DOCTORAL DISSERTATION

Design and synthesis of novel materials for optimization of the active layer morphology and stability of bulk heterojunction organic photovoltaics
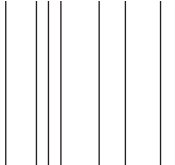
Doctoral dissertation submitted to obtain the degree of
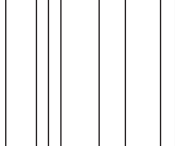Doctor of Science: Chemistry, to be defended by

Pieter Verstappen

Promoter: Prof. Dr Wouter Maes | UHasselt
Co-promoters: Prof. Dr Dirk Vanderzande | UHasselt
　　　　　　　Dr Laurence Lutsen | UHasselt

IMO - IMOMEC
INSTITUUT VOOR MATERIAALONDERZOEK

Chairman: Prof. Dr. Karin Coninx

Promoter: Prof. Dr. Wouter Maes

Copromoters: Prof. Dr. Dirk Vanderzande

                       Dr. Laurence Lutsen, IMO-IMOMEC

Members of the jury: Prof. Dr. Jean Manca, UHasselt

                       Prof. Dr. Peter Adriaensens, UHasselt

                       Prof. Dr. Guy Koeckelberghs, Katholieke

                       Universiteit Leuven

                       Dr. Eva Bundgaard, Technical University of

                       Denmark

TABLE OF CONTENTS

Chapter 3: Fluorination as an Effective Tool to Increase the Open-Circuit Voltage and Charge Carrier Mobility of Organic Solar Cells based on Poly(cyclopenta[2,1-*b*:3,4-*b'*]dithiophene-*alt*-quinoxaline) Copolymers

Chapter 4: Simultaneous Enhancement of the Solar Cell Efficiency and Stability by Reducing the Side Chain Density on Fluorinated PCPDTQx Copolymers

Chapter 5: Enhanced Organic Solar Cell Stability by Polymer (PCPDTBT) Side Chain Functionalization

Chapter 6: Variation of the Central Donor Unit in D-A-D-A-D Small Molecules for Organic Solar Cells

Chapter 7: Summary and Outlook

Chapter 1

Introduction

1.1 ENERGY – CHALLENGE FOR THE 21ST CENTURY

From the start of the Industrial Revolution, the world's economic growth has always gone hand in hand with an insatiable need for energy. Ever since, a vast amount of the required energy has been supplied by (burning) fossil fuels such as oil, gas and coal. Until now, only nuclear energy has been able to take up a significant share of the total energy production (Figure 1). Combustion of these fossil fuel energy resources has led to gigantic emissions of CO_2, likely to be responsible for global warming and the resulting climate change. If global warming is to be kept below 2 °C, a transition from classical CO_2-emissive energy sources to renewable alternatives is eminent.
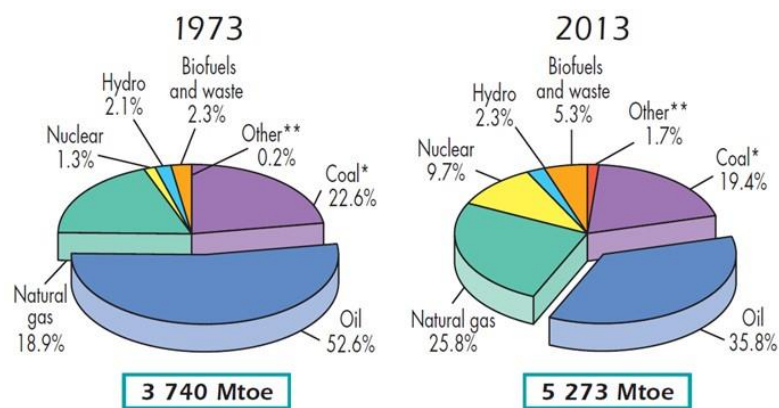
Figure 1: OECD (Organization for Economic Co-operation and Development) total primary energy supply from 1973 to 2013 by fuel. (* Peat and oil shale are aggregated with coal; ** Includes geothermal, wind, solar, etc.; Mtoe = Million tonnes of oil equivalent; Data from *Key World Energy Statistics*, IEA, 2014.[2])

On a world level, there is a growing consensus that CO_2 emissions have to be decreased drastically. The European union has proclaimed some stringent targets which need to be fulfilled by 2020.[1] These so-called 20-20-20 targets include *i*)

a 20% reduction in EU greenhouse gas emissions from 1990 levels, *ii*) raising the share of EU energy consumption produced from renewable resources to 20% and *iii*) a 20% improvement in the EU's energy efficiency. To achieve these commitments it is clear that investments in non-CO_2-emitting energy resources - nuclear, solar, wind, (geo)thermal, etc. - should grow strongly. Further research is required for all of these potential "clean" energy sources and a breakthrough in any of these domains has the prospective to help to supply the world with CO_2 neutral energy.
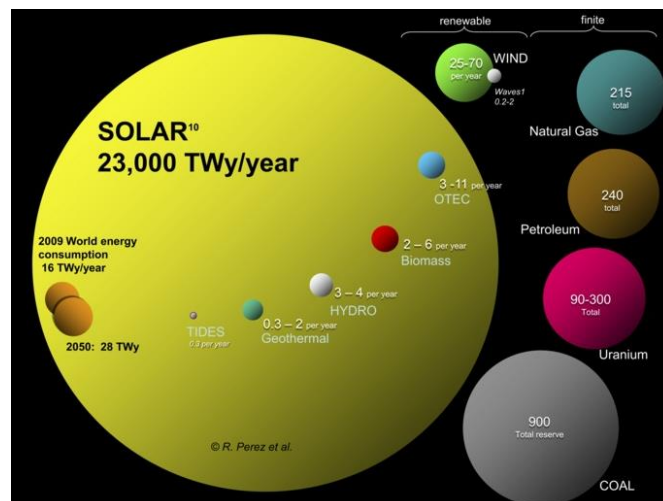
Figure 2: Global energy potential for all energy resources. The renewables are expressed in TW/year, while for the finite sources the total energy amount is expressed in TW. Source: R. Perez and M. Perez, *A fundamental look at the energy reserves for the planet*.[3]

In Figure 2, the maximum amount of energy that can potentially be provided by both finite and renewable resources is shown. From comparison of these numbers with the world's energy consumption of 2009 and the projected energy consumption in 2050, it can be concluded that, from all renewable resources, wind

and especially solar energy hold most potential. However, both energy resources also have a serious drawback, namely the fact that the energy supply is not continuous (as there are frequently periods without sunlight or wind). Therefore, these technologies should always be accompanied by other flexible energy supplies or (improved) energy storage systems.

1.2 SOLAR ENERGY

As can clearly be seen from Figure 2, the potential energy supply by solar light is huge. Every single day the sun provides more energy than mankind yearly consumes on a world scale.[4] Solar energy can typically be harvested in two ways, i.e. *i*) the use of the thermal energy to heat a medium (often water), and *ii*) conversion of the light into a viable energy carrier. To date, a few commercial applications are available that use the thermal energy provided by the sun. The most well-known technologies are probably the vacuum tubes and flat thermal collectors, which can be used to heat household water. Besides these small scale applications, solar heat is also applied in large scale electricity-producing facilities. In February 2014, the Ivanpah Solar Electric Generating System was formally opened in the Mojave Desert.[5] In this electricity plant, a great amount of heliostats (170 000) focus the solar light of the surrounding environment onto a solar tower to generate steam, which then drives steam turbines generating electricity. The expected capacity for electricity production of this plant is 392 MW, which approximately corresponds to the capacity of the nuclear power plants Doel 1 and Doel 2 in Flanders (each 433 MW).

A second technique to transfer solar energy into "useful" energy is the conversion of solar photons. Photosynthesis, Nature's way of harvesting solar energy, can be

categorized under this type of energy conversion. Herein, light is absorbed by the chlorophyll molecules in the plant leaves, converting CO_2 en water into carbohydrates, which can then be used to "fuel" the plant. It should not be surprising that efforts are done to mimic this process in a synthetic environment (called artificial photosynthesis). It has already been shown that sunlight can convert CO_2 into useful fuels such as methanol by the use of appropriate catalysts.[6] Even the photocatalytic conversion of water into H_2 and O_2 has already been reported.[7]

A more generally known technique to harvest solar energy is the direct conversion of photons into electricity by photovoltaic (PV) cells. Nowadays, solar panels are quite generally applied on rooftops. At this moment, the total installed photovoltaic capacity in flanders is ~2150 MW, which is equivalent with two of Belgium's largest nuclear power plants (~1000 MW each). To date, almost all of the employed solar panels are silicon based. However, these types of solar cells are quite expensive and ever since the government decided to cut in the subsidies for the installation of photovoltaic panels, the number of new installations has drastically decreased (from a peak of 84562 installations in 2011 to 4011 in 2013).[8]

1.3 PHOTOVOLTAICS

The construction of the first solar cell, based on silicon, was reported by Chapin *et al.* in 1954, attaining 6% power conversion efficiency (PCE).[9] Silicon solar cells are therefore considered to be the first generation solar cell technology. This technology is nowadays still widely applied for commercial goals. Traditionally, the photoactive layer in this first generation PV technology consists of a thick

crystalline silicon layer, not only leading to high efficiencies but also to a high cost. Therefore, a second generation of photovoltaics has appeared, aiming at cost reduction through the use thin-film technologies. This thin-film technology was based on the first generation materials (crystalline and amorphous silicon) and then extended to other materials such as copper-indium-gallium-selenide (CSGS) and cadmium-telluride (CdTe). Especially the latter two technologies have rapidly evolved and are currently showing PCE's above 20%.[10] Despite the satisfying performances, the scarcity and toxicity of the employed materials are a big disadvantage of these solar cells, hindering wide commercial distribution. This, in turn, pushed the development of a third generation of solar cells, combining low cost and flexibility. This third category includes organic solar cells (OSC's), dye-sensitized solar cells (DSSC's) and hybrid organic/inorganic solar cells. These solar cells rely on organic molecules for light absorption. A main advantage of organic molecules is their high absorption coefficient, often exceeding 10^5 cm^{-1} (~1000 times higher than Si). As a result, this technology allows for the creation of very thin active layers (typically 50–200 nm), leading to devices which are lightweight, semi-transparent and flexible. Moreover, these solar cells can be produced via low cost printing techniques such as roll-to-roll printing, allowing for easy and cheap manufacturing of large surfaces. As can be seen from the NREL chart of best (research) solar cell efficiencies (Figure 3), research on this type of solar cells has rapidly expanded, leading to "booming" PCE values in recent years. Within this third generation of solar cells, organic solar cells are of particular interest because of the possible absence of inorganic materials (all carbon based solar cells), eliminating potential problems of toxicity and scarcity. For organic photovoltaics (OPV's), PCE values around 10% have recently been reported and the first steps toward commercialization are currently explored.[11]
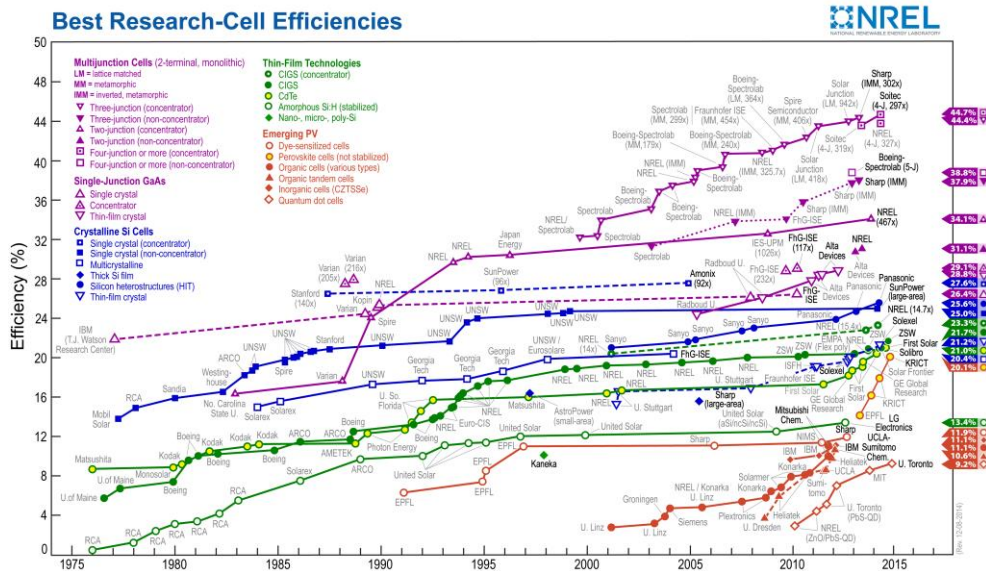
Figure 3: The evolution of the best research-cell efficiencies over the last 40 years (source NREL, 2014-12-21)[12].

1.4 ORGANIC PHOTOVOLTAICS

Although it was already reasoned for quite some time that conjugated polymers could exhibit semiconducting properties and could therefore be very interesting for electronic applications, initial synthetic attempts failed since they yielded insoluble and intractable solids. It was only in the 1970's that a film of poly(acetylene) was successfully prepared, exhibiting a high conductivity (10^5 S/m) after treatment with chlorine, bromine or iodine.[13] Thereafter, interest in conjugated polymers rapidly grew. For their pioneering work, Alan McDiarmid, Hideki Shirakawa and Alan Heeger were awarded the Nobel Price for Chemistry in 2000.

First polymer-based solar cells reported in the 1980's were mostly based on poly(acetylene) and showed rather disappointing performances. It took until 1986

before the first milestone (1% PCE) was reached by Tang *et al.* with a bilayer device consisting of Cu-phthalocyanine as p-type and perylenetetracarboxylic acid as n-type material.[14] An important step forward toward high-efficiency polymer solar cells was taken by Sariciftci and coworkers in 1992, with the discovery of the photoinduced electron transfer from a conjugated polymer to Buckminsterfullerene.[15] In 1995, [6,6]-phenyl-C_{61}-butyric acid methyl ester ($PC_{61}BM$), a more soluble methanofullerene derivative, was reported by Hummelen and Wudl, which to date (together with the $PC_{71}BM$ analogue) is still the most employed acceptor in organic solar cells.[16] In the same year, another major breakthrough was realized when Heeger and Friend introduced the bulk heterojunction (BHJ) concept, which greatly improved the device performance.[17] In a BHJ device, the active layer is constructed by processing a solution containing both the donor and acceptor material.

Although the first solution processed BHJ organic solar cells were reported in 1995, it took another 5 years before the scientific and industrial community realized the potential of this technology, resulting in an almost exponential growth of the number of publications on OPV. While the best solar cell efficiencies reported before 2000 barely reached values above 1%, performances in the proximity (and even beyond) 10% are nowadays reported[9] and the first steps toward commercialization are being taken. The first solar cell park based on organic photovoltaics was installed by the group of Krebs in Denmark.[18] The production of the solar cells proceeded via a variety of printing and roll-to-roll casting techniques with an overall manufacturing speed of 1 m/min for completely encapsulated and tested polymer solar cell foils with a width of 305 mm. The currently employed design consists of a large number of serially connected solar cells, leading to high voltage photovoltaic foils (the "infinity" concept).[19]

Furthermore, it has been demonstrated that these solar cell foils (mounted on a wooden scaffold) have a low energy payback time (277 days when operated in Denmark) in comparison to the classical Si-based solar panels (1.65 to 4.14 years[20]). These polymers even enable a possible energy payback time of 1 day, provided that higher practical large-scale efficiencies are reached and renewable energy is employed in the manufacturing procedure.[21] Nowadays, the device efficiency on these large scale indium tin oxide (ITO) free polymer solar foils is limited to approximately 2%.

1.5 WORKING PRINCIPLE OF ORGANIC SOLAR CELLS

The standard design of an organic solar cell consists of an active layer sandwiched between two electrodes with a different work function (Figure 4). Furthermore, between the photoactive layer and the electrodes, interlayers are added to optimize charge collection. A transparent substrate (usually glass) is typically coated with a thin layer of a transparent electrode (generally ITO). On top, a layer of poly(3,4-ethylenedioxythiophene):poly(styrene sulfonate) (PEDOT:PSS) is deposited as electron blocking (hole transporting) layer. Subsequently, the active layer is spin-coated and the device is finished by thermal evaporation of the low work function cathode, often a combination of calcium and aluminum.
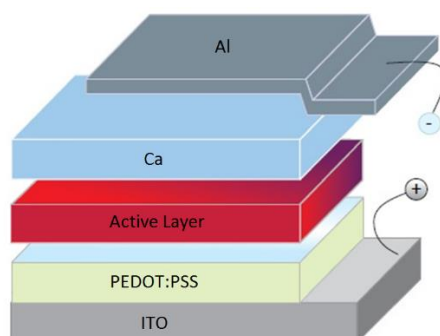
Figure 4: Schematic representation of a standard organic solar cell stack.

An illustration of the general mechanism responsible for the conversion of sunlight to electrical energy is shown in Figure 5. In a first step, photon absorption by the donor material leads to promotion of an electron from the highest occupied molecular orbital (HOMO) (or deeper energy levels) to the lowest unoccupied molecular orbital (LUMO) (or higher energy levels), creating an exciton. These Coulombically bound electron-hole pairs then migrate to the donor-acceptor interphase, where charge transfer occurs, generating free charges. The driving force for charge transfer at the donor-acceptor interphase is provided by the energy difference between the LUMO energy levels of the donor and acceptor materials. A minimum energy difference of ~0.3 eV is required for efficient charge transfer.[22] As a final step, the free charges are transported (holes through the donor and electrons through the acceptor phase) to the electrodes, where they can be collected.
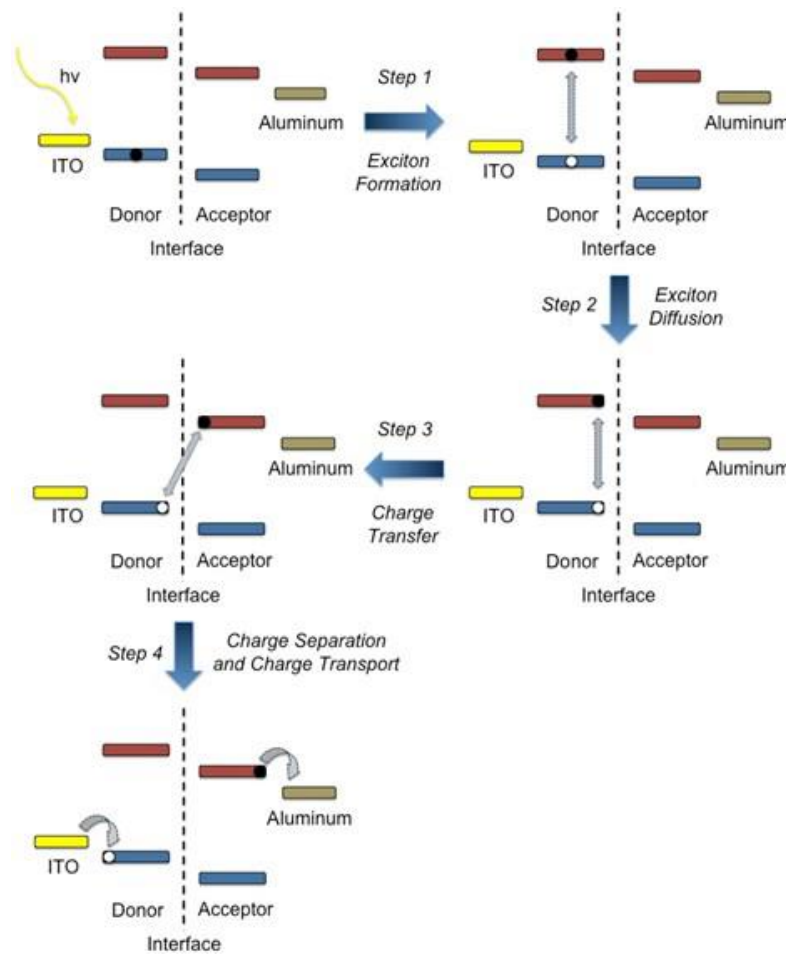
Figure 5: General mechanism for the photoconversion in organic solar cells (HOMO and LUMO energy levels are depicted in blue and red, respectively).

As is clear from the OPV working mechanism, absorption of a photon will not directly create free charges but rather an electron-hole pair, strongly bound via Coulombic interactions (in contrast to what happens in traditional Si-based solar cells). The free charges can only be generated at the interphase between the donor and acceptor material, where enough driving force is present to overcome the binding energy. Due to the very low lifetime of the exciton (typically <1 ns in organic semiconductors),[23] it can only travel over a limited distance (typically 5–

10 nm, referred to as the exciton diffusion length) before recombination occurs. Only excitons generated within this 5–10 nm from the interphase can generate free charges and therefore optimization of the interphase area is very important in OPV. As a consequence, bilayer devices generally exhibit low performances. In BHJ devices, this disadvantage is overcome through the formation of an interpenetrating network of the donor and acceptor material.[14] The surface area of the interphase is largely increased, which decreases the distance the exciton has to travel to the interphase.

In Figure 5, the mechanism for energy conversion is exemplified by photon absorption of the donor material, but of course photon absorption can also proceed through the acceptor material, leading to photocurrent via a similar mechanism as discussed above. Because of its extended absorption in comparison to $PC_{61}BM$, $PC_{71}BM$ is nowadays the most often employed acceptor.[24]

1.6 EVALUATION OF THE SOLAR CELL

Evaluation of the performance of a solar cell under standard simulated conditions (AM1.5G = Air Mass 1.5 Global spectrum, Figure 6a) typically yields a curve as depicted in Figure 6b, which can then be characterized by a series of output parameters. These parameters include the short-circuit current density (J_{SC}), the open-circuit voltage (V_{OC}), the fill factor (FF) and the power conversion efficiency (PCE). The J_{SC} is the maximum current a solar cell can produce and is (mostly) related to the amount of excitons that are generated and separated into free charge carriers, which can be collected at the electrodes. Therefore, the spectral overlap of the absorption spectrum of the solar cell and the solar photon flux is crucial. However, a large fraction of the solar light is also located at higher

wavelengths, indicating the necessity of photoactive materials with extended absorption profiles (ideally into the near-infrared region of the spectrum) (Figure 7). A second important factor governing the J_{SC} is the amount of recombination. Recombination processes can be divided into *i*) geminate recombination (of the exciton), and *ii*) non-geminate recombination (of the free charge carriers).[25] In this respect, purity of the materials is very important to avoid charge traps. The V_{OC}, on the other hand, is the maximum voltage that can be delivered by the device (when no current is flowing). This parameter is related to the energy difference between the HOMO energy level of the donor and the LUMO energy level of the acceptor material. The product of V_{OC} and J_{SC} determines the theoretical maximum power ($P_{theor.\ max}$) which can be extracted from the solar cell. However, under device operation the extracted power is lower than the theoretical maximum power that can be delivered by the solar cell. The ratio of this maximum power and the theoretical maximum power is represented by the fill factor (FF). This parameter depends on the charge dissociation, (balanced) charge carrier transport and recombination properties of the materials.

$$\text{FF} = \frac{P_{max}}{P_{theor.\ max}} = \frac{J_{max} \times V_{max}}{J_{SC} \times V_{OC}}$$

$$\text{PCE} = \frac{P_{max}}{P_{light}} = \frac{J_{SC} \times V_{OC} \times \text{FF}}{P_{light}}$$

Finally, the performance of the solar cell is expressed by the power conversion efficiency, which is determined by the ratio of the maximum power output of the solar cell relative to the power of the input light irradiance under standard test conditions.
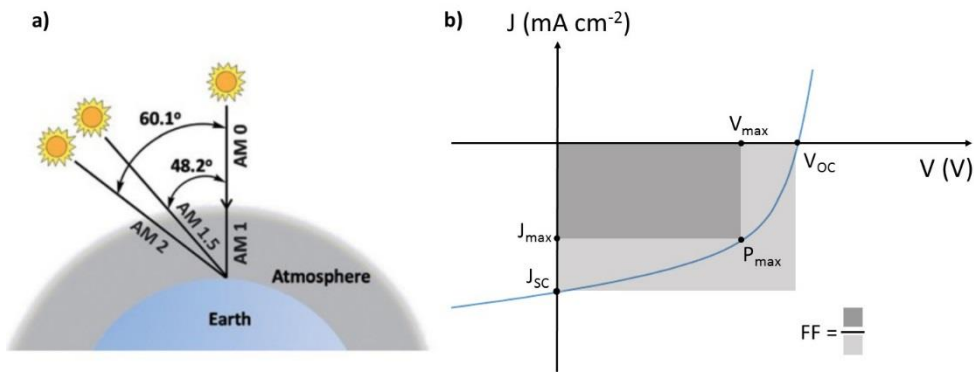
Figure 6: a) Standards used for reporting solar cell efficiencies.[26] b) Current density-voltage curve for a solar cell under illumination with the most important device parameters indicated.
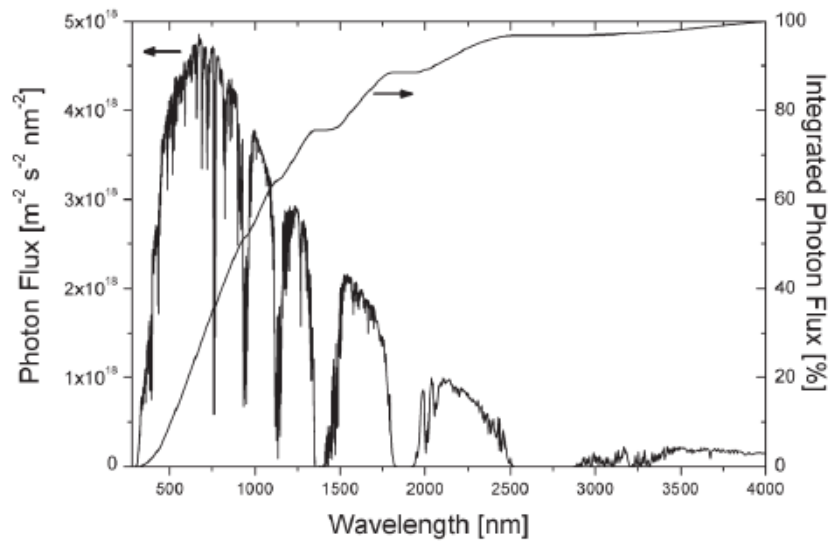
Figure 7: Spectrum of the solar photon flux as a function of wavelength.[27]

1.7 A BRIEF HISTORICAL OVERVIEW OF OPV MATERIALS

1.7.1 Solution-processed polymer solar cells

Since the seminal report of Sariciftci *et al.* on ultrafast electron transfer between poly[2-methoxy-5-(2'-ethylhexyloxy)-1,4-phenylene vinylene] (**MEH-PPV**, Figure 8) and buckminsterfullerene upon illumination, interest in conjugated polymers for the construction of organic solar cells rapidly increased.[12] The first solution-processed BHJ organic solar cell was reported two years later and consisted of a blend of MEH-PPV and $PC_{61}BM$.[14] Since this discovery, a lot of work has been performed on poly(*p*-phenylene vinylene) (PPV) polymers (considered as the first generation of semiconducting polymers for OPV) and some of the basic principles which are nowadays still used, have been discovered on this class of materials. By employing poly[2-methoxy-5-(3',7'-dimethyloctyloxy)-1,4-phenylene vinylene] (**MDMO-PPV**, Figure 8) and variation of the processing solvent, Shaheen *et al.* could greatly improve the solar cell performance from 0.9 to 2.5%.[28] Replacement of toluene by chlorobenzene resulted in a more uniform film with less phase-segregated domains, leading to a vast increase in PCE. Over time, however, it became clear that PPV's posed some intrinsic limitations regarding solar cell performance. The relatively large bandgap (~2 eV) and low mobility for these materials limited the solar cell performance to 3% at best. As a consequence, the interest in the development of new materials with a decreased bandgap and higher hole mobility took off quickly.
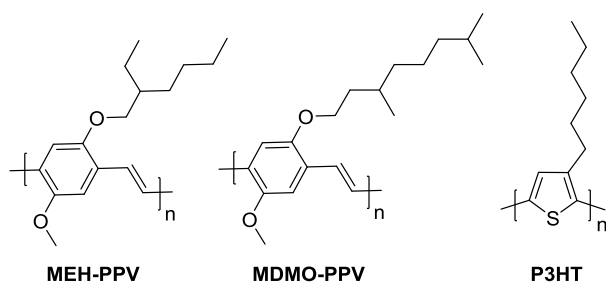
Figure 8: Chemical structures of **MEH-PPV**, **MDMO-PPV** and **P3HT**.

Poly(thiophene)s were rapidly identified as an attractive second generation of electron donating materials for OPV. Especially poly(3-hexylthiophene) (**P3HT**, Figure 8) appeared very promising because of its tendency to organize into microcrystalline structures, which greatly improve the charge transport properties. P3HT quickly became the most popular electron donor polymer, remaining the "workhorse" material for many years. Despite all appealing properties, the initial solar cell performances obtained with this material were rather disappointing. Only in 2002, the first encouraging results were reported, with devices showing J_{SC} values of 8.7 mA/cm^2 and a maximum external quantum efficiency (EQE) of 76%.[29] From that day on, the research community was focused on optimizing the blend morphology. The beneficial effects of thermal annealing were soon discovered, leading to device efficiencies of 3.5%.[30] Besides the physical processing parameters also the chemical properties were optimized by control of the polymerization conditions. Whereas oxidative polymerization leads to the formation of undesired regioisomers, thereby limiting the conjugation length, the discovery of the McCullough, Rieke and GRIM polymerization procedures has enabled the preparation of P3HT exclusively consisting of 2,5-couplings.[31] Additionally, these routes also opened the way to regioregular P3HT, which exhibits superior properties regarding crystallinity and charge mobility.[32]

In combination with $PC_{61}BM$, solar cell performances of 5% were demonstrated for this material.[33] Unfortunately, several limitations have prevented PCE values beyond 5% (in purely organic solar cells). Especially the relatively high HOMO energy level of P3HT, which limits the V_{OC} (P3HT:$PC_{61}BM$ solar cells typically show V_{OC} values around 0.65 V), poses serious restrictions on the final performance. The relatively high bandgap of ~1.9 eV also limits the amount of sunlight that can be absorbed, impeding further improvement. Meanwhile, from theoretical calculations, it has appeared that the "ideal" donor material has a HOMO energy level at -5.4 eV and a bandgap of 1.5 eV, clearly indicating the offset with P3HT.[34]
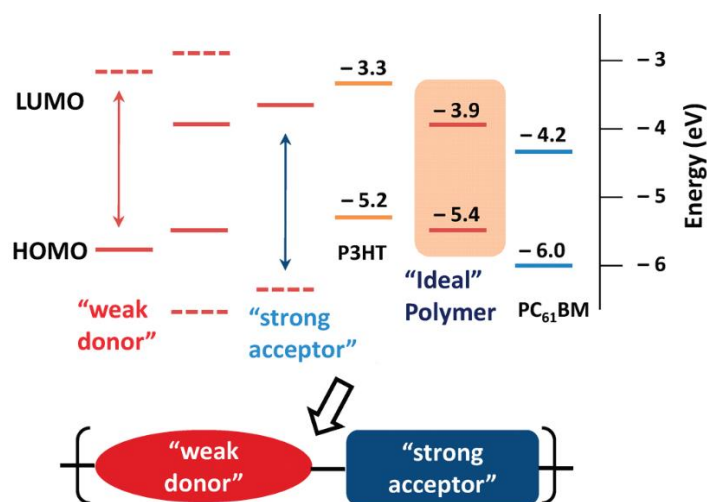
Figure 9: Weak donor-strong acceptor concept and the required energy levels.[22]

In the search for materials that could fulfill these requirements, a third generation of conjugated polymers was developed, i.e. the "push-pull" copolymers, also denoted as donor-acceptor (D-A) copolymers.[35] In these materials, an electron rich and an electron poor building block are copolymerized in an alternating fashion. In such chemical structures, intramolecular charge transfer (ICT) from

the electron rich to the electron poor moiety can occur. This effect stabilizes the quinoid structure of the polymer leading to low bandgap materials. A unique property of these push-pull copolymers is that the HOMO and LUMO energy levels are largely localized on the electron rich and electron poor building block, respectively.[36] This feature can be used to individually tune the bandgap and energy levels of the conjugated polymers. By employing a weak donor-strong acceptor strategy, D-A copolymers with relative low HOMO and high LUMO energy levels have become accessible (Figure 9).[22]

Since the introduction of the donor-acceptor concept, an endless amount of low bandgap copolymers and derived polymer solar cells have been reported. Therefore, this introduction will only handle the most important materials. Early reports on the solar cell performance of these types of materials were again disappointing, mostly due to unfavorable photoactive layer morphologies. Additionally, because most of these materials were rather amorphous, the techniques used to control the morphology of P3HT-based organic solar cells (i.e. thermal and solvent annealing) were not very effective. During the early stages, fluorene and carbazole were often employed as electron rich building blocks in push-pull copolymers. One of the first more successful materials was poly{2,7-[*N*-9-(1'-octylnonyl)-2,7-carbazole]-*alt*-5,5-[4',7'-di(2-thienyl)-2',1',3'-benzothiadiazole]} (**PCDTBT**, Figure 10), reported by Leclerc *et al.*[37] Due to its low HOMO energy level, the resulting PCDTBT:$PC_{71}BM$ photovoltaic devices showed a high V_{OC} of 0.89 V, leading to a PCE of 3.6%. Later on, the efficiency could be improved to 6.1% by the introduction of a TiO_x electron transport layer, which also served as an optical spacer, leading to increased J_{SC} values.[38] However, the wide bandgap of this polymer (1.88 eV) restricts the portion of the solar spectrum that can be absorbed, limiting the J_{SC} of these devices.
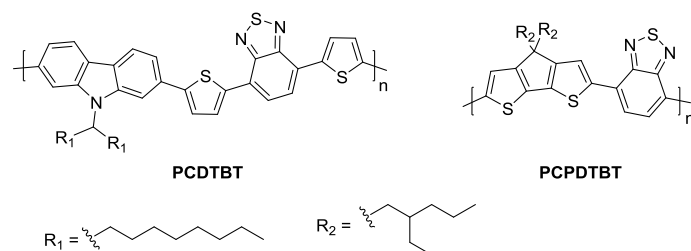
Figure 10: Chemical structures of **PCDTBT** and **PCPDTBT**.

The bandgap could be lowered by the implementation of a more electron rich building block, i.e. cyclopenta[2,1-*b*;3,4-*b'*]dithiophene (CPDT), in the D-A copolymers. Combination with 2,3,1-benzothiadiazole led to the formation of poly[2,6-(4,4-bis-alkyl-4*H*-cyclopenta[2,1-*b*;3,4-*b'*]dithiophene)-*alt*-4,7-(2,1,3-benzothiadiazole)] (**PCPDTBT**, Figure 10), which showed a nearly ideal bandgap of 1.46 eV, leading to improved light harvesting in the near-infrared region.[39] Initially, a rather low PCE of 3.2% was obtained due to the formation of an unfavorable very intimate blend nanomorphology, resulting in short carrier lifetimes and recombination. Interestingly, Heeger *et al.* observed that the solar cell performance drastically increased by the addition of alkanedithiols during active layer processing.[40] Introduction of a small amount (a few v/v%) of this high-boiling additive in the processing solvent optimized the blend morphology, thereby almost doubling the PCE to 5.5%, with J_{SC} values as high as 16.2 mA/cm^2. After this seminal report, various alternative additives were investigated for blend morphology optimization, with 1,8-diiodooctane (DIO) and 1-chloronaphtalene (CN) as some of the most notorious examples, and this technique is nowadays still widely applied to control the blend morphology. Later on, the performance of PCPDTBT-based solar cells could be further improved to over 6% by the incorporation of fluorine atoms on the 2,1,3-benzothiadiazole component (6.6%

for the monofluorinated and 6.5% for the difluorinated analogue).[41] Decreased HOMO and LUMO energy levels were obtained by increasing the electron affinity of 2,1,3-benzothiadiazole, which in turn resulted in higher V_{OC} values (0.73 V and 0.85 V for the mono- and difluorinated copolymer, respectively).
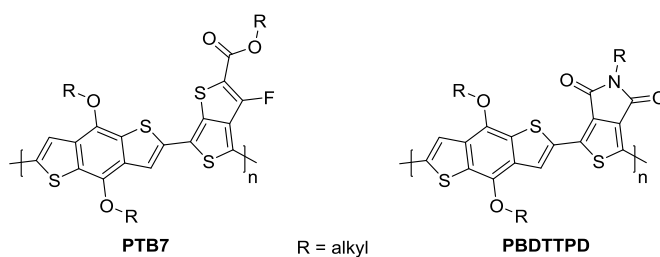
Figure 11: Chemical structures of **PTB7** and **PBDTTPD**.

Further research identified benzo[1,2-*b*:4,5-*b'*]dithiophene (BDT) as another appealing electron rich moiety for the construction of D-A copolymers for OSC's. Showing an intermediate electron density, BDT building blocks can afford both high V_{OC} and J_{SC} values when copolymerized with the appropriate electron poor building blocks. By combining BDT with fluorinated thieno[3,4-*b*]thiophene (TT), the high-performance polymer **PTB7** (Figure 11) has been obtained.[42] The PTB-polymer series has set PCE milestones of 7%, 8% and 9%, strongly boosting the OPV field, and PTB7 is currently (arguably) the number one low bandgap workhorse material. The long and tedious synthesis route toward the TT unit remains a major disadvantage for these materials. Therefore, TT has been replaced by the more easily prepared N-alkylthieno[3,4-*c*]pyrrole-4,6-dione (TPD), yielding poly[2,6-(4,8-bis(alkyloxy)benzo[1,2-*b*:4,5-*b'*]dithiophene)-*alt*-2,8-(N-alkylthieno[3,4-*c*]pyrrole-4,6-dione)] (**PBDTTPD**, Figure 11) copolymers. By optimization of the polymer molar mass, solar cell performances as high as 8.3% have been reported for devices based on this copolymer.[43] Due to the fact

that this polymer is more synthetically accessible than PTB7, more and more research teams have started to apply this material.

1.7.2 Solution-processed small molecule organic solar cells

In the above discussion, only conjugated polymers have been considered as electron donating materials of OPV. These materials have some important drawbacks though. Inherent to their nature, polymers are polydisperse, hindering the use of standard organic synthesis purification techniques (such as column chromatography). Moreover, it has been shown that the molar mass of the polymers is an important factor governing the final solar cell performance.[44] Therefore, quite large batch to batch variations are typically observed when producing solar cells from these materials. Due to their uniform and defined chemical structure, small molecules have the ability to overcome these problems and therefore they are receiving more and more interest. Despite the fact that this is a relatively young domain, some remarkable results have already been reported.

Through extensive optimization, Bazan *et al.* identified a high-performance OPV small molecule. This molecular chromophore is based on a D-A-D-A-D architecture and is composed of fluorinated 2,1,3-benzothiadiazole as acceptor unit, and bithiophene as the outer and dithieno[3,2-*b*:2′,3′-*d*]silole as the inner donor unit, affording 7,7'-[4,4-bis(2′-ethylhexyl)-4*H*-silolo[3,2-*b*:4,5-*b'*]dithiophene-2,6-diyl]bis{6-fluoro-4-[5′-hexyl-(2,2′-bithiophen)-5-yl]benzo[*c*][1,2,5]thiadiazole} (**p-DTS(FBTTh₂)₂**, Figure 12).[45] For this material, high hole mobilities up to 0.14 cm^2(Vs)$^{-1}$ have been obtained, originating from the highly crystalline nature of this small molecule. This resulted in a solar cell performance of 8.0% with a V_{OC} of 0.78 V, a J_{SC} of 14.2 mA/cm^2 and a FF of 73%.
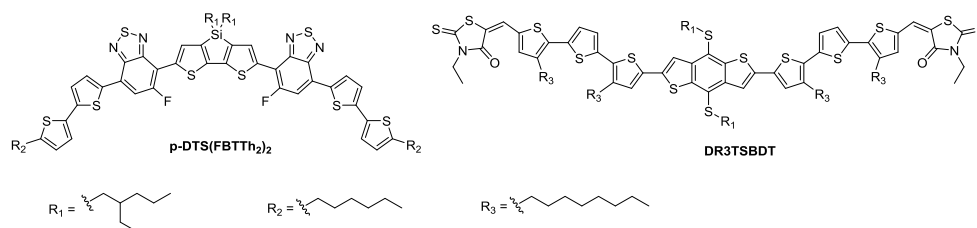
Figure 12: Chemical structures of **p-DTS(FBTTh₂)₂** and **DR3TSBDT**.

Meanwhile, Chen *et al.* reported a small molecule based on an A-D-A strategy affording an even more impressive solar cell performance. Their **DR3TSBDT** molecule consists of a BDT unit as the central donor, which is linked to the outer 3-ethylrhodanine acceptors via a terthiophene linker (Figure 12). It was observed that substitution of the alkoxy side chains by alkylthio moieties could additionally boost the PCE to an astonishing 9.95%.[46]

Despite these excellent recent results, further research is mandatory since no clear design rules for small molecules are defined yet. Small changes of the chemical structure can lead to a large difference in the solar cell performance and, moreover, finding the optimal processing conditions is much more challenging than for polymers. Continuous research is likely to drive the efficiencies further forward and increase the fundamental understanding of small molecule solar cells.

1.8 OUTLINE OF THE THESIS

To become an economically competitive photovoltaic technology, organic solar cells need to step up in terms of production cost, efficiency and stability. In this doctoral thesis, fundamental research is performed in two of these directions, i.e. efficiency and stability. The possibility to produce OPV devices via large area printing and coating technologies is one of the main benefits of this class of solar cells. However, many of the current high-performance materials balance on the edge of solubility, hindering the use of these advanced printing technologies (because of clogging problems). Therefore, one of the main goals of this thesis is to synthesize novel low bandgap copolymers and small molecules exhibiting fairly high solubility and affording high-efficiency devices. Furthermore, (thermal) stabilization of the (nano)morphology of the organic photoactive layers is also pursued.

After a general introduction in **Chapter 1**, **Chapter 2** focuses on the development of convenient (short and high yielding) synthesis routes toward asymmetrically substituted and/or functionalized 4*H*-cyclopenta[2,1-*b*:3,4-*b′*]dithiophenes (CPDT's), one of the main building blocks used in this work. Despite the optimization work performed on the existing three-step (Friedel-Crafts dehydration cyclization) procedure, rather low yields were obtained for more sterically constrained CPDT derivatives. Therefore, an alternative two-step synthetic protocol was developed, involving (i) a Wittig-type carbonyl olefination, and (ii) regioselective alkylation of the exocyclic double bond with LiAlH$_4$ and an alkyl bromide.

Chapter 3 then describes the synthesis of a series of fluorinated PCPDTQx-type low bandgap copolymers and the influence of fluorination on the physicochemical

polymer properties and the resulting polymer solar cell characteristics. A gradual decrease in the HOMO energy level was observed for every fluorine atom added to the quinoxaline constituents, leading to a steady increase in V_{OC} (of ~0.1 V) for the photovoltaic devices.

Chapter 4 continues on the difluorinated PCPDTQx copolymer already reported in Chapter 3. In the active layer of the polymer solar cells based on this material large domains can be seen. In an attempt to reduce the domain size, the side chain density of the polymer is varied, resulting in nicely intermixed blend morphologies. Furthermore, an increase in the T_g of the polymers is noticed when the number of side chains decreases. Both polymer solar cell efficiency and thermal stability are carefully evaluated.

In **Chapter 5** a different approach to stabilize the (nano)morphology of the photoactive layer blend is explored. It has been reported before for polythiophene-based organic solar cells that the introduction of functional groups on the polymer side chains can assist to improve the thermal stability of the resulting devices. In this chapter an effort is done to translate this principle to a push-pull copolymer. As a case study, PCPDTBT is chosen, and it is shown that the incorporation of ester and (especially) alcohol moieties in the alkyl side chains aids to (significantly) improve the lifetime of the resulting polymer:fullerene solar cells under prolonged thermal stress.

The final **Chapter 6** describes the synthesis of four new small molecule donor materials and their OPV device analysis. The central donor unit of the well-known p-DTS(FBTTh$_2$)$_2$ small molecule is altered and the influence of the structural change on the physicochemical material properties and the small molecule solar cells is investigated. It is shown that the purity of the semiconducting materials is of crucial importance and therefore, care has to be taken during the synthesis

protocol to avoid the formation of side products, as they can be very hard to remove and detrimental for solar cell performance.

In **Chapter 7** a general summary of the thesis is presented and an outlook is provided.

1.9 REFERENCES

[1]   http://ec.europa.eu

[2]   http://www.iea.org/publications/freepublications/publication

[3]   Perez, R. and M. Perez, *A fundamental look at energy reserves for the planet.*, IEA SHC Solar Update, **april 2009**, *50*, 5.

[4]   McGehee, M. D.; Goh, C. *The Bridge* **2005**, *35*, 33.

[5]   http://www.ivanpahsolar.com/

[6]   Yang, C.-C.; Yu, Y.-H.; van der Linden, B.; Wu, J. C. S.; Mul, G. *J. Am. Chem. Soc.* **2010**, *132*, 8398.

[7]   Wang, X.; Maeda, K.; Chen, X.; Takanabe, K.; Domen, K.; Hou, Y.; Fu, X.; Antonietti, M. *J. Am. Chem. Soc.* **2009**, *131*, 1680.

[8]   http://www.vreg.be/

[9]   Chapin, D. M.; Fuller, C. S.; Pearson, G. L. *J. Appl. Phys.* **1954**, *25*, 676.

[10]   (a) Aberle, A. G. *Thin Solid Films* **2009**, *517*, 4706; (b) Green, M. A.; Emery, K.; Hishikawa, Y.; Warta, W. *Prog. Photovoltaics Res. Appl.* **2010**, *18*, 346.

[11]   (a) He, Z.; Zhong, C.; Su, S.; Xu, M.; Wu, H.; Cao, Y. *Nat. Photonics* **2012**, *6*, 591; (b) You, J.; Dou, L.; Yoshimura, K.; Kat, T.; Ohya, K.; Moriarty, T.; Emery, K.; Chen, C.-C.; Gao, J.; Li, G.; Yang, Y. *Nat. Commun.* **2012**, *4*, 1446; (c) You, J.; Chen, C.-C.; Hong, Z.; Yoshimura, K.; Ohya, K.; Xu, R.; Ye, S.; Gao, J.; Li, G.; Yang, Y. *Adv. Mater.* **2013**, *25*, 3973; (d) Ye, L.; Zhang, S.; Zhao, W.; Yao, H.; Hou, J. *Chem. Mater.* **2014**, *26*, 3603; (e) Zhang, K.; Zhong, C.; Liu, S.; Mu, C.; Li, Z.; Yan, H.; Huang, F.; Cao, Y. *ACS Appl. Mater. Interfaces* **2014**, *6*, 10429; (f) Liu, Y.; Zhao, J.; Li, Z.; Mu, C.; Ma, W.; Hu, H.; Jiang, K.; Lin, H.; Ade, H.; Yan, H. *Nat. Commun.* **2014**, *5*, 5293.

[12]   http://www.nrel.gov/ncpv/

[13]   (a) Shirakawa, H.; Louis, E. J.; Macdiarmid, A. G.; Chiang, C. K.; Heeger, A. J. *J. Chem. Soc., Chem. Commun.* **1977**, 578; (b) Chiang, C. K.; Fischer, C. R.; Park, Y. W.; Heeger, A. J.; Shirakawa, H.; Louis, E. J.; Gau, S. C.; Macdiarmid, A. G. *Phys. Rev. Lett.* **1977**, *39*, 1098.

[14]   Tang, C. W. *Appl. Phys. Lett.* **1986**, *48*, 183.

[15]   Sariciftci, N. S.; Smilowitz, L.; Heeger, A. J.; Wudl, F. *Science* **1992**, *258*, 1474.

[16]   (a) Wudl, F. *Acc. Chem. Res.* **1992**, *25*, 15716; (b) Hummelen, J. C.; Knight, B. W.; LePeq, F.; Wudl, F.; Yao, J.; Wilkins, C. L. *J. Org. Chem.* **1995**, *60*, 532.

[17]   (a) Yu, G.; Gao, J.; Hummelen, J. C.; Wudl, F.; Heeger, A. J. *Science* **1995**, *270*, 1789; (b) Halls, J. J. M.; Walsh, C. A.; Greenham, N. C.; Marseglia, E. A.; Friend, R. H.; Moratti, S. C.; Holmes, A. B. *Nature* **1995**, *376*, 498.

[18]   Krebs, F. C.; Espinosa, N.; Hösel, M.; Søndergaard, R. R.; Jørgensen, M. *Adv. Mater.* **2014**, *26*, 29.

[19]   Sommer-Larsen, P.; Jørgensen, M.; Søndergaard, R. R.; Hösel, M.; Krebs, F. C. *Energy Technol.* **2013**, *1*, 15.

[20]   Knapp, K.; Jester, T. *Sol. Energy* **2001**, *71*, 165.

[21]   Espinosa, N.; Hösel, M.; Angmo, D.; Krebs, F. C. *Energy Environ. Sci.* **2012**, *5*, 5117.

[22]   Zhou, H.; Yang, L.; You, W. *Macromolecules* **2012**, *45*, 607.

[23]   Scharber, M. C.; Sariciftci, N. S. *Prog. Polym. Sci.* **2013**, *38*, 1929.

[24]   Wienk, M. M.; Kroon, J. M.; Verhees, W. J. H.; Knol, J.; Hummelen, J. C.; van Hal, P. A.; Janssen, R. A. J. *Angew. Chem. Int. Ed.* **2003**, *42*, 3371.

[25]   Proctor, C. M.; Kuik, M.; Nguyen, T.-Q. *Prog. Polym. Sci.* **2013**, *38*, 1941.

[26]   Mishra, A.; Bäuerle, P. *Angew. Chem. Int. Ed.* **2012**, *51*, 2020.

[27]   Kroon, R.; Lenes, M.; Hummelen, J. C.; Blom, P. W. M.; de Boer, B. *Polym. Rev.* **2008**, *48*, 531.

[28]   Shaheen, S. E.; Brabec, C. J.; Sariciftci, N. S.; Padinger, F.; Fromherz, T.; Hummelen, J. C. *Appl. Phys. Lett.* **2001**, *78*, 841.

[29]   Schilinsky, P.; Waldauf, C.; Brabec, C. J. *Appl. Phys. Lett.* **2002**, *81*, 3885.

[30]   Padinger, F.; Rittberger, R. S.; Sariciftci, N. S. *Adv. Funct. Mater.* **2003**, *13*, 1.

[31]   (a) McCullough, R. D.; Lowe, R. D. *J. Chem. Soc., Chem. Commun.* **1992**, *1*, 70; (b) Chen, T. A.; Rieke, R. D. *J. Am. Chem. Soc.* **1992**, *114*, 10087; (c) Chen, T. A.; O'Brien, R. A.; Rieke, R. D. *Macromolecules* **1993**, *26*, 3462; (d) Loewe, R. S.; Ewbank, P. C.; Liu, J.; Zhai, L.; McCullough, R. D. *Macromolecules* **2001**, *34*, 4324.

[32]   Kim, Y.; Cook, S.; Tuladhar, S. M.; Choulis, S. A.; Nelson, J.; Durrant, J. R.; Bradley, D. D. C.; Giles, M.; McCulloch, I.; Ha, C.-S.; Ree, M. *Nat. Mater.* **2006**, *5*, 197.

[33]   (a) Ma, W.; Yang, C.; Gong, X.; Lee, K.; Heeger, A. J. *Adv. Funct. Mater.* **2005**, *15*, 1617; (b) Li, G.; Shrotriya, V.; Huang, J.; Yao, Y.; Moriarty, T.; Emery, K.; Yang, Y. *Nat. Mater.* **2005**, *4*, 864.

[34]   Scharber, M. C.; Mühlbacher, D.; Koppe, M.; Denk, P.; Waldauf, C.; Heeger, A. J.; Brabec, C. J. *Adv. Mater.* **2006**, 18, 789.

[35]   (a) Havinga, E. E.; ten Hoeve, W.; Wynberg, H. *Polym. Bull.* **1992**, *29*, 119; (b) Havinga, E. E.; ten Hoeve, W.; Wynberg, H. *Synth. Met.* **1993**, *55*, 299; (c) van Mullekom, H. A. M.; Vekemans, J. A. J. M.; Havinga, E. E.; Meijer, E. W. *Mater. Sci. Eng., R* **2001**, *32*, 1.

[36]   (a) Brédas, J.-L.; Norton, J. E.; Cornil, J.; Coropceanu, V. *Acc. Chem. Res.* **2009**, *42*, 1691; (b) Zhou, H.; Yang, L.; Stoneking, S.; You, W. *ACS Appl. Mater. Interfaces* **2010**, *2*, 1377.

[37]   (a) Blouin, N.; Michaud, A.; Leclerc, M. *Adv. Mater.* **2007**, *19*, 2295; (b) Blouin, N.; Michaud, A.; Gendron, D.; Wakim, S.; Blair, E.; Neagu-Plesu, R.; Belletête, M.; Durocher, G.; Tao, Y.; Leclerc, M. *J. Am. Chem. Soc.* **2008**, *130*, 732.

[38]   Park, S. H.; Roy, S.; Beaupré, S.; Cho, S.; Coates, N.; Moon, J. S.; Moses, D.; Leclerc, M.; Lee, K.; Heeger, A. J. *Nat. Photonics* **2009**, *3*, 297.

[39]   (a) Mühlbacher, D.; Scharber, M.; Morana, M.; Zhu, Z.; Waller, D.; Gaudiana, R.; Brabec, C. *Adv. Mater.* **2006**, *18*, 2884; (b) Soci, C.; Hwang, I.-W.; Moses, D.; Zhu, Z.; Waller, D.; Gaudiana, R.; Brabec, C. J.; Heeger, A. J. *Adv. Funct. Mater.* **2007**, *17*, 632; (c) Zhang, M.; Tsao, H. N.; Pisula, W.; Yang, C.; Mishra, A. K.; Müllen, K. *J. Am. Chem. Soc.* **2007**, *129*, 3472; (d) Coffin, R. C.; Peet, J.; Rogers, J.; Bazan, G. C. *Nat. Chem.* **2009**, *1*, 657.

[40]   (a) Peet, J.; Kim, J. Y.; Coates, N. E.; Ma, W. L.; Moses, D.; Heeger, A. J.; Bazan, G. C. *Nat. Mater.* **2007**, *6*, 497; (b) Lee, J. K.; Ma, W. L.; Brabec, C. J.; Yuen, J.; Moon, J. S.; Kim, J. Y.; Lee, K.; Bazan, G. C.; Heeger, A. J. *J. Am. Chem. Soc.* **2008**, *130*, 3619.

[41]   (a) Albrecht, S.; Janietz, S.; Schindler, W.; Frisch, J.; Kurpiers, J.; Kniepert, J.; Inal, S.; Pingel, P.; Fostiropoulos, K.; Koch, N.; Neher, D. *J. Am. Chem. Soc.* **2012**, *134*, 14932; (b) Albrecht, S.; Tumbleston, J. R.; Janietz, S.; Dumsch, I.; Allard, S.; Scherf, U.; Ade, H.; Neher, D. *J. Phys. Chem. Lett.* **2014**, *5*, 1131.

[42]   Liang, Y.; Feng, D.; Wu, Y.; Tsai, S.-T.; Li, G.; Ray, C.; Yu, L. *J. Am. Chem. Soc*. **2009**, *131*, 7792; (b) Liang, Y. Y.; Xu, Z.; Xia, J.; Tsai, S. T.; Wu, Y.; Li, G.; Ray, C.; Yu, L. P. *Adv. Mater.* **2010**, *22,* E135.

[43]   Bartelt, J. A.; Douglas, J. D.; Mateker, W. R.; El Labban, A.; Tassone, C. J.; Toney, M. F.; Fréchet, J. M. J.; Beaujuge, P. M.; McGehee, M. D. *Adv. Energy Mater.* **2014**, *4*, 1301733.

[44]   (a) Coffin, R. C.; Peet, J.; Rogers, J.; Bazan, G. C. *Nat. Chem.* **2009**, *1*, 657; (b) Li, W.; Yang, L.; Tumbleston, J. R.; Yan, L.; Ade, H.; You, W. *Adv. Mater.* **2014**, *26*, 4456.

[45]   (a) Kyaw, A. K. K.; Wang, D. H.; Gupta, V.; Zhang, J.; Chand, S.; Bazan G. C.; Heeger, A. J. *Adv. Mater.* **2013**, *25*, 2397; (b) Kyaw, A. K. K.; Wang, D. H.; Gupta, V.; Leong, W. L.; Ke, L.; Bazan G. C.; Heeger, A. J. *ACS Nano* **2013**, *7*, 4569; (c) Coughlin, J. E.; Henson, Z. B.; Welch G. C.; Bazan, G. *Acc. Chem. Res.* **2014**, *47*, 257.
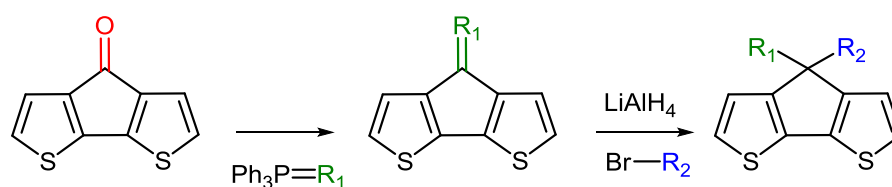
[46]   Kan, B.; Zhang, Q.; Li, M.; Wan, X.; Ni, W.; Long, G.; Wang, Y.; Yang, X.; Feng H.; Chen, Y. *J. Am. Chem. Soc.* **2014**, *136*, 15529.

Chapter 2

Synthetic Routes toward Asymmetrically Substituted (Functionalized) 4*H*-Cyclopenta[2,1-*b*:3,4-*b'*]dithiophenes

ABSTRACT

A two-step synthetic protocol involving (i) a Wittig-type carbonyl olefination, and (ii) regioselective alkylation of the exocyclic double bond with LiAlH$_4$ and an alkyl bromide, was developed as an alternative to the recently reported three-step synthetic approach toward asymmetrically substituted/functionalized 4*H*-cyclopenta[2,1-*b*:3,4-*b′*]dithiophenes. The two routes are rather complementary, with specific advantages depending on the desired substitution pattern, and are of particular appeal for the construction of semiconducting materials to be applied in organic photovoltaics.

2.1 INTRODUCTION

Cyclopentadithiophenes – fused bithiophene heterocycles – have emerged as attractive precursors for advanced materials, notably organic semiconductors and polymerization catalysts. Zr- and Ti-cyclopentadithiophene complexes have been employed as structural units in homogeneous Ziegler-Natta catalysts for 1-olefin polymerization reactions.[1] Cyclopentadithiophenes have also been used as key building blocks in conjugated polymers for optoelectronic applications. To date, they are most prominent in the field of bulk heterojunction organic photovoltaics (OPV) as donor components in low bandgap (donor-acceptor) copolymers.[2,3] The electrochemical, optical and conducting properties of poly(cyclopenta-dithiophenes) bound to various surfaces have extensively been studied by Zotti and co-workers. These materials can be applied as sensors when calixarenes[4] or crown ether[5] moieties are appended since these ligands selectively bind small molecule or ionic guests. Electrochromism was also observed for these homopolymers when viologen groups were attached.[6] Finally, they were also used as conductive matrices for electrochemical drug (DNA) delivery systems.[7]

For optoelectronic applications, 4*H*-cyclopenta[2,1-*b*:3,4-*b'*]dithiophene (CPDT) is by far the most commonly used cyclopentadithiophene isomer (out of the six variants). In general, the 4-position of the CPDT scaffold is dialkylated prior to further chromophore extension and/or polymerization to ensure good solubility of the final materials in the organic solvents used for device processing. **PCPDTBT** (poly[(4,4-bis(2-ethylhexyl)-4*H*-cyclopenta[2,1-*b*:3,4-*b'*]dithiophene-2,6-diyl)-*alt*-(2,1,3-benzothiadiazole-4,7-diyl)], Figure 1) was one of the first donor-acceptor copolymers to be explored for OPV applications, affording power conversion efficiencies above 2.8% in combination with a fullerene acceptor.[8a]

This efficiency was almost doubled in the presence of a suitable processing additive.[8b] As a result, **PCPDTBT** has become one of the workhorse electron donor materials in the field and seminal studies have been conducted using this material (and derivatives thereof).[8] In recent years, CPDT has lost some of its popularity though, partly because other more efficient material combinations popped up, but also due to the rather tedious synthesis of the CPDT monomer. In continuation of previous synthetic endeavors toward CPDT-based materials,[9] we therefore continued our efforts to facilitate the access to CPDT building blocks.

2.2 RESULTS AND DISCUSSION

Over the years, several multistep protocols have been reported affording (mostly dialkylated) CPDT materials.[10-12] In 2010, we have introduced an alternative three-step method (Scheme 1, *vide infra*).[9a] The main benefit of this procedure is that it provides smooth access to asymmetrically dialkylated and/or functionalized CPDTs as well. Nonetheless, it was more recently found that, while surely being an improvement compared to the traditional routes proceeding via the tedious synthesis of the unsubstituted parent CPDT **1** (Figure 1),[10] this approach has a few drawbacks in terms of versatility for particular substituents (e.g. some functionalized or branched alkyl groups). Here, we present some optimization efforts for the above-mentioned three-step protocol and an alternative synthetic approach for the straightforward synthesis of more sophisticated functionalized and/or asymmetrically dialkylated CPDTs in high yields.
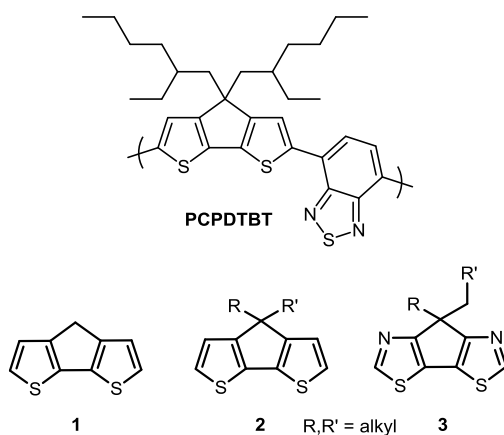
Figure 1: Structure of the low bandgap **PCPDTBT** polymer, parent CPDT **1**, 4,4-dialkyl-CPDTs **2** and 7,7-dialkylcyclopenta[1,2-*d*:4,3-*d*']dithiazoles **3**.

For the synthesis of 4,4-dialkyl-substituted CPDTs **2** (Figure 1) two different synthetic approaches have been reported. One method consists of the synthesis of unsubstituted CPDT **1** followed by a nucleophilic substitution reaction – subtracting the protons on the 4-position – with alkyl halides, either in the presence of KOH as a base[11] or through stepwise lithiation and substitution.[12] For the latter case, a few examples of asymmetric 4,4-dialkyl-substitution have been reported as well.[13] The synthesis of CPDT **1** is, however, quite laborious and involves a minimum of three steps with a rather low overall yield.[10] A second three-step approach to (asymmetrically) substituted CPDTs was reported by Van Mierloo *et al.* (Scheme 1) in 2010.[9a] It comprises of the synthesis of 3-bromo-2,2'-bithiophene (**4**) by a Kumada coupling of 2-thienylmagnesium bromide and 2,3-dibromothiophene, followed by its lithiation and subsequent reaction with (a)symmetrical ketones to afford dialkylated tertiary alcohol derivatives. Finally, Friedel-Crafts dehydration cyclization yields the desired 4,4-dialkyl-CPDTs. Main issues with this route arise in the ring closing step, as low yields and/or troublesome purifications are sometimes encountered.
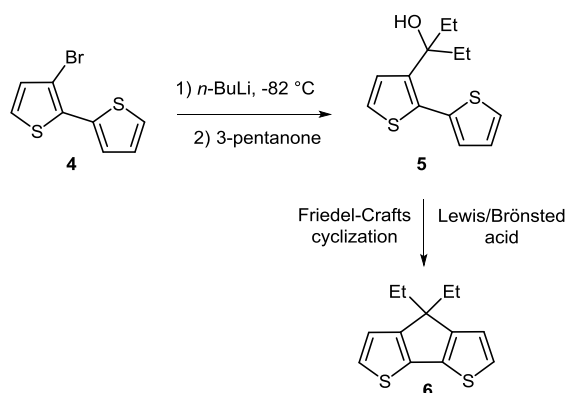
Scheme 1: Three-step synthetic approach by Van Mierloo *et al.*,[9a] illustrated for 4,4-diethyl-CPDT **6**.

For that reason, optimization efforts were done – using 4,4-diethyl-CPDT **6** as a model system (Scheme 1) – in terms of reaction time, Lewis acid, solvent and work-up (see Table S1). As described before, the cyclization to CPDT competes with an elimination reaction to the *Z*- and *E*-alkenes (see Scheme S1).[9a] The reaction conditions were hence evaluated by determination of the relative presence of these alkenes, tertiary alcohol **5** and CPDT **6** in the crude reaction mixture by ^{1}H NMR. Under the previously optimized conditions (octane, H_2SO_4, r.t., 12 h), only CPDT **6** and some undefined impurities were identified. During work-up, extraction was done with diethyl ether instead of CH_2Cl_2, leading to a yield of 74% after column chromatography (compared to 55% before). Also for a shorter reaction time and toluene or hexane as a solvent full conversion was observed. In all cases the formation of a black tar occurred. This was avoided when more polar solvents like diethyl ether or ethanol were employed, but then the alkenes were formed exclusively. This observation, in combination with the discrepancy between the relative abundance of **6** (100%) in the crude reaction mixture and the yield after purification (74%), indicates that degradation is most

likely the limiting factor for the yield of the CPDT. This encouraged us to look for alternative cyclization conditions. When (Lewis) acids such as benzesulfonic acid (BSA) or $FeCl_3.6H_2O$ were employed, only elimination occurred. Also trifluoromethylsulfonic acid anhydride was tested since it was proven to be an effective catalyst for the cyclization of olefins to aza-polycyclic compounds.[14] Unfortunately, also in this case only alkene formation was noticed. However, when $AlCl_3$ was used as a Lewis acid in toluene, the starting product was converted to CPDT **6** in up to 58%, without any tar formation. Further optimization from this lead result could avoid the CPDT degradation seen in the presence of H_2SO_4, and thereby increase the cyclization yield.

Although this three-step method is ideally suited for CPDTs (asymmetrically) substituted with linear alkyl chains, it has its limitations upon the application of functionalized ketones, e.g. keto esters. The introduction of side chain functionalities is of high relevance as the side chains determine to a large extent the blend morphology development and stability in BHJ organic solar cells.[2,15] On the other hand, low yields are generally obtained when branched alkyl side chains are introduced (i.e. with the branching unit close to the CPDT bridge). These observations stimulated us to develop a complementary route based on the reported approach toward 7,7-dialkylated cyclopenta[1,2-*d*:4,3-*d'*]dithiazoles **3** (Figure 1).[16] This route (Scheme 2) – to the best of our knowledge never applied to CPDTs before[17] – starts with a Wittig reaction on CPDT-4-one **7**[10b] with an alkylidenetriphenylphosphorane to introduce a first alkyl chain on the 4 position. The next step is then a regioselective one-pot double bond reduction/substitution with $LiAlH_4$ in the presence of an alkyl bromide. Asymmetric substitution is very straightforward by this method and for both steps the products can be isolated in reasonably high yields (>70%), even if branched alkyl chains are introduced. The

main drawback of this procedure is that it still proceeds via the CPDT-4-one precursor **7** and is hence quite lengthy.
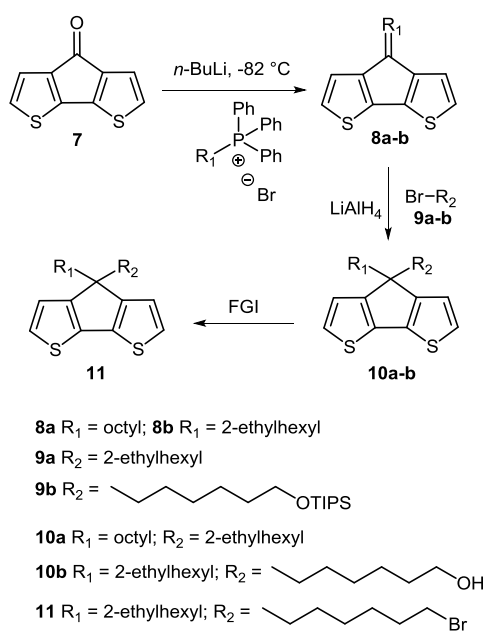
Scheme 2: Wittig route toward asymmetrically substituted/functionalized CPDTs. FGI = functional group interconversion.

As an example, 4-(2-ethylhexyl)-4-octyl-CPDT **10a**[9a] was synthesized via a Wittig reaction with octylidenetriphenylphosphorane, and subsequent reduction of the exocyclic olefin-CPDT **8a** with LiAlH$_4$ in the presence of 2-ethylhexyl bromide (**9a**). Furthermore, functional groups on the CPDT side chains are readily introduced, making this approach well-suited for the synthesis of functionalized asymmetrically substituted CPDTs.[18]

This was demonstrated by the introduction of an alcohol functionality via the use of 6-(bromohexyloxy)triisopropyl silane (**9b**) in the one pot reduction/substitution step of **8b** (Scheme 2).[3a] The crude product was treated with tetrabutylammonium fluoride (TBAF) to hydrolyze the silyl ether, yielding the

alcohol-functionalized CPDT **10b** in 64% overall yield. Finally, this alcohol derivative could easily be converted to brominated CPDT **11** by an Appel reaction (Scheme 2). It is foreseen that this functionalization approach can readily be extended to various other functionalities such as esters (via ortho-esters) or aldehydes (via acetals).

2.3 CONCLUSIONS

In summary, we have developed a convenient synthetic approach to dialkylated CPDTs in high yields, which is of particular interest if one desires to introduce two different functionalized and/or branched alkyl side chains, and is in that sense complementary to the previously reported three-step protocol. Variation of the alkyl bromide in the reduction/substitution step allows the introduction of a wide range of different functionalities on the CPDT building block.

2.4 EXPERIMENTAL SECTION

2.4.1 Materials and instruments

NMR chemical shifts (δ, in ppm) were determined relative to the residual $CHCl_3$ absorption (7.26 ppm) or the ^{13}C resonance shift of $CDCl_3$ (77.16 ppm). High resolution ESI-MS was performed using an LTQ Orbitrap Velos Pro mass spectrometer equipped with an atmospheric pressure ionization source operating in the nebulizer assisted electrospray mode. The instrument was calibrated in the *m/z* range 220−2000 using a standard solution containing caffeine, MRFA and Ultramark 1621.

2.4.2 Synthesis

Unless stated otherwise, all reagents and chemicals were obtained from commercial sources and used without further purification. Solvents were dried by a solvent purification system (MBraun, MB-SPS-800). Cyclopenta[2,1-*b*:3,4-*b*']dithiophen-4-one (**7**)[19] and (2-ethylhexyl)triphenylphosphonium bromide[20] were prepared according to literature procedures.

4-(Octylidene)-4*H*-cyclopenta[2,1-*b*:3,4-*b*']dithiophene (**8a**)

n-BuLi (4.0 mL of a 2.5 M solution in *n*-hexane, 10.0 mmol) was added to a solution of octyltriphenyl-phosphonium bromide (4.55 g, 10.0 mmol) in dry THF (30 mL) at –82 °C under N_2 atmosphere. The mixture was stirred for 30 min at –82 °C and then a solution of CPDT-4-one **7** (1.48 g, 7.69 mmol) in dry THF (30 mL) was added. After stirring for an additional 30 min at this temperature, the mixture was allowed to reach r.t. The reaction was quenched with water and the aqueous layer was extracted with diethyl ether. After drying the combined organic layers over $MgSO_4$, removal of the solvents *in vacuo*, and purification by column chromatography (SiO_2, petroleum ether), a yellow oil was obtained (1.64 g, 74%), ^{1}H NMR (300 MHz, $CDCl_3$): 7.27 (d, *J* = 4.7 Hz, 1H), 7.13 (d, *J* = 4.8 Hz, 1H), 7.12 (d, *J* = 4.8 Hz, 1H), 7.08 (d, *J* = 4.9 Hz, 1H), 6.44 (t, *J* = 7.8 Hz, 1H), 2.68 (q, *J* = 7.5 Hz, 2H), 1.62 (quin, *J* = 7.4 Hz, 2H), 1.48–1.23 (m, 8H), 0.89 (t, *J* = 6.8 Hz, 3H).

4-(2-Ethylhexyl)-4-octyl-4*H*-cyclopenta[2,1-*b*:3,4-*b*']dithiophene

(**10a**)[9a]

A solution of 2-ethylhexylbromide (1.40 g, 7.25 mmol) and CPDT **8a** (2.09 g, 7.25 mmol) in dry THF (25 mL) was added dropwise to a suspension of $LiAlH_4$ (0.275 g, 7.25 mmol) in dry THF (10 mL) under N_2 atmosphere at r.t. After 15 h, Et_2O

(50 mL) and HCl$_{aq}$ (1.0 M, 30 mL) were added carefully. The organic layer was separated and washed with aqueous NaHCO$_3$ and water, followed by drying over MgSO$_4$. Purification by column chromatography (SiO$_2$, petroleum ether) and removal of the solvent under reduced pressure yielded a colorless oil (2.28 g, 78%).

4-(2-Ethylhexylidene)-4*H*-cyclopenta[2,1-*b*:3,4-*b*']dithiophene (**8b**)

According to the procedure as outlined for **8a**: yellow oil (1.75 g, 79%). ^{1}H NMR (300 MHz, CDCl$_3$): 7.29 (d, *J* = 4.9 Hz, 1H), 7.15 (d, *J* = 4.9 Hz, 1H), 7.11 (d, *J* = 4.0 Hz, 1H), 7.09 (d, *J* = 4.0 Hz, 1H), 6.16 (d, *J* = 10.4 Hz, 1H), 2.95–2.81 (m, 1H), 1.75–1.57 (m, 2H), 1.53–1.37 (m, 2H), 1.36–1.20 (m, 4H), 0.96–0.82 (m, 6H). ^{13}C NMR (100 MHz, CDCl$_3$): 146.6, 143.0, 139.4, 137.9, 135.9, 131.2, 124.5, 124.0, 122.8, 119.7, 42.2, 35.4, 29.9, 28.8, 23.0, 14.2, 12.2. HRMS (ESI): calcd for C$_{17}$H$_{21}$S$_2$ [M+H]$^+$: 289.1006; found: 289.1075.

6-(Bromohexyloxy)triisopropyl silane (**9b**)[21]

An iodine-promoted silylation reaction similar to a literature procedure was employed.[22] To a solution of 6-bromohexanol (3.62 g, 20.0 mmol), imidazole (4.08 g, 60.0 mmol) and iodine (12.7 g, 50.0 mmol) in dry CH$_2$Cl$_2$ (60 mL), triisopropylsilyl chloride (4.70 mL, 22.0 mmol) was added. After stirring the reaction mixture for 13 h at r.t., an aqueous HCl solution (1.0 M) was added. The aqueous layer was extracted twice with CH$_2$Cl$_2$ and the combined organic layers were washed with aqueous saturated solutions of NaHSO$_3$ and NaHCO$_3$, and subsequently with water. After drying the organic phase with MgSO$_4$, removal of the solvent *in vacuo*, and purification by column chromatography (SiO$_2$, petroleum ether:diethyl ether, 1:1; visualization with KMnO$_4$ stain) a colorless oil was obtained (4.79 g, 71%). ^{1}H NMR (400 MHz, CDCl$_3$): 3.67 (t, *J* = 6.4 Hz, 2H), 3.40

(t, J = 6.8 Hz, 2H), 1.86 (quin, J = 7.1 Hz, 2H), 1.55 (quin, J = 6.8 Hz, 2H), 1.50–1.32 (m, 4H), 1.08–1.03 (m, 21H).

4-(2-Ethylhexyl)-4-(6-hydroxyhexyl)-4*H*-cyclopenta[2,1-*b*:3,4-*b*']dithiophene (**10b**)

According to the procedure as outlined for **10a** with 6-(bromohexyloxy)triisopropyl silane (**9b**) (2.05 g, 6.07 mmol), CPDT **8b** (1.75 g, 6.07 mmol) and LiAlH$_4$ (230 mg, 6.07 mmol). The crude product was then dissolved in THF (15 mL) and TBAF (2.39 g, 7.59 mmol) was added. The solution was stirred overnight at r.t., followed by the addition of diethyl ether and water. The organic and aqueous layers were separated and the organic layer was dried over MgSO$_4$. Purification of the crude product by column chromatography (SiO$_2$, Et$_2$O) yielded a pale yellow oil (1.28 g, 64%). ^{1}H NMR (400 MHz, CDCl$_3$): 7.13 (d, J = 4.9 Hz, 2H), 6.92 (d, J = 5.1 Hz, 1H), 6.92 (d, J = 4.7 Hz, 1H), 3.55 (t, J = 6.6 Hz, 2H), 1.95–1.76 (m, 4H), 1.50–1.37 (m, 2H), 1.24–1.07 (m, 4H), 1.03–0.82 (m, 10H), 0.75 (t, J = 7.0 Hz, 3H), 0.68–0.61 (m, 1H), 0.59 (t, J = 7.4 Hz, 3H). ^{13}C NMR (75 MHz, CDCl$_3$): 157.9, 157.8, 136.8, 124.4, 122.0, 63.1, 53.3, 35.3, 34.2, 32.8, 29.8, 28.7, 27.3, 24.3, 22.9, 14.2, 10.8. HRMS (ESI): calcd for C$_{23}$H$_{35}$OS$_2$ [M+H]$^+$: 391.2051; found: 391.2134.

4-(6-Bromohexyl)-4-(2-ethylhexyl)-4*H*-cyclopenta[2,1-*b*:3,4-*b*']dithiophene (**11**)

A solution of triphenylphosphine (0.774 g, 2.95 mmol) in dry CH$_2$Cl$_2$ (5 mL) was added dropwise to a mixture of alcohol-functionalized CPDT **10b** (0.823 g, 2.11 mmol) and CBr$_4$ (0.909 g, 2.74 mmol) in dry CH$_2$Cl$_2$ (10 mL) at 0 °C and shielded from light. After stirring the mixture for 50 min at r.t., diethyl ether and water were added. The organic layer was separated and subsequently washed with a

saturated $NaHCO_3$ (aq) solution and water. Drying over $MgSO_4$, purification by flash column chromatography (SiO_2, petroleum ether) and removal of the organic solvent yielded a colorless oil of pure CPDT **11** (0.519 g, 54%). ^{1}H NMR (300 MHz, $CDCl_3$): 7.13 (d, J = 4.9 Hz, 2H), 6.92 (d, J = 4.9 Hz, 1H), 6.91 (d, J = 4.9 Hz, 1H), 3.32 (t, J = 6.8 Hz, 2H), 1.95–1.78 (m, 4H), 1.77–1.66 (m, 2H), 1.33–1.20 (m, 2H), 1.18–1.06 (m, 2H), 1.03–0.80 (m, 10H), 0.75 (t, J = 6.8 Hz, 3H), 0.67–0.53 (m, 4H). ^{13}C NMR (100 MHz, $CDCl_3$): 157.8, 157.7, 136.8, 124.48, 124.46, 122.00, 121.97, 53.3, 41.9, 39.5, 35.3, 34.2, 34.1, 32.8, 29.2, 28.7, 28.0, 27.3, 24.2, 22.9, 14.2, 10.8. HRMS (ESI): calcd for $C_{23}H_{34}BrS_2$ [M+H]$^+$: 453.1207; found: 453.1297.

2.5 NOTES AND REFERENCES

[1]   (a) Senda, T.; Hanaoka, H.; Okado, Y.; Oda, Y.; Tsuguri, H.; Mashima, K. *Organometallics* **2009**, *28*, 6915. (b) De Rosa, C.; Auriemma, F.; Resconi, L. *Angew. Chem. Int. Ed.* **2009**, *48*, 9871.

[2]   Recent reviews on different aspects of OPV: (a) Jorgensen, M.; Norrman, K.; Gevorgyan, S. A.; Tromholt, T.; Andreasen, B.; Krebs, F. C. *Adv. Mater.* **2012**, *24*, 580. (b) Zhou, H.; Yang, L.; You, W. *Macromolecules* **2012**, *45*, 607. (c) Li, Y. *Acc. Chem. Res.* **2012**, *45*, 723. (d) Su, Y.-W; Lan, S.-C.; Wei, K.-H. *Mater. Today* **2012**, *15*, 554. (e) Janssen, R. A. J.; Nelson, J. *Adv. Mater.* **2013**, *25*, 1847.

[3]   Recent materials including the CPDT building block: (a) Lee, U. R.; Lee, T. W.; Hoang, M. H.; Kang, N. S.; Yu, J. W.; Kim, K. H.; Lim, K.-G.; Lee, T.-W.; Jin, J.-I.; Choi, D. H. *Org. Electron.* **2011**, *12*, 269. (b) Hong, Y.-R.; Ng, J. Y.; Wong, H. K.; Moh, L. C. H.; Yip, Y. J.; Chen, Z. K.; Norsten, T. B. *Sol. Energy Mater. Sol. Cells* **2012**, *102*, 58. (c) Cheng, Y.-J.; Ho, Y.-J.; Chen, C.-H.; Kaon, W.-S.; Wu, C.-E.; Hsu, S.-L.; Hsu, C.-S. *Macromolecules* **2012**, *45*, 2690. (d) Lee, S. K.; Seo, J. H.; Cho, N. S.; Cho, S. *Thin Solid Films* **2012**, *520*, 5438. (e) Song, S.; Park, S.; Kwon, S.; Lee, B. H.; Shim, J. Y.; Lee, J.; Park, S. H.; Jin, Y.; Kim, I.; Lee, K.; Suh, H. *Sol. Energy. Mater. Sol. Cells* **2012**, *105*, 229. (f) Jiang, J.-M.; Yang, P.-A.; Yu, C.-M.; Lin, H.-K.; Huang, K.-C.; Wei, K.-H. *J. Polym. Sci Part A.: Polym. Chem.* **2012**, *50*, 3960. (g) Willot, P.; De Cremer, L.; Koeckelberghs, G. *Macromol. Chem. Phys.* **2012**, *213*, 1216. (h) Li, Y.; Zou, J.; Yip, H.-L.; Li, C.-Z.; Zhang, Y.; Chueh, C.-C.; Intemann, J.; Xu, Y.; Liang, P.-W.; Chen, Y.; Jen, A. K.-Y. *Macromolecules* **2013**, *46*, 5497.

[4]   Rizzo, S.; Sannicolò, F.; Benincori, T.; Schiavon, G.; Zecchin, S.; Zotti, G. *J. Mater. Chem.* **2004**, *14*, 1804.

[5]   (a) Sannicolò, F.; Brenna, E.; Benincori, T.; Zotti, G.; Zecchin, S.; Schiavon, G. *Chem Mater.* **1998**, *10*, 2167. (b) Schmittel, M.; Lin, H. *J. Mater. Chem.* **2008**, *18*, 333.

[6]   Ko, H. C.; Yom, J.; Moon, B.; Lee, H. *Electrochim. Acta* **2003**, *48*, 4127.

[7]   (a) Pilar, J.-F; Cougnon, C.; Rault-Berthelot, J.; Berthelot, A.; Hubert, C.; Tran, K. *J. Electroanal. Chem.* **2004**, *568*, 195. (b) Cougnon, C.; Gautier, C.; Pilar, J.-F.; Casse, N.; Chénais, B. *Biosens. Bioelectron.* **2008**, *23*, 1171.

[8]   (a) Mühlbacher, D.; Scharber, M.; Morana, M.; Zhu, Z.; Waller, D.; Gaudiana, R.; Brabec, C. *Adv. Mater.* **2006**, *18*, 2884. (b) Peet, J.; Kim, J. Y.; Coates, N. E.; Ma, W. L.; Moses, D.; Heeger, A. J.; Bazan, G. C. *Nat. Mater.* **2007**, *6*, 497. (c) Tsao, H. N.; Cho, D.; Andreasen, J. W.; Rouhanipour, A.; Breiby, D. W.; Pisula, W.; Müllen, K. *Adv. Mater.* **2009**, *21*, 209. (d) Zoombelt, A. P.; Mathijssen, S. G. J.; Turbiez, M. G. R.; Wienk, M. M.; Janssen, R. A. J. *J. Mater. Chem.* **2010**, *20*, 2240. (e) Kettle, J.; Horie, M.; Majewski, L. A.; Saunders, B. R.; Tuladhar, S.; Nelson, J.; Turner, M. L. *Sol. Energy Mater. Sol. Cells* **2011**, *95*, 2186. (f) Horie, M.; Kettle, J.; Yu, C.-Y.; Majewski, L. A.; Chang, S.-W.; Kirkpatrick, J.; Tuladhar, S. M.; Nelson, J.; Saunders, B. R.; Turner, M. L. *J. Mater. Chem.* **2012**, *22*, 381. (g) Albrecht, S.; Janietz, S.; Schindler, W.; Frisch, J.; Kurpiers, J.; Kniepert, J.; Inal, S.; Pingel, P.; Fostiropoulos, K.; Koch, N.; Neher, D. *J. Am. Chem. Soc.* **2012**, *134*, 14932. (h) Henson, Z. B.; Zhang, Y.; Nguyen, T.-Q.; Seo, J. H.; Bazan, G. C. *J. Am. Chem. Soc.* **2013**, *135*, 4163.

[9]   (a) Van Mierloo S.; Adriaensens P. J.; Maes, W.; Lutsen, L.; Cleij, T. J.; Botek, E.; Champagne, B.; Vanderzande, D. J. *J. Org. Chem.* **2010**, *75*, 7202. (b) Van Mierloo, S.; Hadipour, A.; Spijkman, M.-J.; Van den Brande, N.; Ruttens, B.;

Kesters, J.; D'Haen, J.; Van Assche, G.; de Leeuw, D. M.; Aernouts, T.; Manca, J.; Lutsen, L.; Vanderzande, D. J.; Maes, W. *Chem. Mater.* **2012**, *24*, 587. (c) Marin, L.; Zhang, Y.; Robeyns, K.; Champagne, B.; Adriaensens, P.; Lutsen, L.; Vanderzande, D.; Bevk, D.; Maes, W. *Tetrahedron Lett.* **2013**, *54*, 526. (d) Marin, L.; Van Mierloo, S.; Zhang, Y.; Robeyns, K.; Champagne, B.; Adriaensens, P.; Lutsen, L.; Vanderzande, D.; Maes, W. *Tetrahedron* **2013**, *69*, 2260. (e) Kesters, J.; Ghoos, T.; Penxten, H.; Drijkoningen, J.; Vangerven, T.; Lyons, D. M.; Lutsen, L.; Vanderzande, D.; Manca, J.; Maes, W. *Adv. Energy Mater.* **2013**, *3*, 1180.

[10]   (a) Kraak, A.; Wiersema, A. K; Jordens, P.; Wynberg, H. *Tetrahedron* **1968**, *24*, 3381. (b) Reynolds, J. R.; Brzezinski, J. Z. *Synthesis* **2002**, *8*, 1053. (c) Park, J. H.; Lee, B. Y. *Bull. Korean Chem. Soc.* **2010**, *31*, 1064.

[11]   (a) Coppo, P.; Cupertino, D. C.; Yeates, S. C.; Turner, M. L. *J. Mater. Chem* **2002**, *12*, 2597. (b) Coppo, P.; Cupertino, D. C.; Yeates, S. C.; Turner, M. L. *Macromolecules* **2003**, *36*, 2705.

[12]   Zotti, G.; Schiavon, G.; Berlin, A.; Fontana, G.; Pagani, G. *Macromolecules* **1994**, *27*, 1938.

[13]   (a) Zotti, G.; Zecchin, S.; Schiavon, G.; Berlin, A. *Macromolecules* **2001**, *34*, 3889. (b) Zotti, G.; Zecchin, S.; Berlin, A.; Schiavon, G.; Giro, G. *Chem. Mater.* **2001**, *13*, 43. (c) Zotti, G.; Vercelli, B.; Berlin, A. *Chem. Mater*. **2008**, *20*, 397.

[14]   Li, A.; Gilbert, T. M.; Klumpp, A. *J. Org. Chem.* **2008**, *73,* 3654.

[15]   (a) Vandenbergh, J.; Conings, B.; Bertho, S.; Kesters, J.; Spoltore, D.; Esiner, S.; Zhao, J.; Van Assche, G.; Wienk, M. M.; Maes, W.; Lutsen, L.; Van Mele, B.; Janssen, R. A. J.; Manca, J.; Vanderzande, D. J. M. *Macromolecules* **2011**, *44*, 8470. (b) Bertho, S.; Campo, B.; Piersimoni, F.; Spoltore, D.; D'Haen,

J.; Lutsen, L.; Maes, W.; Vanderzande, D.; Manca, J. *Sol. Energy Mater. Sol. Cells* **2013**, *110*, 69.

[16]   Kudla, J. C.; Dolfen, D.; Schottler, K. J.; Koenen, J.-M.; Breusov, D.; Allard, S.; Scherf, U. *Macromolecules* **2010**, *43*, 7864.

[17]   It has to be mentioned that Turner *et al.* reported a successful Wittig reaction of CPDT-4-one **7** with dodecylidenetriphenylphosphorane: Coppo, P.; Adams, H.; Cupertino, D. C.; Yeates, S. G.; Turner, M. L. *Chem. Commun.* **2003**, 2548.

[18]   A few functionalized asymmetrically dialkylated CPDTs have already been reported (see also ref. 13): (a) Zotti, G.; Zecchin, S.; Schiavon, G.; Berlin, A.; Pagani, G.; Canavesi, A. *Chem. Mater.* **1997**, *9*, 2940. (b) Berlin, A.; Zotti, G.; Schiavon, G.; Zecchin, S. *J. Am. Chem. Soc.* **1998**, *120*, 13453.

[19]   Reynolds, J. R.; Brzezinski, J. Z. *Synthesis* **2002**, 1053.

[20]   Kudla, J. C.; Dolfen, D.; Schottler, K. J.; Koenen, J.-M.; Breusov, D.; Allard, S.; Scherf, U. *Macromolecules* **2010**, *43*, 7864.
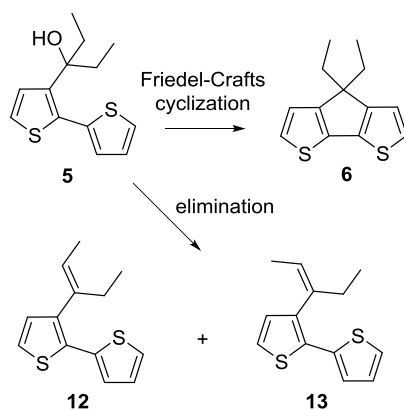
[21]   Pouliot, M.-F.; Mahé, O.; Hamel, J.-D.; Desroches, J.; Paquin, J.-F. *Org. Lett.* **2012**, *14*, 5428.

[22]   Bartoszewicz, A.; Kalek, M.; Stawinski, J. *Tetrahedron* **2008**, *64*, 8843.

2.6 ACKNOWLEDGEMENTS

2.7 SUPPORTING INFORMATION

Scheme S1: Cyclization *vs* alkene formation during the ring-closing step.

Table S1: Overview of the conditions tested for the alkylation-cyclization of 3-([2,2'-bithiophen]-3-yl)pentan-3-ol (**5**).

| Entry	*Reaction conditions*					*Relative abundance (%)*[a]			Observations
	Solvent	Lewis/Brönsted acid	Equiv	T (°C)	Time (h)	5	6	12/13	
1	*n*-octane	H_2SO_4	14	r.t.	12	-	100 (74)[b]	-	black tar
2	*n*-octane	H_2SO_4	14	r.t.	4	-	100	-	black tar
3	*n*-hexane	H_2SO_4	14	r.t.	4	-	100 (69)[b]	-	black tar
4	Et_2O	H_2SO_4	14	r.t.	overnight	-	-	100	-
5	EtOH	H_2SO_4	14	r.t.	overnight	-	-	100	-
6	toluene	H_2SO_4	14	r.t.	48	-	100	-	black tar
7	EtOH	BSA	14	r.t.	72	-	-	100	
8	*n*-pentane	BSA in EtOH	14	r.t.	24			100	
9	*n*-pentane	PPA.SiO₂	cat.	reflux	24	-	-	100	
10	*n*-pentane	TFMS anhydride	1	r.t.	4	-	-	100	
11	$CHCl_3$	TFMS anhydride	1	r.t.	4	-	-	-	
12	nitromethane	FeCl₃.6H₂O	1	r.t.	24	-	-	100	
13	$CHCl_3$	$AlCl_3$	1	0	12	-	6	94	
14	*n*-pentane	$AlCl_3$	1	0	12	-	2	98	
15	toluene	$AlCl_3$	1	r.t.	24	-	20	80	
16	*n*-octane	$AlCl_3$	1	r.t.	24	-	5	95	
17	*n*-octane	$AlCl_3$	0.1	r.t.	24	-	1	99	
18	$CHCl_3$	$AlCl_3$	1	reflux	24	-	39	61	
19	toluene	$AlCl_3$	1	reflux	24	-	58	42	

[a] Determined by ¹H NMR from the crude mixture, assuming presence of only **5**, **6**, **12** and **13**. [b] Yield after work-up and purification by column chromatography.

Chapter 3

Fluorination as an Effective Tool to Increase the Open-Circuit Voltage and Charge Carrier Mobility of Organic Solar Cells based on Poly(cyclopenta[2,1-*b*:3,4-*b*']dithiophene-*alt*-quinoxaline) Copolymers
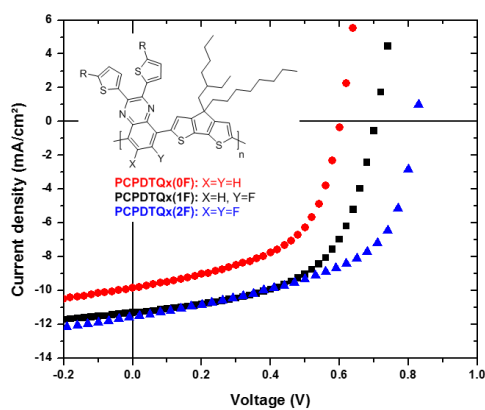
P. Verstappen, J. Kesters, W. Vanormelingen, G. H. L. Heintges, J. Drijkoningen, T. Vangerven, L. Marin, S. Koudjina, B. Champagne, J. Manca, L. Lutsen, D. Vanderzande, W. Maes, *J. Mater. Chem. A*, **2015**, DOI: 10.1039/C4TA06054G.

ABSTRACT

The effect of fluorination on the optoelectronic properties and the polymer:fullerene solar cell characteristics of PCPDTQx-type (poly{4-(2′-ethylhexyl)-4-octyl-4*H*-cyclopenta[2,1-*b*:3,4-*b*′]dithiophene-*alt*-2,3-bis[5′-(2′′-ethylhexyl)thiophen-2′-yl]quinoxaline}) low bandgap copolymers is reported. The introduction of fluorine atoms on the quinoxaline constituents is an effective way to lower the HOMO and LUMO energy levels of the alternating copolymers, resulting in an enhanced open-circuit voltage for the devices based on the fluorinated polymers (~0.1 V per F added). Furthermore, fluorination also improves the charge carrier mobility in the bulk heterojunction blends. Despite the formation of unfavorable photoactive layer morphologies, the best solar cell performance is obtained for the copolymer prepared from the difluorinated quinoxaline monomer, affording a power conversion efficiency of 5.26% under AM 1.5G irradiation, with an open-circuit voltage of 0.83 V, a short-circuit current density of 11.58 mA cm^{-2} and a fill factor of 55%.

3.1 INTRODUCTION

Organic photovoltaics (OPVs) have drawn quite some attention during the last years as a promising technology for renewable energy generation. Organic solar cells offer several advantages in comparison to competing photovoltaic technologies. Their lightweight, flexible, colorful and semi-transparent character opens the door for a number of contemporary applications such as (energy-neutral) building and automotive integration, smart textiles, sunscreens and different consumer goods.[1] The inherent low(er) cost of OPVs offers advantages for fast-deployable PV systems, especially in areas without connection to the classical grid.[2] Depending on the photoactive layer materials, organic solar cells can be produced via low-cost printing techniques, allowing for easy and cheap manufacturing on large surfaces.[3] The power conversion efficiency (PCE) of solution-processed OPV devices has significantly increased over the last few years, to over 10% for the best-performing bulk heterojunction (BHJ) cells, due to the design of novel electron donor conjugated polymers (or related small molecules), the introduction of suitable interfacial charge transport layers and the use of new device architectures.[4,5] In solution-processed BHJ organic solar cells, the active layer consists of an intimate blend of an electron-donating organic semiconductor and an electron-accepting material (usually a fullerene derivative).[1h] Most often low bandgap copolymers are used as the donor materials. These conjugated push-pull polymers are composed of alternating electron rich (donor) and electron poor (acceptor) (heterocyclic) building blocks. Chemical variation of these building blocks allows for fine-tuning of the frontier molecular orbitals and the bandgap. Numerous polymers have been prepared according to this principle and have

afforded a good understanding of the molecular structure-blend morphology-device performance relationships.[1,4,6]

4*H*-Cyclopenta[2,1-*b*:3,4-*b'*]dithiophene (CPDT) is one of the classical building blocks applied in low bandgap copolymers. Due to its relatively electron rich nature (in comparison to other donor moieties such as benzodithiophene and carbazole), rather low bandgaps can be obtained for the polymers based on this moiety, resulting in extended absorption and therefore potentially high short-circuit current density (J_{SC}) values.[1b,7,8] In combination with thieno[3,4-*c*]pyrrole-4,6-dione as electron poor building block, polymer solar cells with a PCE of 6.5% have been obtained.[9] In the last couple of years, CPDT has lost some of its attractiveness though, in part due to the quite laborious synthetic route required to obtain this bridged biheterocycle. Recently, we have optimized two condensed high-yielding synthesis protocols towards CPDT, which have as an additional benefit that they allow smooth asymmetric (alkyl) side chain substitution or the introduction of particular functional groups.[10] As a result, variation in the side chain pattern can simply be obtained, which can be important to further boost the efficiency (and stability) of the solar cells.[4b,11]

On the other hand, quinoxalines (Qx) have emerged as a promising class of electron poor moieties for low bandgap copolymers because of their strong electron affinity, resulting in deep HOMO energy levels and a broad absorption range.[12] Moreover, quinoxalines allow for the introduction of two side chains per monomer, thereby generally providing well-soluble polymer materials. However, most quinoxaline building blocks have been substituted with regular alk(ox)ylated phenyl rings, limiting the absorption coverage. Recently, it was shown that the absorption spectrum can be extended by changing the 2,3-phenyl substituents into alkylated thiophenes.[13]

Although quinoxalines themselves are already quite electron poor, further increase of their electron affinity is pursued in this work. An often employed and effective strategy serving this purpose is the introduction of fluorine atoms on the conjugated backbone. Several groups have shown that fluorination of the electron poor building block can increase the performance of polymer solar cells.[8f,h,14] Most often, this increase in device efficiency cannot be attributed to one single material property, as it is rather an interplay of different parameters which are affected upon fluorination. It has been reported that the incorporation of fluorine atoms decreases both the HOMO and the LUMO energy levels, which leads to an increase of the open-circuit voltage (V_{OC}) with a minimal impact on the bandgap.[8f,h,14] Furthermore it has also been shown that fluorination can affect the hole mobility of the polymer,[15] the active layer morphology,[14j] the internal polarization and crystallinity,[16] charge recombination in the active layer,[14f] and the dielectric constant of the polymer.[17]

In this context, we have synthesized three novel thienyl-substituted quinoxaline monomers (non-, mono- and difluorinated) with broadened absorption features. After copolymerization with an asymmetrically dialkylated 4*H*-cyclopenta[2,1-*b*:3,4-*b'*]dithiophene as the electron rich cross-coupling partner, a unique series of alternating copolymers was obtained, namely poly{4-(2'-ethylhexyl)-4-octyl-4*H*-cyclopenta[2,1-*b*:3,4-*b'*]dithiophene-2,6-diyl-*alt*-2,3-bis[5'-(2''-ethylhexyl)thiophen-2'-yl]quinoxaline-5,8-diyl} (**PCPDTQx(0F)**), poly{4-(2'-ethylhexyl)-4-octyl-4*H*-cyclopenta[2,1-*b*:3,4-*b'*]dithiophene-2,6-diyl-*alt*-6-fluoro-2,3-bis[5'-(2''-ethylhexyl)thiophen-2'-yl]quinoxaline-5,8-diyl} (**PCPDTQx(1F)**) and poly{4-(2'-ethylhexyl)-4-octyl-4*H*-cyclopenta[2,1-*b*:3,4-*b'*]dithiophene-2,6-diyl-*alt*-6,7-difluoro-2,3-bis[5'-(2''-ethylhexyl)thiophen-2'-yl]quinoxaline-5,8-diyl} (**PCPDTQx(2F)**). It was observed that quinoxaline

fluorination is an effective tool to enhance the V_{OC} (approximately 0.1 V for every fluorine atom added) and charge carrier mobility of the resulting PCPDTQx:fullerene solar cells. Using this strategy, BHJ OPV devices with a PCE of more than 5% were obtained for the difluorinated copolymer PCPDTQx(2F), even without an optimal active layer morphology.

3.2 RESULTS AND DISCUSSION

3.2.1 Synthesis and characterization

The polymers were prepared via Stille polycondensation between the distannylated CPDT derivative and the dibrominated Qx acceptors with Pd[P(o-tol)$_3$]$_2$ as a catalyst. The synthetic route towards the Qx building blocks and the final push-pull copolymers is illustrated in Scheme 1. The required Qx monomers were synthesized via a two-step procedure, involving a reduction of the appropriate benzothiadiazole **1a-c**[18] and consecutive condensation of the obtained o-phenylenediamines **2a-c** with 1,2-bis[5'-(2''-ethylhexyl)thiophen-2'-yl]ethane-1,2-dione. After Stille polymerization, the resulting copolymers were precipitated in methanol and filtered off. The collected polymers were subjected to consecutive Soxhlet extractions with methanol, acetone and n-hexane. It is worthwhile to mention that all three polymers could be collected with n-hexane, indicating the high solubility of the materials in common organic solvents (e.g. tetrahydrofuran, chloroform and chlorobenzene). After extraction with an aqueous sodium N,N-diethyldithiocarbamate solution to remove the last traces of palladium,[19] the polymers were subjected to preparative size exclusion chromatography (prep-SEC) to remove the low molar mass parts (and additional purification). Polymer molar masses and their distributions were determined by

analytical SEC. In all instances, high number-average molar masses (M_n) were obtained (47, 69 and 53 kDa for **PCPDTQx(0F)**, **PCPDTQx(1F)** and **PCPDTQx(2F)**, respectively) with polydispersity indices (PDI) around 1.5 (Table 1).
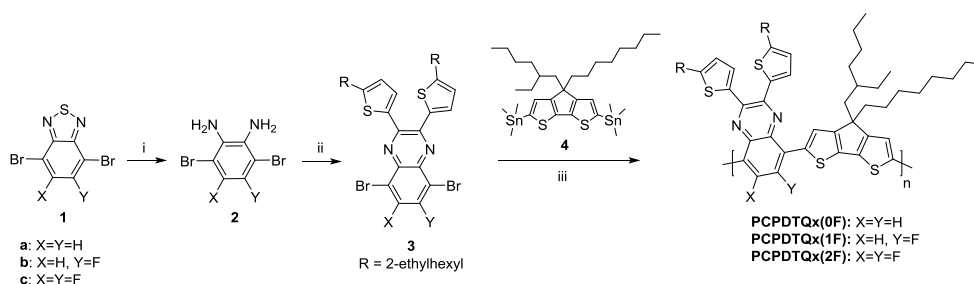
Scheme 1: Synthesis of the quinoxaline monomers and their resulting PCPDTQx copolymers: i) NaBH₄, EtOH; ii) 1,2-bis[5'-(2''-ethylhexyl)thiophen-2'-yl]ethane1,2-dione, p-TsOH, EtOH; iii) Pd₂(dba)₃, P(o-tol)₃, toluene/DMF 4/1, 110 °C, 15 h.

The thermal stability of the copolymers was analyzed via thermogravimetric analysis (TGA) from the onset of the first derivative of the mass loss as a function of temperature (Table 1, Figure S1). All three polymers showed the same mass loss temperature of ~350 °C. Melting points (T_m) and glass transition temperatures (T_g) were investigated via rapid heat-cool calorimetry (RHC) (Table 1, Figure S2). RHC was chosen above regular differential scanning calorimetry (DSC) because of its increased sensitivity to thermal transitions as a result of the fast scanning rates and the low sample amounts required.[20] For **PCPDTQx(0F)**, no clear glass transition could be observed, but the curvature in the baseline may suggest a very broad and gradual change in heat capacity. **PCPDTQx(1F)** and **PCPDTQx(2F)** did show a glass transition occurring at 78 and 65 °C, respectively. Both materials also seem to exhibit a second, higher T_g at 168 and 163 °C,

respectively, and the melting point and melting enthalpy (ΔH_m) increase upon fluorination. Nonetheless, the melting enthalpy remains quite small for all polymers, indicating the low crystalline character for these materials.

Table 1: Molar mass (distribution) and thermal properties for the PCPDTQx copolymer series.

Polymer	$M_n{}^a$ (kDa)	PDI^a	$T_d{}^b$ (°C)	$T_g{}^c$ (°C)	$T_m{}^c$ (°C)	$\Delta H_m{}^c$ (J/g)
PCPDTQx(0F)	47	1.5	350	-	231	0.55
PCPDTQx(1F)	69	1.6	350	78	295	0.70
PCPDTQx(2F)	53	1.5	350	65	312	0.96

^{a} Determined by analytical SEC in THF at 40 °C for the polymer samples after prep-SEC. ^{b} Determined by the onset of the first derivative of the mass loss as a function of temperature. ^{c} Determined by RHC.

The HOMO and LUMO frontier energy levels of the polymers were estimated via cyclic voltammetry (CV) from the onset of the oxidation and reduction peaks, respectively. The oxidation and reduction waves for all polymers are quasi-reversible and the reported values are the means of the first three redox cycles (Table 2). From these results it is clear that the introduction of fluorine on the Qx monomer has a major influence on the HOMO energy level. For each fluorine atom introduced, the HOMO level decreases by approximately 0.1 eV, which corresponds with the results reported in previous work on other fluorinated copolymers.[14] Because of the larger influence on the HOMO energy level in comparison with the LUMO, the electrochemical bandgap ($E_g{}^{EC}$) slightly increases upon fluorination.

Table 2: Experimental optical and electrochemical data and calculated electronic data for the PCPDTQx copolymer series.

Polymer	Experimental						Calculated		
	$\lambda_{max}{}^a$ (nm) solution	$\lambda_{max}{}^b$ (nm) film	$E_g{}^{OPc}$ (eV)	HOMO^d (eV)	LUMO^d (eV)	$E_g{}^{ECe}$ (eV)	HOMO (eV)	LUMO (eV)	E_g (eV)
PCPDTQx(0F)	715	701	1.53	-5.28	-3.31	1.97	-5.20	-2.40	2.80
PCPDTQx(1F)	711	714	1.55	-5.40	-3.35	2.05	-5.25	-2.43	2.82
PCPDTQx(2F)	691	703	1.60	-5.51	-3.37	2.14	-5.34	-2.45	2.90

^{a} The polymers were dissolved in chloroform. ^{b} Films were prepared by drop casting a solution of the polymer in chloroform on a quartz substrate. ^{c} Optical bandgap, determined by the onset of the solid-state UV-Vis spectra. ^{d} Determined by CV from the onset of oxidation and reduction. ^{e} Electrochemical bandgap.

Normalized UV-Vis absorption spectra in solution and thin film for all three copolymers are shown in Figure 1. All copolymers show a similar absorption profile, i.e. a higher energy band arising from the localized π-π* transition and a lower energy band which is attributed to intramolecular charge transfer from the CPDT to the Qx moiety. Due to the strong charge transfer character, the absorption extends to the near-infrared region (absorption edge around 800 nm). Upon fluorination, a small blue-shift is observed, which is in accordance with the increase in bandgap obtained from CV.[16] For the introduction of the first fluorine atom, the blue-shift is very small, whereas upon addition of the second fluorine atom a more pronounced blue-shift of 20 nm is observed. In film, this blue-shift is less distinct. Additionally, only a slight red-shift is observed when moving from solution to the solid state. Upon fluorination, this red-shift increases but stays nevertheless very small.
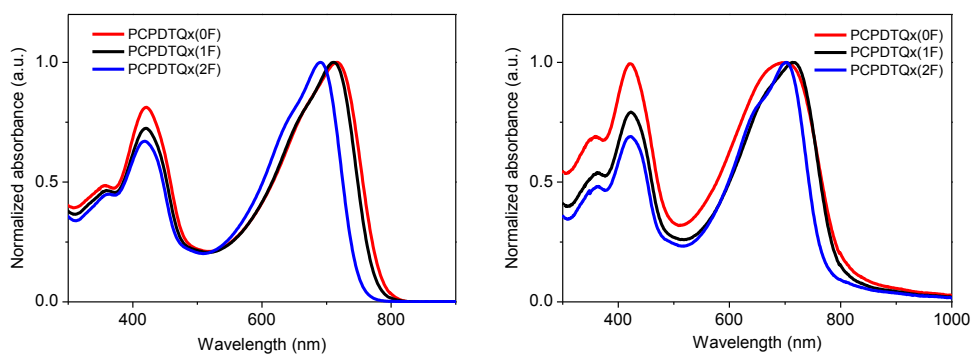

Figure 1: UV-Vis absorption spectra for all copolymers in CHCl$_3$ solution (left) and thin film (right).

3.2.2 DFT calculations

To analyze the impact of the fluorine atoms on the positions of the HOMO and LUMO levels, density functional theory (DFT) calculations were carried out using

the M05[21] exchange-correlation functional and the 6-311G(d) basis set. The effects of the solvent (THF) were taken into account by using the polarizable continuum model.[22] All calculations were carried out using Gaussian09.[23] First, the ground state geometries were fully optimized for the individual donor and acceptor moieties, for the donor-acceptor combinations (DA), as well as for dimers of the donor-acceptor units (DADA). The large alkyl chains were replaced by methyl groups to accelerate the calculations without impacting the results. Several conformations differing by the torsion angles between the donor and acceptor units have been considered. Using the optimized geometries, the energies and the topologies of HOMO and LUMO were determined (Table 2). Since the energies of the *syn* and *anti* conformers differ little, the reported HOMO and LUMO energies were obtained after performing a Boltzmann averaging (T = 298.15 K). The M05 results show that adding fluorine atoms on the quinoxaline moiety stabilizes the HOMO level as well as the LUMO level, but the impact on the former is stronger so that the HOMO-LUMO gap slightly opens with increasing number of fluorine atoms. Then, as shown in Figure 2, the topologies of the HOMO and LUMO are little affected by the number of fluorine atoms with dominant contributions on the donor CPDT (HOMO) and acceptor Qx (LUMO) moieties.
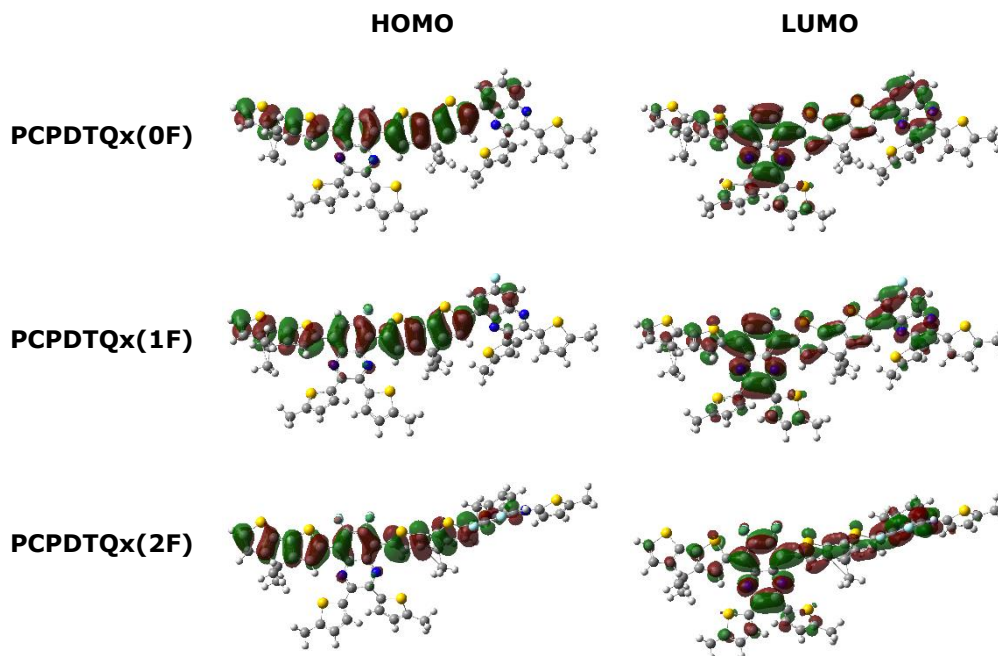
Figure 2: Sketch of the HOMO and LUMO of the DADA dimers for the all-*anti* conformers (isosurfaces of 0.02 a.u.).

3.2.3 Photovoltaic properties

The photovoltaic performances of the three polymers were evaluated in BHJ polymer solar cells fabricated in the standard configuration glass/ITO/PEDOT:PSS/polymer:$PC_{71}BM$/Ca/Al. The active layer processing conditions for the three polymers were optimized independently (Table 3, Table S1–S3). For all polymers the optimal donor:acceptor ratio appeared to be 1:3, except for **PCPDTQx(2F)** (1:2.5 was identified as the optimal ratio for this polymer when processed with 1-chloronaphthalene as an additive). Despite the relative small change in chemical structure (keeping the same side-chain pattern), the best processing conditions (solvent and additive) differ for each polymer, which reflects the large influence of the fluorine atoms on the material properties.

Table 3: Photovoltaic output parameters for the PCPDTQx copolymers in BHJ solar cells with standard configuration glass/ITO/PEDOT:PSS/polymer:PC$_{71}$BM (1:3)/Ca/Al.

| Polymer	Processing solvent[a]	Active layer thickness (nm)	V$_{OC}$ (V)	J$_{SC}$ (mA cm^{-2})	FF	PCE[b] (%)
PCPDTQx(0F)	ODCB	86	0.60	8.63	0.51	2.65 (2.88)
PCPDTQx(0F)	ODCB + 3% CN	77	0.60	9.44	0.54	3.08 (3.24)
PCPDTQx(1F)	CF	110	0.72	7.21	0.52	2.71 (3.10)
PCPDTQx(1F)	CF + 10% ODCB	125	0.71	11.17	0.58	4.56 (4.87)
PCPDTQx(2F)	CB	101	0.78	5.55	0.53	2.28 (2.49)
PCPDTQx(2F)	CB + 3% CN[c]	106	0.83	10.39	0.56	4.86 (5.26)

[a] ODCB = *ortho*-dichlorobenzene, CF = chloroform, CB = chlorobenzene, CN = 1-chloronaphthalene. Polymer concentration for ODCB solutions = 12 mg/mL, CF solutions = 5 mg/mL and CB solutions = 8 mg/mL. [b] Average values over at least 4 devices. The best device performance is shown between brackets. [c] **PCPDTQx(2F)**:PC$_{71}$BM ratio 1:2.5.

The J-V curves for the best solar cells are shown in Figure 3, nicely illustrating the stepwise increase in V$_{OC}$ for each fluorine atom introduced. The insertion of one fluorine on the Qx moiety causes the V$_{OC}$ to increase by ~0.1 V. Upon introduction of the second fluorine atom, the V$_{OC}$ further improved by ~0.1 V to 0.83 V for **PCPDTQx(2F)**. This observation is in good agreement with the observed decrease of 0.1 eV for the HOMO energy level for each fluorine atom added. Besides the V$_{OC}$, also the J$_{SC}$ and fill factor (FF) improved for the monofluorinated copolymer **PCPDTQx(1F)** (to 11.17 mA cm^{-2} and 0.58, respectively), giving rise to an average PCE of 4.56% (4.87% for the top-performing device). For **PCPDTQx(2F)**, a slight decrease in Jsc and FF was observed compared to **PCPDTQx(1F)**, but nonetheless these solar cells showed elevated PCE values due to the strong increase in V$_{OC}$. The external quantum efficiency (EQE) of the solar cells based on the fluorinated polymers was found to be higher at all wavelengths,

exceeding 40% over a broad wavelength range (350−750 nm), with a maximum approaching 60% (at ∼500 nm) for **PCPDTQx(2F)** (Figure 4).
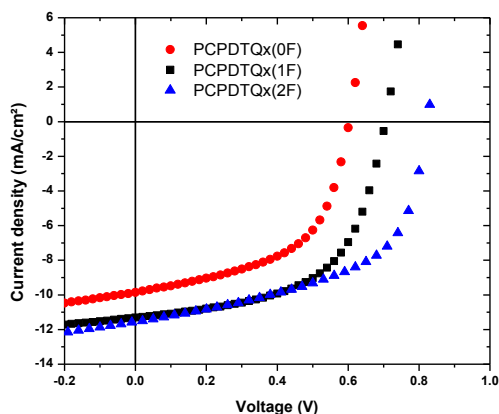
**Figure 3:** J-V curves for the best performing PCPDTQx:PC$_{71}$BM solar cells.
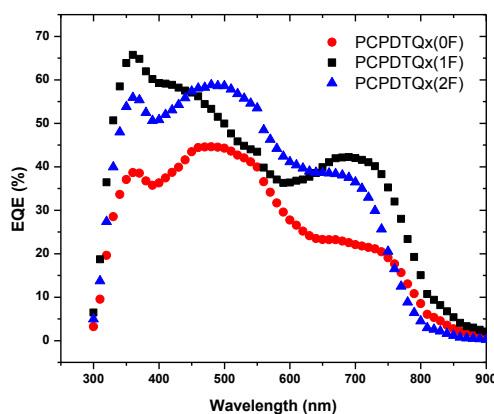
Figure 4: EQE spectra of solar cell devices made from the different PCPDTQx copolymers. The devices employed for the EQE measurements gave a J$_{SC}$ of 8.68, 12.10 and 11.58 mA cm^{-2} for **PCPDTQx(0F)** (in ODCB + 3% CN), **PCPDTQx(1F)** (in CF + 10% ODCB) and **PCPDTQx(2F)** (in CB + 3% CN), respectively, with J$_{EQE}$'s of 8.31, 11.97 and 11.16 mA cm^{-2}.

To investigate the charge transport features of the BHJ blends, photo-induced charge extraction by linearly increasing voltage (photo-CELIV) measurements

were performed. The charge mobility of the active layer (in the appropriate direction of the solar cell mode) was determined to be 6×10^{-4}, 9×10^{-4} and 2×10^{-3} cm^2 V^{-1} s^{-1} for **PCPDTQx(0F)**, **PCPDTQx(1F)** and **PCPDTQx(2F)**, respectively (Figure S3). These results indicate an increased active layer charge mobility upon fluorination.

Based on these results, a higher Jsc could be expected for the device based on **PCPDTQx(2F)**. This raises questions to which extent the obtained blend morphology allows for efficient charge extraction. AFM imaging of the active layer was performed to study the BHJ film topology, revealing extensive domain formation (up to ~250 nm) for the fluorinated copolymer blends (Figure 5), previously attributed to the fluorophobicity of PC$_{71}$BM.[14m,16] Somewhat surprisingly, however, this phenomenon does not seem to be a major limiting factor, as the solar cell performance for both fluorinated polymers increases compared to the non-fluorinated copolymer, which shows a finely intermixed BHJ blend. Similar observations have been made for PTB7-based polymer solar cells, still procuring J_{SC}’s as high as 15 mA cm^{-2}.[24] To understand the nature of the detected domains, DMT (Derjaguin-Muller-Topolov) modulus images were acquired via PeakForce Quantitative Nanomechanical property Mapping (QNM; Figure S4). Since both the observed domains and the surroundings show similar DMT moduli, no major compositional differences are to be expected. A small reduction of the domain size could be obtained by the use of suitable processing additives, giving rise to improved solar cell performances (Table 3, Figure 5). This PCE increase is quite strong for **PCPDTQx(2F)**, with the top efficiency rising from 2.49 to 5.26%. The reduced J_{SC} for the difluorinated copolymer blend compared to the **PCPDTQx(1F)** blend can be related to the (even) less favorable active layer morphology, possibly obscuring the potential high performance of the

devices based on this copolymer. Despite a lot of efforts employing various solvent-additive combinations, the optimal recipe could not be found (yet). For the **PCPDTQx(2F)**:PC$_{71}$BM device, not only the J$_{SC}$ increases upon adding 1-chloronaphthalene to the processing solution, but there is also a noticeable rise in V$_{OC}$ (from 0.78 to 0.83 V; Table 3), which is absent for the devices based on the non- and monofluorinated copolymer. This effect can probably be related to the more significant morphology changes observed for the **PCPDTQx(2F)**:fullerene blend (Figure 5). It has been reported before that the nano- and mesoscopic active layer morphology of polymer solar cells can (strongly) affect the V$_{OC}$.[25]
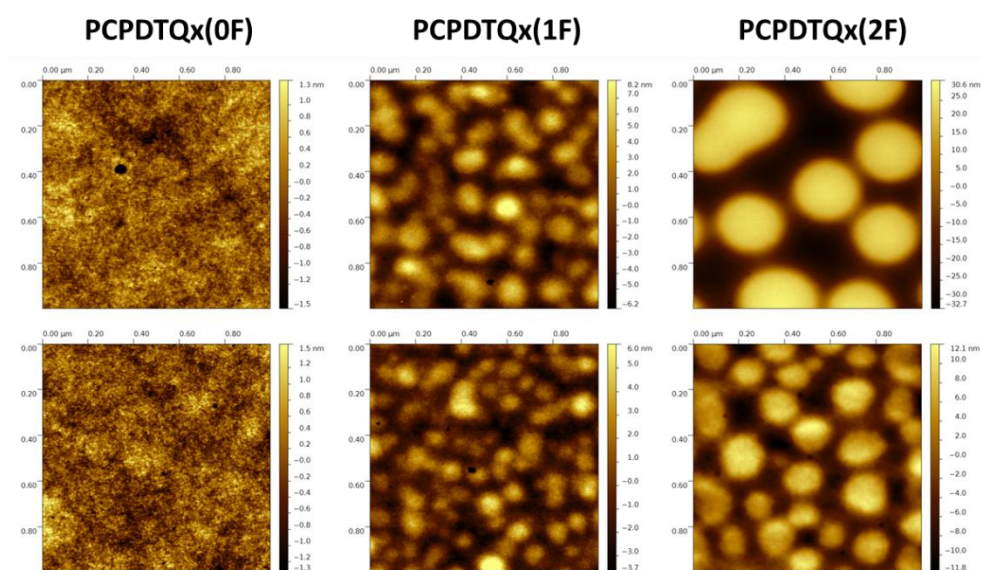
Figure 5: AFM (topography) images of the photoactive layers of the PCPDTQx:PC$_{71}$BM solar cells prepared without (upper row) and with (bottom row) processing additives.

3.3 CONCLUSIONS

For the first time, a complete set of (fluorinated) PCPDTQx(F) copolymers was synthesized. Further structural distinctiveness was provided by the quinoxaline 2,3-bis[5'-(2''-ethylhexyl)thien-2'-yl] substitution pattern and the combination with an asymmetrically dialkylated 4*H*-cyclopenta[2,1-*b*:3,4-*b*']dithiophene. The physicochemical and optical properties of the polymers were influenced only to a minor extent by fluorination, but the HOMO and LUMO energy levels were more seriously affected. For every fluorine atom added, the HOMO energy level decreased by approximately 0.1 eV. This deepening of the HOMO level translated into an increase of the V_{OC} of the resulting polymer solar cell by approximately 0.1 V for every fluorine atom added, leading to a V_{OC} of 0.83 V for the **PCPDTQx(2F)**:$PC_{71}BM$ device. In addition to the V_{OC}, also the J_{SC} and FF increased for **PCPDTQx(1F)** in comparison with the non-fluorinated copolymer, affording a maximum PCE of 4.87%. Despite the further increase in V_{OC} for **PCPDTQx(2F)**, the J_{SC} did not follow this trend, consequently translating in a less pronounced PCE enhancement to 5.26%. The decreased J_{SC} was related to the less favorable photoactive layer morphology, showing large domains up to ~250 nm. Nonetheless, the presented results clearly portray the potential of the combination of cyclopentadithiophene and quinoxaline building blocks. Side chain manipulation may be a way to obtain a nanoscale bicontinuous interpenetrating network in the active layer and activities in this direction are currently pursued. Another aspect of current interest is the thermal and photostability of the PCPDTQx:$PC_{71}BM$ photoactive layers.[1a,26]

3.4 EXPERIMENTAL SECTION

3.4.1 Materials and instruments

Preparative (recycling) size exclusion chromatography was performed on a JAI LC-9110 NEXT system equipped with JAIGEL 1*H*, 2*H* and 3*H* columns (eluent CHCl$_3$, flow rate 3.5 mL/min). NMR chemical shifts (δ, in ppm) were determined relative to the residual CHCl$_3$ (7.26 ppm) absorption or the ^{13}C resonance shift of CDCl$_3$ (77.16 ppm). High resolution electrospray ionization mass spectrometry (ESI-MS) was performed using an LTQ Orbitrap Velos Pro mass spectrometer equipped with an atmospheric pressure ionization source operating in the nebulizer assisted electrospray mode. The instrument was calibrated in the *m/z* range 220−2000 using a standard solution containing caffeine, MRFA and Ultramark 1621. Reported masses are the 100% intensity isotope peaks. UV-Vis measurements were performed on a VARIAN Cary 500 UV-Vis-NIR spectrophotometer at a scan rate of 600 nm/min. The films for the UV-Vis measurements were prepared by drop casting a solution of the polymer in chloroform on a quartz substrate. The solid-state UV-Vis spectra were used to estimate the optical band gaps (from the wavelength at the intersection of the tangent line drawn at the low energy side of the absorption spectrum with the x-axis: E_g (eV) = 1240/(wavelength in nm)). Analysis of the molar masses and molar mass distributions of the polymers was performed on a Tosoh EcoSEC System, comprising of an autosampler, a PSS guard column SDV (50 x 7.5 mm), followed by three PSS SDV analytical linear XL columns (5 μm, 300 x 7.5 mm) and a UV-detector using THF as the eluent at 40 °C with a flow rate of 1.0 mL/min. The SEC system was calibrated using linear narrow polystyrene standards ranging from 474 to 7.5 x 10^6 g/mol (K= 14.1 x 10^{-5} dL/g and α = 0.70). Rapid heat-cool

calorimetry (RHC) experiments were performed on a prototype RHC of TA Instruments, equipped with liquid nitrogen cooling and specifically designed for operation at high scanning rates.[20a,27] RHC measurements were performed at 250 or 500 K min^{-1} in aluminum crucibles, using helium (6 mL min^{-1}) as a purge gas. TGA experiments were performed at 20 K min^{-1} in platinum crucibles on a TA Instruments Q5000 TGA using nitrogen (50 mL min^{-1}) as purge gas. Electrochemical measurements (cyclic voltammetry) were performed with an Eco Chemie Autolab PGSTAT 30 potentiostat/galvanostat using a three-electrode microcell with a platinum working electrode, a platinum counter electrode and a Ag/AgNO$_3$ reference electrode (silver wire dipped in a solution of 0.01 M AgNO$_3$ and 0.1 M NBu$_4$PF$_6$ in anhydrous acetonitrile). The reference electrode was calibrated against ferrocene/ferrocenium as an external standard. Samples were prepared by dip coating the platinum working electrode in the respective polymer solutions (also used for the solid-state UV-Vis measurements). The CV measurements were done on the resulting films with 0.1 M NBu$_4$PF$_6$ in anhydrous acetonitrile as electrolyte solution. To prevent air from entering the system, the experiments were carried out under a curtain of argon. Cyclic voltammograms were recorded at a scan rate of 100 mV s^{-1}. For the conversion of V to eV, the onset potentials of the first oxidation/reduction peaks were used and referenced to ferrocene/ferrocenium, which has an ionization potential of -4.98 eV *vs.* vacuum. This correction factor is based on a value of 0.31 eV for Fc/Fc$^+$ *vs.* SCE[28a] and a value of 4.68 eV for SCE *vs.* vacuum[28b]: E$_{HOMO/LUMO}$ (eV) = -4.98 - E$_{onset\ ox/red}$$^{Ag/AgNO3}$ (V) + E$_{onset\ Fc/Fc+}$ $^{Ag/AgNO3}$ (V).

3.4.2 Monomer synthesis

Unless stated otherwise, all reagents and chemicals were obtained from

commercial sources and used without further purification. Solvents were dried by a solvent purification system (MBraun, MB-SPS-800) equipped with alumina columns. Precursors 4-(2'-ethylhexyl)-4-octyl-4H-cyclopenta[2,1-b:3,4-b']dithiophene,[10b] 1,2-bis[5'-(2''-ethylhexyl)thiophen-2'-yl]ethane-1,2-dione,[13] 3,6-dibromo-1,2-phenylenediamine (**2a**),[13] 3,6-dibromo-4-fluoro-1,2-phenylenediamine (**2b**)[18] and 3,6-dibromo-4,5-difluoro-1,2-phenylenediamine (**2c**)[18] were prepared according to literature procedures.

5,8-Dibromo-2,3-bis[5'-(2''-ethylhexyl)thiophen-2'-yl]quinoxaline (3a)

General Qx monomer synthesis procedure: 3,6-Dibromo-1,2-phenylenediamine (**2a**) (0.690 g, 2.60 mmol) and 1,2-bis[5'-(2''-ethylhexyl)thiophen-2'-yl]ethane-1,2-dione (1.160 g, 2.60 mmol) were dissolved in MeOH (50 mL) and p-toluenesulfonic acid monohydrate (0.050 mg, 0.26 mmol) was added. After heating under reflux for 15 h, the reaction mixture was allowed to cool down and the yellow precipitate was filtered, washed with MeOH and purified with flash column chromatography (silica, eluent dichloromethane (20%) in petroleum ether). After recrystallization from EtOH, yellow, needle like, crystals were obtained (1.370 g, 78%). ^{1}H NMR (400 MHz, CDCl$_3$): δ 7.78 (s, 2H), 7.40 (d, J = 3.7 Hz, 2H), 6.70 (d, J = 3.7 Hz, 2H), 2.80 (d, J = 6.9 Hz, 4H), 1.70–1.60 (m, 2H), 1.45–1.20 (m, 16H), 0.95–0.85 (m, 12H); ^{13}C NMR (100 MHz, CDCl$_3$): δ 150.9 (2C), 147.4 (2C), 138.6 (4C), 132.7 (2C), 130.5 (2C), 126.1 (2C), 123.0 (2C), 41.6 (2C), 34.6 (2C), 32.5 (2C), 29.0 (2C), 25.7 (2C), 23.2 (2C), 14.3 (2C), 11.0 (2C); HRMS (ESI): calcd. for C$_{32}$H$_{41}$Br$_2$N$_2$S$_2$ [M+H]$^+$: 677.1052, found: 677.1046.

5,8-Dibromo-6-fluoro-2,3-bis[5'-(2''-ethylhexyl)thiophen-2'-yl]quinoxaline (3b)

Synthesis according to the general Qx monomer synthesis procedure using 3,6-dibromo-4-fluoro-1,2-phenylenediamine (**2b**) as the starting material. Yellow solid (902 mg, 75%). ^{1}H NMR (400 MHz, CDCl$_3$): δ 7.79 (d, J = 8.1 Hz, 1H), 7.41 (d, J = 3.7 Hz, 1H), 7.39 (d, J = 3.7 Hz, 1H), 6.70–6.65 (m, 2H), 2.81 (d, J = 6.9 Hz, 4H), 1.70–1.60 (m, 2H), 1.45–1.20 (m, 16H), 0.95–0.85 (m, 12H); ^{13}C NMR (100 MHz, CDCl$_3$): δ 159.7 (d, $^1J_{C\text{-}F}$ = 252.7 Hz, 1C), 151.9 (1C), 151.2 (1C), 148.4 (1C), 147.1 (d, $J_{C\text{-}F}$ = 3.0 Hz, 1C), 139.4 (d, $J_{C\text{-}F}$ = 5.7 Hz, 1C), 139.0 (1C), 138.8 (1C), 136.1 (1C), 131.3 (1C), 130.8 (1C), 126.8 (1C), 126.6 (1C), 124.0 (d, $J_{C\text{-}F}$ = 11.1 Hz, 1C), 123.1 (d, $J_{C\text{-}F}$ = 29.2 Hz, 1C), 108.0 (d, $J_{C\text{-}F}$ = 21.1 Hz, 1C), 42.1 (2C), 35.2 (1C), 35.1 (1C), 33.1 (2C), 29.5 (2C), 26.3 (2C), 23.7 (2C), 14.8 (2C), 11.5 (2C); HRMS (ESI): calcd. for C$_{32}$H$_{40}$Br$_2$FN$_2$S$_2$ [M+H]$^+$: 695.0958, found: 695.0953.

5,8-Dibromo-6,7-difluoro-2,3-bis[5'-(2''-ethylhexyl)thiophen-2'-yl]quinoxaline (3c)

Synthesis according to the general Qx monomer synthesis procedure using 3,6-dibromo-4,5-difluoro-1,2-phenylenediamine (**2c**) as the starting material. Yellow solid (589 mg, 56%). ^{1}H NMR (400 MHz, CDCl$_3$): δ 7.40 (d, J = 3.7 Hz, 2H), 6.71 (d, J = 3.7 Hz, 2H), 2.81 (d, J = 6.8 Hz, 4H), 1.70–1.60 (m, 2H), 1.45–1.20 (m, 16H), 0.95–0.85 (m, 12H); ^{13}C NMR (100 MHz, CDCl$_3$): δ 151.2 (2C), 150.3 (dd, $^1J_{C\text{-}F}$ = 257.8, $^2J_{C\text{-}F}$ = 19.8 Hz, 2C), 147.4 (2C), 138.2 (2C), 135.2 (2C), 130.5 (2C), 126.2 (2C), 109.0 (dd, $J_{C\text{-}F}$ = 11.5, 8.8 Hz, 2C), 41.6 (2C), 34.6 (2C), 32.5 (2C), 29.0 (2C), 25.8 (2C), 23.2 (2C), 14.3 (2C), 11.0 (2C); HRMS (ESI): calcd. for C$_{32}$H$_{39}$Br$_2$F$_2$N$_2$S$_2$ [M+H]$^+$: 713.0864, found: 713.0862.

2,6-Bis(trimethylstannyl)-4-(2'-ethylhexyl)-4-octyl-4*H*-cyclopenta[2,1-*b*:3,4-*b*']dithiophene (4)

4-(2'-Ethylhexyl)-4-octyl-4*H*-cyclopenta[2,1-*b*:3,4-*b*']dithiophene (2.93 g, 7.28 mmol) was dissolved in dry THF (60 mL) and the solution was cooled to -78 °C, followed by dropwise addition of *n*-BuLi (29.1 mmol, 2.5 M in *n*-hexane). After stirring an additional hour at -78 °C, a solution of trimethyltin chloride (32.8 mL, 1M in THF) was added. The resulting solution was allowed to warm to room temperature overnight. Water was added and the mixture was extracted with diethyl ether. The organic phase was washed with brine, dried with $MgSO_4$, filtered and the solvents were removed *in vacuo*. The crude mixture was purified via preparative recycling SEC to yield the pure product as a pale yellow oil (3.29 g, 62%). ^{1}H NMR (400 MHz, $CDCl_3$): δ 6.94 (s, 1H), 6.93 (s, 1H), 1.95–1.70 (m, 4H), 1.30–1.05 (m, 10H), 1.05–0.80 (m, 13H), 0.73 (t, *J* = 7.0 Hz, 3H), 0.65–0.55 (m, 4H), 0.36 (s, 18H).

3.4.3 Polymer synthesis

PCPDTQx(0F)

General polymerization method: A solution of CPDT monomer **4** (0.147 g, 0.202 mmol) in dry toluene (4.8 mL) was added to a mixture of Qx monomer **3a** (0.137 g, 0.202 mmol), $Pd_2(dba)_3$ (4.6 mg, 5.0 µmol) and P(*o*-tol)$_3$ (6.1 mg, 20 µmol) in dry DMF (1.2 mL) under nitrogen atmosphere. After purging with N_2 for 15 min, the mixture was heated to 110 °C for 15 h, before 2-(tributylstannyl)thiophene (25 mg, 0.065 mmol) was added. After heating for an additional hour, 2-bromothiophene was added (25 mg, 0.15 mmol) and the mixture was stirred for 1 h. The green polymer solution was then precipitated in methanol and filtered in a Soxhlet thimble. After Soxhlet extractions with MeOH

and acetone, the polymer was collected by Soxhlet extraction with *n*-hexane. The solvent was evaporated and the polymer dissolved in chloroform and mixed vigorously with an aqueous sodium diethyldithiocarbamate solution (10%) for 2 h at 60 °C. The mixture was extracted with chloroform and the organic layer was washed with water. The organic solvent was removed and the obtained polymer was subjected to prep-SEC to remove the low molar mass fraction. After precipitation in MeOH, **PCPDTQx(0F)** was obtained as a greenish black solid (95 mg, 51%). ^{1}H NMR (400 MHz, CDCl$_3$): δ 8.40–7.70 (br, 4H), 7.55–7.40 (m, 2H), 6.85–7.70 (m, 2H), 3.00–2.80 (br, 4H), 2.30–1.90 (br, 4H), 1.80–1.70 (m, 2H), 1.50–0.90 (m, 48H), 0.90–0.70 (m, 4H), 0.70–0.60 (m, 6H); SEC (THF, 40 °C, PS standards): before prep-SEC: M_n = 12 kg mol^{-1}, PDI = 2.6; after prep-SEC: M_n = 47 kg mol^{-1}, PDI = 1.5.

PCPDTQx(1F)

PCPDTQx(1F) was synthesized according to the general polymerization method: CPDT monomer **4** (0.154 g, 0.211 mmol), Qx monomer **3b** (0.147 g, 0.211 mmol), Pd$_2$(dba)$_3$ (4.8 mg, 5.3 µmol) and P(*o*-tol)$_3$ (6.4 mg, 21 µmol) were dissolved in 4.8 mL of dry toluene and 1.2 mL of dry DMF. The polymer was obtained as a greenish black solid (117 mg, 63%). ^{1}H NMR (400 MHz, CDCl$_3$): δ 8.30–8.00 (m, 2H), 8.00–7.80 (m, 1H), 7.60–7.40 (m, 2H), 6.85–7.70 (m, 2H), 3.00–2.80 (br, 4H), 2.40–1.90 (br, 4H), 1.80–1.70 (m, 2H), 1.50–0.90 (m, 48H), 0.90–0.70 (m, 4H), 0.70–0.60 (m, 6H); SEC (THF, 40 °C, PS standards): before prep-SEC: M_n = 26 kg mol^{-1}, PDI = 2.7; after prep-SEC: M_n = 69 kg mol^{-1}, PDI = 1.6.

PCPDTQx(2F)

PCPDTQx(2F) was synthesized according to the general polymerization method:

CPDT monomer **4** (0.178 g, 0.245 mmol), Qx monomer **3c** (0.174 g, 0.245 mmol), $Pd_2(dba)_3$ (5.6 mg, 6.1 µmol) and $P(o\text{-tol})_3$ (7.5 mg, 25 µmol) were dissolved in 4.8 mL of dry toluene and 1.2 mL of dry DMF. The polymer was obtained as a greenish black solid (104 mg, 54%). ^{1}H NMR (400 MHz, $CDCl_3$): δ 8.30–8.15 (m, 2H), 7.55–7.45 (m, 2H), 6.85–7.70 (m, 2H), 3.00–2.80 (br, 4H), 2.40–1.90 (br, 4H), 1.80–1.70 (m, 2H), 1.50–0.90 (m, 48H), 0.90–0.70 (m, 4H), 0.70–0.60 (m, 6H); SEC (THF, 40 °C, PS standards): before prep-SEC: M_n = 22 kg mol^{-1}, PDI = 2.7; after prep-SEC: M_n = 53 kg mol^{-1}, PDI = 1.5.

3.4.4 OPV device fabrication and characterization

Bulk heterojunction polymer solar cells were constructed using the traditional architecture glass/ITO/PEDOT:PSS/active layer/Ca/Al. Prior to processing, the indium tin oxide (ITO, Kintec, 100 nm, 20 Ohm/sq) coated substrates were thoroughly cleaned using soap, demineralized water, acetone, isopropanol and a UV/O_3 treatment. PEDOT:PSS [poly(3,4-ethylenedioxythiophene): poly(styrenesulfonic acid), Heraeus Clevios] was deposited by spincoating to achieve a layer of ~30 nm. Afterwards, processing was continued under nitrogen atmosphere in a glove box, starting off with an annealing step at 130 °C for 15 min to remove any residual water. Subsequently, all PCPDTQx:PC$_{71}$BM (1:3) ([6,6]-phenyl-C$_{71}$-butyric acid methyl ester, Solenne) active layer blends were spincoated with optimal thicknesses of ~80−120 nm, as confirmed by profilometry (DEKTAK^{ST3}). Polymer concentrations for the main solvents chloroform (CF), chlorobenzene (CB) and *ortho*-dichlorobenzene (ODCB) were varied from 5 to 8 and 12 mg/mL, respectively. In a final step, the devices were finished off with Ca and Al as top electrodes, with thicknesses of 20 and 80 nm, respectively, resulting in a device active area of 3 mm². The I-V characteristics were measured using a

Newport class A solar simulator (model 91195A) calibrated with a silicon solar cell to give an AM 1.5G spectrum.

EQE measurements were performed with a Newport Apex illuminator (100 W Xenon lamp, 6257) as light source, a Newport Cornerstone 130° monochromator and a Stanford SR830 lock-in amplifier for the current measurements. A silicon FDS100-CAL photodiode was employed as a reference cell. For AFM imaging, a Bruker Multimode 8 AFM was used in PeakForce tapping mode. The images were produced with a silicon tip on a nitride lever with a spring constant of 4 N m^{-1}. Photo-induced charge extraction by linearly increasing voltage (Photo-CELIV) signals were registered from solar cell devices utilizing a pulsed laser (Continuum minilite II, 532nm), a Tektronix TDS 620B oscilloscope and a Tektronix AFG3101 function generator. The samples were placed in a sample holder filled with nitrogen to avoid exposure to ambient air.

3.5 REFERENCES

[1]   Recent reviews on polymer-based OPV: (*a*) M. Jørgensen, K. Norrman, S. A. Gevorgyan, T. Tromholt, B. Andreasen and F. C. Krebs, *Adv. Mater.*, 2012, **24**, 580; (*b*) H. Zhou, L. Yang and W. You, *Macromolecules*, 2012, **45**, 607; (*c*) Y. Li, *Acc. Chem. Res.*, 2012, **45**, 723; (*d*) Y. Su, S. Lan and K. Wei, *Mater. Today*, 2012, **15**, 554; (*e*) R. A. J. Janssen and J. Nelson, *Adv. Mater.* 2013, **25**, 1847; (*f*) H.-C. Liao, C.-C. Ho, C.-Y. Chang, M.-H. Jao, S. B. Darling and W.-F. Su, *Mater. Today*, 2013, **16**, 326; (*g*) S. Lizin, S. Van Passel, E. De Schepper, W. Maes, L. Lutsen, J. Manca and D. Vanderzande, *Energy Environ. Sci.*, 2013, **6**, 3136; (*h*) A. J. Heeger, *Adv. Mater.* 2014, **26**, 10.

[2]   F. C. Krebs, T. D. Nielsen, J. Fyenbo, M. Wadstrøm and M. S. Pedersen, *Energy Environ. Sci.*, 2010, **3**, 512.

[3]   (*a*) R. Søndergaard, M. Hösel, D. Angmo, T. T. Larsen-Olsen and F. C. Krebs, *Mater. Today*, 2012, **15**, 36; (*b*) R. Søndergaard, M. Hösel and F. C. Krebs, *J. Polym. Sci. Part B: Polym. Phys.*, 2013, **51**, 16.

[4]   (*a*) Z. He, C. Zhong, S. Su, M. Xu, H. Wu and Y. Cao, *Nat. Photonics*, 2012, **6**, 591; (*b*) C. Cabanetos, A. El Labban, J. A. Bartelt, J. D. Douglas, W. M. Mateker, J. M. Fréchet, M. D. McGehee and P. M. Beaujuge, *J. Am. Chem. Soc.*, 2013, **135**, 4656; (*c*) J. You, L. Dou, K. Yoshimura, T. Kato, K. Ohya, T. Moriarty, K. Emery, C.-C. Chen, J. Gao, G. Li and Y. Yang, *Nat. Commun.*, 2013, **4**, 1446; (*d*) M. Zhang, X. Guo, S. Zhang and J. Hou, *Adv. Mater.*, 2014, **26**, 1118; (*e*) L. Ye, S. Zhang, W. Zhao, H. Yao and J. Hou, *Chem. Mater.*, 2014, **26**, 3603; (*f*) K. Zhang, C. Zhong, S. Liu, C. Mu, Z. Li, H. Yan, F. Huang and Y. Cao, *ACS Appl. Mater. Interfaces*, 2014, **6**, 10429; (*g*) Y. Liu, J. Zhao, Z. Li, C. Mu, W. Ma, H. Hu, K.

Jiang, H. Lin, H. Ade and H. Yan, *Nat. Commun.*, 2014, DOI:10.1038/ncomms6293.

[5]   (*a*) Z. He, C. Zhong, X. Huang, W.-Y. Wong, H. Wu, L. Chen, S. Su and Y. Cao, *Adv. Mater.*, 2011, **23**, 4636; (*b*) J. Kesters, T. Ghoos, H. Penxten, J. Drijkoningen, T. Vangerven, D. M. Lyons, B. Verreet, T. Aernouts, L. Lutsen, D. Vanderzande, J. Manca and W. Maes, *Adv. Energy Mater.*, 2013, **3**, 1180; (*c*) W. Zhang, Y. Wu, Q. Bao, F. Gao and J. Fang, *Adv. Energy Mater.*, 2014, **4**, 1400359; (*d*) M. Vasilopoulou, D. G. Georgiadou, A. M. Douvas, A. Soultati, V. Constantoudis, D. Davazoglou, S. Gardelis, L. C. Palilis, M. Fakis, S. Kennou, T. Lazarides, A. G. Coutsolelos and P. Argitis, *J. Mater. Chem. A*, 2014, **2**, 182; (*e*) H. Zhou, Y. Zhang, C.-K. Mai, S. D. Collins, T.-Q. Nguyen, G. C. Bazan and A. J. Heeger, *Adv. Mater.*, 2014, **26**, 780.

[6]   (*a*) R. L. Uy, S. C. Price and W. You, *Macromol. Rapid Commun.*, 2012, **33**, 1162; (*b*) M. Jeffries-EL, B. M. Kobilka and B. J. Hale, *Macromolecules*, 2014, DOI:10.1021/ma501236v.

[7]   J. Peet, J. Y. Kim, N. E. Coates, W. L. Ma, D. Moses, A. J. Heeger and G. C. Bazan, *Nat. Mater.*, 2007, **6**, 497.

[8]   (*a*) C. Soci, I. W. Hwang, D. Moses, Z. Zhu, D. Waller, R. Gaudiana, C. J. Brabec and A. J. Heeger, *Adv. Funct. Mater.*, 2007, **17**, 632; (*b*) M. Zhang, H. N. Tsao, W. Pisula, C. Yang, A. K. Mishra and K. Müllen, *J. Am. Chem. Soc.*, 2007, **129**, 3472; (*c*) A. P. Zoombelt, S. G. J. Mathijssen, M. G. R. Turbiez, M. M. Wienk and R. A. J. Janssen, *J. Mater. Chem.*, 2010, **20**, 2240; (*d*) J. Kettle, M. Horie, L. A. Majewski, B. R. Saunders, S. Tuladhar, J. Nelson and M. L. Turner, *Sol. Energy Mater. Sol. Cells*, 2011, **95**, 2186; (*e*) A. V. Tunc, A. De Sio, D. Riedel, F. Deschler, E. Da Como, J. Parisi and E. von Hauff, *Org. Electron.*, 2012, **13**, 290; (*f*) S. Albrecht, S. Janietz, W. Schindler, J. Frisch, J. Kurpiers, J. Kniepert, S. Inal, P.

Pingel, K. Fostiropoulos, N. Koch and D. J. Neher, *J. Am. Chem. Soc.*, 2012, **134**, 14932; (*g*) S. Van Mierloo, A. Hadipour, M.-J. Spijkman, N. Van den Brande, B. Ruttens, J. Kesters, J. D'Haen, G. Van Assche, D. M. de Leeuw, T. Aernouts, J. Manca, L. Lutsen, D. Vanderzande and W. Maes, *Chem. Mater.*, 2012, **24**, 587; (*h*) Y. Zhang, J. Zou, C.-C. Cheuh, H.-L. Yip and A. K. Y. Jen, *Macromolecules*, 2012, **45**, 5427.

[9]   Z. Li, S.-W. Tsang, X. Du, L. Scoles, G. Robertson, Y. Zhang, F. Toll, Y. Tao, J. Lu and J. Ding, *Adv. Funct. Mater.*, 2011, **21**, 3331.

[10]   (*a*) S. Van Mierloo, P. J. Adriaensens, W. Maes, L. Lutsen, T. J. Cleij, E. Botek, B. Champagne and D. Vanderzande, *J. Org. Chem.*, 2010, **75**, 7202; (*b*) W. Vanormelingen, P. Verstappen, V. Maes, D. Bevk, L. Lutsen, D. Vanderzande and W. Maes, *Synlett*, 2013, **24**, 2389.

[11]   (*a*) S. Massip, P. M. Oberhumer, G. Tu, S. Albert-Seifried, W. T. S. Huck, R. H. Friend and N. C. Greenham, *J. Phys. Chem. C*, 2011, **115**, 25046; (*b*) K. R. Graham, C. Cabanetos, J. P. Jahnke, M. N. Idso A. El Labban, G. O. Ngongang Ndjawa, T. Heumueller, K. Vandewal, A. Salleo, B. F. Chmelka, A. Amassian, P. M. Beaujuge and M. D. McGehee, *J. Am. Chem. Soc.*, 2014, **136**, 9608; (*c*) J. Kesters, S. Kudret, S. Bertho, N. Van den Brande, M. Defour, B. Van Mele, H. Penxten, L. Lutsen, J. Manca, D. Vanderzande and W. Maes, *Org. Electron.*, 2014, **15**, 549.

[12]   (*a*) D. Kitazawa, N. Watanabe, S. Yamamoto and J. Tsukamoto, *Appl. Phys. Lett.*, 2009, **95**, 053701; (*b*) E. Wang, L. Hou, Z. Wang, S. Hellström, F. Zhang, O. Inganäs and M. R. Andersson, *Adv. Mater.*, 2010, **22**, 5240; (*c*) H.-C. Chen, Y.-H. Chen, C.-C. Liu, Y.-C. Chien, S.-W. Chou and P.-T. Chou, *Chem. Mater.*, 2012, **24**, 4766; (*d*) Y. Kim, H. R. Yeom, J. Y. Kim and C. Yang, *Energy Environ. Sci.*, 2013, **6**, 1909; (*e*) H.-C. Chen, Y.-H. Chen, C.-H. Liu, Y.-H. Hsu, Y.-

C. Chien, W.-T. Chuang, C.-Y. Cheng, C.-L. Liu, S.-W. Chou, S.-H. Tung and P.-T. Chou, *Polym. Chem.*, 2013, **4**, 3411; (*f*) J.-H. Kim, C. E. Song, H. U. Kim, A. C. Grimsdale, S.-J. Moon, W. S. Shin, S. K. Choi and D.-H. Hwang, *Chem. Mater.*, 2013, **25**, 2722.

[13]   L. Marin, L. Lutsen, D. Vanderzande and W. Maes, *Org. Biomol. Chem.*, 2013, **11**, 5866.

[14]   (*a*) Z. Li, J. Lu, S.-C. Tse, J. Zhou, X. Du, Y. Tao and J. J. Ding, *J. Mater. Chem.*, 2011, **21**, 3226; (*b*) Y. Zhang, S.-C. Chien, K.-S. Chen, H.-L. Yip, Y. Sun, J. A. Davies, F.-C. Chen and A. K.-Y. Jen, *Chem. Commun.*, 2011, **47**, 11026; (*c*) H. Chang, C. Tsai, Y. Lai, D. Chiou, S. Hsu, C. Hsu and Y. Cheng, *Macromolecules*, 2012, **45**, 9282; (*d*) T. Umeyama, Y. Watanabe, E. Douvogianni and H. J. Imahori, *J. Phys. Chem. C*, 2013, **117**, 21148; (*e*) H. Bronstein, J. M. Frost, A. Hadipour, Y. Kim, C. B. Nielsen, R. S. Ashraf, B. P. Rand, S. Watkins and I. McCulloch, *Chem. Mater.*, 2013, **25**, 277; (*f*) A. C. Stuart, J. R. Tumbleston, H. Zhou, W. Li, S. Liu, H. Ade and Y. Wei, *J. Am. Chem. Soc.*, 2013, **135**, 1806; (*g*) L. Xiao, B. Liu, X. Chen, Y. Li, W. Tang and Y. Zou, *RSC Adv.*, 2013, **3**, 11869; (*h*) W. Zhuang, H. Zhen, R. Kroon, Z. Tang, S. Hellström, L. Hou, E. Wang, D. Gedefaw, O. Inganäs, F. Zhang and M. R. Andersson, *J. Mater. Chem. A*, 2013, **1**, 13422; (*i*) H. Wang, X. Yu, C. Yi, H. Ren, C. Liu, Y. Yang, S. Xiao, J. Zheng, A. Karim, S. Z. D. Cheng and X. Gong, *J. Phys. Chem. C*, 2013, **117**, 4358; (*j*) X. He, S. Mukherjee, S. Watkins, M. Chen, T. Qin, L. Thomsen, H. Ade and C. R. McNeill, *J. Phys. Chem. C*, 2014, **118**, 9918; (*k*) C. Gu, M. Xiao, X. Bao, L. Han, D. Zhu, N. Wang, S. Wen, W. Zhu and R. Yang, *Polym. Chem.*, 2014, **5**, 6551; (*l*) M. Wang, S. Shi, D. Ma, K. Shi, C. Gao, L. Wang, G. Yu, Y. Li, X. Li and H. Wang, *Chem. Asian J.*, 2014, **9**, 2961; (*m*) D. Dang, W. Chen, S. Himmelberger, Q. Tao, A. Lundin, R. Yang, W. Zhu, A. Salleo, C. Müller and E. Wang, *Adv. Energy Mater.*, 2014, **4**, 1400680.

[15]   S. C. Price, A. C. Stuart, L. Yang, H. Zhou and J. Wei, *J. Am. Chem. Soc.*, 2011, **133**, 4625.

[16]   H. J. Son, W. Wang, T. Xu, Y. Liang, Y. Wu, G. Li and L. Yu, *J. Am. Chem. Soc.*, 2011, **133**, 1885.

[17]   (*a*) Y. Lu, Z. Xiao, Y. Yuan, H. Wu, Z. An, Y. Hou, C. Gao, J. Huang, *J. Mater. Chem. C*, 2013, **1**, 630; (*b*) P. Yang, M. Yuan, D. F. Zeigler, S. E. Watkins, J. A. Lee and C. K. Luscombe, *J. Mater. Chem. C*, 2014, **2**, 3278.

[18]   G. K. Dutta, T. Kim, H. Choi, J. Lee, D. S. Kim, J. Y. Kim and C. Yang, *Polym. Chem.*, 2014, **5**, 2540.

[19]   M. Shahid, R. S. Ashraf, Z. Huang, A. J. Kronemeijer, T. McCarthy-Ward, I. McCulloch, J. R. Durrant, H. Sirringhaus and M. Heeney, *J. Mater. Chem.*, 2012, **22**, 12817.

[20]   (*a*) R. L. Danley, P. A. Caulfield and S. R. Aubuchon, *Am. Lab.,* 2008, **40**, 9; (*b*) T. Ghoos, N. Van den Brande, M. Defour, J. Brassinne, C.-A. Fustin, J.-F. Gohy, S. Hoeppener, U. S. Schubert, W. Vanormelingen, L. Lutsen, D. J. Vanderzande, B. Van Mele and W. Maes, *Eur. Polym. J.*, 2014, **53**, 206.

[21]   Y. Zhao, N. E. Schultz and D. G. Truhlar, *J. Chem. Phys*., 2005, **123**, 161103.

[22]   J. Tomasi, B. Mennucci and R. Cammi, *Chem. Rev.*, 2005, **105**, 2999.

[23]   M. J. Frisch, G. W. Trucks, H. B. Schlegel, G. E. Scuseria, M. A. Robb, J. R. Cheeseman, G. Scalmani, V. Barone, B. Mennucci, G. A. Petersson, H. Nakatsuji, M. Caricato, X. Li, H. P. Hratchian, A. F. Izmaylov, J. Bloino, G. Zheng, J. L. Sonnenberg, M. Hada, M. Ehara, K. Toyota, R. Fukuda, J. Hasegawa, M. Ishida, T. Nakajima, Y. Honda, O. Kitao, H. Nakai, T. Vreven, J. A. Montgomery Jr., J. E. Peralta Jr., F. Ogliaro, M. Bearpark, J. J. Heyd, E. Brothers, K. N. Kudin, V. N. Staroverov, R. Kobayashi, J. Normand, K. Raghavachari, A. Rendell, J. C.

Burant, S. S. Iyengar, J. Tomasi, M. Cossi, N. Rega, J. M. Millam, M. Klene, J. E. Knox, J. B. Cross, V. Bakken, C. Adamo, J. Jaramillo, R. Gomperts, R. E. Stratmann, O. Yazyev, A. J. Austin, R. Cammi, C. Pomelli, J. W. Ochterski, R. L. Martin, K. Morokuma, V. G. Zakrzewski, G. A. Voth, P. Salvador, J. J. Dannenberg, S. Dapprich, A. D. Daniels, Ö. Farkas, J. B. Foresman, J. V. Ortiz, J. Cioslowski and D. J. Fox, Gaussian 09, Revision A.1, Gaussian, Inc., Wallingford CT, 2009.

[24]   G. J. Hedly, A. J. Ward, A. Alekseev, C. R. Howells, E. R. Martins, L. A. Serrano, G. Cooke, A. Rruseckas and I. D. W. Samuel, *Nat. Commun.*, 2013, **4**, 2867.

[25]   (*a*) F. Piersimoni, S. Chambon, K. Vandewal, R. Mens, T. Boonen, A. Gadisa, M. Izquierdo, S. Filippone, B. Ruttens, J. D'Haen, N. Martin, L. Lutsen, D. Vanderzande, P. Adriaensens and J. V. Manca, *J. Phys. Chem. C*, 2011, **115**, 10873; (*b*) K. Vandewal, S. Himmelberger and A. Salleo, *Macromolecules*, 2013, **46**, 6379.

[26]   (*a*) M. Manceau, E. Bundgaard, J. E. Carlé, O. Hagemann, M. Helgesen, R. Søndergaard, M. Jørgensen and F. C. Krebs, *J. Mater. Chem.*, 2011, **21**, 4132; (*b*) J. E. Carlé, M. Helgesen, N. K. Zawacka, M. V. Madsen, E. Bundgaard and F. C. Krebs, *J. Polym. Sci. B: Polym. Phys.*, 2014, **52**, 893; (*c*) I. Cardinaletti, J. Kesters, S. Bertho, B. Conings, F. Piersimoni, J. D'Haen, L. Lutsen, M. Nesladek, B. Van Mele, G. Van Assche, K. Vandewal, A. Salleo, D. Vanderzande, W. Maes and J. V. Manca, *J. Photon. Energy*, 2014, **4**, 040997.

[27]   S. Wouters, F. Demir, L. Beenaerts and G. Van Assche, *Thermochim. Acta*, 2012, **530**, 64.

[28]   (*a*) J. Bard and L. R. Faulkner, *Electrochemical methods: fundamentals and applications*, 2nd Ed., 2001, Wiley; (*b*) S. Trasatti, *Pure Appl. Chem.*, 1986, **58**, 955.

3.6 ACKNOWLEDGEMENTS

3.7 SUPPORTING INFORMATION

3.7.1 Optimization of the solar cell performance for each polymer

Table S1: Optimization of the solar cell devices based on **PCPDTQx(0F)**.

Processing solvent[a]	Polymer: PC$_{71}$BM	V_{OC} (V)	J_{SC} (mA cm^{-2})	FF	Average η (%)[b]	Best η (%)
CF	1:3[c]	0.61	6.55	0.53	2.11	2.26
CF + 10% ODCB	1:3	0.60	8.72	0.51	2.65	2.79
CF + 2% DIO	1:3	0.56	4.08	0.44	1.04	1.34
CB	1:3	0.62	6.47	0.49	1.97	2.30
CB + 3% DIO	1:3	0.60	4.73	0.46	1.32	1.45
CB + 3% CN	1:3	0.60	8.41	0.48	2.41	2.75
ODCB[d]	1:3	0.59	7.98	0.49	2.34	2.74
ODCB + 3% DIO[d]	1:3	0.59	4.35	0.45	1.18	1.51
ODCB + 3% CN[d]	1:3	0.60	8.46	0.53	2.70	2.94
ODCB[e]	1:3	0.60	8.63	0.51	2.65	2.88
ODCB + 3% CN[e]	1:3	0.60	9.44	0.54	3.08	3.24

[a] ODCB = *ortho*-dichlorobenzene, CF = chloroform, CB = chlorobenzene, CN = 1-chloronaphthalene, DIO = 1,8-diiodooctane. [b] Average values over at least 4 devices. [c] Optimal polymer:fullerene ratio found after device optimization for **PCPDTQx(1F)**. [d] Polymer concentration 8 mg/mL. [e] Polymer concentration 12 mg/mL

Table S2: Optimization of the solar cell devices based on **PCPDTQx(1F)**.

| Processing solvent[a]	Polymer: PC$_{71}$BM	V$_{OC}$ (V)	J$_{SC}$ (mA cm^{-2})	FF	Average η (%)[b]	Best η (%)
CF	1:3[c]	0.72	7.21	0.52	2.71	3.10
CF + 10% ODCB	1:3	0.71	11.17	0.58	4.56	4.87
CF + 2% DIO	1:3	0.70	3.17	0.46	1.00	1.12
CB	1:3	0.69	6.79	0.47	2.20	2.46
CB + 2% DIO	1:3	0.68	4.16	0.46	1.29	1.62
CB + 3% CN	1:3	0.68	10.85	0.53	3.91	4.47
ODCB[d]	1:3	0.64	8.34	0.48	2.58	2.79
ODCB + 3% DIO[d]	1:3	0.65	2.75	0.42	0.75	0.96
ODCB + 3% CN[d]	1:3	0.61	9.47	0.44	2.50	2.72

[a] ODCB = *ortho*-dichlorobenzene, CF = chloroform, CB = chlorobenzene, CN = 1-chloronaphthalene, DIO = 1,8-diiodooctane. [b] Average values over at least 4 devices. [c] Optimal polymer:fullerene ratio found after device optimization for **PCPDTQx(1F)**. [d] Polymer concentration 8 mg/mL

**Table S3:** Optimization of the solar cell devices based on **PCPDTQx(2F)**.

Processing solvent[a]	Polymer: PC$_{71}$BM	V$_{OC}$ (V)	J$_{SC}$ (mA cm^{-2})	FF	Average η (%)[b]	Best η (%)
CF	1:3[c]	0.73	5.63	0.48	1.98	2.42
CF + 10% ODCB	1:3	0.81	8.46	0.53	3.63	3.78
CF + 3% CN	1:3	0.82	7.92	0.57	3.65	4.07
CB	1:3	0.78	5.55	0.53	2.28	2.49
CB + 3% CN	1:2.5	0.83	10.39	0.56	4.86	5.26
CB + 3% CN	1:3	0.82	8.56	0.56	3.91	4.48
CB + 3% CN	1:3.5	0.80	8.15	0.55	3.57	3.72
ODCB[d]	1:3	0.80	8.11	0.48	3.12[e]	3.12

[a] ODCB = *ortho*-dichlorobenzene, CF = chloroform, CB = chlorobenzene, CN = 1-chloronaphthalene. [b] Average values over at least 4 devices. [c] Optimal polymer: fullerene ratio found after device optimization for **PCPDTQx(1F)**. [d] Polymer concentration 8 mg/mL. [e] Only one device was made.
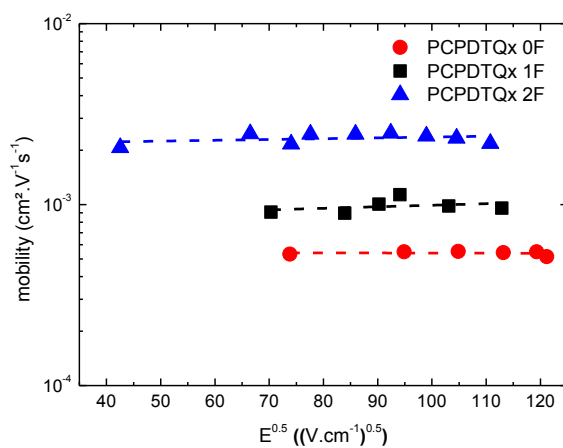
3.7.2 Thermal analysis
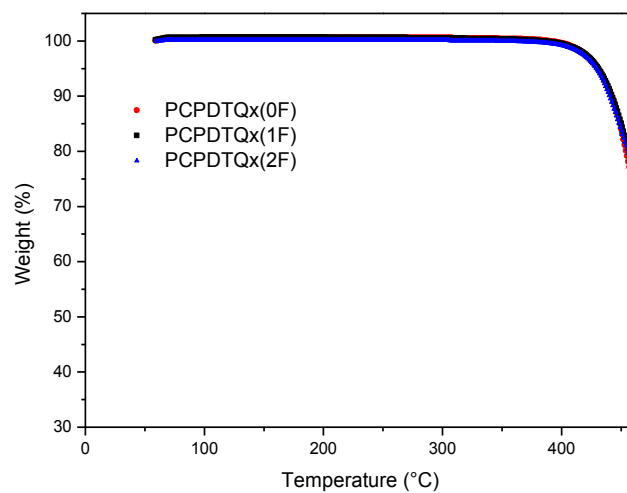
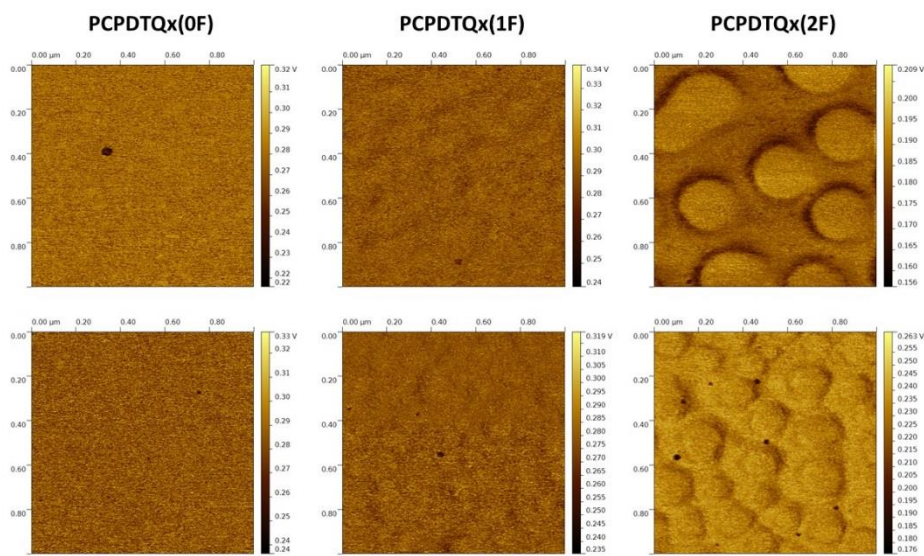**Figure S1:** TGA profiles for the three PCPDTQx copolymers.
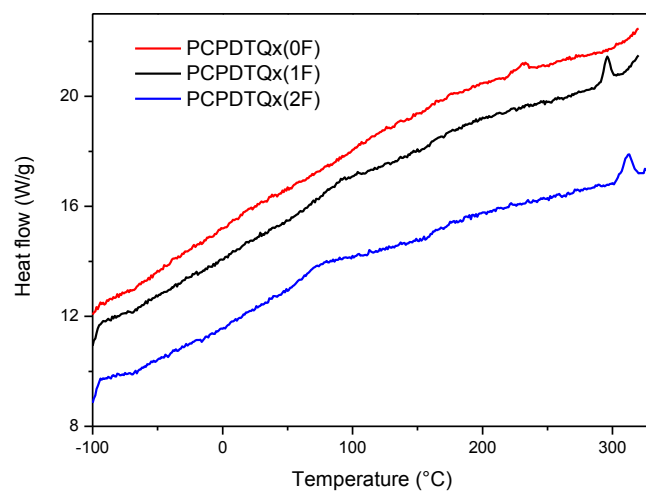
Figure S2: RHC profiles for the three PCPDTQx copolymers.

3.7.3 Photo-CELIV

Figure S3: Photo-CELIV measurements on photovoltaic devices for the three PCPDTQx copolymers.
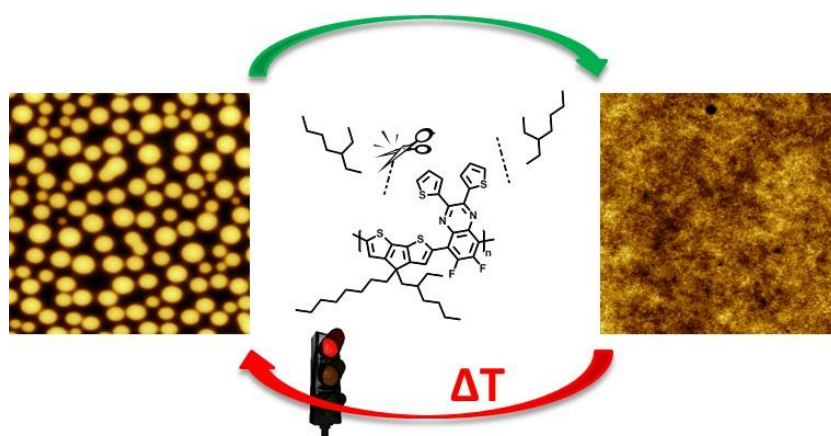
3.7.4 DMT modulus measurements

Figure S4: DMT modulus images of the photoactive layers of the PCPDTQx:PC$_{71}$BM solar cells prepared without (upper row) and with (bottom row) processing additives.

Chapter 4

Simultaneous Enhancement of the Solar Cell Efficiency and Stability by Reducing the Side Chain Density on Fluorinated PCPDTQx Copolymers

P. Verstappen, J. Kesters, L. D'Olieslaeger, J. Drijkoningen, I. Cardinaletti, T. Vangerven, J. D'Haen, J. Manca, L. Lutsen, D. Vanderzande, W. Maes, manuscript submitted.

ABSTRACT

The performance of polymer solar cells is strongly dependent on the morphology of the photoactive layer, which can be optimized by tuning the polymer side chain pattern. Whereas most studies focus on length and bulkiness, the side chain density receives much less attention. In this work, the effect of the number of side chains on PCPDTQx(2F) low bandgap copolymers on material properties and solar cell characteristics is investigated. The active layer morphology is strongly affected, affording more favorable finely intermixed blends when decreasing the side chain density. As a result, the efficiency increases to a maximum of 5.63% for the device based on the copolymer with intermediate side chain density. Moreover, removal of the side chains also has a positive effect on device stability under prolonged thermal stress. A single structural parameter – alkyl side chain density – is hence used for simultaneous enhancement of both solar cell efficiency and lifetime.

4.1 INTRODUCTION

In the quest for alternative energy sources, organic photovoltaics (OPV) have attracted large attention due to their potential low cost and mechanically (light-weight, flexible) and aesthetically (color, uniformity) appealing features.[1] Particularly interesting is the possibility to produce OPV via roll-to-roll processing.[2] First generation OPV applications in energy-neutral buildings, cars, agriculture and shading systems are currently being developed. In state-of-the-art bulk heterojunction (BHJ) polymer-based solar cells, the photoactive layer consists of an intimate blend of a conjugated polymer donor and a (methano)fullerene acceptor material (mostly $PC_{61}BM$ or $PC_{71}BM$).[3] Through the design of new low bandgap copolymers and simultaneous processing and device optimization, the performance of said devices has steadily improved in recent years, to over 10% power conversion efficiency (PCE) for both single junction and tandem polymer solar cells.[4,5] Developing innovative high-performance low bandgap copolymers is a challenging task. In addition to the intrinsic polymer properties which can be controlled synthetically (such as molar mass, position of the energy levels and absorption spectrum), also other, less easily tunable features are of utmost importance. For instance, the interaction of the polymer with the fullerene acceptor[6] and the capability of the donor material to form a favorable active layer blend (nano)morphology[7] are crucial to achieve a high solar cell efficiency. The BHJ active layer should be comprised of a co-continuous network of donor and acceptor domains and the length scale of two phases should be within the range of the exciton diffusion length (10−20 nm) to minimize charge recombination.[3,8] Different procedures to optimize the active layer morphology have been reported. Thermal and solvent annealing proved to be very successful

for P3HT:PC$_{61}$BM solar cells, but this is less straightforward when (rather amorphous) low bandgap copolymers are applied. In 2007, Heeger *et al.* reported on the use of the high-boiling processing additive 1,8-octanedithiol (ODT).[9] Addition of ODT almost doubled the efficiency of PCPDTBT:PC$_{71}$BM polymer solar cells, affording a record PCE of 5.5%. After this seminal report, various alternative additives were investigated for blend morphology optimization, with 1,8-diiodooctane (DIO) and 1-chloronaphtalene (CN) as some of the most notorious examples.[7a,10] Although the detailed mechanism behind the morphology changes is not completely understood,[10c] it has been shown on numerous occasions that these additives have an influence on the extent of nanoscale donor-acceptor phase separation, optimizing the interpenetrating BHJ network by either increasing or decreasing the size and miscibility of the donor and acceptor phases.[10]

Apart from these extrinsic processing parameters, also the intrinsic characteristics of the low bandgap donor polymer determine the final film morphology. The molar mass has been shown to be a major factor governing the final morphology.[11] It should exceed a certain threshold value (M_n = 20–30 kg/mol) for the materials to reveal their true photovoltaic potential. High molar mass polymers tend to aggregate faster, consequently forming a polymer network and preventing the formation of large phase-separated (fullerene) areas. Furthermore, the chemical structure is also of high importance. Conjugated polymers with an increased or decreased affinity for fullerenes will give rise to smaller or larger phase-separated domains, respectively.[12] With regard to this, fluorination, one of the most powerful and regularly employed tools for material chemists to fine-tune the energy levels of low bandgap copolymers, is known to decrease the compatibility of polymers and fullerenes.[13] As a result, the beneficial effects of fluorination, e.g. an increased open-circuit voltage (V_{oc}) via deepening of the HOMO, are often

counteracted by the adverse effects of fluorination on the nanoscale BHJ morphology (affording a reduced fill factor (FF) and short-circuit current density (J_{sc})).[14] Nevertheless, for most systems the morphology can to a certain extent be improved by the use of high-boiling solvent additives. It has to be mentioned though that there are also some disadvantages associated with the use of these additives, including a prolonged fabrication time and reduced lifetime.[15] Another widely employed method to optimize the active layer morphology is to alter the length and bulkiness of the polymer's solubilizing alkyl side chains.[16] In contrast, systematic investigations on the effect of side chain density are very scarce,[17] although similar effects can be expected from such an approach. A limiting factor is obviously polymer solubility, as not all building block combinations leading to successful push-pull low bandgap copolymers allow partial side chain removal while still rendering solution-processable materials.

In this work, the influence of the side chain density on the active layer morphology of BHJ polymer solar cells based on PCPDTQx(2F) is examined. We have recently reported PCE's up to 5.26% for solar cell devices based on this copolymer in combination with $PC_{71}BM$.[18] Fluorination had a major impact on the nanoscale active layer morphology, leading to unfavorable large domains, which could not be remediated through the use of processing additives. As the PCPDTQx(2F) copolymer is highly soluble, it was identified as an ideal test case to investigate the effect of polymer side chain density.

4.2 RESULTS AND DISCUSSION

4.2.1 Synthesis and characterization

The PCPDTQx(2F) (poly{4-(2'-ethylhexyl)-4-octyl-4*H*-cyclopenta[2,1-*b*:3,4-*b*']dithiophene-2,6-diyl-*alt*-6,7-difluoro-2,3-bis[5'-(2''-ethylhexyl)thiophen-2'-yl]quinoxaline-5,8-diyl}) narrow bandgap copolymer combines two well-known OPV buildings blocks, 4*H*-cyclopenta[2,1-*b*:3,4-*b*']dithiophene (CPDT)[9,16b,19] and quinoxaline (Qx)[14b,20], in an alternating push-pull arrangement.[18] Particular structural features of this electron donor polymer are the asymmetrical alkyl side chain substitution on the CPDT component[21] and difluorination[13,19b,c] and 2,3-dithienyl extension[22] of the Qx moiety. Variation of the number of side chains on this copolymer was accomplished by implementing various ratios of two Qx monomers with and without 2-ethylhexyl side chains (**3a** and **3b**, respectively) in the Stille polycondensation with bisstannyl-CPDT derivative **4** (Scheme 1). This is in line with the recent statement that high-performance low bandgap copolymers generally show acceptor parts that are sterically accessible for interaction with the fullerene counterparts.[6b] The Qx monomers were prepared via a condensation reaction between the difluorinated *o*-phenylenediamine **1** and diketone **2a** or **2b**. It was chosen to prepare three copolymers having either alkyl substituents on all Qx components (**P1**), on 50% of the Qx's (**P2**) or on none of the Qx units (**P3**). After Stille polymerization, the polymers were precipitated in MeOH, filtered in a soxhlet timble and soxhlet extractions were performed for purification. Polymers **P1** and **P2** were collected with *n*-hexane, whereas **P3** was only obtained with chloroform, illustrating the reduced solubility upon elimination of the side chains. Traces of palladium were removed via extraction with an aqueous sodium *N,N*-diethyldithiocarbamate solution[23] and the low molar mass fractions of the

copolymers were discarded via preparative size exclusion chromatography (prep-SEC) (Figure S1). The number-average molar masses, as determined by analytical SEC, were 53, 47 and 50 kDa for **P1**, **P2** and **P3**, respectively, with polydispersity indices around 1.5 (Table 1). The molar masses of the three copolymers were nearly identical after prep-SEC. As a result, no particular molar mass effect on the BHJ active layer morphology and final solar cell behavior is to be expected.
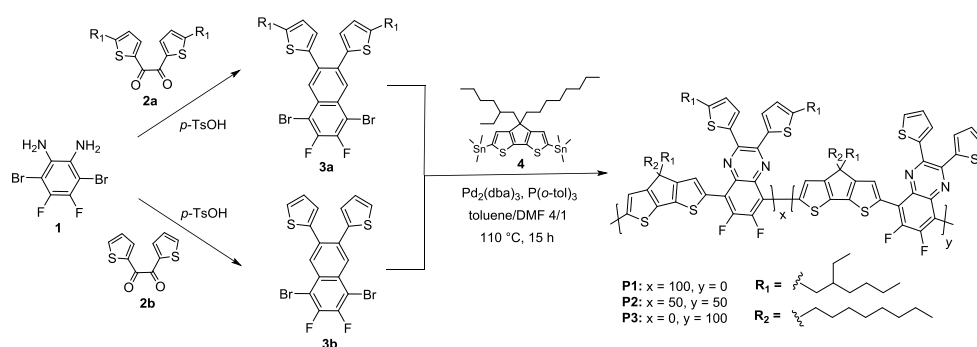
Scheme 1: Synthetic routes toward the employed Qx monomers and the corresponding PCPDTQx(2F) copolymers **P1**−**P3**.

Table 1: Molar mass (distribution), thermal, optical and electrochemical data for the PCPDTQx(2F) copolymer series.

Polymer	$M_n{}^a$ (kDa)	PDI^a	$T_d{}^b$ (°C)	$T_g{}^c$ (°C)	λ_{max} (nm) (CHCl$_3$)	λ_{max} (nm) film	$E_g{}^{OPd}$ (eV)	HOMO^e (eV)	LUMO^e (eV)	$E_g{}^{ECf}$ (eV)
P1	53	1.5	350	65/170^g	691	703	1.60	-5.51	-3.37	2.14
P2	47	1.6	350	135^h	686	692	1.58	-5.45	-3.39	2.06
P3	50	1.4	350	175	694	696	1.55	-5.33	-3.42	1.90

^{a} Determined by analytical SEC in THF at 40 °C for the polymer samples after prep-SEC. ^{b} Determined by the onset of the first derivative of the mass loss as a function of temperature. ^{c} Determined by RHC. ^{d} Optical bandgap, determined by the onset of the solid-state UV-Vis spectrum. ^{e} Determined by CV from the onset of oxidation and reduction. $^f$ Electrochemical bandgap. ^{g} A second T_g at 170 °C is observed as well. ^{h} Exact determination is complicated by the width of the transition.

The thermal stability of the different copolymers was investigated via thermogravimetric analysis (TGA) (Table 1, Figure S2). No influence of the side chain ratio on the onset of the mass loss was observed (the decomposition temperature (T_d) for all three polymers is 350 °C), but mass loss proceeds slightly faster for the polymers with a larger side chain density, suggesting that the side chains are involved in the degradation mechanism.[24] On the other hand, by rapid heat-cool calorimetry (RHC) measurements, a major influence on the glass transition temperature (T_g) was observed (Table 1, Figure S3). RHC was chosen above regular differential scanning calorimetry (DSC) because of its increased sensitivity to thermal transitions as a result of the fast scanning rates and the low sample amounts required.[25] For copolymer **P1**, two T_g's were observed, at approximately 65 and 170 °C, possibly indicating a separate (low T_g) 'phase' imposed by the large amount of flexible alkyl side chains surrounding the (high-T_g) rod-like polymer backbone. On the other hand, one single T_g was obtained for the two other copolymers. By removing all side chains on the Qx units, a steady increase of the T_g up to 175 °C was observed (very close to the second T_g as seen for **P1**), with an intermediate 'broad' T_g of 135 °C for **P2**. As control of the side chain density seems to be a powerful method to regulate the T_g, this may provide a possible pathway toward enhanced thermal stability of (the active layer of) polymer solar cells (*vide infra*).

The electrochemical properties of the three copolymers were investigated via cyclic voltammetry (Table 1). Highest occupied molecular orbital (HOMO) and lowest unoccupied molecular orbital (LUMO) energy levels were estimated from the onset of the oxidation and reduction peaks, respectively. Removal of the side chains mainly influenced the HOMO energy levels (with a minor effect on the LUMO levels), gradually increasing upon reducing the side chain ratio (by 0.18 eV from

P1 to **P3**). The raising HOMO levels result in a slight decrease of the electrochemical bandgaps of the copolymers with reduced amounts of alkyl side chains. Similar UV-Vis absorption spectra were obtained for the three copolymers (Figure 1), with small deviations caused by variation of the side chain density. The wavelength of maximum absorption (λ_{max}) remains more or less unaffected (Table 1), but the low energy absorption band is broadened upon removal of the side chains, in solution as well as in thin film. Hence, the optical bandgap decreases upon reducing the side chain density, in agreement with the trend in electrochemical bandgap. In solution, reduction of the steric bulk caused by the side chains can give rise to smaller torsion angles and thereby extended conjugation. In the solid state, side chain removal can afford a denser packing of the polymer chains, enhancing interchain interactions and leading to a red-shift in the absorption spectrum.[13a]
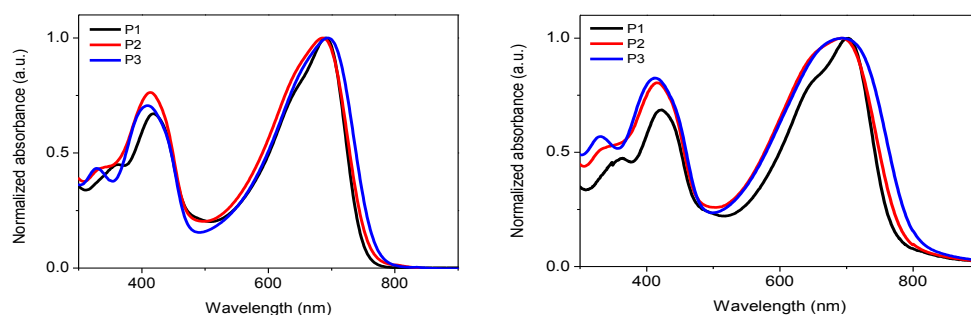
Figure 1: Normalized UV-Vis absorption spectra for the PCPDTQx(2F) copolymers in CHCl₃ solution (left) and thin film (right).

4.2.2 Photovoltaic properties

To investigate the influence of the side chain variation on OPV performance, polymer solar cells were prepared using the standard architecture glass/ITO/PEDOT:PSS/PCPDTQx(2F):PC$_{71}$BM/Ca/Al. The devices based on fully

alkylated polymer **P1** were previously optimized and best results (maximum PCE of 5.26%) were obtained for a 1:2.5 polymer:fullerene ratio and spin-coating from a chlorobenzene solution of the two components containing 3% (v/v) of the processing additive 1-chloronaphthalene (CN) (Table 2 and S1).[18] Device optimization for the two other copolymers was started from these conditions (Table S2 and S3). Enhanced PCE's were achieved for the **P2**:$PC_{71}BM$ and **P3**:$PC_{71}BM$ combinations (Figure 2, Table 2). Slight reductions in V_{oc} (possibly related to the increased HOMO levels) and FF were overcompensated by the increase in J_{sc}. In this way, a maximum efficiency of 5.63% was obtained for the device based on **P2**. Further removal of the side chains did not result in a further enhancement of the J_{sc} and the optimal photovoltaic performance for the **P3** copolymer was 5.11%. The processing solvent did not influence the *J-V* parameters to a large extent, as very similar results were obtained from pure chlorobenzene and pure chloroform solutions (Table 2). Additionally, the use of additives was no longer required to obtain the highest performances, an appealing feature from a processing (and hence commercial) point of view. External quantum efficiency (EQE) measurements performed on the optimized devices showed an upward trend in the polymer contribution (from 40 to 60%) upon progressing from **P1** to **P2** and **P3** (Figure 3). A small red-shift was observed when the side chain density of the polymers was reduced, consistent with the UV-Vis absorption data.

Table 2: Photovoltaic output parameters for copolymers **P1**−**P3** in BHJ solar cells with standard configuration glass/ITO/PEDOT:PSS/PCPDTQx(2F):PC$_{71}$BM/Ca/Al.

Polymer	Polymer:PC$_{71}$BM ratio	Processing solvent[a]	V_{oc} (V)	J_{sc} (mA.cm^{-2})	FF	PCE[b] (%)
P1	1:3	CB	0.78	5.55	0.53	2.28 (2.49)
P1	1:2.5	CB + 3% CN	0.83	10.39	0.56	4.86 (5.26)[c]
P2	1:3	CB	0.77	11.48	0.57	5.04 (5.20)
P2	1:3.5	CF	0.78	11.95	0.55	5.07 (5.63)[c]
P3	1:3	CB	0.78	11.79	0.51	4.72 (5.11)
P3	1:3	CF	0.78	11.43	0.51	4.55 (5.09)[c]

[a] CB = chlorobenzene, CN = 1-chloronaphthalene, CF = chloroform. [b] Average values over at least 4 devices. The best device performance is shown in brackets. [c] Averages taken over 12 devices.
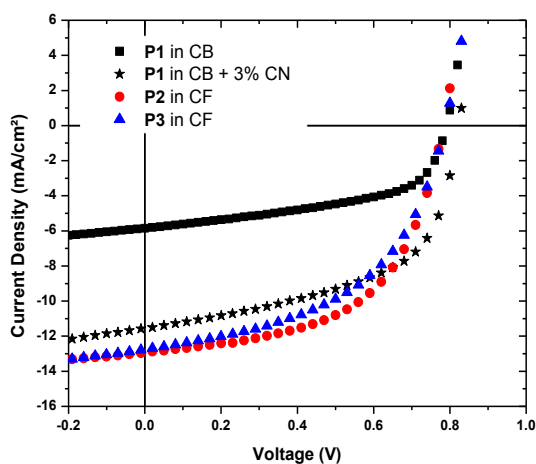

Figure 2: *J-V* curves for the best performing PCPDTQx(2F):PC$_{71}$BM solar cells.
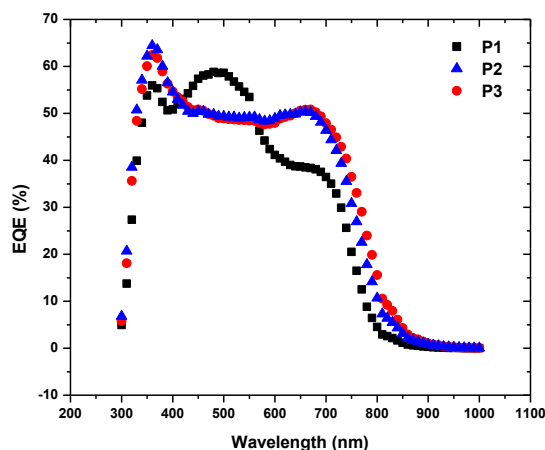
Figure 3: EQE spectra of the solar cell devices made from the different PCPDTQx(2F) copolymers. The devices employed for the EQE measurements gave a J_{SC} of 11.58, 13.03 and 13.16 mA cm^{-2} for **P1** (in CB + 3% CN), **P2** (in CF) and **P3** (in CF), respectively, with J_{EQE}'s of 11.16, 12.56 and 12.95 mA cm^{-2}.

Even though the influence of the side chain density on the photovoltaic parameters did not appear to be very strong, atomic force microscopy (AFM) topography imaging revealed significantly different active layer morphology features (Figure 4). The **P1**:PC$_{71}$BM blend showed a distinct morphology containing large domains, severely deviating from the desired finely intermixed donor:acceptor network. Upon addition of CN, the domain size could be reduced, but remained unfavorable for optimal charge extraction (by the diminished interfacial area).[18] On the other hand, no clear separate domains were visible in the active layer of the solar cells based on copolymers **P2** and **P3**. Removal of 50% of the Qx side chains already resulted in a finely intermixed morphology, and no further identifiable changes were seen when all of the Qx side chains were removed. In addition, AFM revealed no significant morphological changes upon the use of additives (CN) or co-solvents (*ortho*-dichlorobenzene) (Figure S5), consistent with the similar solar cell performances (Table S2 and S3).
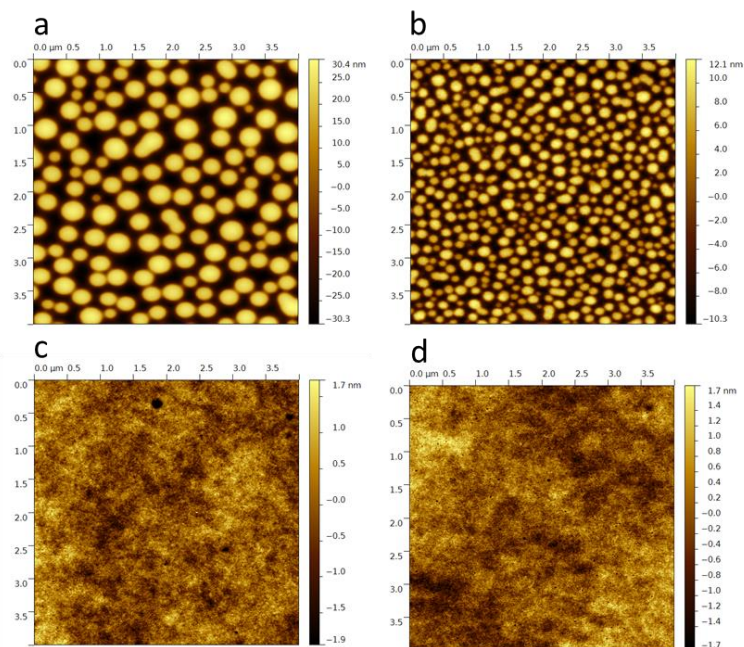
Figure 4: AFM (topography) images (4x4 µm) of the photoactive layers of the (best performing) polymer solar cells based on: a) **P1**:PC$_{71}$BM (in CB), b) **P1**:PC$_{71}$BM (in CB + 3% CN), c) **P2**:PC$_{71}$BM (in CF), and d) **P3**:PC$_{71}$BM (in CF).

Somewhat surprisingly, only a minor improvement in solar cell performance was obtained for the devices based on **P2** and **P3** in comparison to **P1**, despite the strongly enhanced morphology. It has to be noted though that AFM showed no major difference in mechanical properties (DMT (Derjaguin–Müller–Toporov) modulus and deformation images in Figure S6) between the large domains and their surrounding environment, suggesting that both regions might consist of polymer and PC$_{71}$BM. As a result, the effect of the domain formation might not be as detrimental as initially projected.[10c,26] Investigation of the charge transport features of the BHJ blends by photo-induced charge extraction by linearly increasing voltage (photo-CELIV) revealed that the mobilities (in the appropriate direction of the solar cell mode) are in the same (suitable) range for the three

copolymer:$PC_{71}BM$ blends (2×10^{-3}, 6×10^{-4} and 3×10^{-4} cm^2 V^{-1} s^{-1} for the solar cells based on **P1**−**P3**, respectively) (Figure S7). To clarify if the observed gradual reduction in mobility originates from the difference in morphology or is rather an intrinsic material property, field-effect transistors (FET's) were used to investigate the hole mobility of the three pristine copolymers (in absence of the fullerene derivative). By fitting of the FET transfer curves, mobilities were determined to be 2×10^{-3}, 1×10^{-3} and 6×10^{-4} cm^2 V^{-1} s^{-1} for **P1**−**P3**, respectively (Figure S8). These values are in good agreement with the photo-CELIV measurements and indicate a small decrease in hole mobility of the copolymers when reducing the number of side chains, which could (partly) explain the rather small increase in J_{sc} and PCE for the devices based on **P2** and the minor decrease in J_{sc} and PCE for the devices based on **P3**.

4.2.3 Photovoltaic stability

A particular consequence of PCPDTQx(2F) side chain removal is that the double T_g of **P1** disappears and the T_g increases up to 175 °C for **P3** (Table 1), which can have strong consequences for the thermal stability of the resulting polymer:fullerene solar cells. It is well-known that the initially generated high-performance active layer morphology will change during device operation, depending on the T_g's of the involved photoactive species. As regularly demonstrated for the workhorse P3HT:$PC_{61}BM$ combination, exposure to temperatures above the T_g of the blend (i.e. 60 °C for P3HT:$PC_{61}BM$ [27]) results in diffusion and crystallization of the fullerene material, leading to an unfavorable extent of phase separation and therefore strongly reduced device performance.[28] Through the synthesis of high-T_g polymer materials, a more rigid blend morphology can be procured, resulting in prolonged device lifetimes, an important

requirement toward commercial OPV applications.[1,29] Alternative approaches to 'freeze in' or slow down the thermal degradation of the BHJ blend morphology involve the use of compatibilizers[30], nucleating agents,[31] or non-crystalline fullerene additives,[32] thermocleavage of the solubilizing side chains,[33] the incorporation of functional moieties on the polymer side chains[34] and cross-linking of the active materials[35].[36] As instigated by the change in T_g, enhanced thermal stability could be expected for the polymer solar cells based on **P2** and (in particular) **P3**. As the T_g's of the blends (rather than those of the pure polymers) are required to analyze the thermal behavior of the photoactive layers and the resulting solar cell devices, RHC measurements were also performed on the **P1**−**P3**:$PC_{71}BM$ blends affording best solar cell efficiencies (Figure S4). Whereas the **P1**:$PC_{71}BM$ blend showed two T_g's (at 66 and 167 °C, similar to the pure polymer), the T_g's of the blends based on copolymers **P2** and **P3** were found at 160 and 155 °C, respectively. While there does not seem to be a straightforward explanation for these values as compared to those of the pure polymers **P2** and **P3**, they might be attributed to interactions between the polymers and $PC_{71}BM$ (and the different blend ratio).

To investigate the thermal stability of the different polymer solar cells, a dedicated degradation study was performed at 85 °C (cfr. the ISOS-3 standards[37]). This accelerated aging experiment was performed on optimized **P1**−**P3**:$PC_{71}BM$ devices in an automated degradation chamber, with *I-V* measurements at predetermined intervals to investigate the progression of the photovoltaic parameters over time. A strong relative PCE decay was observed for the **P1**:$PC_{71}BM$ device, especially within the first few hours of the experiment, whereas the two other polymers afforded much more stable devices (Figure 5). After 120 hours, the performance of **P1** was reduced to 50% of its initial value,

whereas the relative efficiencies for **P2** and **P3** retained at 72 and 82%, respectively. Deconvolution of the separate *I-V* parameters reveals more details on the nature of the degradation profile at 85 °C (Figure S9). The efficiency decay originates from a combined drop in V_{oc} and J_{sc}, especially at the start of the aging experiment (the 'burn-in' phase[38]), while the FF factor remains practically constant and even slightly increases for the **P3**:PC$_{71}$BM device. Both the V_{oc} and J_{sc} reduction are less prominent for the devices based on **P2** and (especially) **P3**. The strong initial decline in V_{oc} has already been investigated before and has been ascribed to the formation of light-induced charge traps at the interface of the active layer and the top electrode, prominent during the initial phase of the degradation study by the frequent exposure to light.[39] This effect is generally absent upon aging in a dark environment (*vide infra*).
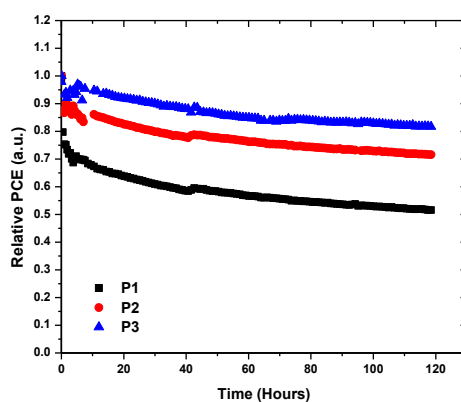

Figure 5: Relative efficiency decay profiles for the three PCPDTQx(2F):PC$_{71}$BM polymer solar cells upon exposure to a temperature of 85 °C for 120 h. The curves are normalized to the first measurement point at 85 °C.

To investigate the influence of the elevated temperature on the (nano)morphology of the various active layer blends, transmission electron microscopy (TEM) analysis was performed (Figure 6). In the pristine **P1**:PC$_{71}$BM film, domains of

~200 nm were observed, supporting the AFM findings. Additionally, selective area electron diffraction (SAED) patterns demonstrated that these domains are not composed of pure $PC_{71}BM$, as no distinct diffraction rings could be observed. The initial **P2**:$PC_{71}BM$ blend displayed a rather intricate intermixed situation, possibly the peak-performing (nano)morphology leading to the higher performance for this donor-acceptor system, whereas the two phases were indistinguishable for the pristine **P3**:$PC_{71}BM$ blend. Upon aging for 120 hours at 85 °C, no formation of micro- or nanocrystals could be observed for any of the materials, as evidenced by TEM and SAED (Figure 6), not even for the **P1**:$PC_{71}BM$ system showing a strong PCE decrease. The thermal treatment did induce some visual morphological rearrangements in the **P2**:$PC_{71}BM$ blend, with minor influence on the device efficiency though. These findings indicate that the observed differences in thermal stability must arise from alternative degradation mechanisms.

To shed more light on the thermal degradation behavior, an additional (manual) aging test was conducted at 120 °C, well above the first T_g of polymer **P1** and the resulting blend, but below the T_g's of the other two polymers and their blends. In this case, the devices were simply heated on a hotplate in the dark with I-V measurements after 0, 2, 5, 8, and 14 hours. The degradation behavior revealed a similar trend, with **P3** procuring the most stable device, preceding **P2** and **P1**, respectively (Figure S10). After 14 hours at 120 °C, the relative PCE for the **P1**−**P3**:$PC_{71}BM$ devices decreased to 19, 67 and 92%, respectively. The absence of light avoided the V_{oc} drop for the solar cells based on **P2** and **P3**. Especially the **P3**:$PC_{71}BM$ device was proven to be remarkably stable, with only a minor initial reduction of the J_{sc} and (once again) a slight improvement in FF. There is a (currently not understood) noteworthy difference between the devices based on copolymers **P2** and **P3**, whereas the T_g's of the active layer blends are very

similar. TEM imaging of the samples aged at 120 °C illustrated large aggregate formation for the **P1**:PC$_{71}$BM system (Figure S11), whereas these were completely absent for the two other blends. The SAED measured for these structures showed a pattern that can be ascribed to PC$_{71}$BM (nano)crystals, pointing to fullerene diffusion and crystallization (with depletion zones around the fullerene domains). This observation seems to be consistent with the low T_g phase observed for the fully alkylated copolymer and its blend with PC$_{71}$BM.
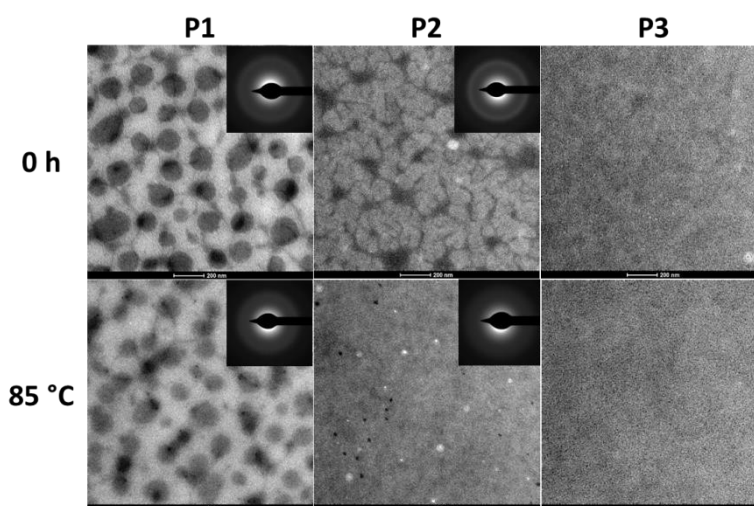
Figure 6: TEM images (with SAED inserts) of the active layers of pristine and aged (120 hours at 85 °C) **P1**−**P3**:PC$_{71}$BM polymer solar cells.

4.3 CONCLUSIONS

For OPV to become an economically viable technology, the two important pillars (besides cost) to be optimized are device efficiency and lifetime. In this work, we have shown that reduction of the polymer side chain density can be beneficially applied to increase both solar cell performance and (thermal) durability. The active layer morphology of PCPDTQx(2F):PC$_{71}$BM BHJ solar cells can to a large

extent be controlled by altering the side chain density on the copolymer (changing the accessible volume for the fullerene acceptor[6b]). Removing (part of) the side chains affords favorable finely intermixed donor-acceptor networks, leading to improved PCE values, even without the use of processing additives. A maximum efficiency of 5.63% is obtained for the device based on the copolymer with intermediate side chain density. The presented approach has also advantages from a synthetic point of view, compared to the classical protocol in which a variety of different side chains (differing in length and steric bulk) are analyzed in a trial and error fashion, as only two different monomers have to be prepared that can then be copolymerized in various ratios. Moreover, removing some of the side chains can also enhance the (thermal) stability of polymer solar cells, as illustrated here for the PCPDTQx(2F) case. Although the improved device lifetime can partly be attributed to a T_g increase (or disappearance of a low T_g phase), this does not suffice to explain all observed differences. Further work in this direction is currently pursued in our group, as is the application of the side chain density concept to other low bandgap copolymers. Another aspect of interest is the photostability of the PCPDTQx(2F):$PC_{71}BM$ active layers.[1a,40]

4.4 EXPERIMENTAL SECTION

4.4.1 Materials and instruments

Preparative (recycling) size exclusion chromatography was performed on a JAI LC-9110 NEXT system equipped with JAIGEL 1*H*, 2*H* and 3*H* columns (eluent $CHCl_3$, flow rate 3.5 mL/min). NMR chemical shifts (δ, in ppm) were determined relative to the residual $CHCl_3$ (7.26 ppm) absorption or the ^{13}C resonance shift of $CDCl_3$ (77.16 ppm). Quantitative ^{13}C NMR measurements were obtained with

chromium(III) acetylacetonate as a relaxation agent. High resolution electrospray ionization mass spectrometry (ESI-MS) was performed using an LTQ Orbitrap Velos Pro mass spectrometer equipped with an atmospheric pressure ionization source operating in the nebulizer assisted electrospray mode. The instrument was calibrated in the *m/z* range 220−2000 using a standard solution containing caffeine, MRFA and Ultramark 1621. Reported masses are the 100% intensity peaks of the isotopic distributions. UV-Vis absorption measurements were performed on a VARIAN Cary 500 UV-Vis-NIR spectrophotometer at a scan rate of 600 nm/min. The films for the UV-Vis measurements were prepared by drop casting chloroform solutions of the polymers on quartz substrates. The solid-state UV-Vis spectra were used to estimate the optical bandgaps (from the wavelength at the intersection of the tangent line drawn at the low energy side of the absorption spectrum with the x-axis: E_g (eV) = 1240/(wavelength in nm)). Analysis of the molar masses and molar mass distributions of the polymers was performed on a Tosoh EcoSEC System, comprising of an autosampler, a PSS guard column SDV (50 x 7.5 mm), followed by three PSS SDV analytical linear XL columns (5 μm, 300 x 7.5 mm) and a UV detector using THF as the eluent at 40 °C with a flow rate of 1.0 mL/min. The SEC system was calibrated using linear narrow polystyrene standards ranging from 474 to 7.5 x 10^6 g/mol (K = 14.1 x 10^{-5} dL/g and a = 0.70). Rapid heat-cool calorimetry experiments were performed on a prototype RHC of TA Instruments, equipped with liquid nitrogen cooling and specifically designed for operation at high scanning rates.[25] RHC measurements were performed at 250 or 500 K min^{-1} in aluminum crucibles, using helium (6 mL min^{-1}) as a purge gas. TGA experiments were performed at 20 K min^{-1} in platinum crucibles on a TA Instruments Q5000 TGA using nitrogen (50 mL min^{-1}) as purge gas. Electrochemical measurements (cyclic voltammetry) were performed with an

Eco Chemie Autolab PGSTAT 30 potentiostat/galvanostat using a three-electrode microcell with a Pt working electrode, a Pt counter electrode and a Ag/AgNO$_3$ reference electrode (Ag wire dipped in a solution of 0.01 M AgNO$_3$ and 0.1 M NBu$_4$PF$_6$ in anhydrous acetonitrile). The reference electrode was calibrated against ferrocene/ferrocenium as an external standard. Samples were prepared by dip coating the Pt working electrode in the respective polymer solutions (also used for the solid-state UV-Vis measurements). The CV measurements were done on the resulting films with 0.1 M NBu$_4$PF$_6$ in anhydrous acetonitrile as electrolyte solution. To prevent air from entering the system, the experiments were carried out under a curtain of Ar. Cyclic voltammograms were recorded at a scan rate of 100 mV s^{-1}. For the conversion of V to eV, the onset potentials of the first oxidation/reduction peaks were used and referenced to ferrocene/ferrocenium, which has an ionization potential of -4.98 eV *vs.* vacuum. This correction factor is based on a value of 0.31 eV for Fc/Fc$^+$ *vs.* SCE[41a] and a value of 4.68 eV for SCE *vs.* vacuum[41b]: $E_{HOMO/LUMO}$ (eV) $= -4.98 - E_{onset\ ox/red}^{Ag/AgNO3}$ (V) $+ E_{onset\ Fc/Fc+}^{Ag/AgNO3}$ (V). The reported values are the means of the first five redox cycles.

4.4.2 Synthesis

Unless stated otherwise, all reagents and chemicals were obtained from commercial sources and used without further purification. Solvents were dried by a solvent purification system (MBraun, MB-SPS-800) equipped with alumina columns. Precursor 3,6-dibromo-4,5-difluoro-1,2-phenylenediamine (**1**)[42] and monomers 5,8-dibromo-6,7-difluoro-2,3-bis[5'-(2''-ethylhexyl)thiophen-2'-yl]quinoxaline (**3a**)[18] and 2,6-bis(trimethylstannyl)-4-(2'-ethylhexyl)-4-octyl-4*H*-cyclopenta[2,1-*b*:3,4-*b'*]dithiophene (**4**)[18] were prepared according to literature procedures.

5,8-Dibromo-6,7-difluoro-2,3-bis(thiophen-2'-yl)quinoxaline (3b). 3,6-Dibromo-4,5-difluoro-1,2-phenylenediamine (**1**) (694 mg, 2.30 mmol) and 2,2'-thenil (511 mg, 2.30 mmol) were dissolved in MeOH (50 mL) and *p*-toluenesulfonic acid monohydrate (44 mg, 0.23 mmol) was added. After heating under reflux for 15 h, the reaction mixture was allowed to cool down and the yellow precipitate was filtered off, washed with MeOH and purified with flash column chromatography (silica, eluent dichloromethane (2%) in petroleum ether). After recrystallization from EtOH, the pure product was obtained as yellow needles (763 mg, 68%). ^{1}H NMR (300 MHz, CDCl$_3$): δ 7.58 (dd, J = 5.0 Hz, J = 1.0 Hz, 2H), 7.49 (dd, J = 3.8 Hz, J = 1.0 Hz, 2H), 7.06 (dd, J = 5.0 Hz, J = 3.8 Hz, 2H); ^{13}C NMR (100 MHz, CDCl$_3$): δ 150.6 (dd, $^1J_{C\text{-}F}$ = 258.8, $^2J_{C\text{-}F}$ = 19.9 Hz, 2C), 147.3 (2C), 140.5 (2C), 135.5 (2C), 130.7 (2C), 130.3 (2C), 127.9 (2C), 109.1 (dd, $^2J_{C\text{-}F}$ = 12.0, $^3J_{C\text{-}F}$ = 8.3 Hz, 2C); HRMS (ESI): Calcd. for C$_{16}$H$_7$Br$_2$F$_2$N$_2$S$_2$$^+$ [M+H]$^+$: *m/z* 488.8360, found: 488.8349.

P1 (General polymerization method). 2,6-Bis(trimethylstannyl)-4-(2'-ethylhexyl)-4-octyl-4*H*-cyclopenta[2,1-*b*:3,4-*b*']dithiophene (**4**) (0.178 g, 0.245 mmol) was dissolved in dry toluene (4.8 mL) and added to a solution of Qx monomer **3a** (0.174 g, 0.245 mmol), Pd$_2$(dba)$_3$ (5.6 mg, 6.1 µmol) and P(*o*-tol)$_3$ (7.5 mg, 25 µmol) in dry DMF (1.2 mL). The mixture was purged with N$_2$ for 15 min and heated to 110 °C for 15 h, before 2-(tributylstannyl)thiophene (25 mg, 0.065 mmol) was added. After heating for an additional hour, 2-bromothiophene was added (25 mg, 0.15 mmol) and the mixture was stirred for 1 h. The resulting polymer was precipitated in MeOH and filtered off in a soxhlet thimble. Soxhlet extractions were performed with MeOH, acetone and *n*-hexane, respectively. Subsequently, an aqueous solution of sodium *N,N*-diethyldithiocarbamate (10%)

was added to the polymer solution in *n*-hexane and the mixture was stirred for 2 h at 60 °C. After separation from the aqueous layer, the organic phase was evaporated *in vacuo* and the obtained polymer was subjected to prep-SEC to remove the low molar mass fractions. After precipitation in MeOH, polymer **P1** was finally obtained as a greenish black solid (104 mg, 54%). ^{1}H NMR (400 MHz, CDCl$_3$): δ 8.30–8.15 (m, 2H), 7.55–7.45 (m, 2H), 6.85–7.70 (m, 2H), 3.00–2.80 (br, 4H), 2.40–1.90 (br, 4H), 1.80–1.70 (m, 2H), 1.50–0.90 (m, 48H), 0.90–0.70 (m, 4H), 0.70–0.60 (m, 6H); SEC (THF, 40 °C, PS standards): before prep-SEC: M_n = 22 kg mol^{-1}, PDI = 2.7; after prep-SEC: M_n = 53 kg mol^{-1}, PDI = 1.5.

P2. P2 was prepared according to the general polymerization method: CPDT monomer **4** (0.146 g, 0.200 mmol), Qx monomer **3a** (0.0713 g, 0.100 mmol), Qx monomer **3b** (0.0488 g, 0.100 mmol), Pd$_2$(dba)$_3$ (4.6 mg, 5.0 µmol) and P(*o*-tol)$_3$ (6.1 mg, 20 µmol) were dissolved in 4.6 mL of dry toluene and 1.1 mL of dry DMF. The polymer was finally obtained as a greenish black solid (94 mg, 56%). ^{1}H NMR (400 MHz, CDCl$_3$): δ 8.32–8.14 (m, 2H), 8.14–7.97 (m, 2H), 7.70–7.56 (m, 4H), 7.56–7.44 (m, 2H), 7.21–7.05 (m, 2H), 6.84–6.70 (m, 2H), 3.01–2.79 (m, 4H), 2.44–1.82 (br, 8H), 1.82–1.65 (m, 2H), 1.50–0.91 (m, 64H), 0.91–0.84 (m, 6H), 0.84–0.75 (m, 6H), 0.75–0.59 (m, 12H); SEC (THF, 40 °C, PS standards): before prep-SEC: M_n = 19 kg mol^{-1}, PDI = 2.3; after prep-SEC: M_n = 47 kg mol^{-1}, PDI = 1.6.

P3. P3 was prepared according to the general polymerization method: CPDT monomer **4** (0.157 g, 0.216 mmol), Qx monomer **3b** (0.106 g, 0.216 mmol), Pd$_2$(dba)$_3$ (4.9 mg, 5.4 µmol) and P(*o*-tol)$_3$ (6.6 mg, 22 µmol) were dissolved in 5.0 mL of dry toluene and 1.2 mL of dry DMF. Soxhlet extractions were performed with MeOH, acetone, *n*-hexane and CHCl$_3$. The polymer was finally obtained as a

greenish black solid (99 mg, 63%). ^{1}H NMR (400 MHz, CDCl$_3$): δ 8.27–7.95 (m, 2H), 7.75–7.42 (m, 4H), 7.21–7.04 (m, 2H), 2.43–1.77 (br, 4H), 1.37–0.89 (m, 21H), 0.89–0.75 (t, J = 6.6 Hz, 3H), 0.75–0.59 (m, 6H); SEC (THF, 40 °C, PS standards): before prep-SEC: M_n = 31 kg mol^{-1}, PDI = 1.8; after prep-SEC: M_n = 50 kg mol^{-1}, PDI = 1.4.

4.4.3 OPV device fabrication and characterization

Bulk heterojunction polymer solar cells were constructed using the traditional architecture glass/ITO/PEDOT:PSS/active layer/Ca/Al. Prior to processing, the indium tin oxide (ITO, Kintec, 100 nm, 20 Ohm/sq) coated substrates were thoroughly cleaned using soap, demineralized water, acetone, isopropanol and a UV/O$_3$ treatment. PEDOT:PSS [poly(3,4-ethylenedioxythiophene): poly(styrenesulfonic acid); Heraeus Clevios] was deposited by spin-coating to achieve a layer of ~30 nm. Afterwards, processing was continued under nitrogen atmosphere in a glove box, starting off with an annealing step at 130 °C for 15 min to remove any residual water. Subsequently, all PCPDTQx(2F):PC$_{71}$BM ([6,6]-phenyl-C$_{71}$-butyric acid methyl ester; Solenne) active layer blends were spin-coated with optimal thicknesses of ~80−120 nm, as confirmed by profilometry (DEKTAK^{ST3}). Polymer concentrations for the main solvents chloroform, chlorobenzene, and $ortho$-dichlorobenzene were varied from 5 to 8 and 12 mg/mL, respectively. In a final step, the devices were finished off with Ca and Al as top electrodes, with thicknesses of 20 and 80 nm, respectively, resulting in a device active area of 3 mm². The I-V characteristics were measured using a Newport class A solar simulator (model 91195A) calibrated with a silicon solar cell to give an AM 1.5G spectrum. EQE measurements were performed with a Newport Apex illuminator (100 W Xenon lamp, 6257) as light source, a Newport Cornerstone

130° monochromator and a Stanford SR830 lock-in amplifier for the current measurements. A calibrated silicon FDS100 photodiode was employed as a reference cell. Photo-induced charge extraction by linearly increasing voltage (Photo-CELIV) signals were registered from solar cell devices utilizing a pulsed laser (Continuum minilite II, 532nm), a Tektronix TDS 620B oscilloscope and a Tektronix AFG3101 function generator. The samples were placed in a sample holder filled with nitrogen to avoid exposure to ambient air. For AFM imaging, a Bruker Multimode 8 AFM was used in PeakForce tapping mode, employing ScanAsyst. The images were produced with a silicon tip on a nitride lever with a spring constant of 4 N m^{-1}.

4.4.4 FET preparation and characterization

FETs were prepared in the bottom gate bottom contacts configuration by spin-coating solutions of **P1**, **P2**, and **P3** in chloroform with a concentration of 8 mg/mL on 200 nm of SiO$_2$, thermally grown on a highly n-doped Si substrate with pre-patterned contacts comprising of a stack of Ti/Au (10/100 nm), obtained from Philips. In the case of **P3**, a self-assembled monolayer of HMDS (hexamethyldisilazane) passivated the bare SiO$_2$ surface. The channel length was 10 μm. Two Keithley 2400 source meters were used to measure the current at the drain and correct it for leakage through the gate electrode. All FET preparation and characterization was carried out in a N$_2$ filled glove box.

4.4.5 Solar cell degradation under thermal stress

To investigate the thermal degradation behavior, the solar cells were positioned in an automated degradation chamber in nitrogen atmosphere (glove box) at a constant temperature of 85 °C. The *I-V* characteristics were measured at regular time intervals (initially every 5 min, later on every hour) using a White 5500 K

LED (Lamina). The manual degradation experiment at 120 °C was performed with the aid of a hotplate (280 x 200 mm, type PZ28-2ET, Harry Gestigkeit GmbH, with a PR5 programmer controller). TEM measurements were performed on a FEI Tecnai Spirit using an accelerating voltage of 120 kV. TEM samples were prepared from pristine solar cells, the devices utilized in the automated degradation chamber (after a thermal stress of 85 °C for 120 h), and the devices degraded on a hotplate at 120 °C. By washing away the PEDOT:PSS layer with water, freestanding films were obtained. For the samples degraded at 120 °C, the freestanding films had to be procured through the use of HF.

4.5 REFERENCES

[1]   (a) Jørgensen, M.; Norrman, K.; Gevorgyan, S. A.; Tromholt, T.; Andreasen, B.; Krebs, F. C. *Adv. Mater.* **2012**, *24*, 580. (b) Zhou, H.; Yang, L.; You, W. *Macromolecules* **2012**, *45*, 607. (c) Li, Y. *Acc. Chem. Res.* **2012**, *45*, 723. (d) Su, Y.; Lan, S.; Wei, K. *Mater. Today* **2012**, *15*, 554. (e) Janssen, R. A. J.; Nelson, J. *Adv. Mater.* **2013**, *25*, 1847. (f) Lizin, S.; Van Passel, S.; De Schepper, E.; Maes, W.; Lutsen, L.; Manca, J.; Vanderzande, D. *Energy Environ. Sci.* **2013**, *6*, 3136. (g) Xu, T.; Yu, L. *Mater. Today* **2014**, *17*, 11. (h) Roncali, J.; Leriche, P.; Blanchard P. *Adv. Mater.* **2014**, *26*, 3821.

[2]   Søndergaard, R.; Hösel, M.; Angmo, D.; Larsen-Olsen, T. T.; Krebs, F. C. *Mater. Today* **2012**, *15*, 36.

[3]   Heeger, A. J. *Adv. Mater.* **2014**, *26*, 10.

[4]   Single junction: (a) He, Z.; Zhong, C.; Su, S.; Xu, M.; Wu, H.; Cao, Y. *Nat. Photonics* **2012**, *6*, 591. (b) Ye, L.; Zhang, S.; Zhao, W.; Yao, H.; Hou, J. *Chem. Mater.* **2014**, *26*, 3603. (c) Zhang, K.; Zhong, C.; Liu, S.; Mu, C.; Li, Z.; Yan, H.; Huang, F.; Cao, Y. *ACS Appl. Mater. Interfaces* **2014**, *6*, 10429. (d) Liu, Y.; Zhao, J.; Li, Z.; Mu, C.; Ma, W.; Hu, H.; Jiang, K.; Lin, H.; Ade, H.; Yan, H. *Nat. Commun.* **2014**, doi: 10.1038/ncomms6293.

[5]   Tandem: (a) You, J.; Dou, L.; Yoshimura, K.; Kat, T.; Ohya, K.; Moriarty, T.; Emery, K.; Chen, C.-C.; Gao, J.; Li, G.; Yang, Y. *Nat. Commun.* **2012**, *4*, 1446. (b) You, J.; Chen, C.-C.; Hong, Z.; Yoshimura, K.; Ohya, K.; Xu, R.; Ye, S.; Gao, J.; Li, G.; Yang, Y. *Adv. Mater.* **2013**, *25*, 3973.

[6]   (a) Tumbleston, J. R.; Collins, B. A.; Yang, L.; Stuart, A. C.; Gann, E.; Ma, W.; You, W.; Ade, H. *Nat. Photonics* **2014**, *8*, 385. (b) Graham, K. R.; Cabanetos, C.; Jahnke, J. P.; Idso M. N.; El Labban, A.; Ngongang Ndjawa, G. O.; Heumueller,

T.; Vandewal, K.; Salleo, A.; Chmelka, B. F.; Amassian, A.; Beaujuge, P. M.; McGehee, M. D. *J. Am. Chem. Soc.* **2014**, *136*, 9608.

[7]   (a) Liao, H.-C.; Ho, C.-C.; Chang, C.-Y.; Jao, M.-H.; Darling, S. B.; Su, W.-F. *Mater. Today* **2013**, *16*, 326. (b) Dang, M. T.; Hirsch, L.; Wantz, G.; Wuest, J. D. *Chem. Rev.* **2013**, *113*, 3734. (d) Huang, Y.; Kramer, E. J.; Heeger, A. J.; Bazan, G. C. *Chem. Rev.* **2014**, *114*, 7006.

[8]   (a) Bartelt, J. A.; Beiley, Z. M.; Hoke, E. T.; Mateker, W. R.; Douglas, J. D.; Collins, B. A.; Tumbleston, J. R.; Graham, K. R.; Amassian, A.; Ade, H.; Fréchet, J. M. J.; Toney, M. F.; McGehee, M. D. *Adv. Energy Mater.* **2013**, *3*, 364. (b) Proctora, C. M.; Kuik, M.; Nguyen, T.-Q. *Prog. Polym. Sci.* **2013**, *38*, 1941. (c) Kesava, S. V.; Fei, Z.; Rimshaw, A. D.; Wang, C.; Hexemer, A.; Asbury, J. B.; Heeney, M.; Gomez, E. D. *Adv. Energy Mater.* **2014**, *4*, 1400116.

[9]   Peet, J.; Kim, J. Y.; Coates, N. E.; Ma, W. L.; Moses, D.; Heeger, A. J.; Bazan, G. C. *Nat. Mater.* **2007**, *6*, 497.

[10]   (a) Lou, S. J.; Szarko, J. M.; Xu, T.; Yu, L.; Marks, T. J.; Chen, L. X. *J. Am. Chem. Soc.* **2011**, *133*, 20661. (b) Wang, D. H.; Morin, P.-O.; Lee, C.-L.; Kyaw, A. K. K.; Leclerc, M.; Heeger, A. J. *J. Mater. Chem. A* **2014**, *2*, 15052. (c) Schmidt, K.; Tassone, C. J.; Niskala, J. R.; Yiu, A. T.; Lee, O. P.; Weiss, T. M.; Wang, C.; Fréchet, J. M. J.; Beaujuge, P. M.; Toney, M. F. *Adv. Mater.* **2014**, *26*, 300.

[11]   (a) Bartelt, J. A.; Douglas, J. D.; Mateker, W. R.; El Labban, A.; Tassone, C. J.; Toney, M. F.; Fréchet, J. M. J.; Beaujuge, P. M.; McGehee, M. D. *Adv. Energy Mater.* **2014**, *4*, 1301733. (b) Li, W.; Yang, L.; Tumbleston, J. R.; Yan, L.; Ade, H.; You, W. *Adv. Mater.* **2014**, *26*, 4456.

[12]   (a) Treat, N. D.; Varotto, A.; Takacs, C. J.; Batara, N.; Al-Hashimi, M.; Heeney, M. J.; Heeger, A. J.; Wudl, F.; Hawker, C. J.; Chabinyc, M. L. *J. Am.*

Chem. Soc. **2012**, *134*, 15869. (b) Tumbleston, J. R.; Yang, L.; You, W.; Ade, H. *Polymer* **2014**, *55*, 4884. (c) Chen, H.; Peet, J.; Hsiao, Y.-C.; Hu, B.; Dadmun, M. *Chem. Mater.* **2014**, *26*, 3993.

[13]   (a) Son, H. J.; Wang, W.; Xu, T.; Liang, Y.; Wu, Y.; Li, G.; Yu, L. *J. Am. Chem. Soc.* **2011**, *133*, 1885. (b) Bronstein, H.; Frost, J. M.; Hadipour, A.; Kim, Y.; Nielsen, C. B.; Ashraf, R. S.; Rand, B. P.; Watkins, S.; McCulloch, I. *Chem. Mater.* **2013**, *25*, 277. (c) Stuart, A. C.; Tumbleston, J. R.; Zhou, H.; Li, W.; Liu, S.; Ade, H.; Wei, Y. *J. Am. Chem. Soc.* **2013**, *135*, 1806. (d) Zhuang, W.; Zhen, H.; Kroon, R.; Tang, Z.; Hellström, S.; Hou, L.; Wang, E.; Gedefaw, D.; Inganäs, O.; Zhang, F.; Andersson, M. R. *J. Mater. Chem. A* **2013**, *1*, 13422. (e) Dang, D.; Chen, W.; Himmelberger, S.; Tao, Q.; Lundin, A.; Yang, R.; Zhu, W.; Salleo, A.; Müller, C.; Wang, E. *Adv. Energy Mater.* **2014**, *4*, 1400680. (f) Yang, P.; Yuan, M.; Zeigler, D. F.; Watkins, S. E.; Lee, J. A.; Luscombe, C. K. *J. Mater. Chem. C* **2014**, *2*, 3278.

[14]   (a) Zhou, H.; Yang, L.; Stuart, A. C.; Price, S. C.; Liu, S.; You, W. *Angew. Chem. Int. Ed.* **2011**, *50*, 2995. (b) Chen, H.-C.; Chen, Y.-H.; Liu, C.-C.; Chien, Y.-C.; Chou, S.-W.; Chou, P.-T. *Chem. Mater.* **2012**, *24*, 4766. (c) Schroeder, B. C.; Huang, Z.; Ashraf, R. S.; Smith, J.; D'Angelo, P.; Watkins, S. E.; Anthopoulos, T. D.; Durrant, J. R.; McCulloch, I. *Adv. Funct. Mater.* **2012**, *22*, 1663. (d) He, X.; Mukherjee, S.; Watkins, S.; Chen, M.; Qin, T.; Thomsen, L.; Ade, H.; McNeill, C. R. *J. Phys. Chem. C* **2014**, *118*, 9918. (e) Liu, P.; Zhang, K.; Liu, F.; Jin, Y.; Liu, S.; Russell, T. P.; Yip, H.-L.; Huang, F.; Cao, Y. *Chem. Mater.* **2014**, *26*, 3009.

[15]   Waters, H.; Bristow, N.; Moudam, O.; Chang, S.-W.; Su, C.-J.; Wu, W.-R.; Jeng, U.-S.; Horie, M.; Kettle, J. *Org. Electron.* **2014**, *15*, 2433.

[16]   (a) Zoombelt, A. P.; Leenen, M. A. M.; Fonrodona, M.; Nicolas, Y.; Wienk, M. M.; Janssen, R. A. J. *Polymer* **2009**, *50*, 4564. (b) Li, Z.; Tsang, S.-W.; Du, X.; Scoles, L.; Robertson, G.; Zhang, Y.; Toll, F.; Tao, Y.; Lu, J.; Ding, J. *Adv. Funct. Mater.* **2011**, *21*, 3331. (c) Cabanetos, C.; El Labban, A.; Bartelt, J. A.; Douglas, J. D.; Mateker, W. M.; Fréchet, J. M.; McGehee, M. D.; Beaujuge, P. M. *J. Am. Chem. Soc.* **2013**, *135*, 4656. (d) Mei, J.; Bao, Z. *Chem. Mater.* **2014**, *26*, 604. (e) Lee, J.; Kim, M.; Kang, B.; Jo, S. B.; Kim, H. G.; Shin, J.; Cho, K. *Adv. Energy Mater*. **2014**, *4*, 1400087.

[17]   Tessarolo, M.; Gedefaw, D.; Bolognesi, M.; Liscio, F.; Henriksson, P.; Zhuang, W.; Milita, S.; Muccini, M.; Wang, E.; Seri, M.; Andersson, M. R. *J. Mater. Chem. A* **2014**, *2*, 11162.

[18]   Verstappen, P.; Kesters, J.; Vanormelingen, W.; Heintges, G. H. L.; Drijkoningen, J.; Vangerven, T.; Marin, L.; Koudjina, S.; Champagne, B.; Manca, J.; Lutsen, L.; Vanderzande, D.; Maes, W. *J. Mater. Chem. A* **2015**, DOI: 10.1039/C4TA06054G.

[19]   (a) Kettle, J.; Horie, M.; Majewski, L. A.; Saunders, B. R.; Tuladhar, S.; Nelson, J.; Turner, M. L. *Sol. Energy Mater. Sol. Cells* **2011**, *95*, 2186. (b) Albrecht, S.; Janietz, S.; Schindler, W.; Frisch, J.; Kurpiers, J.; Kniepert, J.; Inal, S.; Pingel, P.; Fostiropoulos, K.; Koch, N.; Neher, D. J. *J. Am. Chem. Soc.* **2012**, *134*, 14932. (c) Zhang, Y.; Zou, J.; Cheuh, C.-C.; Yip, H.-L.; Jen, A. K. Y. *Macromolecules* **2012**, *45*, 5427.

[20]   (a) Wang, E.; Hou, L.; Wang, Z.; Hellström, S.; Zhang, F.; Inganäs, O.; Andersson, M. R. *Adv. Mater.* **2010**, *22*, 5240. (b) Kim, Y.; Yeom, H. R.; Kim, J. Y.; Yang, C. *Energy Environ. Sci.* **2013**, *6*, 1909. (c) Chen, H.-C.; Chen, Y.-H.; Liu, C.-H.; Hsu, Y.-H.; Chien, Y.-C.; Chuang, W.-T.; Cheng, C.-Y.; Liu, C.-L.; Chou, S.-W.; Tung, S.-H.; Chou, P.-T. *Polym. Chem.* **2013**, *4*, 3411. (d) Kim, J.-

H.; Song, C. E.; Kim, H. U.; Grimsdale, A. C.; Moon, S.-J.; Shin, W. S.; Choi, S. K.; Hwang, D.-H. *Chem. Mater.* **2013**, *25*, 2722.

[21]   (a) Van Mierloo, S.; Adriaensens, P. J.; Maes, W.; Lutsen, L.; Cleij, T. J.; Botek, E.; Champagne, B.; Vanderzande, D. *J. Org. Chem.* **2010**, *75*, 7202. (b) Van Mierloo, S.; Hadipour, A.; Spijkman, M.-J.; Van den Brande, N.; Ruttens, B.; Kesters, J.; D'Haen, J.; Van Assche, G.; de Leeuw, D. M.; Aernouts, T.; Manca, J.; Lutsen, L.; Vanderzande, D.; Maes, W. *Chem. Mater.* **2012**, *24*, 587. (c) Vanormelingen, W.; Verstappen, P.; Maes, V.; Bevk, D.; Lutsen, L.; Vanderzande, D.; Maes, W. *Synlett* **2013**, *24*, 2389.

[22]   Marin, L.; Lutsen, L.; Vanderzande, D.; Maes, W. *Org. Biomol. Chem.* **2013**, *11*, 5866.

[23]   Shahid, M.; Ashraf, R. S.; Huang, Z.; Kronemeijer, A. J.; McCarthy-Ward, T.; McCulloch, I.; Durrant, J. R.; Sirringhaus, H.; Heeney, M. *J. Mater. Chem.* **2012**, *22*, 12817.

[24]   Marin, L.; Penxten, H.; Van Mierloo, S.; Carleer, R.; Lutsen, L.; Vanderzande, D.; Maes, W. *J. Polym. Sci. A: Polym. Chem.* **2013**, *51*, 4912.

[25]   (a) Danley, R. L.; Caulfield, P. A.; Aubuchon, S. R. *Am. Lab.* **2008**, *40*, 9. (b) Wouters, S.; Demir, F.; Beenaerts, L.; Van Assche, G. *Thermochim. Acta* **2012**, *530*, 64.

[26]   Hedley, G. J.; Ward, A. J.; Alekseev, A.; Howells, C. T.; Martins, E. R.; Serrano, L. A.; Cooke, G.; Ruseckas, A.; Samuel, I. D.W. *Nat. Commun.* **2013**, *4*, 2867.

[27]   (a) Zhao, J.; Swinnen, A.; Van Assche, G.; Manca, J.; Vanderzande, D.; Van Mele, B. *J. Phys. Chem. B* **2009**, *113*, 1587. (b) Demir, F.; Van den Brande, N.; Van Mele, B.; Bertho, S.; Vanderzande, D.; Manca, J.; Van Assche, G. *J. Therm. Anal. Calorim.* **2011**, *105*, 845.

[28]   (a) Jørgensen, M.; Norrman, K.; Krebs, F. C. *Sol. Energy Mater. Sol. Cells* **2008**, *92*, 686. (b) Bertho, S.; Janssen, G.; Cleij, T. J.; Conings, B.; Moons, W.; Gadisa, A.; D'Haen, J.; Goovaerts, E.; Lutsen, L.; Manca, J.; Vanderzande, D. *Sol. Energy Mater. Sol. Cells* **2008**, *92*, 753. (c) Lee, J. U.; Jung, J. W.; Jo, J. W.; Jo, W. H. *J. Mater. Chem.* **2012**, *22*, 24265. (d) Bundgaard, E.; Helgesen, M.; Carlé, J. E.; Krebs, F. C.; Jorgensen, M. *Macromol. Chem. Phys.* **2013**, *214*, 1546.

[29]   (a) Johansson, D. M.; Srdanov, G.; Yu, G.; Theander, M.; Inganas, O.; Andersson, R. M. *Macromolecules* **2000**, *33*, 2525. (b) Vandenbergh, J.; Conings, B.; Bertho, S.; Kesters, J.; Spoltore, D.; Esiner, S.; Zhao, J.; Van Assche, G.; Wienk, M. M.; Maes, W.; Lutsen, L.; Van Mele, B.; Janssen, R. A. J.; Manca, J.; Vanderzande, D. J. M. *Macromolecules* **2011**, *44*, 8470.

[30]   (a) Sivula, K.; Ball, Z. T.; Watanabe, N.; Fréchet, J. M. J. *Adv. Mater.* **2006**, *18*, 206. (b) Lee, J. U.; Jung, J. W.; Emrick, T.; Russell, T. P.; Jo, W. H. *Nanotechnology* **2010**, *21*, 105201. (c) Lee, J. U.; Jung, J. W.; Emrick, T.; Russel, T. P.; Jo, W. H. *J. Mater. Chem.* **2010**, *20*, 3287.

[31]   Lindqvist, C.; Bergqvist, J.; Feng, C.-C.; Gustafsson, S.; Bäcke, O.; Treat, N. D.; Bounioux, C.; Henriksson, P.; Kroon, R.; Wang, E.; Sanz-Velasco, A.; Kristiansen, P. M.; Stingelin, N.; Olsson, E.; Inganäs, O.; Andersson, M. R.; Müller, C. *Adv. Energy Mater.* **2014**, *4*, 1301437.

[32]   Liu, H. W.; Chang, D.-Y.; Chiu, W.-Y.; Rwei, S.-P.; Wang, L. *J. Mater. Chem.* **2012**, *22*, 15586.

[33]   (a) Krebs, F. C.; Spanggaard, H. *Chem. Mater.* **2005**, *17*, 5235. (b) Petersen, M. H.; Gevorgyan, S. A.; Krebs, F. C. *Macromolecules* **2008**, *41*, 8986.

[34]   (a) Tanenbaum, D. M.; Hermenau, M.; Voroshazi, E.; Lloyd, M. T.; Galagan, Y.; Zimmermann, B.; Hösel, M.; Dam, H. F.; Jørgensen, M.; Gevorgyan, S. A.; Kudret, S.; Maes, W.; Lutsen, L.; Vanderzande, D.; Würfel, U.; Andriessen,

R.; Rösch, R.; Hoppe, H.; Lira-Cantu, M.; Rivaton, A.; Uzunoğlu, G. Y.; Germack, D.; Andreasen, B.; Madsen, M. V.; Norrman, K.; Krebs, F. C. *RSC Adv.* **2012**, *2*, 882. (b) Bertho, S.; Campo, B.; Piersimoni, F.; Spoltore, D.; D'Haen, J.; Lutsen, L.; Maes, W.; Vanderzande, D.; Manca, J. *Sol. Energy Mater. Sol. Cells* **2013**, *110*, 69. (c) Kesters, J.; Kudret, S.; Bertho, S.; Van den Brande, N.; Defour, M.; Van Mele, B.; Penxten, H.; Lutsen, L.; Manca, J.; Vanderzande, D. J. M.; Maes, W. *Org. Electron.* **2014**, *15*, 549.

[35]   (a) Griffini, G.; Douglas, J. D.; Piliego, C.; Holcombe, T. W.; Turri, S.; Fréchet, J. M. J.; Mynar, J. L. *Adv. Mater.* **2011**, *23*, 1660. (b) Carlé, J. E.; Andreasen, B.; Tromholt, T.; Madsen, M. V.; Norrman, K.; Jørgensen, M.; Krebs, F. C. *J. Mater. Chem.* **2012**, *22*, 24417.

[36]   Cardinaletti, I.; Kesters, J.; Bertho, S.; Conings, B.; Piersimoni, F.; D'Haen, J.; Lutsen, L.; Nesladek, M.; Van Mele, B.; Van Assche, G.; Vandewal, K.; Salleo, A.; Vanderzande, D.; Maes, W.; Manca, J. V. *J. Photon. Energy* **2014**, *4*, 040997.

[37]   Reese, M. O.; Gevorgyan, S. A.; Jørgensen, M.; Bundgaard, E.; Kurtz, S. R.; Ginley, D. S.; Olson, D. C.; Lloyd, M. R.; Morvillo, P.; Katz, E. A.; Elschner, A.; Haillant, O.; Currier, T. R.; Shrotriya, V.; Hermenau, M.; Riede, M.; Kirov, K. R.; Trimmel, G.; Rath, T.; Inganäs, O.; Zhang, F.; Andersson, M.; Tvingstedt, K.; Lira-Cantu, M.; Laird, D.; McGuiness, C.; Gowrisanker, S. J.; Pannone, M.; Xiao, M.; Hauch, J.; Steim, R.; DeLongchamp, D. M.; Rösch, R.; Hoppe, H.; Espinosa, N.; Urbina, A.; Yaman-Uzunoglu, G.; Bonekamp, J.-B.; van Breemen, A. J. J. M.; Girotto, C.; Voroshazi, E.; Krebs, F. C. *Sol. Energy Mater. Sol. Cells* **2011**, *95*, 1253.

[38]   (a) Peters, C. H.; Sachs-Quintana, I. T.; Kastrop, J. P.; Beaupré, S.; Leclerc, M.; McGehee, M. D. *Adv. Energy Mater.* **2011**, *1*, 491. (b) Peters, C. H.;

Sachs-Quintana, I. T.; Mateker, W. R.; Heumueller, T.; Rivnay, J.; Noriega, R.; Beiley, Z. M.; Hoke, E. T.; Salleo, A.; McGehee, M. D. *Adv. Mater.* **2012**, *24*, 663. (c) Mateker, W. R.; Douglas, J. D.; Cabanetos, C.; Sachs-Quintana, I. T.; Bartelt, J. A.; Hoke, E. T.; Labban, A. E.; Beaujuge, P. M.; Fréchet, J. M. J.; McGehee, M. D. *Energy Environ. Sci.* **2013**, *6*, 2529. (d) Sachs-Quintana, I. T.; Heumüller, T.; Mateker, W. R.; Orozco, D. E.; Cheacharoen, R.; Sweetnam, S.; Brabec, C. J.; McGehee, M. D. *Adv. Funct. Mater.* **2014**, *24*, 3978.

[39]   (a) Heumueller, T.; Mateker, W. R.; Sachs-Quintana, I. T.; Vandewal, K.; Bartelt, J. A.; Burke, T. M.; Ameri, T.; Brabec, C. J.; McGehee, M. D. *Energy Environ. Sci.* **2014**, *7*, 2974. (b) Voroshazi, E.; Cardinaletti, I.; Conard, T.; Rand, B. P. *Adv. Energy Mater.* DOI:10.1002/aenm.201400848.

[40]   (a) Manceau, M.; Bundgaard, E.; Carlé, J. E.; Hagemann, O.; Helgesen, M.; Søndergaard, R.; Jørgensen, M.; Krebs, F. C. *J. Mater. Chem.* **2011**, *21*, 4132. (b) Carlé, J. E.; Helgesen, M.; Zawacka, N. K.; Madsen, M. V.; Bundgaard, E.; Krebs, F. C. *J. Polym. Sci. B: Polym. Phys.* **2014**, *52*, 893.

[41]   (a) Bard, J.; Faulkner, L. R. *Electrochemical methods: fundamentals and applications*, 2nd Ed., 2001, Wiley. (b) Trasatti, S. *Pure Appl. Chem.* **1986**, *58*, 955.

[42]   Dutta, G. K.; Kim, T.; Choi, H.; Lee, J.; Kim, D. S.; Kim, J. Y.; Yang, C. *Polym. Chem.* **2014**, *5*, 2540.

4.6 ACKNOWLEDGEMENTS

4.7 SUPPORTING INFORMATION

## 4.7.1   Analytical size exclusion chromatograms
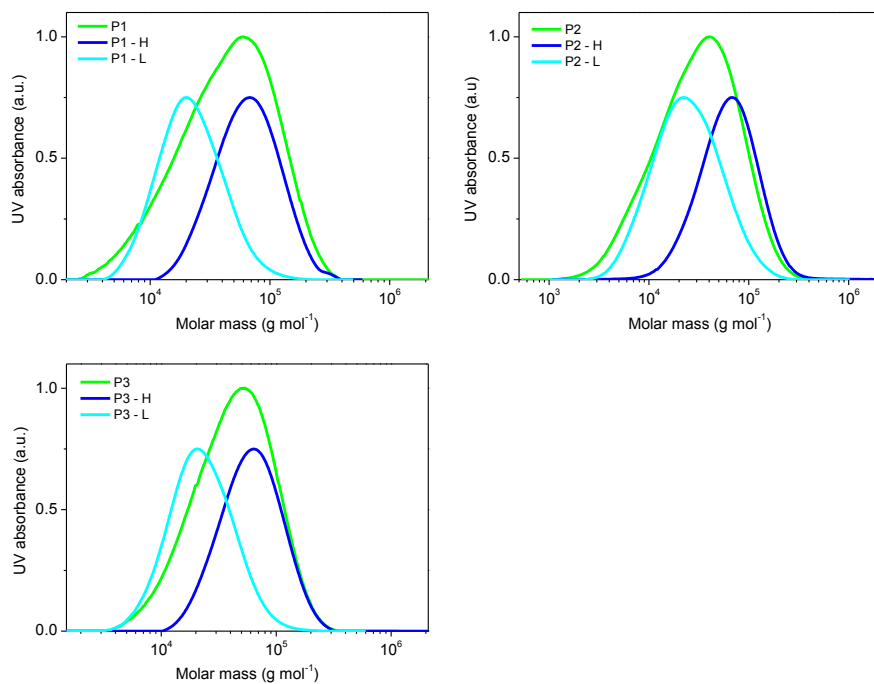
Figure S1: Analytical size exclusion chromatograms (THF, 40 °C, UV detection at 254 nm) of the crude copolymers (after Soxhlet extractions) and their low (denoted with **-L**) and high (denoted with **-H**) molar mass fractions as obtained after fractionation by prep-SEC.
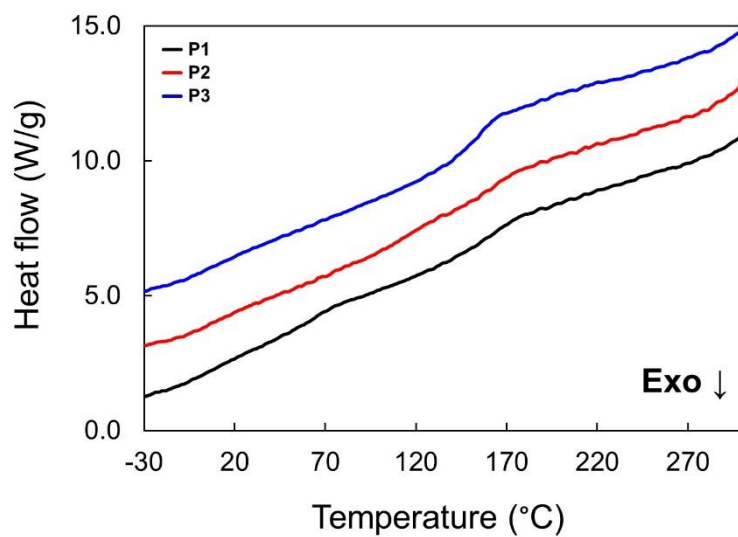
4.7.2 Thermal analysis
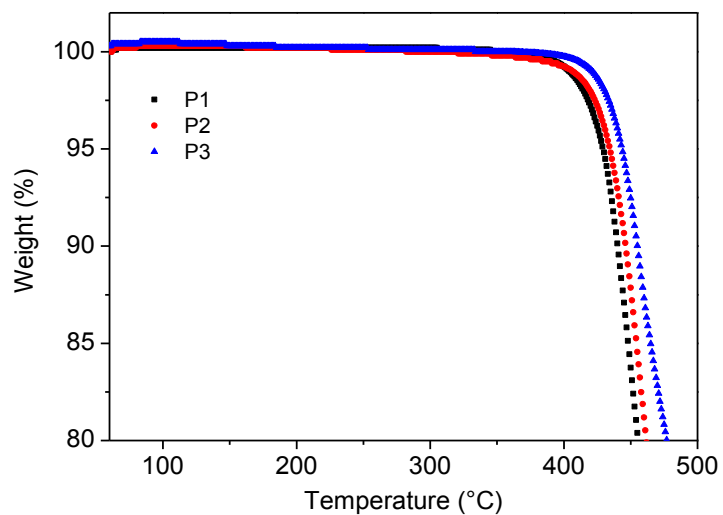
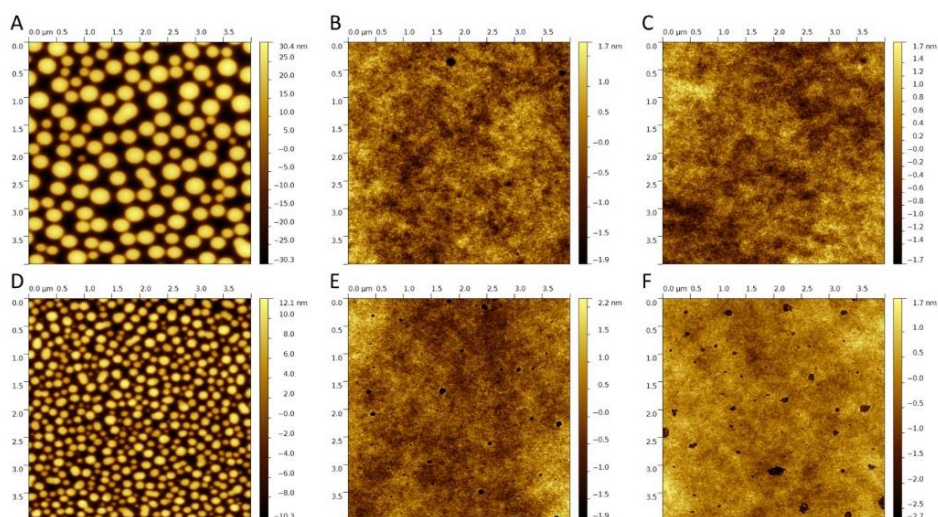**Figure S2:** TGA profiles for the three PCPDTQx(2F) copolymers.
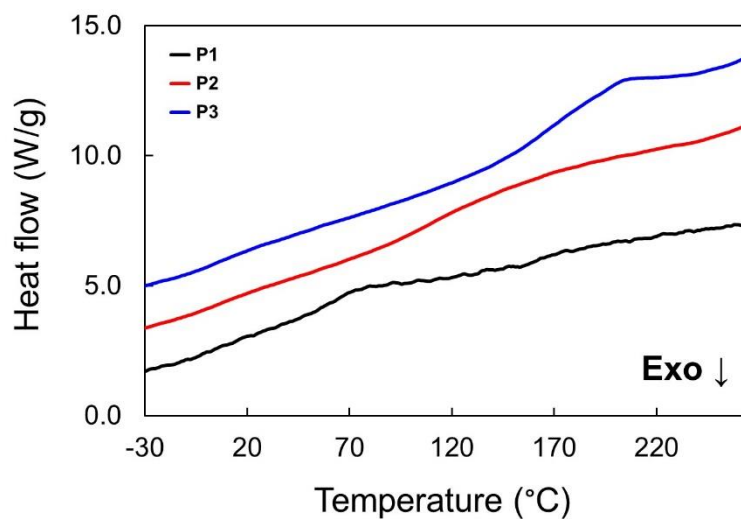
Figure S3: RHC profiles for the three PCPDTQx(2F) copolymers (curves shifted vertically for clarity).
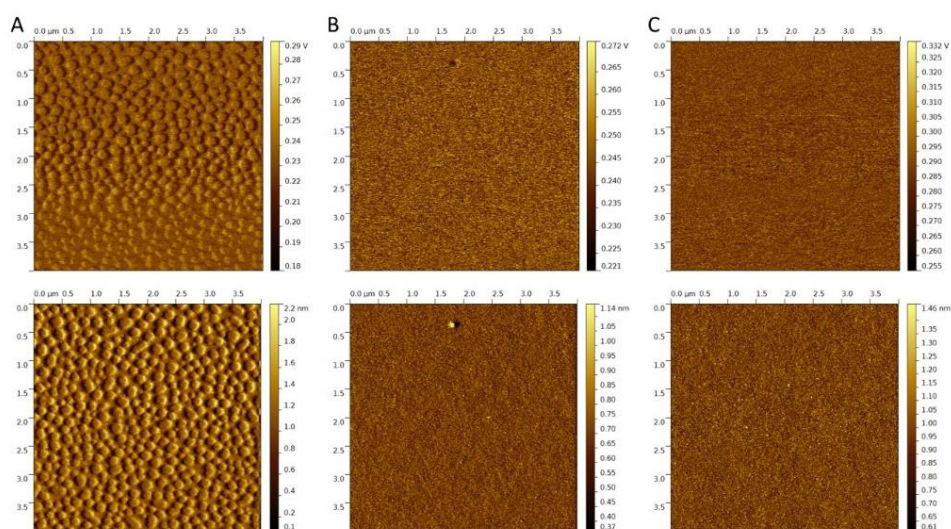
Figure S4: RHC profiles for the three optimum copolymer:PC$_{71}$BM blends: **P1**:PC$_{71}$BM 1:2.5 (black line), **P2**:PC$_{71}$BM 1:3.5 (red line), and **P3**:PC$_{71}$BM 1:3 (blue line) (curves shifted vertically for clarity).

4.7.3 AFM images

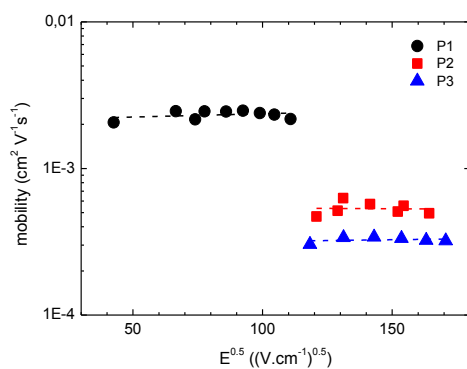**Figure S5:** AFM topography images (4x4 μm) of the active layers of the polymer solar cells based on: A) **P1** in CB, B) **P2** in CF, C) **P3** in CF, D) **P1** in CB + 3% CN, E) **P2** in CF +10% ODCB, and F) **P3** in CF + 10% ODCB.
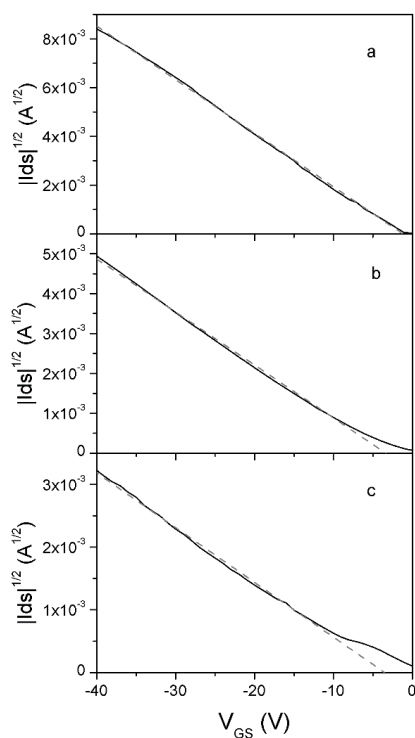

Figure S6: AFM DMT modulus (upper row) and deformation (lower row) images of the active layers of the polymer solar cells based on: A) **P1** in CB + 3% CN, B) **P2** in CF, and C) **P3** in CF.

4.7.4 Mobility data

Figure S7: Photo-CELIV measurements on photovoltaic devices for the three PCPDTQx(2F) copolymers.

Figure S8: Transfer curves (solid lines) for FETs of the pure donor polymers **P1** (a), **P2** (b), and **P3** (c). The measurements were performed in saturation regime at V_{DS} = -40 V. The dotted lines were used to fit the mobilities.

4.7.5 Optimization of the solar cell performance for each polymer

Table S1: Optimization of the solar cell devices based on **P1.**

Processing solvent[a]	Polymer: $PC_{71}BM$ ratio	V_{oc} (V)	J_{sc} (mA cm^{-2})	FF	Average η (%)[b]	Best η (%)
CF	1:3	0.73	5.63	0.48	1.98	2.42
CF + 10% ODCB	1:3	0.81	8.46	0.53	3.63	3.78
CF + 3% CN	1:3	0.82	7.92	0.57	3.65	4.07
CB	1:3	0.78	5.55	0.53	2.28	2.49
CB + 3% CN	1:2.5	0.83	10.39	0.56	4.86	5.26
CB + 3% CN	1:3	0.82	8.56	0.56	3.91	4.48
CB + 3% CN	1:3.5	0.80	8.15	0.55	3.57	3.72

[a] CF = chloroform, ODCB = *ortho*-dichlorobenzene, CN = 1-chloronaphthalene, CB = chlorobenzene. [b] Average values over at least 4 devices.

Table S2: Optimization of the solar cell devices based on **P2.**

| Processing solvent[a]	Polymer: $PC_{71}BM$ ratio	V_{oc} (V)	J_{sc} (mA cm^{-2})	FF	Average η (%)[b]	Best η (%)
CF[c]	1:2.5	0.80	11.29	0.51	4.65	4.92
CF	1:3	0.77	11.36	0.57	5.02	5.24
CF[d]	1:3.5	0.78	12.73	0.51	5.11	5.46
CF + 10% ODCB	1:3	0.78	10.60	0.54	4.47	4.74
CF + 3% CN	1:3	0.78	10.37	0.53	4.26	4.90
CB	1:3	0.77	11.48	0.57	5.04	5.20
CB + 3% CN[e]	1:3	0.77	10.22	0.49	3.82	4.13

[a] CF = chloroform, ODCB = *ortho*-dichlorobenzene, CN = 1-chloronaphthalene, CB = chlorobenzene. [b] Average values over at least 4 devices. [c] polymer concentration 6 mg/mL. [d] polymer concentration 4.5 mg/mL. [e] polymer concentration 7 mg/mL.

**Table S3:** Optimization of the solar cell devices based on **P3.**

Processing solvent[a]	Polymer: PC$_{71}$BM ratio	V_{oc} (V)	J_{sc} (mA cm^{-2})	FF	Average η (%)[b]	Best η (%)
CF[c]	1:2.5	0.80	11.69	0.50	4.70	4.96
CF	1:3	0.78	11.43	0.51	4.55	5.09
CF[d]	1:3.5	0.78	11.44	0.51	4.53	4.86
CF + 10% ODCB	1:3	0.77	11.63	0.52	4.65	4.76
CF + 3% CN	1:3	0.77	11.69	0.50	4.52	4.70
CB	1:3	0.78	11.79	0.51	4.72	5.11
CB + 3% CN[e]	1:3	0.76	11.51	0.52	4.52	4.91
CB + 3% DIO	1:3	0.76	9.75	0.50	3.69	4.19

[a] CF = chloroform, ODCB = *ortho*-dichlorobenzene, CN = 1-chloronaphthalene, CB = chlorobenzene. [b] Average values over at least 4 devices. [c] polymer concentration 6 mg/mL. [d] polymer concentration 4.5 mg/mL. [e] polymer concentration 7 mg/mL.

4.7.6   Additional degradation data
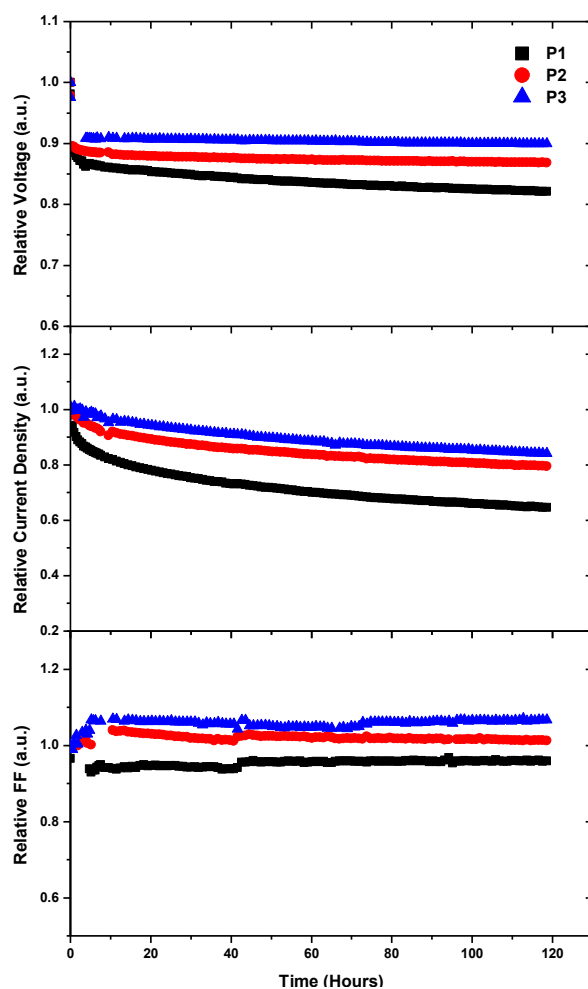
Figure S9: Degradation profiles (V_{oc}, J_{sc} and FF) for the PCPDTQx(2F):PC$_{71}$BM solar cells heated at 85 °C for 120 hours. The curves are normalized to the first measurement point at 85 °C.
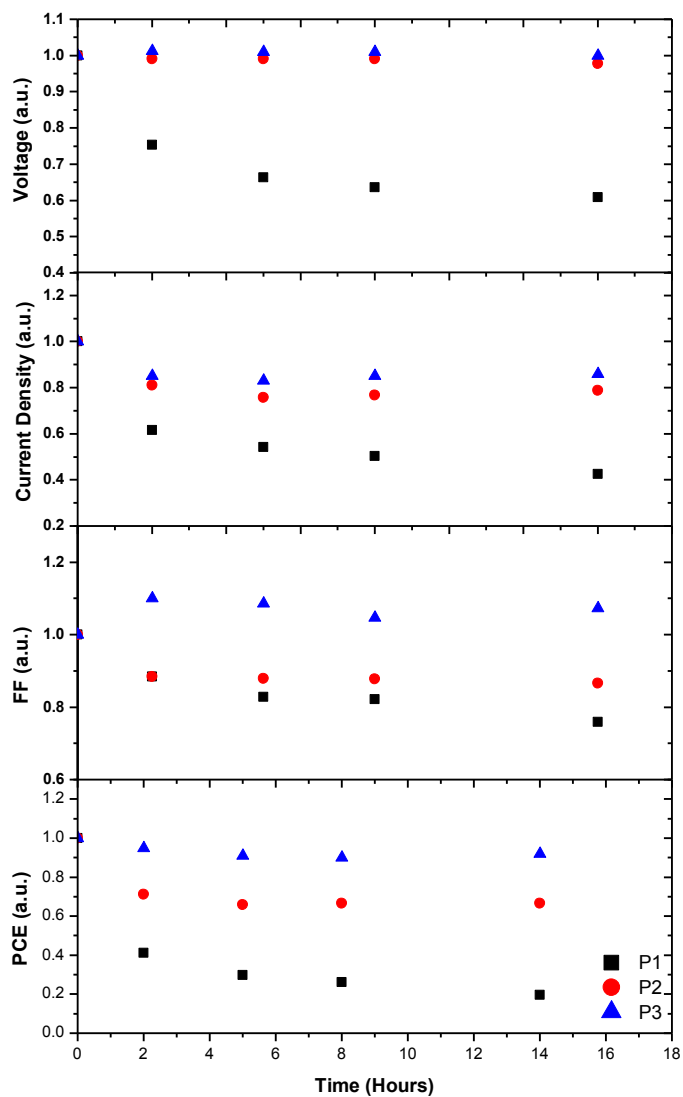
Figure S10: Degradation profiles (V_{oc}, J_{sc}, FF, and PCE) for the PCPDTQx(2F):PC$_{71}$BM solar cells heated at 120 °C for 14 hours. The curves are normalized to the first measurement point at 120 °C.
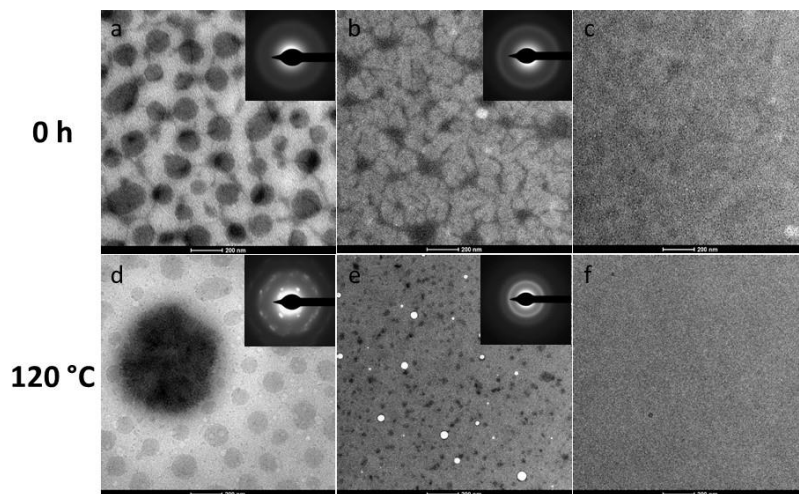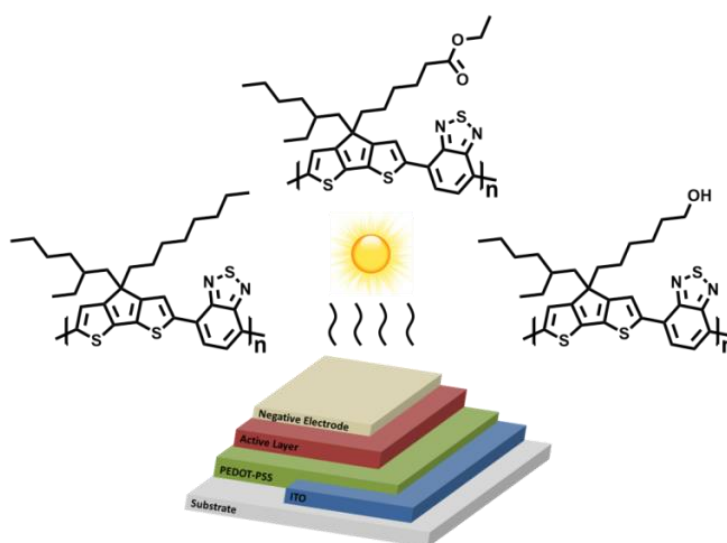
Figure S11: TEM images (with SAED inserts) of the active layers of pristine and aged (14 h at 120 °C) **P1**−**P3**:PC$_{71}$BM polymer solar cells.

Chapter 5

Enhanced Organic Solar Cell Stability by Polymer (PCPDTBT) Side Chain Functionalization

ABSTRACT

Organic photovoltaics represent a promising thin-film solar cell technology with appealing mechanical, aesthetical and cost features. In recent years, a strong growth in power conversion efficiency (to over 10%) has been realized for organic solar cells through extensive material and device research. To be competitive in the renewable energy market, further improvements are mandatory though, both with respect to efficiency and lifetime. High intrinsic stability of the photoactive layer is obviously a crucial requirement for long lifetimes, but the generally applied bulk heterojunction blends and their components are prone to light-induced and thermal degradation processes. In the present contribution, the high-T_g polymer strategy is combined with specific side chain functionalization to address the thermal stability of polymer solar cells. These two design concepts are applied to a prototype low bandgap copolymer, PCPDTBT. Accelerated aging tests (at 85 °C) indicate an improved thermal durability of the PCPDTBT:PC$_{71}$BM blends and the resulting devices by the insertion of ester or alcohol moieties on the polymer side chains. The different stages in the efficiency decay profiles are addressed by dedicated experiments to elucidate the (simultaneously occurring) degradation mechanisms.

5.1 INTRODUCTION

Over the past two decades, organic photovoltaics (OPV) have evolved into an attractive solar energy technology.[1] Besides the general advantages of thin-film photovoltaics – reduced weight, flexibility and (semi-)transparency – organic solar cells show additional interesting features such as improved low-light performance, narrow band widths, design freedom (color and uniformity), and compatibility to large scale (roll-to-roll) printing techniques, further decreasing production costs. At present, power conversion efficiencies (PCE's) in the range of 10% have been achieved for single junction solution-processed OPV devices through simultaneous photoactive material, interlayer and device optimization.[2] However, for OPV to become an economically viable technology, with projected integration in (energy neutral) buildings, vehicles and specific fast-deployable consumer goods, further leaps forward are required with respect to both efficiency and stability. Improving the lifetime of organic solar cells has for a long time been underexposed compared to the chase for enhanced efficiencies, but the field has recently caught up with a number of encouraging results in terms of durability.[3] A first important step was taken by the concept of inverted solar cells, procuring P3HT:PC$_{61}$BM devices retaining 90% of their initial performance for over 1.5 years under exposure to direct sunlight.[4] Optimization of the charge transport layers was also performed to increase device stability. Doping PEDOT:PSS with WO$_x$ was shown to provide more efficient and durable devices, with only 5% reduced performance over 5000 hours in ambient conditions.[5] On the opposite side of the (standard) organic solar cell stack, Ca, which is sensitive to oxidation,[6] was replaced by an n-type TiO$_x$ buffer layer, affording devices which are more resistant to the intrusion of oxygen and moisture.[7] The bulk heterojunction (BHJ) photoactive layer at the heart of

an organic solar cell is one of the most challenging components to optimize for improved device lifetime. Even when properly encapsulated, keeping oxygen and moisture out of the device as much as possible, intrinsic active layer degradation can be induced by light or by the elevated temperatures imposed by continued exposure to sunlight.[8] Photochemical (oxidative) degradation of the active layer (polymer) materials and blends is examined extensively within the group of Gardette and Rivaton, suggesting rearrangements of the chemical structures, the formation of oxidation products, crosslinking and chain scissions as the main malefactors.[9]

In this work, the main focus lies on the thermal degradation of the active layer donor:acceptor blend in polymer:fullerene BHJ solar cells. Under the influence of elevated temperatures, reorganization of the active layer components may occur, depending on the glass transition temperature (T_g) of the blend (components). The peak-performing active layer nanomorphology, a finely intermixed interpenetrating network of the electron donor and acceptor compounds, gradually changes during device operation, whether it be through diffusion and demixing (depending on the T_g), degradation of the bulk materials or interface-related processes. For the workhorse P3HT:PC$_{61}$BM combination, operating at an optimal polymer:fullerene ratio of 1:0.8, it has been observed that the fullerene material diffuses into microcrystals upon heating the blend (well) above 60 °C (i.e. above the T_g of the P3HT:PC$_{61}$BM blend[10]), leading to a near-to-complete phase separation and strongly reduced device efficiency.[11] Important insights on the thermal stabilization of OPV materials and devices were obtained within the McGehee group at Stanford.[12] They emphasized the importance of material purity when aiming for long-term stability of polymer solar cells.[12c] Additionally, through the investigation of polymer:fullerene blends at temperatures above the

T_g of the polymer, it was found that a thin polymer layer is formed at the interface between the active layer and the top electrode, thereby lowering the device performance over time.[12d] To alleviate (or at least slow down) polymer solar cell degradation under thermal stress, various approaches to 'freeze in' the top-performing BHJ blend (nano)morphology have been explored in the past years, including, amongst others, thermocleavage of the solubilizing side chains,[13] the use of non-crystalline fullerene additives,[14] compatibilizers[15] or the addition of nucleating agents[16]. Another acknowledged pathway involves the synthesis of polymer materials with a higher T_g, resulting in more rigid polymer:fullerene blends, hindering fullerene diffusion and crystallization and hence procuring OPV devices with longer lifetimes.[11b,17] Thermal stabilization of the photoactive blend has also been achieved through the application of (photo)crosslinkable polymer and/or fullerene derivatives.[18]

In previous work, we have noted a remarkable improvement of the intrinsic stability of the OPV active layer blend morphology by the incorporation of functional moieties (ester, alcohol or cinnamoyl) on the side chains of P3HT-based copolymers, even for fairly low built-in ratios (5–15%) and without crosslinking to covalently anchor the polymer and/or fullerene molecules.[19] Moreover, these alterations did not influence the initial PCE to a large extent. As such, this approach can be regarded as an attractive paradigm for OPV active layer stability. In this manuscript, this concept is extended to a proof-of-concept low bandgap copolymer, PCPDTBT, simultaneously targeting high efficiency and improved (thermal) stability by combining the high-T_g and side chain functionalization strategies. PCPDTBT (poly{4,4-dialkyl-4H-cyclopenta[2,1-b;3,4-b']dithiophene-2,6-diyl-alt-2,1,3-benzothiadiazole-4,7-diyl}) has attracted quite some interest from the OPV community as it was the first push-pull low bandgap copolymer,

with an extended absorption beyond 800 nm, affording a PCE above 5% in polymer solar cells.[20,21] Despite the high initial PCE, the applicability of PCPDTBT in OPV is hampered by its rapidly decreasing performance under thermal stress (during operation or annealing), and only preliminary efforts were made to improve the device lifetime.[22] PCPDTBT copolymers containing crosslinkable functional groups at the end of the alkyl side chains were synthesized and the resulting polymer solar cells displayed an enhanced stability under ambient conditions[22a] or during light-soaking aging[22b] experiments. Based on the reasonable efficiency of PCPDTBT-based solar cells, the limited intrinsic stability of these devices and our previously established synthetic procedures toward smooth CPDT side chain variation (vide infra), PCPDTBT was regarded as an ideal test case for our hypothesis of combined high efficiency and improved lifetime by polymer side chain modification.

5.2 RESULTS AND DISCUSSION

5.2.1 Synthesis and characterization

Functionalization of the alkyl side chains on 4,4-dialkyl-4*H*-cyclopenta[2,1-*b*;3,4-*b'*]dithiophene (CPDT) derivatives has been performed by several research groups for specific purposes.[22-25] Bazan and co-workers introduced ionic groups to achieve conjugated poly- and oligoelectrolytes.[23] The introduction of functional groups has also been prevailed as a tool to alter the solubility of the resulting conjugated polymers, enabling processing from more benign solvents.[24] The Müllen group introduced double bonds in the alkyl side chains of PCPDTBT to tune the packing and solubility of this material.[25] In all of the examples mentioned above, symmetrically functionalized CPDT moieties were obtained through

application of the rather tedious classical CPDT synthesis route.[26] Our group previously developed two shortened, convenient synthetic protocols, which additionally allow smooth asymmetric alkyl side chain substitution. In 2010, a three-step synthetic strategy – (i) synthesis of 3-bromo-2,2'-bithiophene by a Kumada coupling, (ii) lithiation and subsequent reaction with a ketone to afford a dialkylated tertiary alcohol derivative, and (iii) Friedel-Crafts dehydration cyclization – toward 4,4-dialkyl-CPDT building blocks was reported.[27] Although this procedure provides straightforward access to asymmetrically dialkylated (functionalized) CPDT's, it suffers from relatively low yields for more bulky side chain patterns. Therefore, an alternative synthesis protocol was developed.[28] In this approach, the first side chain is introduced by a Wittig-type carbonyl olefination reaction between 4*H*-cyclopenta[2,1-*b*:3,4-*b*']dithiophen-4-one and an alkylidenetriphenylphosphorane, yielding a 4-alkylidene-4*H*-cyclopenta[2,1-*b*:3,4-*b*']dithiophene (e.g. compound **1** in Scheme 1). Subsequently, the second side chain is introduced via regioselective reductive alkylation of the exocyclic double bond. In this way, asymmetric substitution is easily achieved and for both steps the products can be isolated in reasonably high yields (>70%), hence favoring the Wittig route as the most versatile procedure for asymmetric CPDT side chain functionalization.

Based on the previously employed series of side chain functionalized poly(3-alkylthiophene)s,[19c] it was envisaged to introduce ester and alcohol groups at the end of one of the CPDT alkyl side chains, and an asymmetrically dialkylated CPDT derivative was synthesized as a reference compound. Both the alcohol and ester moieties enable further side chain variation by different pre- or post-polymerization functional group interconversions. The synthetic strategy affording the monomers and final polymers is depicted in Scheme 1.
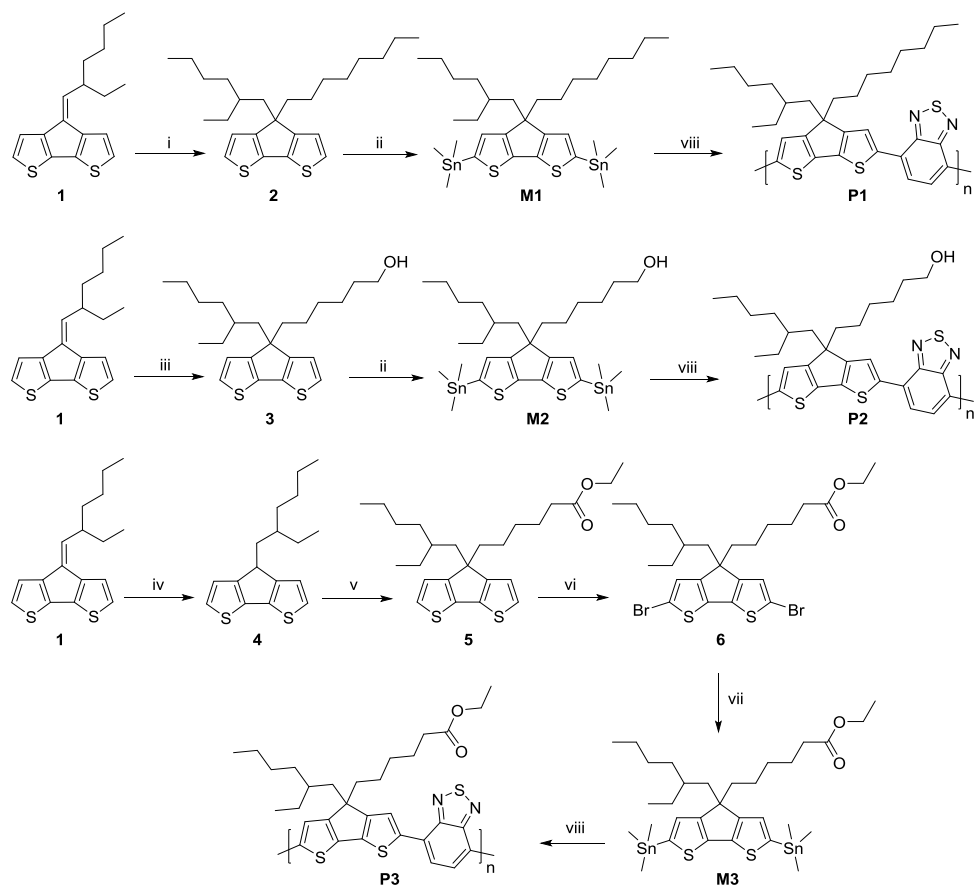
Scheme 1: Synthesis of the different CPDT monomers and PCPDTBT polymers:
i) LiAlH$_4$, n-octylbromide, THF; ii) n-BuLi, Me$_3$SnCl, THF; iii) A: LiAlH$_4$, (6-bromohexyloxy)triisopropylsilane, THF; B: TBAF, THF; iv) LiAlH$_4$, THF; v) A: t-BuOK, 6-bromohexanoic acid, KI, DMSO; B: EtOH, H$_2$SO$_4$; vi) NBS, CHCl$_3$; vii) hexamethylditin, LiCl, Pd(PPh$_3$)$_4$, toluene; viii) 4,7-dibromo-2,1,3-benzothiadiazole, Pd$_2$(dba)$_3$, P(o-tol)$_3$, toluene/DMF 4/1, 110 °C, 15 h.

In a first step, 4-(2'-ethylhexylidene)-4H-cyclopenta[2,1-b:3,4-b']dithiophene (**1**) was reductively alkylated to obtain the asymmetrically dialkylated CPDT's **2** and **3**.[28] For compound **3**, the alcohol functional group had to be protected (as a silyl ether) during this step. Next, both building blocks were stannylated via lithiation and reaction with trimethyltin chloride, affording the required CPDT monomers

M1 and **M2**. For the ester-functionalized monomer **M3**, a slightly adapted procedure had to be followed. Attempts to protect the ester functional group as an ortho-ester or 2-alkyl-1,3-oxazoline failed. On the other hand, milder reducing agents such as $NaBH_4$ and DIBAL were not capable of reducing the exocyclic double bond. Therefore, the double bond was first reduced with $LiAlH_4$ in a separate step. Alkylation was then performed with 6-bromohexanoate instead of ethyl 6-bromohexanoate to avoid competition between the bromide and the ester groups in the nucleophilic substitution reaction. After the alkylation reaction, the obtained carboxylic acid functionalized CPDT was immediately transformed to the ethyl ester analogue **5** via an acid-catalyzed esterification in ethanol. The ester-functionalized CPDT was also synthesized via the older three-step route,[27a] but purification was less straightforward in this case. Ester-CPDT **5** was dibrominated and further converted to monomer **M3** via stannylation with hexamethylditin in the presence of $Pd(PPh_3)_4$.

Since monomer purity is crucial to obtain high molar mass species in polycondensation-type polymerization reactions, all three CPDT monomers were further purified by preparative recycling size exclusion chromatography (prep-SEC). After Stille polymerization with 4,7-dibromo-2,1,3-benzothiadiazole (BT), the PCPDTBT copolymers were purified by soxhlet extractions with methanol, acetone, n-hexane and chloroform, respectively. All three polymers were collected with chloroform and the low molar mass fractions of polymers **P1** and **P3** were removed via prep-SEC. Due to its limited solubility in chloroform, alcohol-functionalized PCPDTBT copolymer **P2** could not be subjected to prep-SEC. The number average molar masses (M_n) and polydispersity indices (PDI) of the polymers are gathered in Table 1. While the molar masses of **P1** and **P3** were reasonably high, a relatively low value was obtained for **P2**.

Table 1: Molar mass, thermal and electrochemical data for PCPDTBT copolymers **P1**–**P3**.

| Polymer	M_n[a] [kDa]	PDI[a]	T_g[b] [°C]	HOMO[c] [eV]	LUMO[c] [eV]	E_g^{OP}[d] [eV]
P1	26	3.2	174	-5.09	-3.34	1.40
P2	13	2.5	198	-4.95	-3.36	1.40
P3	46	1.7	161	-4.95	-3.41	1.37

[a] Determined by analytical SEC using polystyrene standards in THF at 40 °C. [b] Determined by RHC. [c] Determined by CV from the onset of oxidation/reduction. [d] Optical bandgap, as determined by the onset of the solid-state UV-Vis spectra.

The thermal transitions of the three novel copolymers were investigated via rapid heat-cool calorimetry (RHC),[29] preferred above regular differential scanning calorimetry (DSC) because of its increased sensitivity to thermal transitions (as a result of the fast scanning rates) and the low sample amounts required. The glass transition temperatures were determined to be 174, 198 and 161 °C for **P1**–**P3**, respectively (Figure S1), and no melting transitions could be observed, suggesting a highly amorphous polymer nature. The (very) high T_g values for the three copolymers, well above the ISOS-3 temperature of 85 °C employed for standard aging tests,[30] suggest a minor influence of T_g during OPV device stability tests. In this respect, it has to be mentioned that, despite its huge importance for device stability, there is a noteworthy lack of (accurate) T_g values for (OPV) low bandgap copolymers in literature.

The HOMO and LUMO energy levels of the PCPDTBT alternating copolymers were estimated via cyclic voltammetry (CV) from the onset of the oxidation and reduction peaks, respectively. The frontier molecular orbital energy levels of the functionalized copolymers **P2** and **P3** show comparable values to the reference polymer **P1**. Normalized UV-Vis absorption spectra in solution and thin film for the

three copolymers are shown in Figure 1. In all cases, the absorption extends to the near-IR region of the solar spectrum and the profiles are very similar, even more so in thin film. Therefore, it can be concluded that modification of the side chains does not influence the opto-electronic solid-state properties of the PCPDTBT copolymers to a large extent. The functional groups do seem to influence (i.e. to reduce) the aggregation tendency of the polymers in solution, as the long-wavelength shoulder is affected by the presence and the nature of the functional groups.
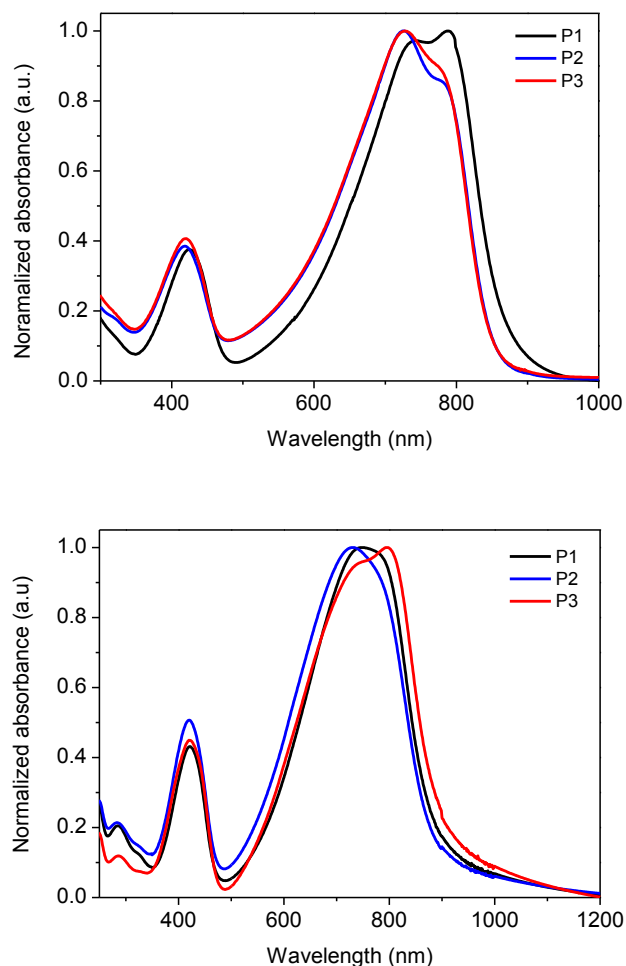
Figure 1: Normalized UV-Vis absorption spectra for the three PCPDTBT
copolymers in chloroform solution (top) and thin film (bottom).

5.2.2 Polymer solar cells

To evaluate the influence of the side chain modification on photovoltaic
performance, polymer solar cells were prepared using the standard architecture
glass/ITO/PEDOT:PSS/active layer/Ca/Al. For the photoactive layers, blend
solutions were prepared in a 1:3 ratio with $PC_{71}BM$. Whereas **P1** and **P3** could
readily be dissolved in chloroform (CF), polymer **P2** required a mixture of *ortho-*

dichlorobenzene (oDCB) and 4% of N-methylpyrrolidone (NMP) due to its higher aggregation tendency. Nonetheless, as evidenced by the I-V parameters summarized in Table 2 and Figure 2, the incorporation of the functional moieties on the PCPDTBT side chains hardly affected the average PCE's. The slightly lower performance for **P2** might be attributed to the lower M_n for this material and/or the addition of NMP to the blend solution, affecting mainly the short-circuit current density (Jsc) and resulting in a slightly lower average PCE of 2.05% (in comparison to 2.46% for the reference device). The solar cells based on ester-functionalized copolymer **P3** showed an enhanced fill factor (FF) (from 43−44% to 49%), combined with a slightly reduced open-circuit voltage (Voc) (from 0.59 to 0.56 V). In literature, optimized device efficiencies up to 5.5% were obtained for PCPDTBT:PC$_{71}$BM through the addition of 1,8-octanedithiol (ODT) as an additive to the active layer blend solution.[20] Recent work indicated, however, that even though the initial performance can be enhanced significantly by inclusion of the additive, the lifetime of these solar cells decreased more rapidly under light-soaking conditions.[22c] To avoid complications due to the effect of (different optimal) additives and to isolate the influence of the side chain moieties, the use of additives was omitted during these studies.

Table 2: Photovoltaic parameters for the pristine solar cell devices based on PCPDTBT copolymers **P1**−**P3**.

Material	Processing solvent	V_{OC} [V]	J_{SC} [mA cm^{-2}]	FF	Best PCE [%]	Average PCE [a)] [%]
P1	CF	0.59	9.49	0.44	2.76	2.46
P2	oDCB + 4% NMP	0.59	7.94	0.43	2.43	2.05
P3	CF	0.56	9.12	0.49	3.21	2.50

[a)]Averages were taken across 16−20 devices, with an active area of 3 mm².
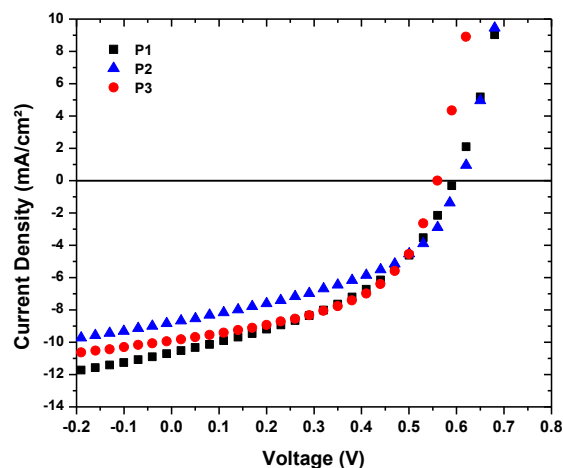
Figure 2: *J-V* curves for the best solar cell devices produced from the **P1**−**P3**:PC$_{71}$BM(1:3) blends.

In the external quantum efficiency (EQE) spectra, photocurrent generation over a broad wavelength range, up to 900 nm, was observed (Figure 3). The **P2**:PC$_{71}$BM device showed lower EQE values, in line with the lower J_{SC} observed in the *I-V* measurements, in particular in the spectral range where the polymer contribution is seen. The integrated current densities (J_{EQE}'s) correspond rather well with the measured J_{SC}'s, in line with standard measurement deviations.
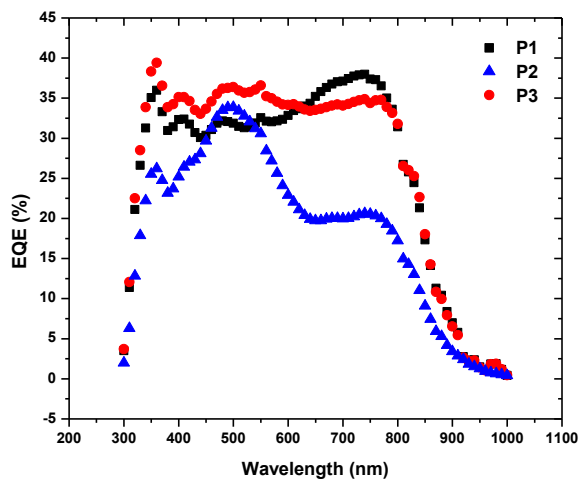
Figure 3: EQE spectra for the solar cell devices based on **P1**−**P3** (measured Jsc's: 10.01, 7.81 and 11.08 mA cm^{-2}; J_{EQE}'s: 10.49, 7.33 and 10.67 mA cm^{-2} for **P1**, **P2** and **P3**, respectively).

5.2.3 Photovoltaic behavior under prolonged thermal stress

In a next step, the solar cells were mounted in an automated degradation chamber and subdued to a precisely controlled temperature of 85 °C for 650 hours, with I-V measurements at predetermined intervals to investigate the progression of the photovoltaic parameters over time. The temperature chosen for this accelerated aging test was instigated by the ISOS-3 standards and the desire to stay well below the T_g of all materials.[30] All three PCPDTBT:PC$_{71}$BM polymer solar cells showed a strong initial drop in efficiency (within the first 50 hours), followed by a more 'linear' degradation regime for the remainder of the lifetime experiment (Figure 4; separate Jsc, Voc and FF profiles in Figure S2). After 150 hours of exposure to 85 °C, more indicative differences in relative PCE's are revealed. The **P1**:PC$_{71}$BM reference device still exhibits a rather steep slope, resulting in a final PCE diminished to 26% of its initial value after 650 hours. In contrast, the relative efficiencies of the polymer solar cells based on side chain functionalized PCPDTBT

copolymers **P2** and **P3** remain more stable after the initial 'burn-in' phase (vide infra), with values of 53 and 40% of the starting performance after 650 hours, respectively.
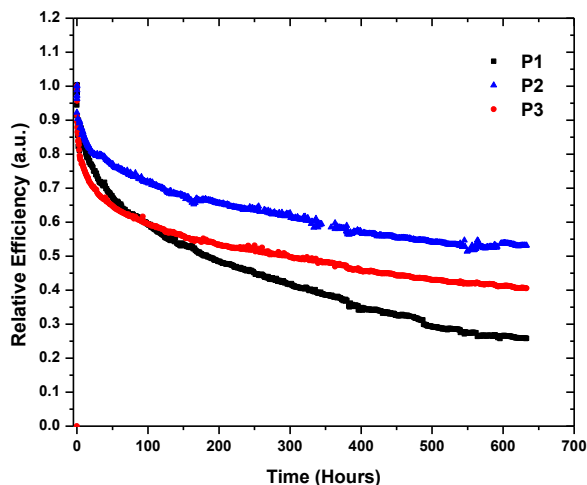
Figure 4: Relative efficiency decay profiles for the three PCPDTBT:PC_{71}BM polymer solar cells upon exposure to a temperature of 85 °C for 650 h. The curves are normalized to the first measurement point at 85 °C.

For P3HT:PC_{61}BM BHJ OPV devices, a similar thermal stress results in the appearance of a multitude of crystalline structures in the photoactive layer, indicative of diffusion and phase separation of the polymer donor and fullerene acceptor.[11] Polythiophene side chain functionalization (by ester and in particular alcohol moieties) was shown to reduce this crystallization and demixing tendency considerably, thereby diminishing the efficiency drop.[19b,c] To analyze the BHJ blend nanomorphology of the PCPDTBT:PC_{71}BM polymer solar cells and its evolution over time, transmission electron microscopy (TEM) and atomic force microscopy (AFM) imaging was performed (Figure 5 and 6). For the pristine solar cells from ester-PCPDTBT **P3**, a slightly different bulk morphology and topography (increased peak to peak distance and somewhat higher roughness, Table S1) was

observed, possibly corroborating with the slightly reduced Voc and higher FF (Table 2). After exposure of the devices to a temperature of 85 °C for 650 hours, no crystallization or large demixing was observed (Figure 5 and 6), which can be linked to the high T_g's of all copolymers and, as a result, the high T_g's of the polymer:fullerene active layer blends. The T_g's of the blends were also determined by RHC and they were found at 143, 158 and 148 °C for the **P1**−**P3**:PC$_{71}$BM (1:3) blends, respectively (Figure S1). These values are all below the T_g's of the separate blend components (174, 198 and 161 °C for **P1**−**P3**, respectively, and 170 °C for PC$_{71}$BM). The TEM-selected area electron diffraction (SAED) patterns show no formation of crystalline structures in the films, not even after 650 hours of aging (Figure 5). For completeness, TEM was also performed on similarly prepared films exposed for 3 hours to a temperature of 220 °C on a hotplate in the dark, i.e. above the T_g of all individual polymers and polymer:PC$_{71}$BM blends (Figure 5 and S3). Obviously, the PEDOT:PSS layer and the top electrode are not resistant to such elevated temperatures, and device characterization is not representative. Nevertheless, crystallization and extensive phase separation did occur at this temperature, although not in equal amounts for the three different blends. The most deteriorated active layer morphology was found for the **P1**:PC$_{71}$BM reference system, followed by **P3**:PC$_{71}$BM and finally **P2**:PC$_{71}$BM, in line with the relative efficiency decay profiles as observed at 85 °C (Figure 4). Additionally, SAED for the **P1**:PC$_{71}$BM blend revealed the presence of microcrystals in the center of the 'aggregated' domains (as illustrated in more detail in Figure S3). Noteworthy, the amount of phase separation varies quite strongly, even though the T_g's of the blends are similar, indicating that the incorporation of the functional moieties enhances the resistivity of the blends toward diffusion and crystallization (of PC$_{71}$BM).
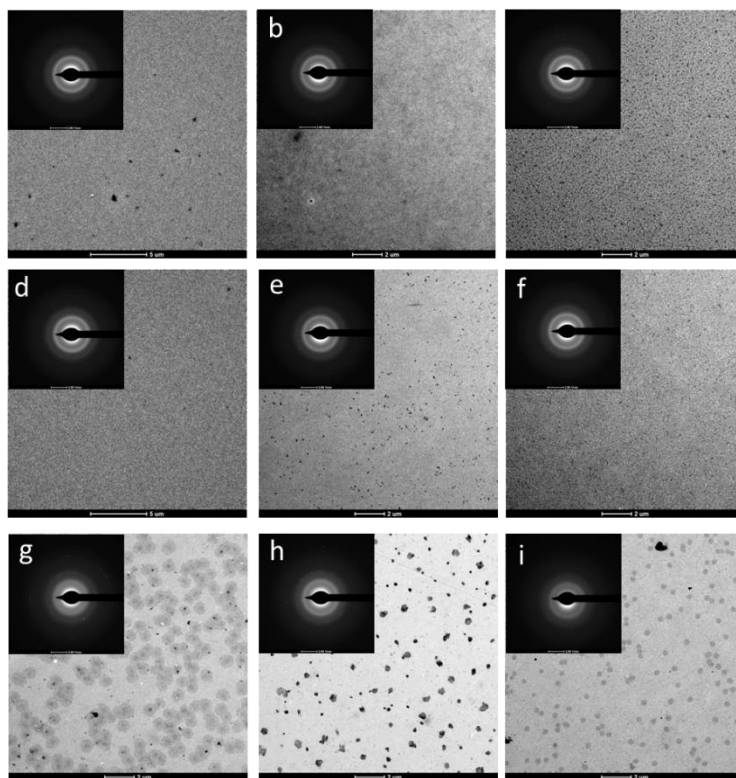
Figure 5: TEM images for **P1**:PC$_{71}$BM (a, d, g), **P2**:PC$_{71}$BM (b, e, h) and **P3**:PC$_{71}$BM (c, f, i) BHJ blends annealed at 85 °C for 0 h (top row), 85 °C for 650 h (middle row) and 220 °C for 3 h (bottom row).
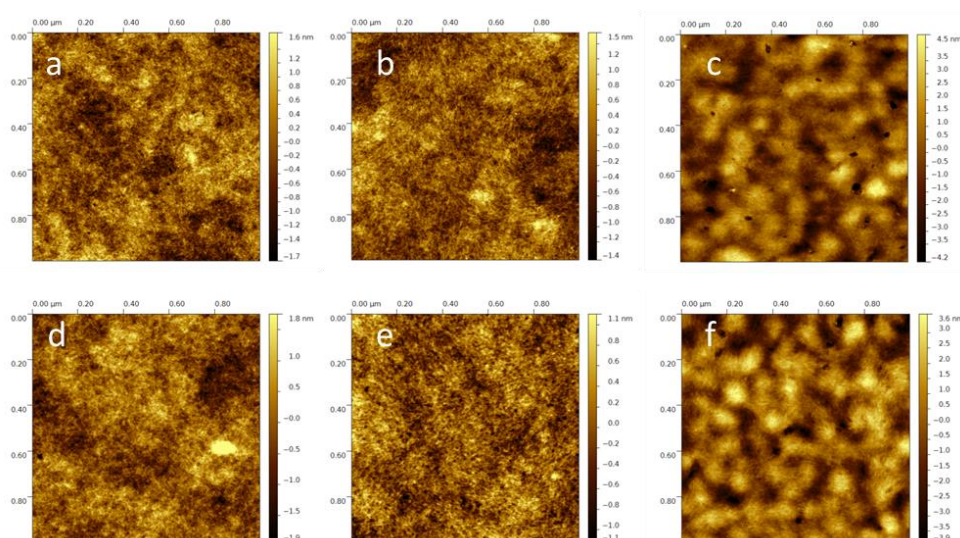
Figure 6: AFM images for **P1**:PC$_{71}$BM (a, d), **P2**:PC$_{71}$BM (b, e,) and **P3**:PC$_{71}$BM (c, f) polymer solar cells before (top row) and after (bottom row) thermal aging for 650 h at 85 °C.

Last year, the groups of Durrant and Manca independently reported on the light-induced dimerization of fullerenes, hindering phase separation in polymer:fullerene systems.[31] As our aging experiments require frequent exposure to light (measurement intervals of 5 minutes for the initial phase, with a total sweep time of approximately 4 minutes over 16 devices, followed by intervals up to 1 hour at later stages), light and thermally-induced effects might intermix, especially in the initial phase of the degradation experiment. To address this concern, a new set of solar cell samples was prepared which were continuously annealed at 85 °C in the dark (on a hotplate) prior to the *I-V* measurements. After 150 hours, the non-illuminated samples still did not show any crystallites, as confirmed by TEM (Figure S4), suggesting that the specific nature of the thermal stabilization effect originates from a different (i.e. non-light-induced) mechanism.

More detailed investigation of the degradation profiles allows for a further deconvolution of the degradation process(es) occurring in the thermally stressed PCPDTBT:PC$_{71}$BM photovoltaic devices. The exponential efficiency decay within the first 100 hours of the aging experiment can be attributed to the combination of a rapid decay in the Voc (reducing by 20%) and a more drawn-out decrease in Jsc, resulting in an overall strong reduction of the PCE (by 30% for **P2** and up to 40% for **P1** and **P3**). The strong initial loss in Voc is higher for **P3** than for **P1** and **P2**, explaining the stronger initial PCE decay for the device based on the ester-functionalized copolymer (Figure 4). This initial strong efficiency drop has been referred to as the 'burn-in' phase.[12] The McGehee group has recently provided more thorough understandings of the initial Voc loss and the burn-in stage through light-induced aging of several polymer:fullerene systems, including both crystalline and amorphous polymers.[12e] The fast initial loss in Voc was found to be characteristic for amorphous systems (such as the PCPDTBT polymer under investigation here), whereas light-induced traps, as revealed by transient photocurrent measurements, were observed for both material types upon aging. Related work by Voroshazi *et al.* on the light soaking of PCDTBT:PC$_{71}$BM devices revealed that the initial Voc could almost completely be recovered through re-deposition of the top electrode after the aging experiment, supporting the hypothesis of light-induced traps.[32] Consequently, as the initial phase of our aging experiment is characterized by frequent exposure to light, additional mechanisms (i.e. light soaking) other than those induced by pure thermal stress are likely to affect the overall degradation process. To shed more light on this, a set of PCPDTBT:PC$_{71}$BM samples was exposed to 85 °C in a dark environment. This control experiment revealed that the initial reduction in Voc was almost non-existent in comparison with the results obtained from the automated degradation

chamber (PCE drop <5% vs 20%) (Table S2), confirming the attribution of the burn-in phase to a light-induced (Voc loss) effect. Exclusion of the light-induced effects does, however, not clarify the continuous reduction in Jsc, with observable differences for the **P1**−**P3** copolymers, indicating other mechanisms must be present.

It is generally known that the quality of the interface between the active layer and the top electrode is worsening when applying external stress factors, thereby leading to a reduced charge extraction. Plausible causes reported in literature include the delamination of the top electrode and the creation of voids or electrically insulating patches at the interface.[33] To investigate the active layer-top electrode interface, the three different PCPDTBT:PC$_{71}$BM films were exposed to 85 °C for 85 hours in the dark prior to electrode deposition (since the standard solar cell architecture employed in this work did not allow for smooth peeling off of the top electrode). Simultaneously, 12 operational devices were processed from the same batch solutions to grant I-V results comparable with the pristine solar cells. As summarized in Table 3, comparison of the average Jsc's of the blend films degraded with and without Ca/Al top electrodes revealed a less pronounced decay for the latter. After 85 hours at 85 °C in the dark, no reduction in Voc was observed, supporting the previous findings. Moreover, the Jsc showed a relatively small decay, to approximately 92% of the initial Jsc for all three copolymers (in comparison to the average Jsc of the 12 pristine devices). The resulting PCE's remained at 90, 92 and 85% of their starting values, demonstrating the strong influence of the thermal treatment on the quality of the interface between the active layer and the top electrode. The slightly lower performance of the device based on ester-PCPDTBT **P3** could be ascribed to the (stronger) loss in FF. Combination of all gathered data suggests that the relative difference in

performance stability within the **P1**−**P3** copolymer series as observed in the initial degradation experiment can possibly be ascribed to a higher resistance of **P2**, and to a lesser extent **P3**, to diminishing active layer-top electrode interface quality upon thermal stress.

Table 3: Comparison of the pristine photovoltaic devices based on copolymers **P1**−**P3** with devices containing a post-evaporated (Ca/Al) top electrode after exposure to 85 °C for 85 h in the dark.

Polymer	Treatment	V_{OC} [V]	J_{SC} [mA cm^{-2}]	FF	Average PCE[a] [%]
P1	pristine	0.59	9.26	0.44	2.38
P1	85h at 85 °C + post-evap	0.59	8.64	0.42	2.15
P2	pristine	0.59	7.83	0.43	1.98
P2	85h at 85 °C + post-evap	0.59	7.23	0.43	1.82
P3	pristine	0.56	8.98	0.47	2.38
P3	85h at 85 °C + post-evap	0.56	8.50	0.42	2.02

[a]Averages were taken across 4−8 devices, with an active area of 3 mm².

5.3 CONCLUSIONS

A small series of side chain functionalized PCPDTBT low bandgap copolymers was efficiently prepared with the general aim to improve the intrinsic thermal stability of the photovoltaic devices based on these donor materials, while maintaining the power conversion efficiency for standard PCPDTBT:PC$_{71}$BM polymer solar cells. Accelerated aging tests at a temperature of 85 °C showed that the stability of the photovoltaic cells under prolonged thermal stress was enhanced by the insertion of ester or alcohol moieties on the CPDT side chains, with the best results being obtained for the alcohol-functionalized PCPDTBT derivative. A relative efficiency up to 55% of its starting value could be maintained after 650 hours at 85 °C, whereas the reference device exhibited a relative performance of only 26%. TEM

and AFM imaging revealed the absence of (extensive) phase separation and crystallization after the aging experiment at 85 °C, which can be attributed to the high T_g's of the PCPDTBT-type copolymers and the corresponding photoactive layer blends, obviating crosslinking approaches. Stepwise examination of some of the various possible degradation pathways revealed that the decay in photovoltaic performance can be attributed to a combination of light-induced and thermal processes, resulting (amongst others) in a decrease of the active layer-top electrode interface quality. Further efforts in our group will be directed toward the extension of the presented functionalized side chain method to alternative high(er) performance low bandgap copolymers. Additionally, the degradation behavior of encapsulated devices in climate chamber conditions will be addressed, in combination with an in-depth analysis of the mechanism(s) governing the deteriorating interface quality upon continued thermal stress. On the other hand, the observed differences in light-induced burn-in (stronger for the ester-functionalized PCPDTBT) are worth a closer look as well.

The presented work emphasizes the importance of polymer (side chain) engineering as a powerful tool to improve the lifetime of polymer solar cells. Long-term stability will be a conditio sine qua non for OPV to survive in the harsh battle for market share with alternative PV technologies. In this respect, the booming field of perovskite-based hybrid solar cells can be considered a serious competitor, albeit also struggling with durability issues.[34] Improved thermal stability is also mandatory if OPV is to take benefit from its positive temperature coefficient, attractive for energy harvesting under extreme (e.g. aerospace) conditions.

5.4 EXPERIMENTAL SECTION

5.4.1   Materials and instruments

Preparative (recycling) size exclusion chromatography (prep-SEC) was performed on a JAI LC-9110 NEXT system equipped with JAIGEL 1*H*, 2*H* and 3*H* columns (eluent CHCl$_3$, flow rate 3.5 mL min^{-1}). NMR chemical shifts (δ, in ppm) were determined relative to the residual CHCl$_3$ (7.26 ppm) absorption or the ^{13}C resonance shift of CDCl$_3$ (77.16 ppm). High resolution electrospray ionization mass spectrometry (ESI-MS) was performed using an LTQ Orbitrap Velos Pro mass spectrometer equipped with an atmospheric pressure ionization source operating in the nebulizer assisted electrospray mode. The instrument was calibrated in the *m/z* range 220−2000 using a standard solution containing caffeine, MRFA and Ultramark 1621. MALDI-TOF spectra were recorded on a Bruker Daltonics Ultraflex II Tof/Tof. 1 µL of the matrix solution (4 mg mL^{-1} DTCB (*trans*-2-[3-(4-*tert*-butylphenyl)-2-methyl-2-propenylidene]malononitrile) in CHCl$_3$) was spotted onto an MTP Anchorchip 600/384 MALDI plate. The spot was allowed to dry and 1 µL of the analyte solution (0.5 mg mL^{-1} in CHCl$_3$) was spotted on top of the matrix. Reported masses are the 100% intensity peaks of the isotopic distributions. UV-Vis measurements were performed on a VARIAN Cary 500 UV-Vis-NIR spectrophotometer at a scan rate of 600 nm/min. The films for the UV-Vis measurements were prepared by drop casting a solution of the polymer in chloroform on a quartz substrate. The solid-state UV-Vis spectra were used to estimate the optical band gaps (from the wavelength at the intersection of the tangent line drawn at the low energy side of the absorption spectrum with the x-axis: E_g (eV) = 1240/(wavelength in nm)). Analysis of the molar masses and molar mass distributions of the polymers was performed on a Tosoh EcoSEC

System, comprising of an autosampler, a PSS guard column SDV (50 x 7.5 mm), followed by three PSS SDV analytical linear XL columns (5 μm, 300 x 7.5 mm), and a UV detector using THF as the eluent at 40 °C with a flow rate of 1.0 mL/min. The SEC system was calibrated using linear narrow polystyrene standards ranging from 474 to 7.5×10^6 g mol^{-1} (K = 14.1×10^{-5} dL g^{-1} and α = 0.70). Rapid heat-cool calorimetry (RHC) experiments were performed on a prototype RHC of TA Instruments, equipped with liquid nitrogen cooling and specifically designed for operation at high scanning rates.[29,35] RHC measurements were performed at 500 K min^{-1} in aluminum crucibles, using helium (10 mL min^{-1}) as a purge gas. Electrochemical measurements (cyclic voltammetry) were performed with an Eco Chemie Autolab PGSTAT 30 potentiostat/galvanostat using a three-electrode microcell with a platinum working electrode, a platinum counter electrode and a Ag/AgNO$_3$ reference electrode (silver wire dipped in a solution of 0.01 M AgNO$_3$ and 0.1 M NBu$_4$PF$_6$ in anhydrous acetonitrile). The reference electrode was calibrated against ferrocene/ferrocenium as an external standard. Samples were prepared by dip coating the platinum working electrode in the respective polymer solutions (also used for the solid-state UV-Vis measurements). The CV measurements were done on the resulting films with 0.1 M NBu$_4$PF$_6$ in anhydrous acetonitrile as electrolyte solution. To prevent air from entering the system, the experiments were carried out under a curtain of argon. Cyclic voltammograms were recorded at a scan rate of 100 mV s^{-1}. For the conversion of V to eV, the onset potentials of the first oxidation/reduction peaks were used and referenced to ferrocene/ferrocenium, which has an ionization potential of -4.98 eV *vs.* vacuum. This correction factor is based on a value of 0.31 eV for Fc/Fc$^+$ *vs.* SCE[36a] and a value of 4.68 eV for SCE *vs.* vacuum[36b]: $E_{HOMO/LUMO}$ (eV) = -4.98 - $E_{onset\ ox/red}^{Ag/AgNO3}$ (V) + $E_{onset\ Fc/Fc+}^{Ag/AgNO3}$ (V).

5.4.2 OPV device fabrication and characterization

Bulk heterojunction polymer solar cells were prepared using the standard architecture substrate/ITO/PEDOT:PSS/polymer:$PC_{71}BM$/Ca/Al. Prior to device processing, the ITO-coated substrates (100 nm, Kintec, Sheet resistivity 20 Ω/sq) were subjected to a standard cleaning procedure using soap, demineralized water, acetone and isopropanol, followed by a UV/O_3 treatment for 15 min. Subsequently, PEDOT:PSS was deposited via spin-coating with a thickness of approximately 30 nm. Afterwards, the samples were transferred to a glove box containing a nitrogen atmosphere and an annealing step was performed at 130 °C for 15 min to remove any residual water. In a next step, the PCPDTBT:$PC_{71}BM$ (Solenne) layers were deposited through spin-coating. The blend solutions were prepared in a 1:3 ratio polymer:$PC_{71}BM$, with total concentrations of 12, 16 and 32 mg mL^{-1} for **P1**, **P2** and **P3**, respectively. Whereas **P1** and **P2** could readily be dissolved in pure chloroform, **P3** required a mixture of o-dichlorobenzene and NMP (4 v/v%). Finally, the devices were finished by evaporation of the top electrodes Ca and Al, with layer thicknesses of ~30 and 80 nm, respectively, at a pressure of 2 x 10^{-6} mbar. In this way, devices with an active area of 3 mm² were obtained. Initial device performance measurements were done using a Newport class A solar simulator (model 91195A), calibrated with a silicon solar cell to give an AM 1.5G spectrum. EQE measurements were performed with a Newport Apex illuminator (100 W xenon lamp, 6257) as a light source, a Newport Cornerstone 130° monochromator, and a Stanford SR830 lock-in amplifier for the current measurements. A silicon FDS100-CAL photodiode was employed as a reference cell.

5.4.3 Solar cell degradation under thermal stress

To investigate the thermal degradation behavior, the solar cells were positioned in an automated degradation chamber in nitrogen atmosphere (glove box) with a constant temperature of 85 °C. The *I-V* characteristics were measured at regular time intervals (initially every 5 min, later on every hour) using a White 5500 K LED (Lamina). Duplo experiments on identically processed samples were performed to confirm the findings. Dedicated degradation experiments focusing either on the absence of light or aging without the presence of top electrodes were performed using a hotplate (280 x 200 mm, type PZ28-2ET, Harry Gestigkeit GmbH, with a PR5 programmer controller).

5.4.4 TEM and AFM characterization

TEM measurements were performed on a FEI Tecnai Spirit using an accelerating voltage of 120 kV. TEM samples were prepared from devices placed in the dark utilizing a hotplate to initiate thermal degradation or, in the case of the accelerated aging test over 650 hours, from the devices utilized in the automated degradation chamber. By washing away the PEDOT:PSS layer with water, freestanding films were obtained. For AFM imaging, a Bruker Multimode 8 AFM was used in PeakForce tapping mode, employing ScanAsyst. The images were produced with a silicon tip on a nitride lever with a spring constant of 4 N m^{-1}.

5.5 REFERENCES

[1]   a) B. Kippelen, J.-L. Brédas, *Energy Environ. Sci.* **2009**, *2*, 251; b) Y. Su, S. Lan, K. Wei, *Mater. Today* **2012**, *15*, 554; c) L. Dou, J. You, Z. Hong, Z. Xu, G. Li, R. A. Street, Y. Yang, *Adv. Mater.* **2013**, *25*, 6642; d) S. Lizin, S. Van Passel, E. De Schepper, W. Maes, L. Lutsen, J. Manca, D. Vanderzande, *Energy Environ. Sci.* **2013**, *6*, 3136.

[2]   a) Z. C. He, C. M. Zhong, S. J. Su, M Xu, H. B. Wu, Y. Cao, *Nat. Photonics* **2012**, *6*, 591; b) A. K. K. Kyaw, D. H. Wang, D. Wynands, J. Zhang, T. -Q. Nguyen, G. C. Bazan, A. J. Heeger, *Nano Lett.* **2013**, *13*, 3796; c) K. H. Hendriks, G. H. L. Heintges, S. Gevaerts, M. M. Wienk, R. A. J. Janssen, *Angew. Chem.* **2013**, *125*, 8499; *Angew. Chem. Int. Ed.* **2013**, *52*, 8341; d) C. Cabanetos, A. E. Labban, J. A. Bartelt, J. D. Douglas, W. M. Mateker, J. M. Fréchet, M. D. McGehee, P. M. Beaujuge, *J. Am. Chem. Soc.* **2013**, *135*, 4556; e) Y. Liu, Y. Yang, C.-C. Chen, Q. Chen, L. Dou, Z. Hong, G. Li, Y. Yang, *Adv. Mater.* **2013**, *25*, 4657; f) W. Zhang, Y. Wu, Q. Bao, F. Gao, J. Fang, *Adv. Energy Mater.* **2014**, *4*, 1400359; g) B. Kan, Q. Zhang, M. Li, X. Wan, W. Ni, G. Long, Y. Wang, X. Yang, H. Feng, Y. Chen, *J. Am. Chem. Soc.* **2014**, *136*, 15529; h) Y. Liu, J. Zhao, Z. Li, C. Mu, W. Ma, H. Hu, K. Jiang, H. Lin, H. Ade, H. Yan, *Nat. Commun.*, **2014**, *5*, 5293.

 [3]   a) N Grossiord, J. M. Kroon, R. Andriessen, P. W. M. Blom, *Org. Electron.* **2012**, *13*, 432; b) M. Jorgensen, K. Norrman, S. A. Gevorgyan, T. Tromholt, B. Andreasen, F. C. Krebs, *Adv. Mater.* **2012**, *24*, 580; c) M. Manceau, A. Rivaton, J.-L. Gardette, *Photochemical stability of materials for OPV*, in *Stability and Degradation of Organic and Polymer Solar Cells* (Ed: F. C. Krebs), Wiley, **2012**, 71; d) S. K. Gupta, K. Dharmalingam, L. S. Pali, S. Rastogi, A. Singh, A. Garg,

Nanomater. Energy **2013**, *2*, 42; e) R. Roesch, K.-R. Eberhardt, S. Engmann, G. Gobsch, H. Hoppe, *Sol. Energy Mater. Sol. Cells* **2013**, *117*, 59; f) H. Cao, W. He, Y. Mao, X. Lin, K. Ishikawa, J. H. Dickerson, W. P. Hess, *J. Power Sources* **2014**, *264*, 168; g) D. Angmo, P. M. Sommeling, R. Gupta, M. Hösel, S. A. Gevorgyan, J. M. Kroon, G. U. Kulkarni, F. C. Krebs, *Adv. Eng. Mater.* **2014**, *16*, 8.

[4]   a) F. C. Krebs, *Sol. Energy Mater. Sol. Cells* **2008**, *92*, 715; b) B. Zimmermann, U. Würfel, M. Niggemann, *Sol. Energy Mater. Sol. Cells* **2009**, *93*, 491.

[5]   A. Kanwat, J. Jang, *J. Mater. Chem. C.* **2014**, *2*, 901.

[6]   a) S. Gevorgyan, M. Jørgensen, F. C. Krebs, K.O. Sylvester-Hvid, *Sol. Energy Mater. Sol. Cells* **2011**, *95*, 1389; b) R. Rösch, D. M. Tanenbaum, M. Jørgensen, M. Sealand, M. Barenklau, M. Hermenau, E. Voroshazi, M. T. Lloyd, Y. Galagan, B. Zimmermann, U. Würfel, M. Hösel, H. F. Dam, S. Gevorgyan, S. Kudret, W. Maes, L. Lutsen, D. Vanderzande, R. Andriessen, M. Teran-Escobar, M. Lira-Cantu, A. Rivaton, G. Y. Uzunoglu, D. Germack, B. Andreasen, M. V. Madsen, K. Norrman, H. Hoppe, F. C. Krebs, *Energy Environ. Sci.* **2012**, *5*, 6521.

[7]   K. Lee, J. Y. Kim, S. H. Park, S. H. Kim, S. Cho, A. J. Heeger, *Adv. Mater.* **2007**, *19*, 2445.

[8]   I. Cardinaletti, J. Kesters, S. Bertho, B. Conings, F. Piersimoni, J. D'Haen, L. Lutsen, M. Nesladek, B. Van Mele, G. Van Assche, K. Vandewal, A. Salleo, D. Vanderzande, W. Maes, J. V. Manca, *J. Photon. Energy* **2014**, *4*, 040997.

[9]   a) J.-L. Gardette, *Fundamental and technical aspects of the photooxidation of polymers*, in *Handbook of Polymer Degradation*, 2nd Edn., Vol. 1 (Ed: S. H. Hamid), Marcel Dekker, New York, **2000**, 671; b) A. Tournebize, P.-O. Bussière, A. Rivaton, J.-L. Gardette, H. Medlej, R. C. Hiorns, C. Dagron-Lartigau, F. C. Krebs, K. Norrman, *Chem. Mater.* **2013**, *25*, 4522; c) A.

Tournebize, P.-O. Bussière, P. Wong-Wah-Chung, S. Thérias, A. Rivaton, J.-L. Gardette, S. Beaupré, M. Leclerc, *Adv. Energy Mater.* **2013**, *3*, 478; d) A. Rivaton, A. Tournebize, J. Gaume, P.-O. Bussière, J.-L. Gardette, S. Thérias, *Polym. Int.* **2014**, *63*, 1335.

[10]   a) J. Zhao, A. Swinnen, G. Van Assche, J. Manca, D. Vanderzande, B. Van Mele, *J. Phys. Chem. B* **2009**, *113*, 1587; b) F. Demir, N. Van den Brande, B. Van Mele, S. Bertho, D. Vanderzande, J. Manca, G. Van Assche, *J. Therm. Anal. Calorim.* **2011**, *105*, 845.

[11]   a) M. Jorgensen, K. Norrman, F. C. Krebs, *Sol. Energy Mater. Sol. Cells* **2008**, *92*, 686; b) S. Bertho, G. Janssen, T. J. Cleij, B. Conings, W. Moons, A. Gadisa, J. D'Haen, E. Goovaerts, L. Lutsen, J. Manca, D. Vanderzande, *Sol. Energy Mater. Sol. Cells* **2008**, *92*, 753; c) J. U. Lee, J. W. Jung, J. W. Jo, W. H. Jo, *J. Mater. Chem.* **2012**, *22*, 24265; d) E. Bundgaard, M. Helgesen, J. E. Carlé, F. C. Krebs, M. Jorgensen, *Macromol. Chem. Phys.* **2013**, *214*, 1546.

[12]   a) C. H. Peters, I. T. Sachs-Quintana, J. P. Kastrop, S. Beaupré, M. Leclerc, M. D. McGehee, *Adv. Energy Mater.* **2011**, *1*, 491; b) C. H. Peters, I. T. Sachs-Quintana, W. R. Mateker, T. Heumueller, J. Rivnay, R. Noriega, Z. M. Beiley, E. T. Hoke, A. Salleo, M. D. McGehee, *Adv. Mater.* **2012**, *24*, 663; c) W. R. Mateker, J. D. Douglas, C. Cabanetos, I. T. Sachs-Quintana, J. A. Bartelt, E. T. Hoke, A. E. Labban, P. M. Beaujuge, J. M. J. Fréchet, M. D. McGehee, *Energy Environ. Sci.* **2013**, *6*, 2529; d) I. T. Sachs-Quintana, T. Heumüller, W. R. Mateker, D. E. Orozco, R. Cheacharoen, S. Sweetnam, C. J. Brabec, M. D. McGehee, *Adv. Funct. Mater.* **2014**, *24*, 3978; e) T. Heumueller, W. R. Mateker, I. T. Sachs-Quintana, K. Vandewal, J. A. Bartelt, T. M. Burke, T. Ameri, C. J. Brabec, M. D. McGehee, *Energy Environ. Sci.* **2014**, *7*, 2974.

[13]   a) F. C.Krebs, H. Spanggaard, *Chem. Mater.* **2005**, *17*, 5235; b) M. H. Petersen, S. A. Gevorgyan, F. C. Krebs, *Macromolecules* **2008**, *41*, 8986.

[14]   H. W. Liu, D. Y. Chang, W. Y. S. P. Chiu Rwei, L. Wang, *J. Mater. Chem.* **2012**, *22*, 15586.

[15]   a) K. Sivula, Z. T. Ball, N. Watanabe, J. M. J. Fréchet, *Adv. Mater.* **2006**, *18*, 206; b) J. U. Lee, J. W. Jung, T. Emrick, T. P. Russell, W. H. Jo, *Nanotechnology* **2010**, *21*, 105201; c) J. U. Lee, J. W. Jung, T. Emrick, T. P. Russel, W. H. Jo, *J. Mater. Chem.* **2010**, *20*, 3287.

[16]   C. Lindqvist, J. Bergqvist, C.-C. Feng, S. Gustafsson, O. Bäcke, N. D. Treat, C. Bounioux, P. Henriksson, R. Kroon, E. Wang, A. Sanz-Velasco, P. M. Kristiansen, N. Stingelin, E. Olsson, O. Inganäs, M. R. Andersson, C. Müller, *Adv. Energy Mater.* **2014**, *4*, 1301437.

[17]   a) D. M. Johansson, G. Srdanov, G. Yu, M. Theander, O. Inganas, R. M. Andersson, *Macromolecules* **2000**, *33*, 2525; b) V. Deimede, J. K. Kallitsis, T. Pakula, *J. Polym. Sci. A: Polym. Chem.* **2001**, *39*, 3168; c) J. Vandenbergh, B. Conings, S. Bertho, J. Kesters, D. Spoltore, S. Esiner, J. Zhao, G. Van Assche, M. M. Wienk, W. Maes, L. Lutsen, B. Van Mele, R. A. J. Janssen, J. Manca, D. J. M. Vanderzande, *Macromolecules* **2011**, *44*, 8470.

[18]   a) S. Miyanishi, K. Tajima, H. Kazuhito, *Macromolecules* **2009**, *42*, 1610; b) B. J. Kim, Y. Miyamoto, B. Ma, J. M. J. Fréchet, *Adv. Funct. Mater.* **2009**, *19*, 2273; c) C.-H. Hsieh, Y.-J. Cheng, P.-J. Li, C.-H. Chen, M. Dubosc, R.-M. Liang, C.-S. Hsu, *J. Am. Chem. Soc.* **2010**, *132*, 4887; d) G. Griffini, J. D. Douglas, C. Piliego, T. W. Holcombe, S. Turri, J. M. J. Fréchet, J. L. Mynar, *Adv. Mater.* **2011**, *23*, 1660; e) H. J. Kim, A.-R. Han, C.-H. Cho, H. Kang, H.-H. Cho, M. Y. Lee, J. M. J. Fréchet, J. H. Oh, B. J. Kim, *Chem. Mater.* **2012**, *24*, 215; f) C.-Y. Nam, Y. Qin, Y. S. Park, H. Hlaing, X. Lu, B. M. Ocko, C. T. Black, R. B. Grubbs, *Macromolecules*

2012, *45*, 2338; g) F. Ouhib, M. Tomassetti, J. Manca, F. Piersimoni, D. Spoltore, S. Bertho, H. Moons, R. Lazzaroni, S. Desbief, C. Jérôme, C. Detrembleur, *Macromolecules* **2013**, *46*, 785; h) G. Brotas, J. Farinhas, Q. Ferreira, R. Rodrigues, I. L. Martins, J. Morgado, A. Charas, *J. Polym. Sci. A: Polym. Chem.* **2014**, *52*, 652; i) L. Derue, O. Dautel, A. Tournebize, M. Drees, H. Pan, S. Berthumeyrie, B. Pavageau, E. Cloutet, S. Chambon, L. Hirsch, A. Rivaton, P. Hudhomme, A. Facchetti, G. Wantz, *Adv. Mater.* **2014**, *26*, 5831.

[19] a) D. M. Tanenbaum, M. Hermenau, E. Voroshazi, M. T. Lloyd, Y. Galagan, B. Zimmermann, M. Hösel, H. F. Dam, M. Jørgensen, S. A. Gevorgyan, S. Kudret, W. Maes, L. Lutsen, D. Vanderzande, U. Würfel, R. Andriessen, R. Rösch, H. Hoppe, M. Lira-Cantu, A. Rivaton, G. Y. Uzunoğlu, D. Germack, B. Andreasen, M. V. Madsen, K. Norrman, F. C. Krebs, *RSC Adv.* **2012**, *2*, 882; b) S. Bertho, B. Campo, F. Piersimoni, D. Spoltore, J. D'Haen, L. Lutsen, W. Maes, D. Vanderzande, J. Manca, *Sol. Energy Mater. Sol. Cells* **2013**, *110*, 69; c) J. Kesters, S. Kudret, S. Bertho, N. Van den Brande, M. Defour, B. Van Mele, H. Penxten, L. Lutsen, J. Manca, D. J. M. Vanderzande, W. Maes, *Org. Electron.* **2014**, *15*, 549.

[20] a) D. Mühlbacher, M. Scharber, M. Morana, Z. Zhu, D. Waller, R. Gaudiana, C. Brabec, *Adv. Mater.* **2006**, *18*, 2884; b) J. Peet, J. Y. Kim, N. E. Coates, W. L. Ma, D. Moses, A. J. Heeger, G. C. Bazan, *Nat. Mater.* **2007**, *6*, 497; c) J. K. Lee, W. L. Ma, C. J. Brabec, J. Yuen, J. S. Moon, J. Y. Kim, K. Lee, G. C. Bazan, A. J. Heeger, *J. Am. Chem. Soc.* **2008**, *130*, 3619.

[21] a) C. I. Soci, W. Hwang, D. Moses, Z. Zhu, D. Waller, R. Gaudiana, C. J. Brabec, A. J. Heeger, *Adv. Funct. Mater.* **2007**, *17*, 632; b) M. Zhang, H. N. Tsao, W. Pisula, C. Yang, A. K. Mishra, K. Müllen, *J. Am. Chem. Soc.* **2007**, *129*, 3472; c) A. P. Zoombelt, S. G. J. Mathijssen, M. G. R. Turbiez, M. M. Wienk, R. A. J. Janssen, *J. Mater. Chem.* **2010**, *20*, 2240; d) J. Kettle, M. Horie, L. A. Majewski,

B. R. Saunders, S. Tuladhar, J. Nelson, M. I. Turner, *Sol. Energy Mater. Sol. Cells* **2011**, *95*, 2186; e) A. V. Tunc, A. De Sio, D. Riedel, F. Deschler, E. Da Como, J. Parisi, E. von Hauff, *Org. Electron.* **2012**, *13*, 290; f) S. Albrecht, S. Janietz, W. Schindler, J. Frisch, J. Kurpiers, J. Kniepert, S. Inal, P. Pingel, K. Fostiropoulos, N. Koch, D. J. Neher, *J. Am. Chem. Soc.* **2012**, *134*, 14932; g) L. Marin, H. Penxten, S. Van Mierloo, R. Carleer, L. Lutsen, D. Vanderzande, W. Maes, *J. Polym. Sci. A: Polym. Chem.* **2013**, *51*, 4912.

[22]   a) U. R. Lee, T. W. Lee, M. H. Hoang, N. S. Kang, J. W. Yu, K. H. Kim, K.-G. Lim, T.-W. Lee, J.-I. Jin, D. H. Choi, *Org. Electron.* **2011**, *12*, 269; b) H. Waters, J. Kettle, S.-W. Chang, C.-J. Su, W.-R. Wu, U.-S. Jeng, Y.-C. Tsai, M. Horie, *J. Mater. Chem. A* **2013**, *1*, 7370; c) H. Waters, N. Bristow, O. Moudam, S.-W. Chang, C.-J. Sun, W.-R. Wu, U.-S. Jeng, M. Horie, J. Kettle, *Org. Electron.* **2014**, *15*, 2433.

[23]   a) C.-K. Mai, H. Zhou, Y. Zhang, Z. B. Henson, T.-Q. Nguyen, A. J. Heeger, G. C. Bazan, *Angew. Chem.* **2013**, *125*, 13112; *Angew. Chem. Int. Ed.* **2013**, *52*, 12874; b) A. W. Thomas, Z. B. Henson, J. Du, C. A. Vandenberg, G. C. Bazan, *J. Am. Chem. Soc.* **2014**, *136*, 3736; c) H. Zhou, Y. Zhang, C.-K. Mai, S. D. Collins, T.-Q. Nguyen, G. C. Bazan, A. J. Heeger, *Adv. Mater.* **2014**, *26*, 780.

[24]   Z. B. Henson, P. Zalar, X. Chen, G. C. Welch, T.-Q. Nguyen, G. C. Bazan, *J. Mater. Chem. A* **2013**, *1*, 11117.

[25]   F. Hinkel, T. Marszalek, W. Zajaczkowski, S. R. Puniredd, M. Baumgarten, W. Pisula, K. Müllen, *Chem. Mater.* **2014**, *26*, 4844.

[26]   a) A. Kraak, A. K. Wiersema, P. Jordens, H. Wynberg, *Tetrahedron* **1968**, *24*, 3381; b) J. R. Reynolds, J. Z. Brzezinski, *Synthesis* **2002**, 1053; c) P. Coppo, D. C. Cupertino, S. C. Yeates, M. L. Turner, *J. Mater. Chem.* **2002**, *12*, 2597; d)

P. Coppo, D. C. Cupertino, S. C. Yeates, M. L. Turner, *Macromolecules* **2003**, *36*, 2705; e) J. H. Park, B. Y. Lee, *Bull. Korean Chem. Soc.* **2010**, *31*, 1064.

[27]   a) S. Van Mierloo, P. J. Adriaensens, W. Maes, L. Lutsen, T. J. Cleij, E. Botek, B. Champagne, D. J. Vanderzande, *J. Org. Chem.* **2010**, *75*, 7202; b) S. Van Mierloo, A. Hadipour, M.-J. Spijkman, N. Van den Brande, B. Ruttens, J. Kesters, J. D'Haen, G. Van Assche, D. M. de Leeuw, T. Aernouts, J. Manca, L. Lutsen, D. Vanderzande, W. Maes, *Chem. Mater.* **2012**, *24*, 587.

[28]   W. Vanormelingen, P. Verstappen, V. Maes, D. Bevk, L. Lutsen, D. Vanderzande, W. Maes, *Synlett* **2013**, *24*, 2389.

[29]   a) R. L. Danley, P. A. Caulfield, S. R. Aubuchon, *Am. Lab.* **2008**, *40*, 9; b) T. Ghoos, N. Van den Brande, M. Defour, J. Brassinne, C.-A. Fustin, J.-F. Gohy, S. Hoeppener, U. S. Schubert, W. Vanormelingen, L. Lutsen, D. J. Vanderzande, B. Van Mele, W. Maes, *Eur. Polym. J.* **2014**, *53*, 206.

[30]   M. O. Reese, S. A. Gevorgyan, M. Jørgensen, E. Bundgaard, S. R. Kurtz, D. S. Ginley, D. C. Olson, M. R. Lloyd, P. Morvillo, E. A. Katz, A. Elschner, O. Haillant, T. R. Currier, V. Shrotriya, M. Hermenau, M. Riede, K. R. Kirov, G. Trimmel, T. Rath, O. Inganäs, F. Zhang, M. Andersson, K. Tvingstedt, M. Lira-Cantu, D. Laird, C. McGuiness, S. J. Gowrisanker, M. Pannone, M. Xiao, J. Hauch, R. Steim, D. M. DeLongchamp, R. Rösch, H. Hoppe, N. Espinosa, A. Urbina, G. Yaman-Uzunoglu, J. -B. Bonekamp, A. J. J. M. van Breemen, C. Girotto, E. Voroshazi, F. C. Krebs, *Sol. Energy Mater. Sol. Cells* **2011**, *95*, 1253.

[31]   a) Z. Li, H. C. Wong, Z. Huang, H. Zhong, C. H. Tan, W. C. Tsoi, J. S. Kim, J. R. Durrant, J. T. Cabral, *Nat. Commun.* **2013**, *4*, 2227; b) F. Piersimoni, G. Degutis, S. Bertho, K. Vandewal, D. Spoltore, T. Vangerven, J. Drijkoningen, M. K. Van Bael, A. Hardy, J. D'Haen, W. Maes, D. Vanderzande, M. Nesladek, J. Manca, *J. Polym. Sci. B: Polym. Phys.* **2013**, *51*, 1209.

[32]   E. Voroshazi, I. Cardinaletti, T. Conard, B. P. Rand, *Adv. Energy Mater.* **2014**, DOI:10.1002/aenm.201400848.

[33]   a) M. O. Reese, M. S. White, G. Rumbles, D. S. Ginley, S. E. Shaheen, *Appl. Phys. Lett.* **2008**, *92*, 053307; b) M. T. Lloyd, D. C. Olson, P. Lu, E. Fang, D. L. Moore, M. S. White, M. O. Reese, D. S. Ginley, J. W. P. Hsu, *J. Mater. Chem.* **2009**, *19*, 7638.

[34]   a) M. M. Lee, J. Teuscher, T. Miyasaka, T. N. Murakami, H. J. Snaith, *Science* **2012**, *338*, 643; b) S. Kazim, M. K. Nazeeruddin, M. Grätzel, S. Ahmad, *Angew. Chem.* **2014**, *126*, 2854; *Angew. Chem. Int. Ed.* **2014**, *53*, 2812; c) H. Zhou, Q. Chen, G. Li, S. Luo, T.-B. Song, H.-S. Duan, Z. Hong, J. You, Y. Liu, Y. Yang, *Science* **2014**, *345*, 542.

[35]   S. Wouters, F. Demir, L. Beenaerts, G. Van Assche, *Thermochim. Acta* **2012**, *530*, 64.

[36]   a) J. Bard, L. R. Faulkner, *Electrochemical methods: fundamentals and applications*, 2nd Ed., Wiley, **2001**; b) S. Trasatti, *Pure Appl. Chem.* **1986**, *58*, 955.

5.6 ACKNOWLEDGEMENTS

5.7 SUPPORTING INFORMATION

5.7.1 Monomer and polymer synthesis

Unless stated otherwise, all reagents and chemicals were obtained from commercial sources and used without further purification. Solvents were dried by a solvent purification system (MBraun, MB-SPS-800) equipped with alumina columns. 4-(2'-Ethylhexylidene)-4*H*-cyclopenta[2,1-*b*:3,4-*b*']dithiophene (**1**),[1] 4-(2'-ethylhexyl)-4-octyl-4*H*-cyclopenta[2,1-*b*:3,4-*b*']dithiophene (**2**)[1], 4-(2'-ethylhexyl)-4-(6'-hydroxyhexyl)-4*H*-cyclopenta[2,1-*b*:3,4-*b*']dithiophene (**3**),[1] and 4,7-dibromo-2,1,3-benzothiadiazole[2] were prepared according to literature procedures.

2,6-Bis(trimethylstannyl)-4-(2'-ethylhexyl)-4-octyl-4H-cyclopenta[2,1-b:3,4-b']dithiophene (M1)

4-(2'-Ethylhexyl)-4-octyl-4*H*-cyclopenta[2,1-*b*:3,4-*b*']dithiophene (**2**) (2.93 g, 7.28 mmol) was dissolved in dry THF (60 mL) and the solution was cooled down to -78 °C before a solution of *n*-BuLi in *n*-hexane (2.5 M; 11.6 mL, 29.1 mmol) was added dropwise. After stirring an additional hour at -78 °C, a solution of trimethyltin chloride (1 M in THF; 32.8 mL) was added. The resulting solution was allowed to warm gently to room temperature (overnight). Water was added and the mixture was extracted with diethyl ether. The organic phase was washed with brine, dried with $MgSO_4$, filtered and evaporated to dryness. The crude product was purified via preparative recycling SEC to yield the pure monomer as a pale yellow oil (3.29 g, 62%). ^{1}H NMR (400 MHz, $CDCl_3$, δ): 6.94 (s, 1H), 6.93 (s, 1H), 1.95–1.70 (m, 4H), 1.30–1.05 (m, 10H), 1.05–0.80 (m, 13H), 0.73 (t, *J* = 7.0 Hz, 3H), 0.65–0.55 (m, 4H), 0.36 (s, 18H).

2,6-Bis(trimethylstannyl)-4-(2′-ethylhexyl)-4-(6′-hydroxyhexyl)-4H-cyclopenta[2,1-b:3,4-b′]dithiophene (M2)

To a solution of 4-(2′-ethylhexyl)-4-(6′-hydroxyhexyl)-4*H*-cyclopenta[2,1-*b*:3,4-*b*′]dithiophene (**3**) (0.404 g, 1.03 mmol) in dry THF (18 mL), *n*-BuLi (2.5 M in *n*-hexane; 1.36 mL, 3.40 mmol) was added dropwise at -15 °C under a N_2 atmosphere. The resulting mixture was stirred for 20 min at -15 °C and a solution of trimethyltin chloride (1 M in THF; 3.71 mL) was added. The solution was allowed to warm gently to room temperature (overnight) and water was added. After extraction with diethyl ether, the organic phase was washed with brine, dried with Na_2SO_4, filtered and evaporated to dryness. The crude product was purified via preparative recycling SEC to yield the pure monomer as a pale yellow oil (0.393 g, 53%). ^{1}H NMR (300 MHz, $CDCl_3$, δ): 6.93 (s, 1H), 6.92 (s, 1H), 3.57 (td, *J* = 6.6, 5.4 Hz, 2H), 1.93–1.70 (m, 4H), 1.45 (q, *J* = 6.7 Hz, 2H), 1.32–1.08 (m, 5H), 1.07–0.79 (m, 10H), 0.78–0.68 (t, *J* = 6.9 Hz, 3H), 0.64–0.53 (m, 4H), 0.36 (s, 18H).

4-(2′-Ethylhexyl)-4H-cyclopenta[2,1-b:3,4-b']dithiophene (4)

A solution of 4-(2′-ethylhexylidene)-4*H*-cyclopenta[2,1-*b*:3,4-*b*′]dithiophene (**1**) (930 mg, 3.23 mmol) in dry THF (30 mL) was added dropwise to a suspension of $LiAlH_4$ (264 mg, 6.96 mmol) in THF (30 mL). The resulting mixture was stirred for 2 h at room temperature, cooled down to 0 °C and water was carefully added. After extraction with diethyl ether, the organic layer was dried with $MgSO_4$, filtered and the solvent was removed under vacuum. Purification of the crude product by column chromatography (silica, eluent petroleum ether) yielded the pure product as a colorless oil (730 mg, 78%). ^{1}H NMR (400 MHz, $CDCl_3$, δ): 7.16 (d, *J* = 4.9 Hz, 2H), 7.06 (d, *J* = 4.9 Hz, 1H), 7.05 (d, *J* = 4.9 Hz, 1H), 3.70 (t, *J* = 7.7 Hz,

1H), 1.73–1.54 (m, 3H), 1.53–1.35 (m, 4H), 1.35–1.20 (m, 4H), 0.93–0.83 (m, 6H); ^{13}C NMR (75 MHz, CDCl$_3$, δ): 154.9, 154.8, 137.5, 124.4, 122.8, 42.4, 37.4, 36.1, 32.8, 28.7, 25.9, 23.2, 14.3, 10.6; MS (MALDI-TOF) *m/z*: 289.8 ([M]$^+$).

Ethyl 6-{4'-(2''-ethylhexyl)-4H-cyclopenta[2,1-b:3,4-b']dithiophen-4'-yl}hexanoate (5)

4-(2'-Ethylhexyl)-4*H*-cyclopenta[2,1-*b*:3,4-*b*']dithiophene (**4**) (630 mg, 2.18 mmol), 6-bromohexanoic acid (468 mg, 2.40 mmol) and KI (30 mg, 0.18 mmol) were dissolved in DMSO (16 mL) and *t*-BuOK (612 mg, 5.45 mmol) was added. After stirring at room temperature for 15 h, an aqueous HCl (1 M) solution was added and the mixture was extracted with hexanes. After drying the organic phase with MgSO$_4$, filtration and solvent removal under vacuum, the obtained product was dissolved in EtOH (15 mL) and H$_2$SO$_4$ (0.5 mL) was added. After reaction for 1 h at room temperature, ice water was added and the mixture was extracted with diethyl ether. The collected organic layers were washed with a saturated NaHCO$_3$ solution, dried with MgSO$_4$, filtered and the solvent was removed under vacuum. After column chromatographic purification (silica, eluent petroleum ether:diethyl ether, 97:3), the pure product was obtained as a colorless oil (785 mg, 83%). ^{1}H NMR (300 MHz, CDCl$_3$, δ): 7.13 (d, *J* = 4.9 Hz, 2H), 6.91 (d, *J* = 4.9 Hz, 1H), 6.90 (d, *J* = 4.9 Hz, 1H), 4.08 (q, *J* = 7.1 Hz, 2H), 2.15 (t, *J* = 7.5 Hz, 2H), 1.95–1.75 (m, 4H), 1.55–1.40 (m, 2H), 1.30–1.15 (m, 5H), 1.15–0.80 (m, 10H), 0.75 (t, *J* = 6.9 Hz, 3H), 0.70–0.55 (m, 4H); ^{13}C NMR (100 MHz, CDCl$_3$, δ): 173.8, 157.7, 157.6, 136.7, 124.4, 121.9, 60.2, 53.2, 41.7, 39.3, 35.2, 34.3, 34.1, 29.4, 28.6, 27.2, 24.7, 23.9, 22.8, 14.3, 14.1, 10.7; HRMS (ESI) *m/z*: [M+Na]$^+$ calcd. for C$_{25}$H$_{36}$O$_2$S$_2$Na, 455.2049; found, 455.2038.

Ethyl 6-{2',6'-dibromo-4'-(2''-ethylhexyl)-4H-cyclopenta[2,1-b:3,4-b']-dithiophen-4'-yl}hexanoate (6)

Ethyl 6-{4'-(2''-ethylhexyl)-4H-cyclopenta[2,1-b:3,4-b']dithiophen-4'-yl}hexa-noate (**5**) (785 mg, 1.81 mmol) was dissolved in $CHCl_3$ (15 mL) and the solution was cooled down to 0 °C. NBS (678 mg, 3.81 mmol) was added and the resulting solution was stirred for 2 h at room temperature. Water was added and the mixture was extracted with diethyl ether. After drying with $MgSO_4$, filtration, solvent evaporation in vacuo and purification via column chromatography (silica, eluent petroleum ether:diethyl ether, 97:3), the pure product was obtained as a colorless oil (931 mg, 87%). ^{1}H NMR (400 MHz, $CDCl_3$, δ): 6.92 (s, 1H), 6.91 (s, 1H), 4.09 (q, J = 7.1 Hz, 2H), 2.18 (t, J = 7.5 Hz, 2H), 1.88–1.70 (m, 4H), 1.52–1.42 (m, 2H), 1.23 (t, J = 7.1 Hz, 3H), 1.19–1.09 (m, 2H), 1.07–0.81 (m, 10H), 0.78 (t, J = 7.0 Hz, 3H), 0.68–0.57 (m, 4H); ^{13}C NMR (100 MHz, $CDCl_3$, δ): 173.8, 155.7, 155.6, 136.6, 124.9, 124.8, 111.2, 111.1, 60.3, 55.0, 41.7, 39.2, 35.4, 34.4, 34.0, 29.5, 28.6, 27.4, 24.8, 24.0, 22.9, 14.4, 14.2, 10.8; HRMS (ESI) m/z: [M+Na]$^+$ calcd. for $C_{25}H_{34}Br_2O_2S_2Na$, 613.0239; found, 613.0204.

Ethyl 6-{4'-(2''-ethylhexyl)-2',6'-bis(trimethylstannyl)-4H-cyclopenta-[2,1-b:3,4-b']dithio-phen-4'-yl}hexanoate (M3)

Ethyl 6-{2',6'-dibromo-4'-(2''-ethylhexyl)-4H-cyclopenta[2,1-b:3,4-b']dithio-phen-4'-yl}hex-anoate (**6**) (931 mg, 1.58 mmol), hexamethylditin (2.00 g, 6.10 mmol), LiCl (234 mg, 5.53 mmol) and Pd(PPh$_3$)$_4$ (92 mg, 0.079 mmol) were dissolved in dry degassed toluene (10 mL) under N_2 atmosphere and heated at 105 °C for 1 h. The mixture was cooled down to room temperature and water was added. After extraction with diethyl ether, the organic phase was washed with water, dried over $MgSO_4$, filtered and evaporated to dryness. The crude product

was passed through a silica plug and purification with preparative recycling SEC yielded the pure product as a pale yellow oil (694 mg, 58%). ^{1}H NMR (400 MHz, CDCl$_3$, δ): 6.93 (s, 1H), 6.92 (s, 1H), 4.08 (q, *J* = 7.1 Hz, 2H), 2.17 (t, *J* = 7.6 Hz, 2H), 1.91–1.75 (m, 4H), 1.54–1.45 (m, 2H), 1.22 (t, *J* = 7.1 Hz, 3H), 1.20–1.11 (m, 2H), 1.03–0.80 (m, 10H), 0.73 (t, *J* = 7.0 Hz, 3H), 0.63–0.55 (m, 4H), 0.36 (s, 18H).

Poly{4-(2'-ethylhexyl)-4-octyl-4H-cyclopenta[2,1-b:3,4-b']dithiophene-2,6-diyl-alt-2,1,3-benzothiadiazole-4,7-diyl} (P1)

A solution of 2,6-bis(trimethylstannyl)-4-(2'-ethylhexyl)-4-octyl-4*H*-cyclopenta[2,1-*b*:3,4-*b'*]dithiophene (**M1**) (102 mg, 0.140 mmol) in dry toluene (3.2 mL) was added to a mixture of 4,7-dibromo-2,1,3-benzothiadiazole (41.2 mg, 0.140 mmol), Pd$_2$(dba)$_3$ (3.2 mg, 0.0035 mmol) and P(*o*-tol)$_3$ (4.3 mg, 0.014 mmol) in dry DMF (0.8 mL) under a N$_2$ atmosphere. After purging with N$_2$ for 30 min, the mixture was heated to 110 °C for 15 h. The green-black solution was added dropwise to MeOH and the resulting precipitate was filtered in a Soxhlet timble. The crude polymer was purified by subsequent Soxhlet extractions with methanol, acetone, hexanes and chloroform. The chloroform fraction was further purified by preparative SEC and finally precipitated in MeOH to yield a greenish black solid (43.7 mg, 57%). ^{1}H NMR (400 MHz, CDCl$_3$, δ): 9.1–7.5 (br, 2H), 7.5–6.1 (br, 2H), 3.0–0.2 (br, 34H); SEC (THF, 40 °C, PS standards): before prep-SEC: *M$_n$* 20 kDa, PDI 2.4; after prep-SEC: *M$_n$* 26 kDa, PDI 3.2.

Poly{4-(2'-ethylhexyl)-4-(6'-hydroxyhexyl)-4H-cyclopenta[2,1-b:3,4-b']dithiophene-2,6-diyl-alt-2,1,3-benzothiadiazole-4,7-diyl} (P2)

P2 was prepared similar to **P1**. CPDT monomer **M2** (0.393 g, 0.548 mmol), 4,7-dibromo-2,1,3-benzothiadiazole (0.161 g, 0.548 mmol), Pd$_2$(dba)$_3$ (12.5 mg, 13.7

µmol) and P(o-tol)$_3$ (16.7 mg, 54.8 µmol) were dissolved in 9.0 mL of dry toluene and 2.3 mL of dry DMF. Soxhlet extractions were subsequently performed with hexanes, acetone and CHCl$_3$. Due to the rather limited solubility of the polymer in CHCl$_3$, purification by preparative SEC was not performed on this material. The final polymer was obtained as a greenish black solid (223 mg, 77%). ^{1}H NMR (400 MHz, CDCl$_3$, δ): 8.6–7.6 (br, 2H), 7.6–6.8 (br, 2H), 4.0–3.3 (br, 2H), 3.0–0.2 (br, 28H); SEC (THF, 40 °C, PS standards): M_n 13 kDa, PDI 2.5.

Poly{4-(2'-ethylhexyl)-4-(6'-ethoxy-6'-oxohexyl)-4H-cyclopenta[2,1-b:3,4-b']dithiophene-2,6-diyl-alt-2,1,3-benzothiadiazole-4,7-diyl} (P3)

P3 was prepared similar to **P1**. CPDT monomer **M3** (0.162 g, 0.214 mmol), 4,7-dibromo-2,1,3-benzothiadiazole (0.063 g, 0.214 mmol), Pd$_2$(dba)$_3$ (4.9 mg, 5.3 µmol) and P(o-tol)$_3$ (6.5 mg, 21.4 µmol) were dissolved in 5.0 mL of dry toluene and 1.2 mL of dry DMF. The final polymer was obtained as a greenish black solid (66 mg, 55%). ^{1}H NMR (400 MHz, CDCl$_3$, δ): 8.3–7.6 (br, 2H), 7.6–6.7 (br, 2H), 4.4–3.8 (br, 2H), 3.0–0.3 (br, 30H); SEC (THF, 40 °C, PS standards): before prep-SEC: M_n 39 kDa, PDI 3.0; after prep-SEC: M_n 46 kDa, PDI 1.7.
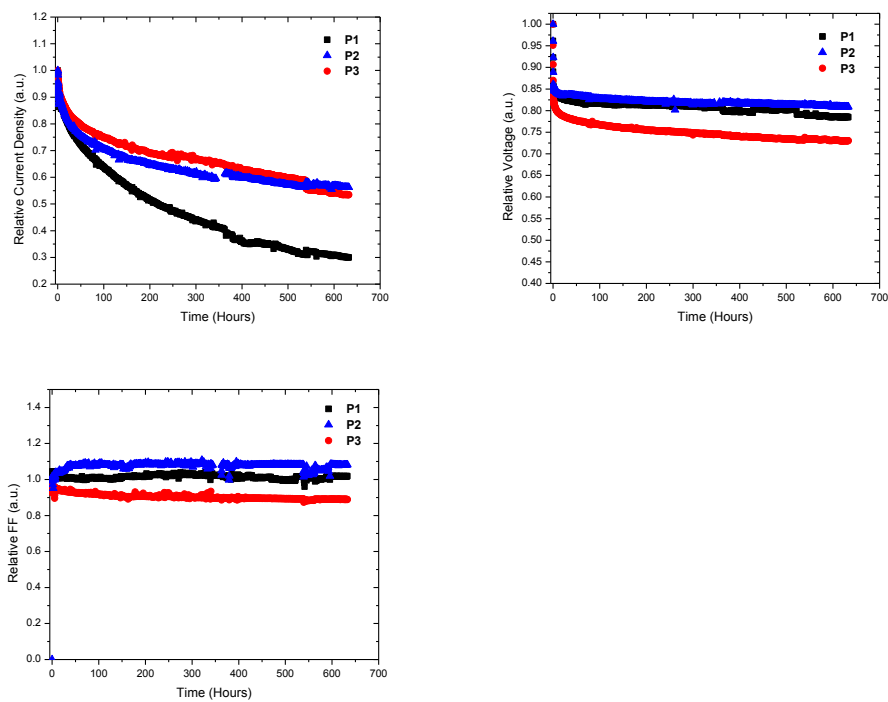
5.7.2 Thermal analysis
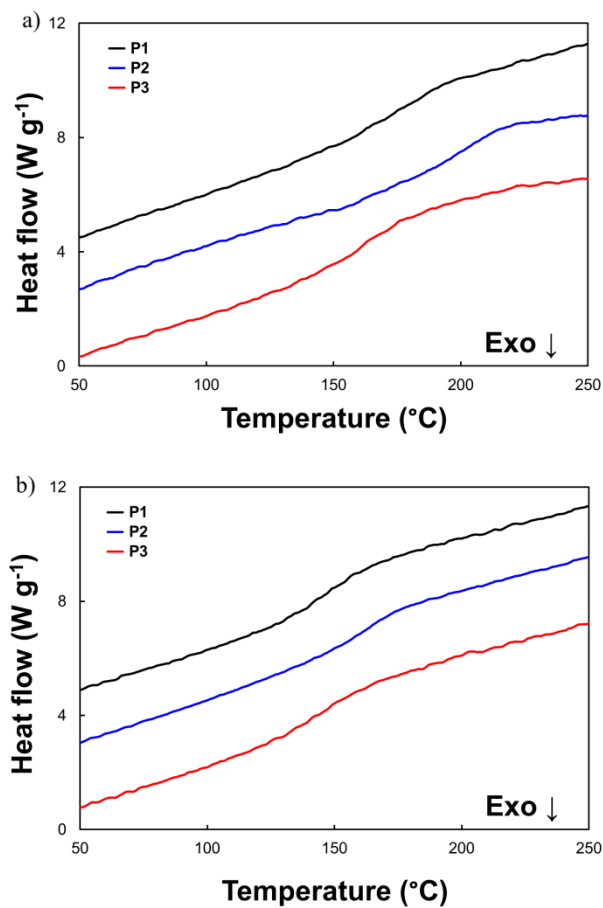
Figure S1: RHC profiles for a) the three PCPDTBT copolymers, and b) the **P1**−**P3**:PC$_{71}$BM(1:3) blends (curves shifted vertically for clarity).

5.7.3 Additional solar cell degradation data and TEM figures

Figure S2: Degradation curves (V_{OC}, J_{SC} and FF) for the polymer solar cells based on **P1**–**P3** (650 h at 85 °C). The curves are normalized to the first measurement point at 85 °C.
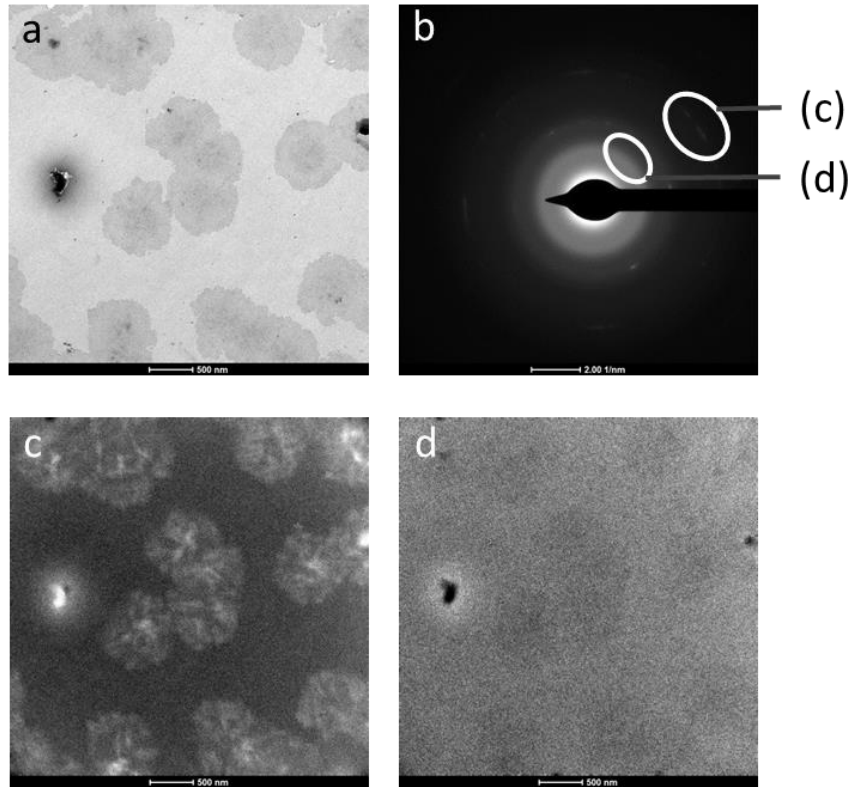
Figure S3: (a) TEM bright field image of a **P1**:PC$_{71}$BM blend film annealed at 220 °C for 3 h, showing the formation of microcrystals and phase separation. (b) SAED image procured from aggregated domains in the bright field image, illustrating the formation of crystalline regions, most likely to be ascribed to PC$_{71}$BM. (c) Circular dark field image made by electrons scattered into the sharp diffraction ring. (d) Circular dark field image made by electrons scattered into the diffuse diffraction ring, indicating the more amorphous matrix in the polymer:PC$_{71}$BM blend.
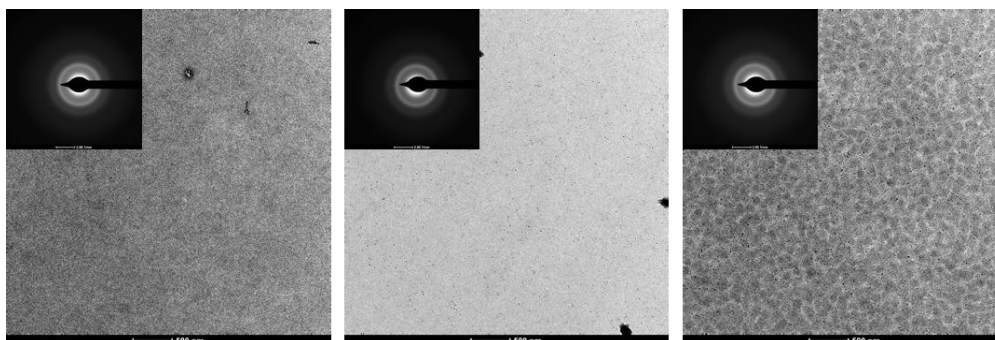
Figure S4: TEM images of **P1**−**P3**:PC$_{71}$BM (left to right) BHJ blends exposed to 85 °C for 150 h in the dark.

Table S1: Roughness and peak to peak (P2P) distance data procured from AFM measurements and polymer solar cell devices.

Polymer	Treatment	R_a	R_q	P2P
P1	0 h at 85 °C	0.61	1.11	37.62
P1	650 h at 85 °C	0.56	0.98	43.94
P2	0 h at 85 °C	0.43	0.55	9.02
P2	650 h at 85 °C	0.36	0.46	5.55
P3	0 h at 85 °C	1.09	1.38	19.56
P3	650 h at 85 °C	1.09	1.37	13.96

Table S2: *I-V* characteristics of the polymer solar cells based on **P1**−**P3** after aging in the dark at 85 °C for 0, 6 and 25 h.

Polymer	Treatment	V_{OC} [V]	J_{SC} [mA cm^{-2}]	FF	Best PCE [%]	Average PCE [a] [%]
P1	pristine	0.59	9.57	0.44	2.57	2.49
P1	dark + 6 h at 85 °C	0.59	7.04	0.43	1.90	1.78
P1	dark + 25 h at 85 °C	0.59	6.58	0.43	1.71	1.67
P2	pristine	0.59	7.54	0.44	1.99	1.94
P2	dark + 6 h at 85 °C	0.59	6.58	0.45	1.80	1.76
P2	dark + 25 h at 85 °C	0.59	6.17	0.45	1.67	1.64
P3	pristine	0.56	9.58	0.51	3.21	2.72
P3	dark + 6 h at 85 °C	0.54	7.45	0.47	2.18	1.78
P3	dark + 25 h at 85 °C	0.55	6.58	0.46	1.70	1.64

[a]Averages were taken across 4−8 devices, with an active area of 3 mm².

5.7.4 References

[1]   Vanormelingen, W.; Verstappen, P.; Maes, V.; Bevk, D.; Lutsen, L.; Vanderzande, D.; Maes, W. *Synlett* **2013**, *24*, 2389.

[2]   Karsten, B. P.; Bijleveld, J. C.; Viani, L.; Cornil, J.; Gierschner, J.; Janssen, R. A. J. *J. Mater. Chem.* **2009**, *19*, 5343.

Chapter 6

Variation of the Central Donor Unit in D-A-D-A-D Small Molecules for Organic Solar Cells

Increased crystalline character
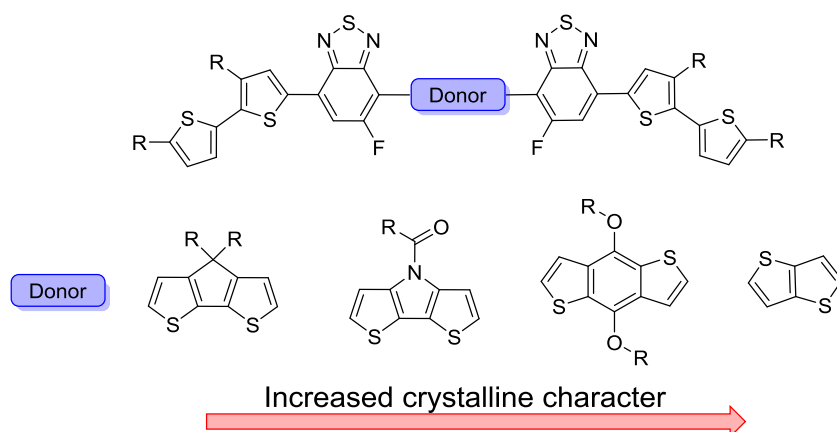
P. Verstappen, I. Cardinaletti, T. Vangerven, W. Vanormelingen, L. Lutsen, D. Vanderzande, J. Manca, W. Maes, *to be submitted*

ABSTRACT

Replacing conjugated polymers by small molecules as donor materials for organic photovoltaics can offer several advantages. However, general understanding of the structure-device property relations is less developed for small molecule solar cells in comparison to the polymer counterparts. In this respect, herein, the central donor unit in the well-known high-performance small molecule p-DTS(FBTTh$_2$)$_2$ is altered to CPDT, BDT, DTP and TT, and the influence thereof on the physicochemical material properties and solar cell characteristics is reported. Variation of the central donor entity has a pronounced effect on the crystallinity of the small molecules. However, only a minor effect on the solar cell efficiency is observed as almost equal performances are obtained for the highest and lowest crystallinity materials (with a maximum PCE of 3.10%). Additionally, it is shown that homo-coupled products can be generated during Stille cross-coupling reactions, which are hard to remove and are detrimental to solar cell performance.

6.1 INTRODUCTION

Organic solar cells have attracted great attention as a promising sustainable energy-producing technology due to some appealing features such as their aesthetically pleasing, flexible and light-weight character and the possibility to produce large area devices via simple and cheap printing processes.[1] In state of the art bulk heterojunction (BHJ) organic solar cells, the active layer consists of two finely intermixed materials, an electron rich donor and an electron poor acceptor.[2] Although efforts have been done to identify viable alternatives for (methano)fullerene n-type materials, phenyl-C_{61}-butyric acid methyl ester ($PC_{61}BM$) and phenyl-C_{71}-butyric acid methyl ester ($PC_{71}BM$) are still most often employed.[3] On the other hand, the donor material has undergone quite some evolution over time. During the early days of organic solar cells, almost all work was focused on poly(*p*-phenylene vinylene) (PPV) and poly(3-hexylthiophene) (P3HT) as "workhorse" materials generating power conversion efficiencies (PCE's) of approximately 3% and 5%, respectively.[4] In recent years, the focus has shifted to "push-pull" copolymers as electron donor materials. These polymers are composed of electron rich and electron poor (heterocyclic) moieties, copolymerized in an alternating fashion. By employing this strategy, intramolecular charge transfer occurs, lowering the bandgap of these copolymers and allowing them to harvest significantly more light in comparison to homopolymers, leading to current reports of efficiencies around 10%.[5] The advent of the push-pull concept has delivered a toolbox to synthetic chemists to regulate the highest occupied molecular orbital (HOMO) and lowest unoccupied molecular orbital (LUMO) energy levels.[1b,6] Therefore, sufficiently low bandgaps can already be obtained with relatively short chain small molecules, eliminating

even the need for polymeric materials. Moreover, these "small molecules" offer some additional advantages compared to their polymer counterparts, i.e. (1) less problems because of batch-to-batch variations due to their uniform and defined molecular structures, (2) easily tunable frontier energy levels due to dedicated chemical structure design, and (3) a generally intrinsic higher mobility and open-circuit voltage (V_{oc}).[1i,7] As a result, the interest in small molecule organic solar cells has rapidly grown and although this type of devices have much less been investigated, PCE's in the proximity of 10% have also been reported recently.[8] Bazan *et al.* developed a D-A-D-A-D strategy based on fluorinated benzothiadiazole and dithienosilole (affording the well-known small molecule p-DTS(FBTTh$_2$)$_2$) leading to PCE's exceeding 8%,[8b,9] whereas Chen *et al.* employed a D-A-D concept to achieve 8% efficiency.[8c,10] However, it is generally accepted that small changes to the chemical structure can lead to strong variation in final solar cell performance. For example, it was recently reported that substitution of the alkoxy side chains by alkylthio groups can effectively improve the solar cell efficiency, leading to devices with almost 10% efficiency.[8c] It was also shown that side chain length and position is of major importance for the development of high-performance small molecule solar cells.[11] Despite the outstanding results achieved in recent years, additional investigation of the structure-device relations is certainly necessary to make further advances in the field.

In this work, the central donor unit in the well-known p-DTS(FBTTh$_2$)$_2$ small molecule[8b, 9] was varied and its impact on the physicochemical properties of the resulting materials and the final solar cell characteristics was studied. Four different donor units were chosen, based on their behavior in low bandgap copolymers for OPV devices, i.e. 4*H*-cyclopenta[2,1-*b*:3,4-*b'*]dithiophene (CPDT),[1b,12] benzo[1,2-*b*:4,5-*b'*]dithiophene (BDT),[1b,13] *N*-acyl-substituted

dithieno[3,2-*b*:2′,3′-*d*]pyrrole (DTP)[14] and thieno[3,2-*b*]thiophene (TT)[15]. The small molecules were fully characterized and their solar cell properties were determined, along with studies on the film morphology and charge carrier mobility of the donor materials and their blends.

6.2 RESULTS AND DISCUSSION

6.2.1 Synthesis and characterization
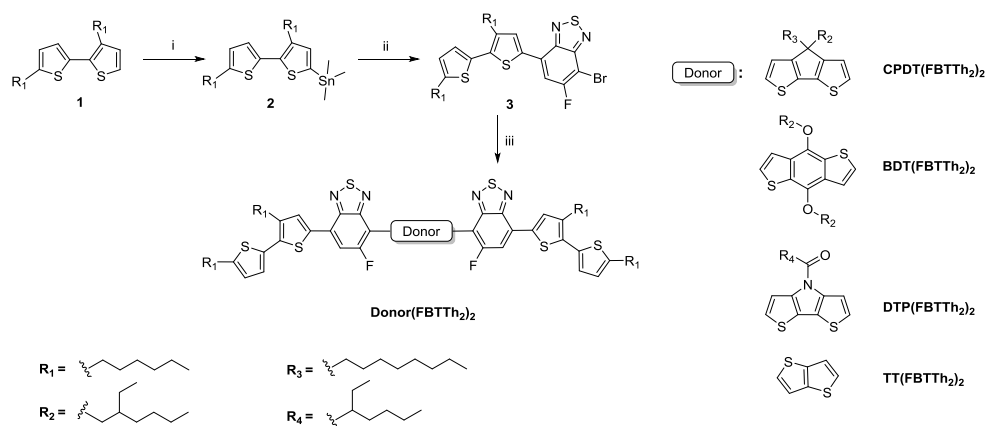
Scheme 1: Synthetic route toward the four small molecules: i) 1: *n*-BuLi, Et$_2$O, 2: Me$_3$SnCl; ii) 4,7-dibromo-5-fluorobenzo[*c*][1,2,5]thiadiazole, Pd(PPh$_3$)$_4$, DMF/toluene 1/1, 80 °C, 15 h (64% yield); iii) bis(trimethylstannyl) derivative of the appropriate donor molecule, Pd(PPh$_3$)$_4$, DMF/toluene 1/1, 110 °C, 15 h.

All four small molecules were synthesized following the synthetic pathway outlined in Scheme 1. 3,5′-Dihexyl-2,2′-bithiophene (**1**) was prepared according to a literature procedure and subsequently stannylated.[16] Stille cross-coupling of precursor **2** with 4,7-dibromo-5-fluorobenzo[*c*][1,2,5]thiadiazole then yielded molecule **3**. In this reaction, a statistical mixture of the non-, mono- and di-reacted product was formed, leading to a modest yield for the desired product (64%). The targeted small molecules were then obtained via Stille cross-coupling

of precursor **3** with the bis(trimethylstannyl) derivatives of the appropriate donor molecules. Except for **TT(FBTTh$_2$)$_2$**, all small molecules showed excellent solubility in common organic solvents (e.g. tetrahydrofuran, chloroform and toluene). **TT(FBTTh$_2$)$_2$**, on the other hand, only showed reasonably high solubility in CS$_2$ at room temperature or in chlorinated solvents (e.g. 1,1,2,2-tetrachloroethane and chlorobenzene) at elevated temperatures. Since material purity is of major importance for the fabrication of electronic devices, all small molecules except **TT(FBTTh$_2$)$_2$** were purified by standard column chromatography (on silica) and recycling preparative size exclusion chromatography (prep-SEC). Due to its limited solubility, **TT(FBTTh$_2$)$_2$** was purified through Soxhlet extractions with methanol, acetone, *n*-hexane and chloroform.

Despite the extensive purification procedures, the ^{1}H NMR spectrum of **DTP(FBTTh$_2$)$_2$** showed some minor impurities (~5%) (see ESI). To understand the nature of these impurities, all molecules were analyzed by MALDI-TOF mass spectrometry (see ESI). For **DTP(FBTTh$_2$)$_2$**, additional signals (besides the parent molecular ion) could be observed. The most abundant impurity showed a mass of 1577.1 Da, which correlates to the molecule with an extra DTP unit. Since homo-coupling is a known side reaction of the Stille cross-coupling, it can be expected that molecules with two adjacent DTP core moieties were formed during the reaction.[17] The MALDI-TOF spectrum even revealed the presence of trace amounts of molecules with three DTP units (*m/z* = 1880.3 Da). Also for **BDT(FBTTh$_2$)$_2$**, a minor amount of homo-coupling was observed (*m/z* = 1858.7 Da), although not noticeable by ^{1}H NMR. For both **CPDT(FBTTh$_2$)$_2$** and **TT (FBTTh$_2$)$_2$**, no significant impurities could be seen through MALDI-TOF analysis. It should be noted that the homo-coupling defect structures were less readily

observed from the electrospray mass spectra. These observations clearly demonstrate the importance of using multiple analysis techniques to evaluate the purity of (electronic) materials.

The thermal properties of the small molecules were investigated by rapid heat-cool calorimetry (RHC) (Figure 1, Table 1). RHC was chosen above regular differential scanning calorimetry (DSC) because of its increased sensitivity to thermal transitions as a result of the fast scanning rates and the low sample amounts required.[18] From the obtained results it is clear that variation of the central donor unit has a major impact on both the melting temperature (T_m) and the melting enthalpy (ΔH_m). Furthermore, two of the small molecules – **BDT(FBTTh₂)₂** and **TT(FBTTh₂)₂** – seem to exhibit two melting temperatures. As anticipated, the small molecule with the highest degree of crystallinity was acquired by employing thieno[3,2-*b*]thiophene as the central donor unit.[15] Moreover, this material showed two melting temperatures, one at a relative low temperature (120 °C) and a second at high temperature (230 °C), with the latter one exhibiting a large ΔH_m (48.8 J/g), indicating a highly crystalline character. Also **BDT(FBTTh₂)₂** exhibited two melting peaks with relatively high ΔH_m values. In contrast to **TT(FBTTh₂)₂**, however, this molecule showed the highest ΔH_m for the first melting peak. On the other hand, for both **CPDT(FBTTh₂)₂** and **DTP(FBTTh₂)₂** relatively low ΔH_m values were observed, demonstrating a more amorphous nature. For **CPDT(FBTTh₂)₂**, the low melting enthalpy was accompanied by a low melting temperature. For comparison, RHC measurements on p-DTS(FBTTh₂)₂ were performed as well (Figure S1). The T_m and ΔH_m were determined to be 209 °C and 55.3 J/g respectively, which indicates a highly crystalline character for this small molecule, even higher than for **TT(FBTTh₂)₂**.
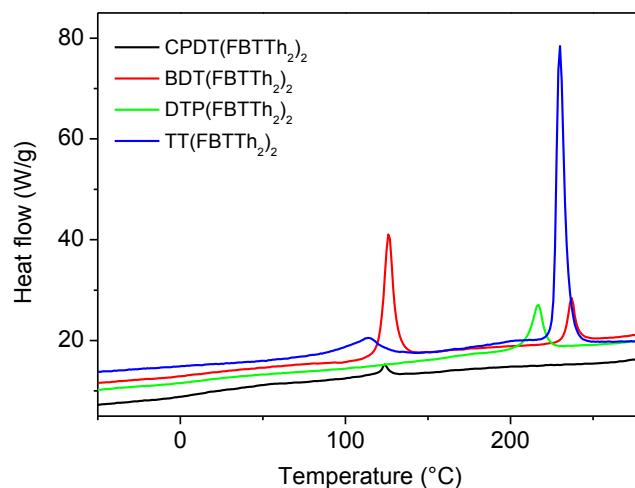
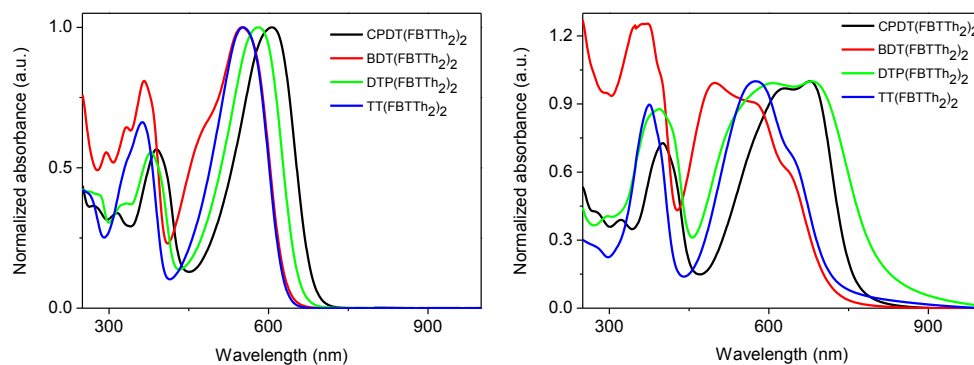**Figure 1:** RHC profiles of the four small molecules (curves shifted vertically for clarity).

Table 1: Thermal, optical and electrochemical properties of the small molecules.

	$T_m{}^a$ (°C)	$\Delta H_m{}^a$ (J/g)	$\lambda_{max}{}^b$ (nm) solution	λ_{max} (nm) film	$E_g{}^{OPc}$ (eV)	HOMO^d (eV)	LUMO^d (eV)	$E_g{}^{ECe}$ (eV)
CPDT(FBTTh₂)₂	124	2.6	607	677	1.64	-5.43	-3.41	2.03
BDT(FBTTh₂)₂	126/237	24.1/6.6	550	499	1.74	-5.41	-3.40	2.01
DTP(FBTTh₂)₂	217	11.0	581	681	1.52	-5.35	-3.43	1.92
TT(FBTTh₂)₂	120/230	11.6/48.8	553	575	1.72	-5.63	-3.38	2.25

^{a} Determined by RHC. ^{b} In chloroform. ^{c} Optical bandgap, determined by the onset of the solid-state UV-Vis spectra. ^{d} Determined by CV from the onset of oxidation and reduction. ^{e} Electrochemical bandgap.

Normalized UV-Vis absorption spectra of all small molecules in solution (CHCl₃) and thin film are shown in Figure 2. The UV-Vis spectra in solution nicely demonstrate that the introduction of more electron rich donor units results in red-shifted absorption spectra. Both **BDT(FBTTh₂)₂** and **TT(FBTTh₂)₂** showed λ_{max} values around 550 nm. When the central donor unit was altered to DTP, a red-shift of 30 nm was acquired, and an even higher wavelength was obtained when the electron rich CPDT unit was incorporated. In thin film, the absorption profiles

were broadened and red-shifted, except for **BDT(FBTTh$_2$)$_2$**. It was also observed that the absorption profile of **CPDT(FBTTh$_2$)$_2$** and **DTP(FBTTh$_2$)$_2$** was more strongly red-shifted in comparison to the other two small molecules, despite the higher degree of crystallinity of the latter, as perceived from RHC measurements. From the UV-Vis spectra in thin film, the optical bandgaps were calculated (Table 1). The smallest optical bandgap was observed for **DTP(FBTTh$_2$)$_2$** (1.52 eV). Modifying the central donor to CPDT slightly increased the bandgap, which further raised by implementation of TT and BDT as central donor units.

Figure 2: UV-Vis absorption spectra for the four small molecule materials in chloroform solution (top) and in thin film (bottom).

The HOMO and LUMO frontier energy levels of the small molecules were estimated via cyclic voltammetry (CV) from the onset of the oxidation and reduction peaks, respectively. All small molecules showed quasi-reversible oxidation and reduction behavior and the reported values are the means of the first four redox cycles (Table 1). While similar LUMO energy levels were observed for all small molecules, the HOMO energy level was significantly influenced by the variation of the central donor unit. Incorporation of TT as central donor unit seemed to yield small

molecules with deep HOMO levels, while introduction of DTP resulted in higher HOMO energy levels.

6.2.2 Solar cell characterization

To evaluate the performance of the small molecules in BHJ organic solar cells, the materials were used to fabricate standard architecture photovoltaic cells, in combination with $PC_{61}BM$ or $PC_{71}BM$ (Table 2, Table S1−S4). The devices were prepared by spin-coating the active layer blends on a hole transport layer of poly(3,4-ethylenedioxythiophene):poly(styrene sulfonate) PEDOT:PSS, deposited on an indium tin oxide (ITO) transparent electrode. The optimal processing conditions were found to be different for each material, and they are reported in Table 2, together with the average output parameters determining the performance. The *J-V* curves of the best performing small molecule solar cells are shown in Figure 3a. While chloroform was found to be the best casting solvent for **BDT(FBTTh₂)₂**, chlorobenzene allowed to reach higher performances (mainly in terms of short-circuit current density, J_{sc}) for the devices employing **CPDT(FBTTh₂)₂**, **DTP(FBTTh₂)₂** and **TT(FBTTh₂)₂**. In particular, due the low solubility imposed by the TT moiety, the latter had to be deposited from a high temperature solution. The use of 1,8-diiodooctane (DIO) allowed for an additional increase of current for the **TT(FBTTh₂)₂**:$PC_{71}BM$ device, reaching an efficiency of 3.0%.

A remarkably low V_{OC} was acquired for the solar cell devices based on **DTP(FBTTh₂)₂**. Since only a small increase in the HOMO energy level was observed by cyclic voltammetry, such a large deviation in V_{OC} was not expected for this small molecule. As it was recently reported that the presence of homo-coupled products can lead to reduced V_{OC} values in polymer solar cells,[19] the

presence of homo-coupling for this material, as confirmed by MALDI-TOF, might provide an explanation for the low V_{OC} obtained. The PCE's for the **BDT(FBTTh₂)₂**:PC₇₁BM devices were also quite disappointing, especially since BDT is one of the key building blocks leading to high performing push-pull copolymers.[1b,13] Although in this case the V_{OC} and FF were reasonably high, the J_{SC} values were found to remain low, despite extensive optimization of the processing parameters. For both **CPDT(FBTTh₂)₂** and **TT(FBTTh₂)₂**, reasonable solar cell results were obtained, however, still by far not as good as the "Bazan molecule" p-DTS(FBTTh₂)₂ (in our lab PCE values up to 6.6% were obtained with this small molecule, V_{OC} = 0.78 V, J_{SC} = 12.7 mA cm^{-2}, FF = 66%).

Table 2: Processing and output parameters of the standard architecture organic solar cells based on the four small molecule materials.

	Acceptor	D:A ratio	Solvent[a]	J_{sc} (mA/cm²)	V_{oc} (V)	FF (%)	PCE[b] (%)
CPDT(FBTTh₂)₂	PC₇₁BM	1:3	CB	8.39	0.85	39.7	2.83 (3.10)
BDT(FBTTh₂)₂[c]	PC₆₁BM	1:3	CF	2.44	0.76	50.3	0.93 (0.98)
DTP(FBTTh₂)₂	PC₇₁BM	1:2	CB	6.75	0.50	39.6	1.34 (1.37)
TT(FBTTh₂)₂[d]	PC₇₁BM	1:2	CB + 0.2% DIO	9.13	0.79	36.4	2.63 (2.96)

[a] CB = chlorobenzene, CF = chloroform, DIO = 1,8-diiodooctane. [b] Average values over at least 3 devices. The best device performance is shown in brackets. [c] Post-annealed at 100 °C. [d] Processed at 85 °C.

The parameters that participate the most to limiting the final efficiency of the devices presented in this study are the fill factor (FF) and, to a lesser extent, the J_{SC}, which can possibly be related to the occurrence of recombination processes or imbalanced charge carrier mobilities.[20] To evaluate charge transport, the hole mobility was assessed for the small molecule materials. Field-effect transistors (FETs) were prepared in the bottom gate bottom contacts configuration by

depositing **CPDT(FBTTh₂)**$_2$, **BDT(FBTTh₂)**$_2$ and **TT(FBTTh₂)**$_2$ from chlorobenzene on a SiO_2 layer, thermally grown on highly n-doped Si. Gold source and drain contacts were pre-patterned on the substrate, on top of a Ti adhesion layer. The same method could not be used for **DTP(FBTTh₂)₂** due to difficulties with solution deposition on the SiO_2 substrate. Although the high threshold voltages observed (see ESI) suggest the possibility of bias stress occurring,[21] the estimated mobilities do not deviate too far from the values reported for other commonly employed organic semiconductors ($\sim 10^{-4}$ for P3HT[22]). Comparable hole mobilities were extracted for **CPDT(FBTTh₂)₂** and **TT(FBTTh₂)₂**, 4.5×10^{-4} and 3.5×10^{-4} cm^2(Vs)$^{-1}$, respectively, while **BDT(FBTTh₂)₂** afforded a FET mobility of only 1.3×10^{-5} cm^2(Vs)$^{-1}$. These results correlate well with the observed solar cell performances and the lower mobility for **BDT(FBTTh₂)₂** is in line with the low J_{SC} values attained for solar cells based on this small molecule. For p-DTS(FBTTh$_2$)$_2$, FET hole mobilities as high as 0.14 cm^2(Vs)$^{-1}$ were reported, which might explain the significant higher performance of this material.[9b]
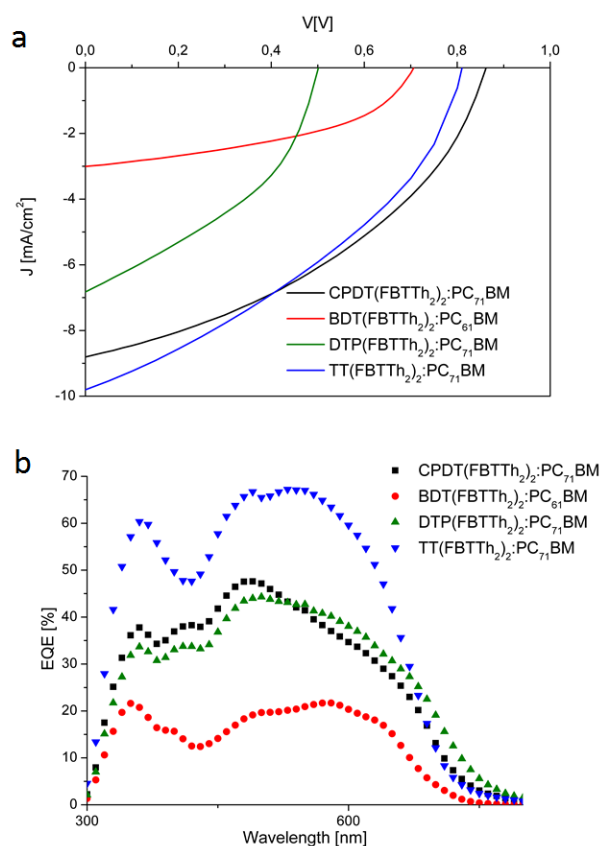
Figure 3: *J-V* characteristics (a) and EQE spectra (b) of the best solar cells prepared. The devices employed for the EQE measurements gave a J_{sc} of 8.81, 2.57, 6.83 and 9.80 mA cm^{-2} for **CPDT(FBTTh$_2$)$_2$**, **BDT(FBTTh$_2$)$_2$**, **DTP(FBTTh$_2$)$_2$**, and **TT(FBTTh$_2$)$_2$**, respectively, with J_{EQE}'s of 7.58, 2.63, 7.85 and 11.16 mA cm^{-2}.

EQE spectra for the best solar cell devices of all four molecules are shown in Figure 3b. The shape of the EQE profiles correlates well to the UV-Vis spectra of the small molecules and for all molecules a clear contribution of both the donor material and the fullerene derivative is observed. For the solar cell device based on **BDT(FBTTh$_2$)$_2$**, no major difference in shape is observed compared to the other

small molecules, but the whole spectrum shifted toward lower EQE values, justifying the lower performance in terms of J_{sc}.

To examine the active layer blend morphology on the nanoscale, atomic force microscopy (AFM) images were acquired in peak force tapping mode. In most cases, the best performing films appear to be fully intermixed, with no evidence of phase separation nor crystallization (Figure 4). **BDT(FBTTh$_2$)$_2$** exceptionally exhibits needle-like features that may be linked to the already reported п-п stacking tendency.[13]
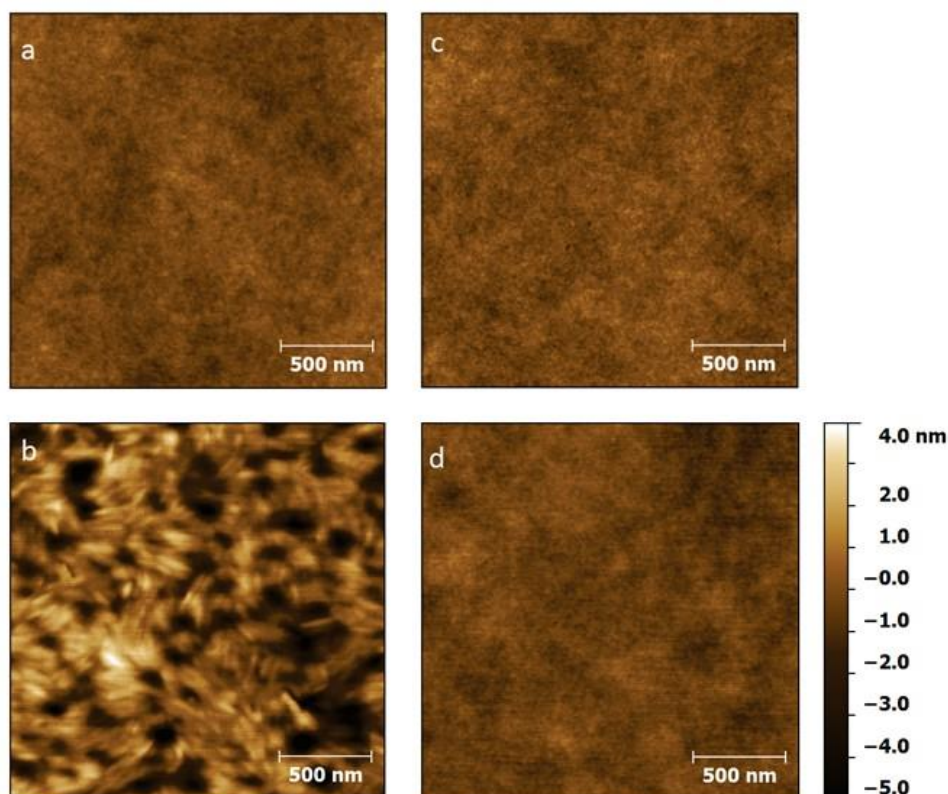

Figure 4: Peak force tapping scans of the active layer blends resulting in best solar cell performances for **CPDT(FBTTh$_2$)$_2$** (a), **BDT(FBTTh$_2$)$_2$** (b), **DTP(FBTTh$_2$)$_2$** (c), and **TT(FBTTh$_2$)$_2$** (d).

While it is possible that the elongated grains comprise entirely of small molecule, and that the methanofullerene remained on a bottom layer, mapping of the nano-mechanical properties does not indicate a clear difference in DMT (Derjaguin–Müller–Toporov) modulus (Figure 5) between the needles and the surrounding area, supporting the possibility of a rather homogeneous material blend.
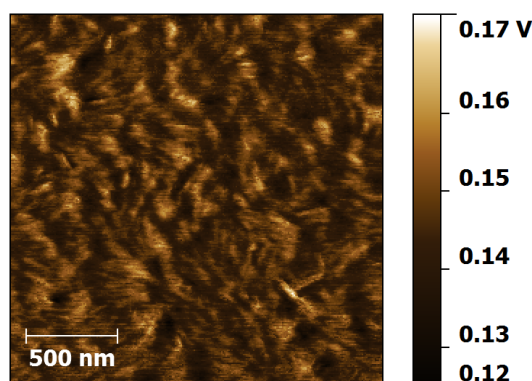
Figure 5: DMT-modulus of the optimal **BDT(FBTTh$_2$)$_2$**:PC$_{61}$BM blend, showing no strong difference in stiffness between the needle-like features and the surroundings.

Surface imaging on non-optimized blends confirmed the tendency of **BDT(FBTTh$_2$)$_2$** to crystallize, and of the other 3 presented small molecules to form more amorphous films. It is also worth to mention that the strongly ordered character of the TT moiety is shown when the **TT(FBTTh$_2$)$_2$**:PC$_{61}$BM blend is processed from tetrachloroethane or, less evidently, in pure form. In these cases, long domains are visible (Figure 6), although the more ordered morphology is again not directly represented by a higher light-conversion efficiency (Table S4).
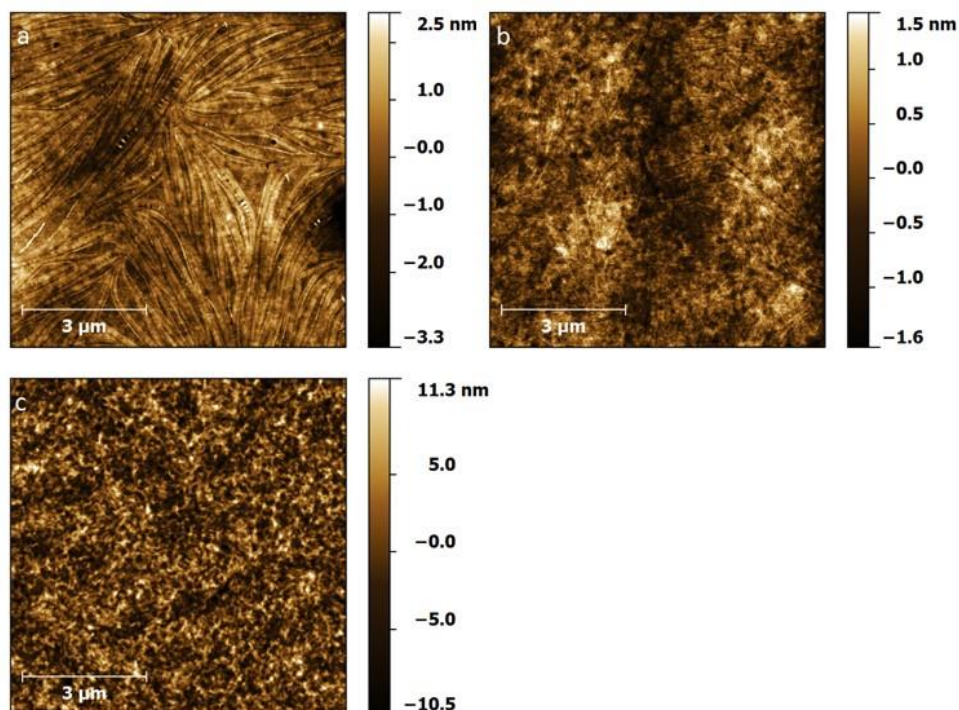
Figure 6: AFM scans of **TT(FBTTh₂)₂**:PC₆₁BM processed from tetrachloroethane in a 1:1 (a) and 1:2 (b) ratio, showing elongated features. A similar morphology is observed for pure **TT(FBTTh₂)₂** when processed from chlorobenzene (c).

The two best-performing small molecules emerged to be the least and the most crystalline ones (**CPDT(FBTTh₂)₂** and **TT(FBTTh₂)₂**) (cfr. RHC data), which leaves the question whether a highly ordered nanoscale structure is to be preferred above a more amorphous system. These two small molecules were then also used to prepare inverted solar cell devices. The resulting solar cells did not exhibit enhanced photovoltaic performances (Figure S5) and the final blend morphology showed no difference compared to the active layers on top of PEDOT:PSS (Figure S4).

6.3 CONCLUSIONS

Small molecules can be viable alternatives for conjugated polymers as electron donor materials in organic solar cells. Generally, these molecules have the advantage of a more easy and reproducible synthesis, combined with the possibility of purifying these materials effectively by classical organic purification methodologies such as column chromatography and recrystallization. However, in this study, we have shown that purification of these "small" molecules is not as straightforward as often projected. Notwithstanding the use of recycling preparative size exclusion chromatography in combination with standard column chromatography, the presence of minor amounts of side products could be demonstrated by MALDI-TOF MS analysis. These impurities could be related to the use of the Stille cross-coupling reaction, as they were identified as homo-coupled products. The presence of these side products seemed to have a detrimental effect on the final solar cell performance. Therefore, considerable care is required to avoid the formation of homo-coupled side products and these small molecules can actually be versatile model systems to optimize Stille reactions as standardly applied for low bandgap copolymers. Furthermore it is shown that variation of the central donor unit greatly affects the physicochemical properties of these small molecule materials. The crystalline character could be modified from almost completely amorphous (**CPDT(FBTTh$_2$)$_2$**) to highly crystalline (**TT(FBTTh$_2$)$_2$**). Despite the large difference in crystallinity, these material showed very comparable solar cell performances (~3% PCE). These values are, however, far below the PCE values reported for p-DTS(FBTTh$_2$)$_2$, which could be related to the reduced mobility for the small molecules reported in this manuscript. In general, it has been confirmed that it is very tough to establish general design rules for

small molecule solar cells, as optimization of a certain parameter very often leads to (unexpected) negative effects.

6.4 EXPERIMENTAL SECTION

6.4.1 Materials and instruments

Preparative (recycling) size exclusion chromatography was performed on a JAI LC-9110 NEXT system equipped with JAIGEL 1*H* and 2*H* columns (eluent $CHCl_3$, flow rate 3.5 mL/min). NMR chemical shifts (δ, in ppm) were determined relative to the residual $CHCl_3$ (7.26 ppm) absorption or the ^{13}C resonance shift of $CDCl_3$ (77.16 ppm). High resolution electrospray ionization mass spectrometry (ESI-MS) was performed using an LTQ Orbitrap Velos Pro mass spectrometer equipped with an atmospheric pressure ionization source operating in the nebulizer assisted electrospray mode. The instrument was calibrated in the *m/z* range 220−2000 using a standard solution containing caffeine, MRFA and Ultramark 1621. MALDI-TOF mass spectra were recorded on a Bruker Daltonics Ultraflex II Tof/Tof. 1 μL of the matrix solution (16 mg mL^{-1} DTCB (*trans*-2-[3-(4-*tert*-butylphenyl)-2-methyl-2-propenylidene]malononitrile) in $CHCl_3$) was spotted onto an MTP Anchorchip 600/384 MALDI plate. The spot was allowed to dry and 1 μL of the analyte solution (0.5 mg mL^{-1} in $CHCl_3$) was spotted on top of the matrix. Reported masses are for the first isotope peak of the isotopic pattern. UV-Vis measurements were performed on a VARIAN Cary 500 UV-Vis-NIR spectrophotometer at a scan rate of 600 nm/min. The films for the UV-Vis measurements were prepared by drop casting a solution of the small molecule in chloroform on a quartz substrate. The solid-state UV-Vis spectra were used to estimate the optical band gaps (from the wavelength at the intersection of the tangent line drawn at the low energy

side of the absorption spectrum with the x-axis: E_g (eV) = 1240/(wavelength in nm)). Rapid heat-cool calorimetry (RHC) experiments were performed on a prototype RHC of TA Instruments, equipped with liquid nitrogen cooling and specifically designed for operation at high scanning rates.[18] RHC measurements were performed at 250 or 500 K min^{-1} in aluminum crucibles, using helium (6 mL min^{-1}) as a purge gas. Electrochemical measurements (cyclic voltammetry) were performed with an Eco Chemie Autolab PGSTAT 30 potentiostat/galvanostat using a three-electrode microcell with a platinum working electrode, a platinum counter electrode and a Ag/AgNO$_3$ reference electrode (silver wire dipped in a solution of 0.01 M AgNO$_3$ and 0.1 M NBu$_4$PF$_6$ in anhydrous acetonitrile). The reference electrode was calibrated against ferrocene/ferrocenium as an external standard. Samples were prepared by dip coating the platinum working electrode in the respective small molecule solutions (also used for the solid-state UV-Vis measurements). The CV measurements were done on the resulting films with 0.1 M NBu$_4$PF$_6$ in anhydrous acetonitrile as electrolyte solution. To prevent air from entering the system, the experiments were carried out under a curtain of argon. Cyclic voltammograms were recorded at a scan rate of 100 mV s^{-1}. For the conversion of V to eV, the onset potentials of the first oxidation/reduction peaks were used and referenced to ferrocene/ferrocenium, which has an ionization potential of -4.98 eV *vs.* vacuum. This correction factor is based on a value of 0.31 eV for Fc/Fc$^+$ *vs.* SCE[23a] and a value of 4.68 eV for SCE *vs.* vacuum[23b]:

$E_{HOMO/LUMO}$ (eV) = $-4.98 - E_{onset\ ox/red}^{Ag/AgNO3}$ (V) $+ E_{onset\ Fc/Fc+}^{Ag/AgNO3}$ (V).

6.4.2 Synthesis

Unless stated otherwise, all reagents and chemicals were obtained from commercial sources and used without further purification. Solvents were dried by

a solvent purification system (MBraun, MB-SPS-800) equipped with alumina columns. Precursors 3,5'-dihexyl-2,2'-bithiophene,[16] 2,6-bis(trimethylstannyl)-4-(2'-ethylhexyl)-4-octyl-4H-cyclopenta[2,1-b:3,4-b']dithiophene,[24] 2,6-bis(trimethylstannyl)-4,8-bis[(2-ethylhexyl)oxy]benzo[1,2-b:4,5-b']dithiophene[25] and 2,6-bis(trimethylstannyl)-N-(2-ethylhexanoyl)dithieno[3,2-b:2',3'-d]pyrrole[14] were prepared according to literature procedures. 2,5-Bis(trimethylstannyl)thieno[3,2-b]thiophene was purchased from Sigma-Aldrich. p-DTS(FBTTh$_2$)$_2$ was obtained from 1-material.

[3,5'-Dihexyl-(2,2'-bithiophen)-5-yl]trimethylstannane (2)

To an ice cooled solution of 3,5'-dihexyl-2,2'-bithiophene (7.09 g, 21.2 mmol) in dry diethyl ether (30 mL), n-BuLi (2.5 M in n-hexane; 9.4 mL, 23.5 mmol) was added under a N$_2$ atmosphere. The mixture was stirred for 30 min at 0 °C and Me$_3$SnCl (1 M in THF; 27.4 mL) was added. The solution was allowed to warm gently to room temperature (overnight) and water was added. After extraction with diethyl ether, the organic phase was washed with brine, dried with MgSO$_4$, filtered and evaporated to dryness. The crude product was used without further purification.

4-Bromo-7-[3,5'-dihexyl-(2,2'-bithiophen)-5-yl]-5-fluorobenzo[c][1,2,5]thiadiazole (3)

[3,5'-Dihexyl-(2,2'-bithiophen)-5-yl]trimethylstannane (1.50 g, 3.02 mmol) and 4,7-dibromo-5-fluorobenzo[c][1,2,5]thiadiazole (0.940 g, 3.02 mmol) were dissolved in dry DMF (10 mL) and dry toluene (10 mL) under N$_2$ atmosphere. Pd(PPh$_3$)$_4$ (0.100 g, 0.0865 mmol) was added and the mixture was stirred for 15 h at 80 °C. The solution was allowed to cool to room temperature and water was added. After extraction with diethyl ether, the organic layer was washed with

brine, dried with $MgSO_4$, filtered and the solvent was removed under vacuum. Purification by column chromatography (silica, petroleum ether:dichloromethane, 70:30) and recycling prep-SEC yielded the pure product as an orange solid (1.10 g, 1.94 mmol, 64%). ^{1}H NMR (400 MHz, $CDCl_3$): δ 7.96 (s, 1H), 7.65 (d, J = 10.1 Hz, 1H), 7.05 (d, J = 3.6 Hz, 1H), 6.77 (d, J = 3.6, 1H), 2.82 (q, J = 7.8 Hz, 4H), 1.71 (quint, J = 7.3 Hz, 4H), 1.48–1.23 (m, 12H), 0.96–0.82 (m, 6H); ^{13}C NMR (100 MHz, $CDCl_3$): δ 160.9 (d, $^1J_{C\text{-}F}$ = 251.2 Hz, 1H), 154.4 (d, $^3J_{C\text{-}F}$ = 7.4 Hz, 1H), 149.1 (1H), 147.3 (1H), 140.2 (1H), 135.0 (1H), 134.1 (1H), 133.0 (1H), 132.3 (1H), 127.5 (d, $^3J_{C\text{-}F}$ = 10.3 Hz, 1H), 126.3 (1H), 124.8 (1H), 115.5 (d, $^2J_{C\text{-}F}$ = 30.9 Hz, 1H), 95.8 (d, $^2J_{C\text{-}F}$ = 24.8 Hz, 1H), 31.8 (1H), 31.7 (2H), 30.7 (1H), 30.3 (1H), 29.6 (1H), 29.4 (1H), 29.0 (1H), 22.8 (1H), 22.7 (1H), 14.3 (2H).

7,7'-[4-(2'-Ethylhexyl)-4-octyl-4*H*-cyclopenta[2,1-*b*:3,4-*b*']dithiophene-2,6-diyl]bis{4-[3,5'-dihexyl-(2,2'-bithiophen)-5-yl]-6-fluorobenzo[c][1,2,5]thiadiazole} [CPDT(FBTTh₂)₂]

General synthesis protocol for the small molecules: Precursor **3** (200 mg, 0.354 mmol), 2,6-bis(trimethylstannyl)-4-(2'-ethylhexyl)-4-octyl-4*H*-cyclopenta[2,1-*b*:3,4-*b'*]dithiophene (126 mg, 0.173 mmol) and Pd(PPh₃)₄ (10 mg, 0.0087 mmol) were dissolved in a mixture of dry DMF (2 mL) and dry toluene (2 mL). The solution was purged with N₂ gas for 30 min and heated to 110 °C for 15 h. The resulting mixture was allowed to cool to room temperature and was precipitated in methanol. After filtration, the crude material was further purified by column chromatography (silica, petroleum ether:dichloromethane, 60:40) and recycling prep-SEC and the pure material was collected as a dark blue solid (185 mg, 0.135 mmol, 78%).

^{1}H NMR (400 MHz, CDCl$_3$): δ 8.24 (s, 1H), 8.22 (s, 1H), 7.97 (d, J = 1.3 Hz, 2H), 7.73 (dd, J = 13.4, 1.3 Hz, 2H), 7.06 (d, J = 3.6 Hz, 2H), 6.77 (d, J = 3.6, 2H), 2.84 (q, J = 7.5, 8H), 2.16–1.93 (m, 4H), 1.80–1.65 (m, 8H), 1.50–1.27 (m, 25H), 1.24–1.10 (m, 10H), 1.10–0.95 (m, 10H), 0.95–0.83 (m, 12H), 0.83–0.73 (m, 3H), 0.71–0.59 (m, 6H); HRMS (ESI): calcd. for C$_{77}$H$_{96}$F$_2$N$_4$S$_8$Na [M+Na]$^+$: 1393.5261, found: 1393.5240; MS (MALDI-TOF) m/z: 1370.52 ([M]$^+$)

7,7'-{4,8-Bis[(2-ethylhexyl)oxy]benzo[1,2-*b*:4,5-*b'*]dithiophene-2,6-diyl}bis{4-(3,5'-dihexyl-[2,2'-bithiophen]-5-yl)-6-fluorobenzo[*c*][1,2,5]thiadiazole} [BDT(FBTTh$_2$)$_2$]

BDT(FBTTh$_2$)$_2$ was prepared according to the general synthesis protocol for small molecules: Precursor **3** (200 mg, 0.354 mmol), 2,6-bis(trimethylstannyl)-4,8-bis[(2-ethylhexyl)oxy]benzo[1,2-*b*:4,5-*b'*]dithiophene (133 mg, 0.172 mmol) and Pd(PPh$_3$)$_4$ (10 mg, 0.0087 mmol) were dissolved in a mixture of dry DMF (2 mL) and dry toluene (2 mL). The pure material was obtained as a dark purple solid (175 mg, 0.124 mmol, 72%).

^{1}H NMR (400 MHz, CDCl$_3$) δ 8.60 (s, 2H), 7.85 (s, 2H), 7.57 (d, J = 13.2 Hz, 2H), 6.96 (d, J = 3.5 Hz, 2H), 6.70 (d, J = 3.5, 2H), 4.28 (s, 4H), 2.79 (t, J = 7.7 Hz, 4H), 2.71 (t, J = 8.0 Hz, 4H), 1.95–1.76 (m, 6H), 1.75–1.47 (m, 33H), 1.47–1.28 (m, 25H), 1.16 (t, J = 7.3 Hz, 6H), 1.04 (t, J = 7.0 Hz, 6H), 0.96–0.87 (m, 12H); HRMS (ESI): calcd. for C$_{78}$H$_{96}$F$_2$N$_4$O$_2$S$_8$Na [M+Na]$^+$: 1437.5159, found: 1437.5172; MS (MALDI-TOF) m/z: 1414.50 ([M]$^+$)

1-(2,6-Bis{7-[3,5'-dihexyl-(2,2'-bithiophen)-5-yl]-5-fluorobenzo[*c*][1,2,5]thiadiazol-4-yl}-4*H*-dithieno[3,2-*b*:2',3'-*d*]pyrrol-4-yl)-2-ethylhexan-1-one [DTP(FBTTh₂)₂]

DTP(FBTTh₂)₂ was prepared according to the general synthesis protocol for small molecules: Precursor **3** (200 mg, 0.354 mmol), 2,6-bis(trimethylstannyl)-*N*-(2-ethylhexanoyl)dithieno[3,2-*b*:2',3'-*d*]pyrrole (107 mg, 0.170 mmol) and Pd(PPh₃)₄ (10 mg, 0.0087 mmol) were dissolved in a mixture of dry DMF (2 mL) and dry toluene (2 mL). The pure material was obtained as a dark blue solid (150 mg, 0.117 mmol, 69%).

^{1}H NMR (400 MHz, CDCl₃) δ 8.70–8.05 (br, 2H), 7.60–7.25 (br, 2H), 7.13 (d, J = 13.7 Hz, 2H), 6.75 (s, 2H), 6.57 (s, 2H), 3.32 (quint, J = 6.2 Hz, 1H), 2.81–2.60 (m, 4H), 2.56–2.26 (br, 4H), 2.21–2.01 (m, 2H), 2.01–1.80 (m, 2H), 1.78–1.43 (m, 19H), 1.42–1.20 (m, 27H), 1.09 (t, J = 7.2 Hz, 3H), 0.92 (t, J = 6.7 Hz, 12H); HRMS (ESI): calcd. for C₆₈H₇₇F₂N₅OS₈Na [M+Na]⁺: 1296.3754, found: 1296.3750; MS (MALDI-TOF) *m/z*: 1273.91 ([M]⁺)

2,5-Bis{7-[3,5'-dihexyl-(2,2'-bithiophen)-5-yl]-5-fluorobenzo[*c*][1,2,5]thiadiazol-4-yl}thieno[3,2-*b*]thiophene [TT(FBTTh₂)₂]

Precursor **3** (250 mg, 0.442 mmol), 2,5-bis(trimethylstannyl)thieno[3,2-*b*]thiophene (103 mg, 0.221 mmol) and Pd(PPh₃)₄ (15 mg, 0.013 mmol) were dissolved in a mixture of dry DMF (2 mL) and dry toluene (2 mL). The solution was purged with N₂ gas for 30 min and heated to 110 °C for 15 h. The mixture was cooled down to room temperature and the formed precipitate was filtered in a Soxhlet timble. Soxhlet extractions were subsequently performed with methanol, acetone, *n*-hexane and chloroform. The chloroform fraction was

precipitated in acetone and the resulting dark purple solid was collected through filtration (181 mg, 0.164 mmol, 74%). Due to its limited solubility in $CHCl_3$, the product could not be further purified by recycling prep-SEC.

^{1}H NMR (400 MHz, $CDCl_3$) δ 8.59 (s, 2H), 7.99 (s, 2H), 7.66 (d, J = 13.4 Hz, 2H), 6.97 (d, J = 3.6 Hz, 2H), 6.72 (d, J = 3.6 Hz, 2H), 2.85 (t, J = 7.6 Hz, 4H), 2.79 (t, J = 7.8 Hz, 4H), 1.79–1.67 (m, 8H), 1.52–1.32 (m, 26H), 1.00–0.91 (m, 12H); HRMS (ESI): calcd. for $C_{58}H_{62}F_2N_4S_8Na$ $[M+Na]^+$: 1131.2600, found: 1131.2565; MS (MALDI-TOF) m/z: 1108.33 ($[M]^+$)

6.4.3 Solar cell and FET preparation and characterization

Solar cells in standard architecture were prepared with a layout glass/ITO/PEDOT:PSS/small molecule:methanofullerene/Ca/Al. Substrates with pre-patterned ITO on glass were purchased from Kintec (100 nm, 20 Ohm/sq) and cleaned through sonication in soap, deionized water, acetone and isopropyl alcohol before proceeding with the spin-coating of PEDOT:PSS (Heraeus Clevios AI 4083). Substrates were subsequently brought inside a N_2 filled glovebox and annealed during 10 min at 130 °C to remove residual humidity. All subsequent steps of processing and characterization were conducted in inert atmosphere. The active layers in the various blend compositions (see Table 2 and ESI) were spin-casted on the PEDOT:PSS layer. The optimal concentrations were found to be 35 mg/mL for **CPDT-**, **DTP-**, and **TT(FBTTh₂)₂** (in the aforementioned solvents) and 20 mg/mL for **BDT(FBTTh₂)₂**. In case of additives present in the processing solution, the films were kept under vacuum for a minimum of 2 h to remove eventual solvent remainders before thermally evaporating Ca/Al (30/80 nm) stacks as top contacts, defining device areas of 0.03 cm^2 through the use of masks. Inverted architecture devices with the structure glass/ITO/ZnO/small

molecule:methanofullerene/MoO$_3$/Ag were fabricated by spin-coating a zinc acetate based precursor on the glass/ITO substrates. An annealing step in air at 300 °C was necessary to obtain ZnO. The active layers were then deposited as described above for standard devices. MoO$_3$ (15 nm) and Ag (80 nm) were thermally evaporated to serve as top hole-extracting contact. Electrical characterization was carried out under illumination from a Newport class A solar simulator (model 91195A), calibrated with a silicon solar cell to give an AM 1.5G spectrum. EQE measurements were performed with a Newport Apex illuminator (100 W Xenon lamp, 6257) as light source, a Newport Cornerstone 130 monochromator and a Stanford SR830 lock-in amplifier for the current measurements. A silicon-calibrated FDS-100 photodiode was employed as a reference cell. Peak Force Tapping AFM images were acquired with a Bruker Multimode 8 AFM, employing ScanAsyst. The silicon nitride tip had a spring constant of 4 N m^{-1}. FET's were prepared by spin-coating solutions of **CPDT(FBTTh$_2$)$_2$**, **BDT(FBTTh$_2$)$_2$** and **TT(FBTTh$_2$)$_2$** in chlorobenzene with a concentration of 15, 15 and 8 mg/mL, respectively, on 200 nm of thermally grown SiO$_2$. The gate contact consisted of highly n-doped Si. Source and drain electrodes were pre-patterned, comprising of a stack of Ti/Au (10/100 nm). FET substrates were acquired from Philips. The channel length was 10 μm. Two Keithley 2400 source meters were used to measure the I_{DS} and correct it for leakage through the gate electrode. All FET preparations and characterizations were carried out in a N$_2$ filled glove box.

6.5 ACKNOWLEDGEMENTS

6.6 REFERENCES

[1]   Recent reviews on organic solar cells: (*a*) M. Jørgensen, K. Norrman, S. A. Gevorgyan, T. Tromholt, B. Andreasen and F. C. Krebs, *Adv. Mater.*, 2012, **24**, 580; (*b*) H. Zhou, L. Yang and W. You, *Macromolecules*, 2012, **45**, 607; (*c*) Y. Li, *Acc. Chem. Res.*, 2012, **45**, 723; (*d*) Y. Su, S. Lan and K. Wei, *Mater. Today*, 2012, **15**, 554; (*e*) R. Søndergaard, M. Hösel, D. Angmo, T. T. Larsen-Olsen and F. C. Krebs, *Mater. Today*, 2012, **15**, 36; (*f*) R. A. J. Janssen and J. Nelson, *Adv. Mater.*, 2013, **25**, 1847; (*g*) S. Lizin, S. Van Passel, E. De Schepper, W. Maes, L. Lutsen, J. Manca and D. Vanderzande, *Energy Environ. Sci.*, 2013, **6**, 3136; (*h*) T. Xu and L. Yu, *Mater. Today*, 2014, **17**, 11; (*i*) J. Roncali, P. Leriche and P. Blanchard, *Adv. Mater.*, 2014, **26**, 3821.

[2]   (*a*) G. Yu, J. Gao, J. Hummelen, F. Wudl and A. Heeger, *Science*, 1995, **270**, 1789; (b) A. J. Heeger, *Adv. Mater.*, 2014, **26**, 10.

[3]   (*a*) A. Facchetti, *Mater Today*, 2013, **16**, 123; (*b*) Y. Linac and X. Zhan, *Mater. Horiz.*, 2014, **1**, 470; (*c*) A. F. Eftaiha, J.-P. Sun, I. G. Hill and G. C. Welch, *J. Mater. Chem. A*, 2014, **2**, 120.

[4]   (*a*) K. M. Coakley and M. D. McGehee, *Chem. Mater.*, 2004, **16***,* 4533; (*b*) S. Günes, H. Neugebauer and N. S. Sariciftci, *Chem. Rev.*, 2007, **107**, 1324; (*c*) B. C. Thompson and J. M. J. Fréchet, *Angew. Chem. Int. Ed.*, 2008, **47**, 58.

[5]   (*a*) Z. He, C. Zhong, S. Su, M. Xu, H. Wu and Y. Cao, *Nat. Photonics*, 2012, **6**, 591; (*b*) L. Ye, S. Zhang, W. Zhao, H. Yao and J. Hou, *Chem. Mater.*, 2014, **26**, 3603; (*c*) K. Zhang, C. Zhong, S. Liu, C. Mu, Z. Li, H. Yan, F. Huang and Y. Cao, *ACS Appl. Mater. Interfaces*, 2014, **6**, 10429; (*d*) Y. Liu, J. Zhao, Z. Li, C. Mu, W. Ma, H. Hu, K. Jiang, H. Lin, H. Ade and H. Yan, *Nat. Commun.*, 2014, **5**, 5293.

[6]   (*a*) R. L. Uy, S. C. Price and W. You, *Macromol. Rapid Commun.*, 2012, **33**, 1162; (*b*) M. Jeffries-EL, B. M. Kobilka and B. J. Hale, *Macromolecules*, 2014, **47**, 7253.

[7]   (*a*) A. Mishra and P. Bäuerle, *Angew. Chem. Int. Ed.*, 2012, **51**, 2020; (*b*) Y. Chen, X. Wan and G. Long, *Acc. Chem. Res.*, 2013, **46**, 2645.

[8]   (*a*) Y. Liu, C.-C. Chen, Z. Hong, J. Gao, Y. M. Yang, H. Zhou, L. Dou, G. Li and Y. Yang, *Scientific Reports*, 2013, **3**, 3356; (*b*) A. K. K. Kyaw, D. H. Wang, V. Gupta, J. Zhang, S. Chand, G. C. Bazan and A. J. Heeger, *Adv. Mater.*, 2013, **25**, 2397; (*c*) B. Kan, Q. Zhang, M. Li, X. Wan, W. Ni, G. Long, Y. Wang, X. Yang, H. Feng and Y. Chen, *J. Am. Chem. Soc.*, 2014, **136**, 15529.

[9]   (*a*) T. S. van der Poll, J. A. Love, T.-Q. Nguyen and G. C. Bazan, *Adv. Mater.*, 2012, **24**, 3646; (*b*) A. K. K. Kyaw, D. H. Wang, V. Gupta, W. L. Leong, L. Ke, G. C. Bazan and A. J. Heeger, *ACS Nano*, 2013, **7**, 4569; (*c*) J. E. Coughlin, Z. B. Henson, G. C. Welch and G. Bazan, *Acc. Chem. Res.*, 2014, **47**, 257.

[10]   (*a*) J. Zhou, Y. Zuo, X. Wan, G. Long, Q. Zhang, W. Ni, Y. Liu, Z. Li, G. He, C. Li, B. Kan, M. Li and Y. Chen, *J. Am. Chem. Soc.*, 2013, **135**, 8484; (*b*) Y. Chen, X. Wan and G. Long, *Acc. Chem. Res.*, 2013, **46**, 2645.

[11]   (*a*) J. Min, Y. N. Luponosov, A. Gerl, M. S. Polinskaya, S. M. Peregudova, P. V. Dmitryakov, A. V. Bakirov, M. A. Shcherbina, S. N. Chvalun, S. Grigorian, N. Kaush-Busies, S. A. Ponomarenko, T. Ameri and C. J. Brabec, *Adv. Energy Mater*., 2014, **5**, 1301234; (*b*) V. S. Gevaerts, E. M. Herzig, M. Kirkus, K. H. Hendriks, M. M. Wienk, J. Perlich, P. Müller-Buschbaum and R. A. J. Janssen, *Chem. Mater.*, 2014, **26**, 916; (*c*) M. Jung, Y. Yoon, J. H. Park, W. Cha, A. Kim, J. Kang, S. Gautam, D. Seo, J. H. Cho, H. Kim, J. Y. Choi, K. H. Chae, K. Kwak, H. J. Son, M. J. Ko, H. Kim, D.-K. Lee, J. Y. Kim, D. H. Choi and B. Kim, *ACS Nano*, 2014, **8**,

5988; (*d*) H. Qin, L. Li, F. Guo, S. Su, J. Peng, Y. Cao and X. Peng, *Energy Environ. Sci.*, 2014, **7**, 1397.

[12]   (*a*) J. Peet, J. Y. Kim, N. E. Coates, W. L. Ma, D. Moses, A. J. Heeger and G. C. Bazan, *Nat. Mater.*, 2007, **6**, 497; (*b*) A. P. Zoombelt, S. G. J. Mathijssen, M. G. R. Turbiez, M. M. Wienk and R. A. J. Janssen, *J. Mater. Chem.*, 2010, **20**, 2240; (*c*) S. Albrecht, S. Janietz, W. Schindler, J. Frisch, J. Kurpiers, J. Kniepert, S. Inal, P. Pingel, K. Fostiropoulos, N. Koch and D. J. Neher, *J. Am. Chem. Soc.*, 2012, **134**, 14932; (*d*) S. Van Mierloo, A. Hadipour, M.-J. Spijkman, N. Van den Brande, B. Ruttens, J. Kesters, J. D'Haen, G. Van Assche, D. M. de Leeuw, T. Aernouts, J. Manca, L. Lutsen, D. Vanderzande and W. Maes, *Chem. Mater.*, 2012, **24**, 587.

[13]   (*a*) L. Huo, S. Zhang, X. Guo, F. Xu, Y. Li, and J. Hou, *Angew. Chem. Int. Ed.*, 2011, **50**, 9697; (*b*) L. Lu and L. Yu, *Adv. Mater.*, 2014, **26**, 4413.

[14]   (*a*) W. Vanormelingen, J. Kesters, P. Verstappen, J. Drijkoningen, J. Kudrjasova, S. Koudjina, V. Liégeois, B. Champagne, J. Manca, L. Lutsen, D. Vanderzande and W. Maes, *J. Mater. Chem. A*, 2014, **2**, 7535; (*b*) J. Kesters, P. Verstappen, W. Vanormelingen, J. Drijkoningen, T. Vangerven, L. Marin, B. Champagne, J. Manca, L. Lutsen, D. Vanderzande and W. Maes, *Sol. Energy Mater. Sol. Cells*, revised manuscript submitted.

[15]   (a) H. Bronstein, Z. Chen, R. S. Ashraf, W. Zhang, J. Du, J. R. Durrant, P. S. Tuladhar, K. Song, S. E. Watkins, Y. Geerts, M. M. Wienk, R. A. J. Janssen, T. Anthopoulos, H. Sirringhaus, M. Heeney and I. McCulloch, *J. Am. Chem. Soc.*, 2011, **133**, 3272; (*b*) J. C. Bijleveld, R. A. M. Verstrijden, M. M. Wienk and R. A. J. Janssen, *J. Mater. Chem.*, 2011, **21**, 9224; (*c*) Y. S. Choi and W. H. Jo, *Org. Electron.*, 2013, **14**, 1621.

[16]   C.-Y. Kuo, W. Nie, H. Tsai, H.-J. Yen, A. D. Mohite, G. Gupta, A. M. Dattelbaum, D. J. William, K. C. Cha, Y. Yang, L. Wang and H.-L. Wang, *Macromolecules*, 2014, **47**, 1008.

[17]   V. Farina, V. Krishnamurthy and W. J. Scott, *The Stille Reaction. Organic Reactions.* 50:1:1–652, 2004, Wiley.

[18]   (*a*) R. L. Danley, P. A. Caulfield and S. R. Aubuchon, *Am. Lab.*, 2008, **40**, 9; (*b*) T. Ghoos, N. Van den Brande, M. Defour, J. Brassinne, C.-A. Fustin, J.-F. Gohy, S. Hoeppener, U. S. Schubert, W. Vanormelingen, L. Lutsen, D. J. Vanderzande, B. Van Mele and W. Maes, *Eur. Polym. J.*, 2014, **53**, 206.

[19]   K. H. Hendriks, W. Li, G. H. L. Heintges, G. W. P. van Pruissen, M. M. Wienk and R. A. J. Janssen, *J. Am. Chem. Soc.*, 2014, **136**, 11128.

[20]   L. J. A. Koster, V. D. Mihailetchi and P. W. M. Blom, *Appl. Phys. Lett.*, 2006, **88**, 052104.

[21]   A. Salleo and R. A. Street, *J. Appl. Phys.*, 2003, **94**, 471.

[22]   J.-C. Bolsée and J. Manca, *Synthetic Met.*, 2011, **161**, 789.

[23]   (*a*) J. Bard and L. R. Faulkner, *Electrochemical methods: fundamentals and applications*, 2nd Ed., 2001, Wiley; (*b*) S. Trasatti, *Pure Appl. Chem.*, 1986, **58**, 955.

[24]   P. Verstappen, J. Kesters, W. Vanormelingen, G. H. L. Heintges, J. Drijkoningen, T. Vangerven, L. Marin, S. Koudjina, B. Champagne, J. Manca, L. Lutsen, D. Vanderzande and W. Maes, *J. Mater. Chem. A*, 2015, DOI: 10.1039/C4TA06054G.

[25]   J. Hou, M.-H. Park, S. Zhang, Y. Yao, L.-M. Chen, J.-H. Li and Y. Yang, *Macromolecules*, 2008, **41**, 6012.

6.7 SUPPORTING INFORMATION

6.7.1   NMR spectra of the small molecules
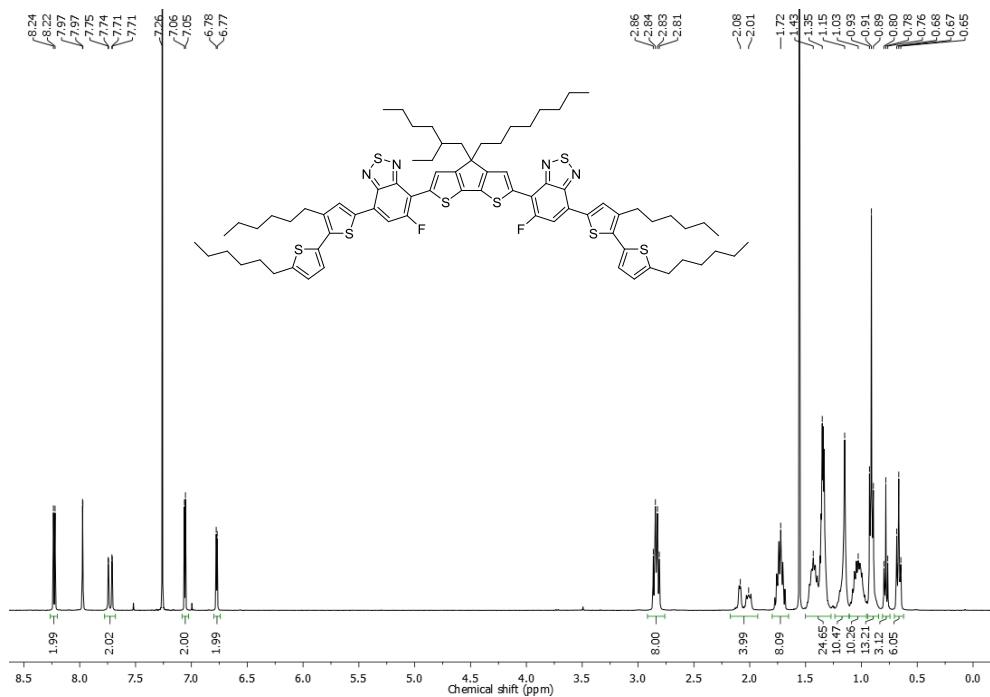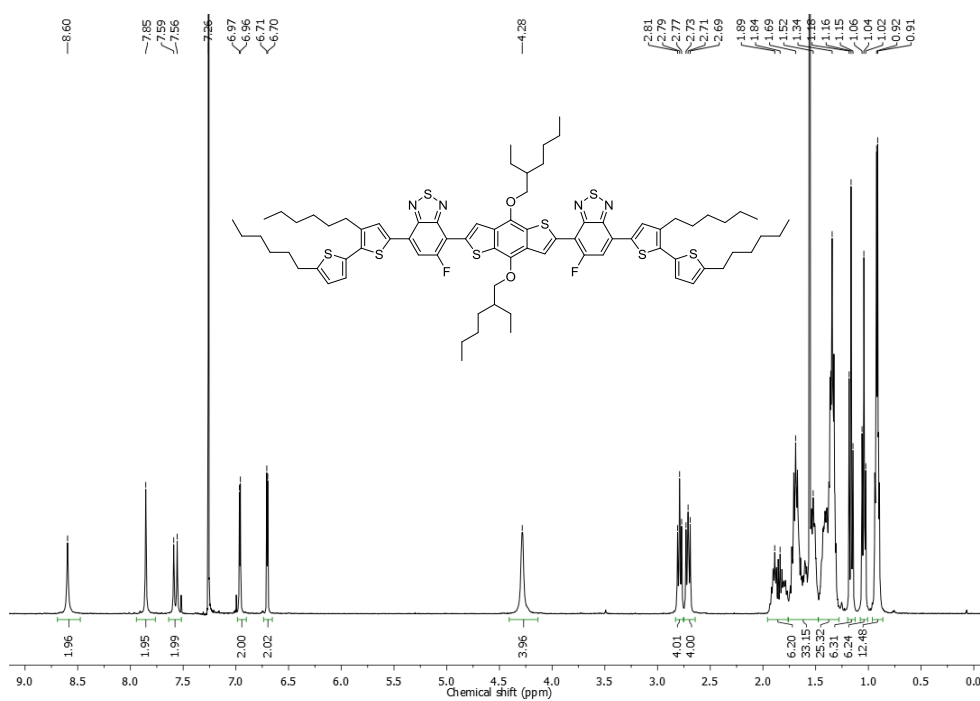
CPDT(FBTTh₂)₂
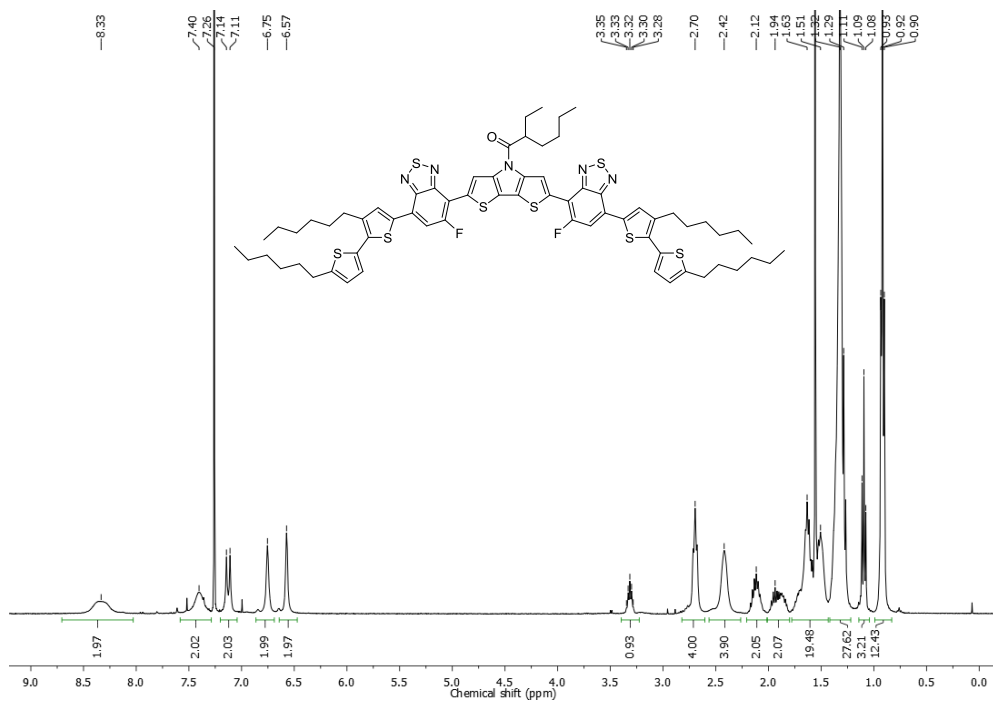
BDT(FBTTh₂)₂

DTP(FBTTh₂)₂
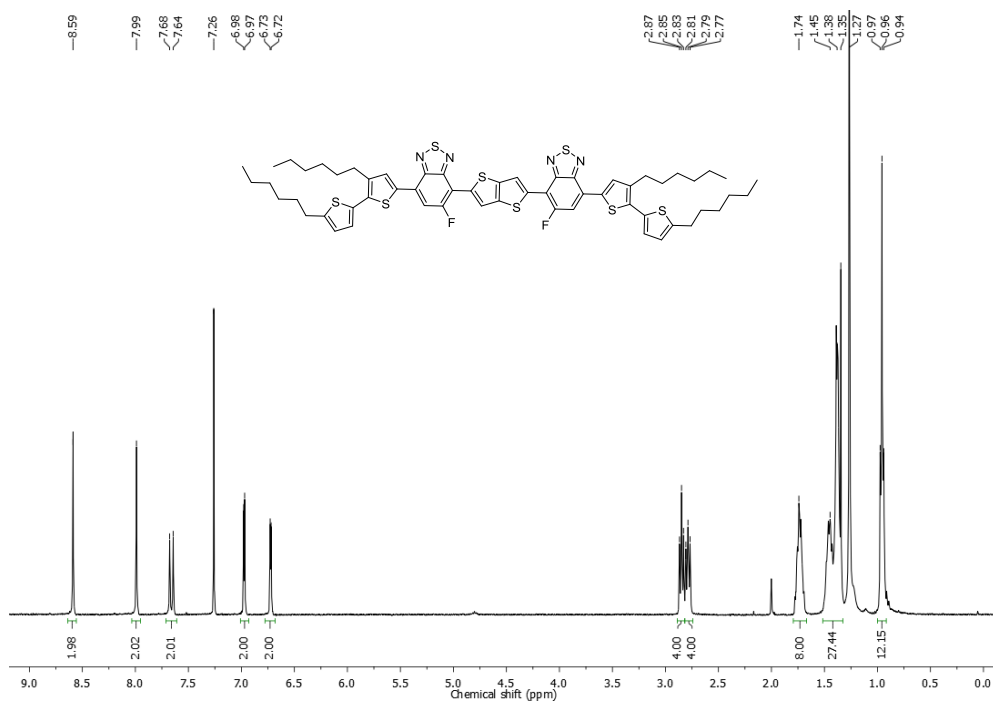
TT(FBTTh₂)₂

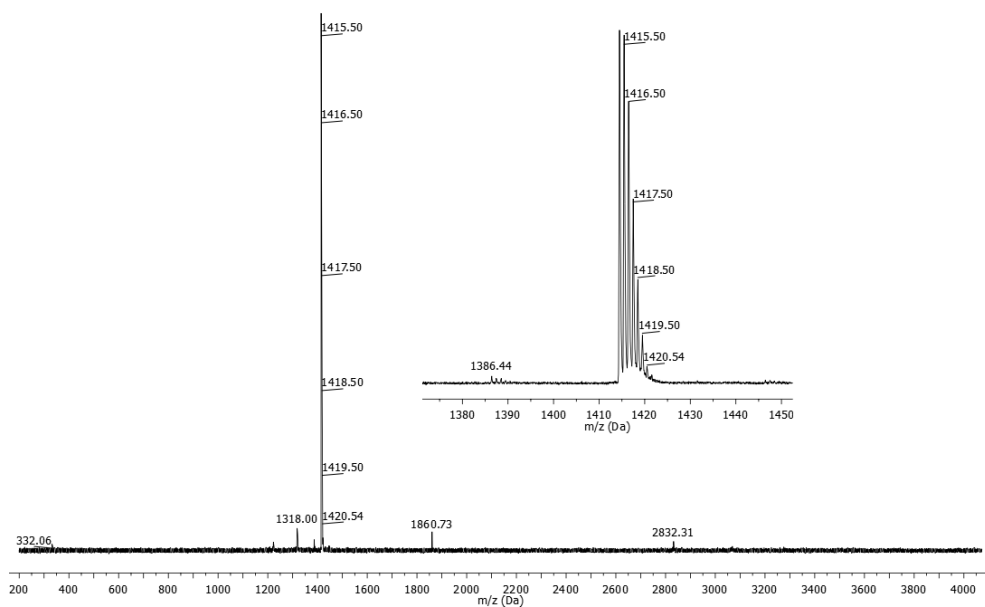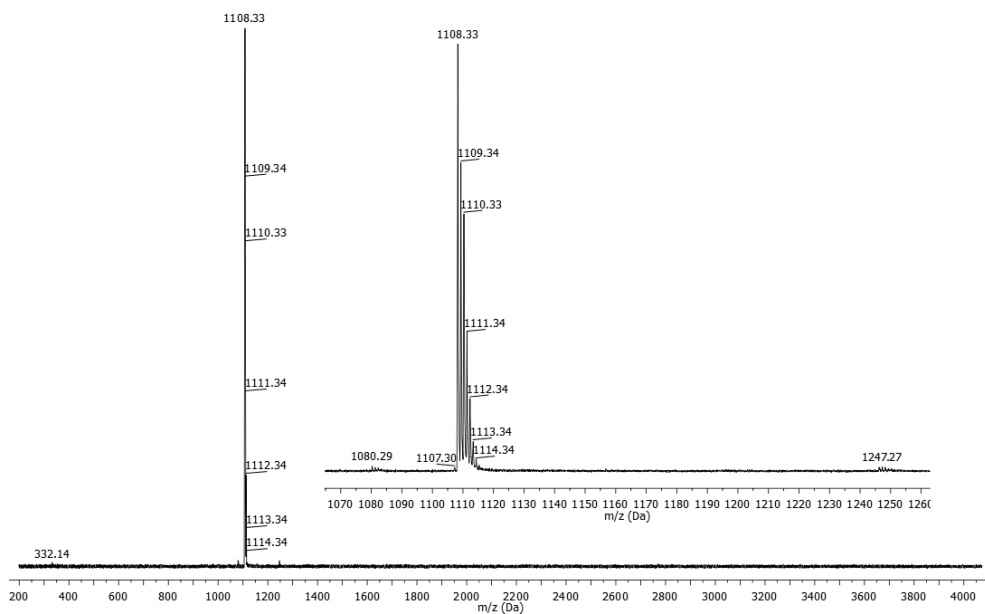### 6.7.2 MALDI-TOF spectra of the small molecules
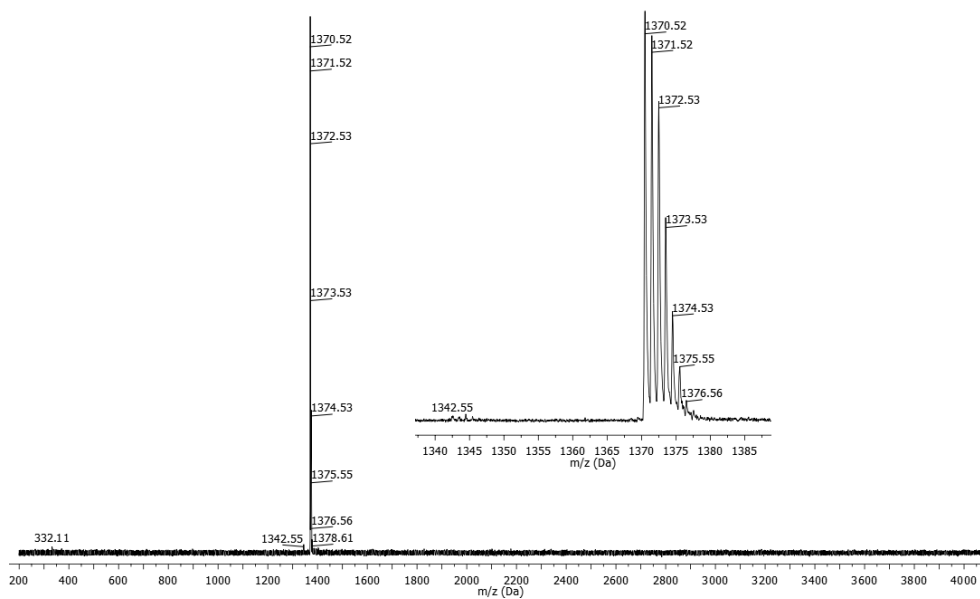
CPDT(FBTTh$_2$)$_2$

BDT(FBTTh₂)₂

DTP(FBTTh₂)₂
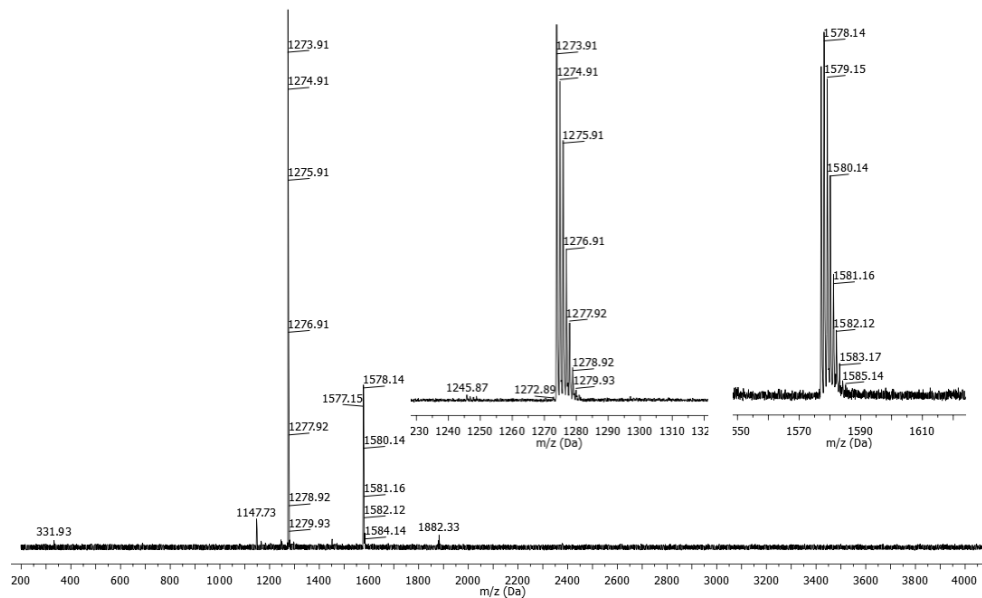
TT(FBTTh₂)₂

6.7.3 RHC spectrum of p-DTS(FBTTh$_2$)$_2$
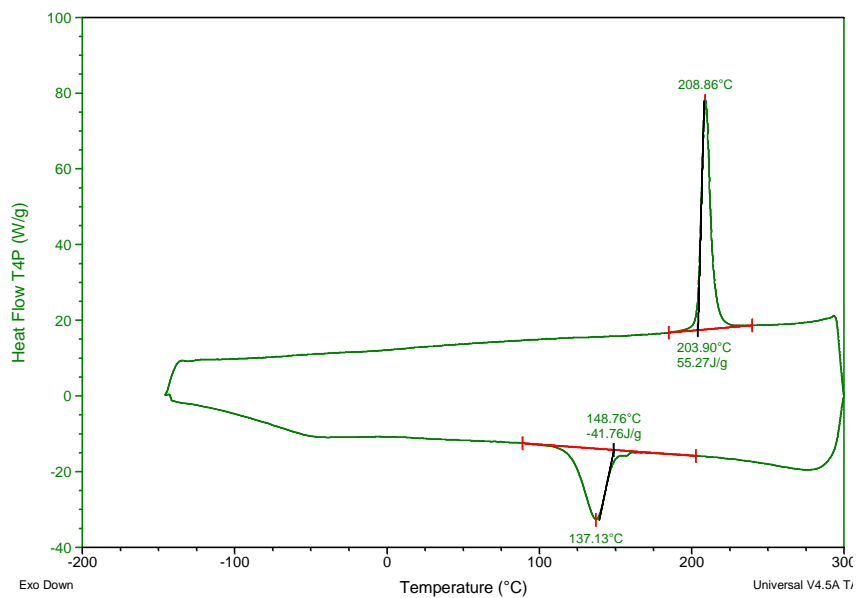
Figure S1: RHC profile for p-DTS(FBTTh$_2$)$_2$. The melting point (T_m) was determined to be 209 °C with a melting enthalpy (ΔH_m) of 55.3 J/g.

6.7.4 Optimization of the solar cell performance for each small molecule

Table S1: Optimization of the solar cell devices based on **CPDT(FBTTh$_2$)$_2$**.

Acceptor	Ratio	Solvent[a]	J_{sc} (mA/cm^2)	V_{oc} (V)	FF (%)	PCE[b] (%)
PC$_{61}$BM	1:2	CF	4.79	0.81	30	1.17 (1.22)
PC$_{61}$BM	1:2	CF	4.88	0.86	30	1.28 (1.33)[c]
PC$_{61}$BM	1:3	CF	5.12	0.79	32	1.29 (1.33)
PC$_{61}$BM	1:3	CF	5.47	0.84	32	1.40 (1.46)[c]
PC$_{71}$BM	1:2	CB	8.44	0.85	38	2.77 (3.00)
PC$_{71}$BM	1:3	CB	8.39	0.85	40	2.83 (3.10)
PC$_{71}$BM	1:2	oDCB	7.74	0.83	41	2.61 (2.74)
PC$_{71}$BM	1:3	oDCB	7.63	0.82	39	2.46 (2.53)
PC$_{71}$BM	1:3	CB + 0.1% DIO	8.02	0.83	36	2.38 (2.58)
PC$_{71}$BM	1:3	CB + 0.3% DIO	7.90	0.83	37	2.42 (2.52)
PC$_{71}$BM	1:3	CB + 0.1% CN	8.40	0.84	39	2.72 (2.93)
PC$_{71}$BM	1:3	CB + 0.3% CN	8.31	0.83	38	2.64 (2.70)

[a] CF = chloroform, CB = chlorobenzene, oDCB = *ortho*-dichlorobenzene, DIO = 1,8-diiodooctane, CN = 1-chloronaphthalene. [b] Averaged over at least 3 devices. The best device performance is shown between brackets. [c] Post-annealed at 100°C.

Table S2: Optimization of the solar cell devices based on **BDT(FBTTh$_2$)$_2$**.

Acceptor	Ratio	Solvent[a]	J_{sc} (mA/cm^2)	V_{oc} (V)	FF (%)	PCE[b] (%)
PC$_{71}$BM	1:1	CF	1.69	0.70	40	0.47
PC$_{71}$BM	2:1	CF	1.32	0.70	33	0.30
PC$_{71}$BM	3:1	CF	0.44	0.70	31	0.10
PC$_{71}$BM	1:1	CF + 0.1% DIO	2.79	0.68	45	0.85
PC$_{71}$BM	1:1	CF + 0.3% DIO	2.13	0.67	43	0.62
PC$_{61}$BM	1:1	CF	1.95	0.70	43	0.58
PC$_{61}$BM	1:1	CF + 0.1% DIO	2.62	0.69	47	0.84 (0.97)
PC$_{61}$BM	1:1	CF + 0.1% DIO	2.66	0.76	41	0.83 (0.91)[c]
PC$_{61}$BM	1:2	CF	1.57	0.73	67	0.77 (0.83)
PC$_{61}$BM	1:2	CF	1.99	0.76	60	0.93 (0.98)[c]
PC$_{61}$BM	1:3	CF	1.80	0.69	59	0.73 (0.79)
PC$_{61}$BM	1:3	CF	2.37	0.76	50	0.90 (0.98)[c]
PC$_{61}$BM	1:2	CB	1.92	0.70	59	0.79 (0.84)

[a] CF = chloroform, CB = chlorobenzene, DIO = 1,8-diiodooctane. [b] Averaged over at least 3 devices. The best device performance is shown between brackets. [c] Post-annealed at 100 °C.

Table S3: Optimization of the solar cell devices based on **DTP(FBTTh$_2$)$_2$**.

Acceptor	Ratio	Solvent[a]	J_{sc} (mA/cm^2)	V_{oc} (V)	FF (%)	PCE[b] (%)
PC$_{61}$BM	1:2	CF	3.96	0.45	42	0.75 (0.80)
PC$_{61}$BM	1:3	CF	2.72	0.43	45	0.52 (0.53)
PC$_{71}$BM	1:1	CB	5.52	0.59	33	1.08 (1.11)
PC$_{71}$BM	1:2	CB	6.75	0.50	40	1.34 (1.37)

[a] CF = chloroform, CB = chlorobenzene. [b] Averaged over at least 3 devices. The best device performance is shown between brackets.

Table S4: Optimization of the solar cell devices based on **TT(FBTTh$_2$)$_2$**.

Acceptor	Ratio	Solvent[a]	J_{sc} (mA/cm^2)	V_{oc} (V)	FF (%)	PCE[b] (%)
PC$_{61}$BM	1:1	TCE[c]	4.36	0.80	36	1.26 (1.32)
PC$_{61}$BM	1:2	TCE[c]	5.28	0.71	38	1.42 (1.74)
PC$_{61}$BM	1:2	CB[d]	6.25	0.77	33	1.60 (1.68)
PC$_{61}$BM	1:3	CB[d]	4.45	0.76	34	1.14 (1.37)
PC$_{61}$BM	1:2	CB + 0.1% CN[d]	5.35	0.76	32	1.28 (1.60)
PC$_{61}$BM	1:2	CB + 0.3% CN[d]	5.53	0.69	31	1.16 (1.56)
PC$_{71}$BM	1:2	CB[d]	8.75	0.72	32	1.97 (2.19)
PC$_{71}$BM	1:2	CB + 0.2% DIO[d]	9.13	0.79	36	2.63 (2.96)
PC$_{71}$BM	1:2	oDCB[d]	8.11	0.65	34	1.79 (2.22)

[a] TCE = 1,1,2,2-tetrachloroethane, CB = chlorobenzene, oDCB = *ortho*-dichlorobenzene, CN = 1-chloronaphthalene, DIO = 1,8-diiodooctane. [b] Averaged over at least 3 devices. The best device performance is shown between brackets. [c] Processed at 85 °C. [d] Processed at 95 °C.

6.7.5 FET mobility measurements
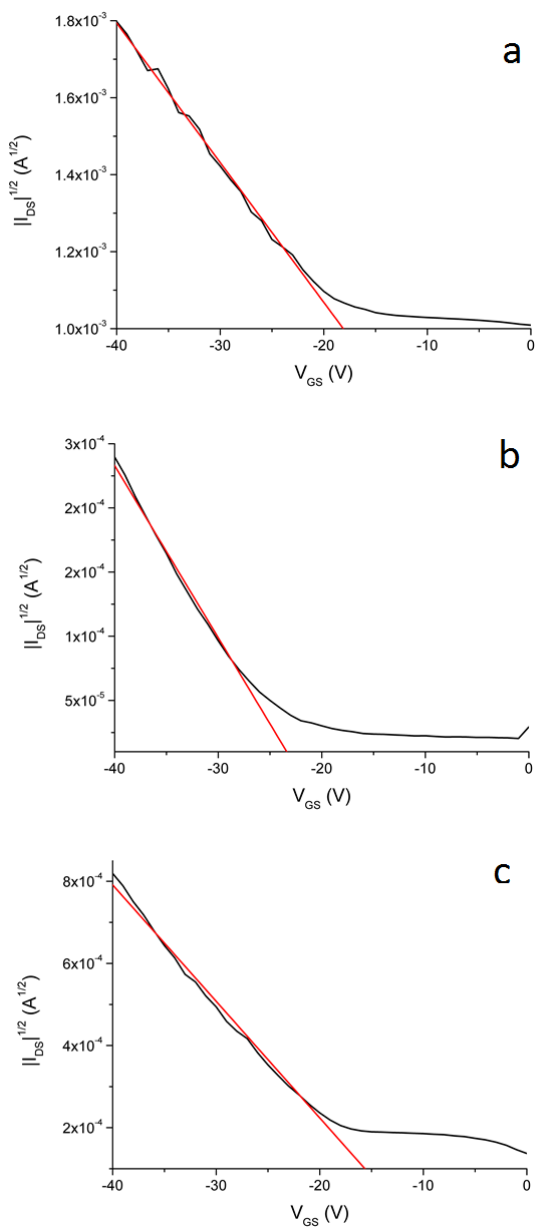
Figure S2: FET transfer characteristics for **CPDT(FBTTh₂)₂** (a), **BDT(FBTTh₂)₂** (b), and **TT(FBTTh₂)₂** (c). The lines used to fit the mobilities in the saturation regime (V_{DS} = -40 V) are shown in red.

6.7.6 AFM images
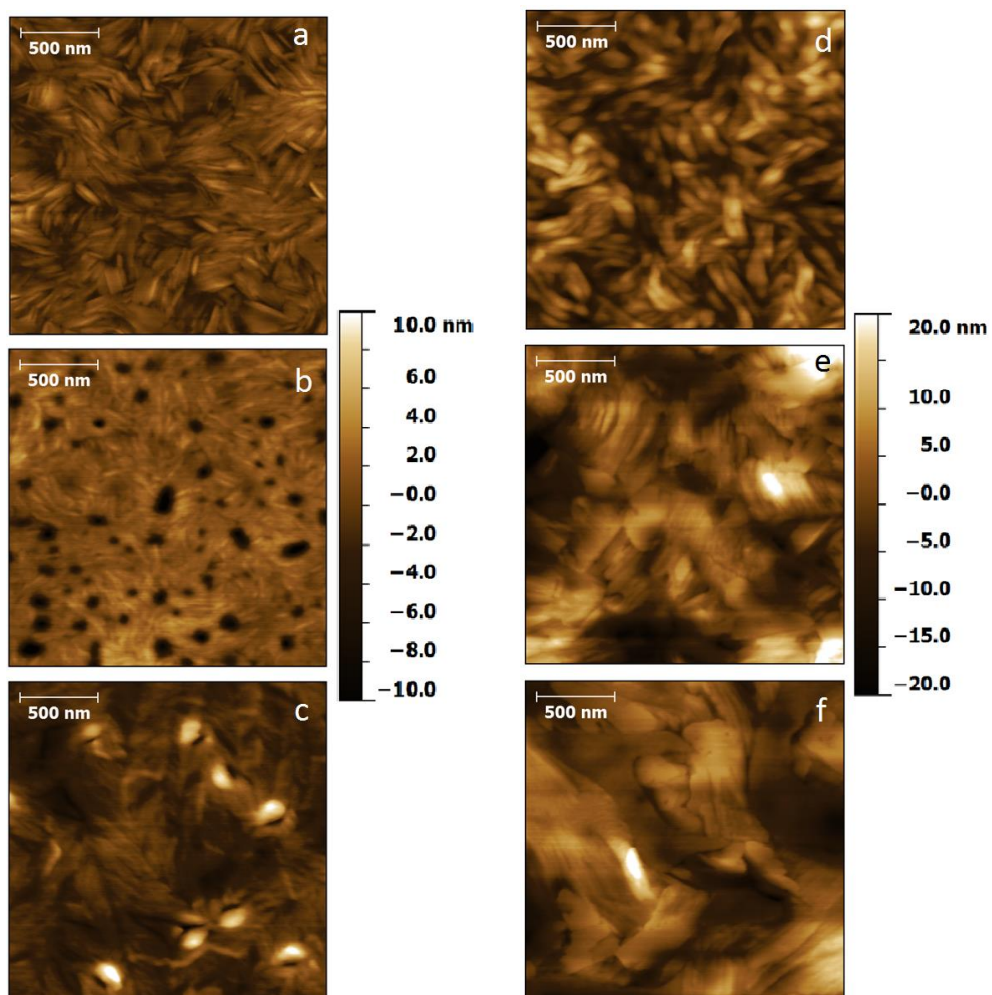
Figure S3: AFM scans for blends of **BDT(FBTTh₂)₂**:PC₆₁BM (1:2) in chloroform, post-annealed at 100 °C (a), (1:3) in chloroform (b), (1:2) in chlorobenzene (c), (1:1) in chloroform + 0.1% DIO (d), (1:2) in chloroform (e), (1:2) in chlorobenzene annealed at 100 °C (f).
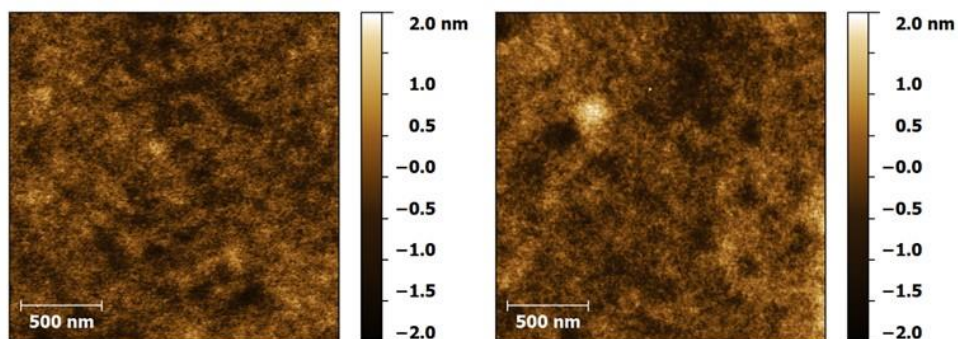
Figure S4: AFM images for the inverted devices based on **CPDT(FBTTh₂)₂**:PC₇₁BM (top) and **TT(FBTTh₂)₂**:PC₇₁BM (bottom) on ZnO.

6.7.7 J-V curves for the inverted solar cells
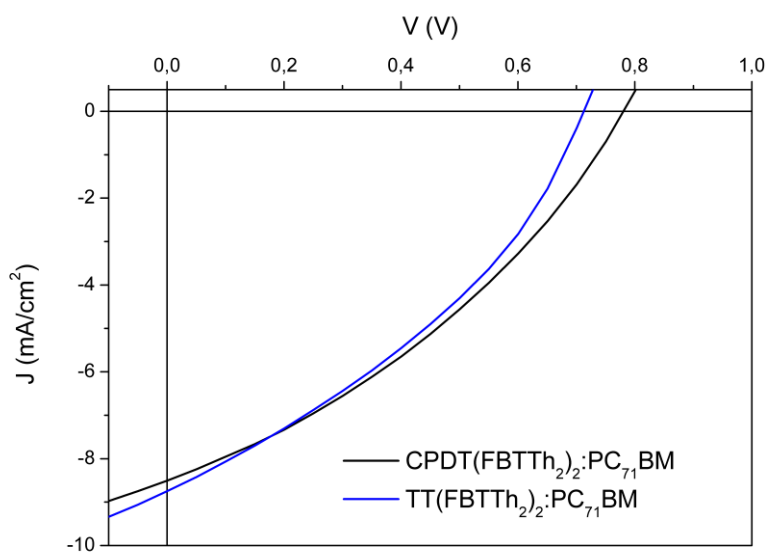
Figure S5: *J-V* characteristics for the inverted solar cells comprising of glass/ITO/ZnO/active layer (in legend)/MoO₃/Ag. The best efficiencies were 2.31% for **CPDT(FBTTh₂)₂**:PC₇₁BM and 2.21% for **TT(FBTTh₂)₂**:PC₇₁BM.

Chapter 7

Summary and Outlook

7.1 SUMMARY

Due to the tremendous amount of research performed during the last decade, the performance of organic solar cells has strongly been improved and power conversion efficiencies (PCE's) over 10% are currently reported for single junction polymer-based solar cells. However, for organic photovoltaics (OPV) to evolve into an economically viable technology, three major requirements need to be fulfilled, i.e. a high efficiency, a sufficiently long lifetime and the possibility to produce the solar cells at low cost. In this PhD thesis, work was performed on two of these parameters, performance and stability, through the development of new low bandgap copolymers and small molecule analogues and evaluation of their solar cell characteristics.

At first instance, we have focused on the optimization of the synthesis protocol for alkylated 4*H*-cyclopenta[2,1-*b*:3,4-*b′*]dithiophenes (CPDT's), one of the main building blocks used throughout this thesis. To circumvent the long and tedious classical synthesis route, in 2010, an alternative three step protocol was developed in our group, which additionally allows for the straightforward introduction of (asymmetrically) functionalized side chains. Since this procedure suffers from relatively low yields for the final ring-closing step, some optimization

efforts were performed. By (mainly) variation of the extraction solvent, the yield for this step could be improved from 55 to 74%. Despite the improved reaction efficiency, issues were still observed for more voluminous side chain patterns. This prompted us to develop a complementary synthesis protocol based on a Wittig-type carbonyl olefination reaction and subsequent reductive alkylation. For both steps, the products can be isolated in reasonably high yields (>70%), hence rendering this Wittig route more versatile (for sure for the more complex side chains).

After optimization of the monomer synthesis route, CPDT was copolymerized with a particular thiophene-extended quinoxaline (Qx) derivative to yield a PCPDTQx-type low bandgap copolymer. Due to the electron rich nature of the CPDT unit, this polymer did not only exhibit a small bandgap (1.5–1.6 eV), but also a relatively high HOMO energy level, limiting the solar cell performance through the moderate open-circuit voltage (V_{OC}). In an effort to overcome this, fluorine atoms (1 or 2) were introduced on the Qx unit and the influence on the physicochemical material features and device properties was investigated. While affecting the optical properties to only a minor extent, a significant influence on the positions of the HOMO and LUMO energy levels was observed. For every fluorine atom added, the HOMO level decreased by ~0.1 eV, which translated into an increase of the V_{OC} for the corresponding polymer solar cells by ~0.1 V (up to a maximum V_{OC} of 0.83 V for the PCPDTQx(2F):PC$_{71}$BM device). However, fluorination also influenced the active layer morphology of the solar cells, leading to the formation of unfavorable large domains (~250 nm) for the PCPDTQx(2F):PC$_{71}$BM blend, which could not be prevented by the use of high boiling additives, limiting the polymer solar cell performance to 5.26%.

In follow-up work, the amount of side chains on the backbone of the PCPDTQx(2F) polymer was then varied. It was found that the side chain density largely affects the active layer morphology of the solar cells. Whereas domains of approximately 250 nm were observed for the PCPDTQx(2F):PC$_{71}$BM active layer, a finely intermixed blend composition was obtained by removing 50% of the side chains on the Qx unit, leading to a maximum device performance of 5.63%. Furthermore, besides the influence on the active layer morphology, a large effect on the glass transition temperature (T_g) of the polymers was observed as well. Since the T_g of the polymer:fullerene blend is a crucial factor determining the thermal stability of polymer solar cells, the impact of the side chain density on the thermal stability of the solar cells was also evaluated. Complete removal of the side chains on all Qx units resulted in the best solar cell lifetime. PCE values of >80% of the initial value could be recovered for solar cells based on this polymer after 120 h exposure to a continuous thermal stress of 85 °C, whereas only 50% of the initial efficiency was retained for the device based on the fully alkylated copolymer.

Within our group, it was already shown that the incorporation of functional moieties (ester, alcohol, cinnamoyl) on the side chains of poly(3-alkylthiophenes) can enhance the (thermal) stability of polymer solar cells. This improvement is related to a decreased tendency for phase separation of the polymer and fullerene component (and fullerene crystallization) in the photoactive layer. In this thesis, an effort was done to translate this approach to low bandgap copolymers, affording higher solar cell efficiencies. To this extent, PCPDTBT-type copolymers (BT = 2,1,3-benzothiadiazole) containing alcohol or ester functional groups in the side chains were prepared. For both functionalized copolymers, the resulting polymer:fullerene solar cells showed an improved thermal stability during accelerated aging tests at 85 °C (in comparison to the non-functionalized

analogue). However, in contrast to the polythiophene results, the enhanced lifetime could not be attributed to delayed phase separation because of the high T_g values (> 160 °C) for all of the materials (and the resulting blends), even the pristine PCPDTBT. From preliminary deconvolution of the various degradation pathways it seems that the incorporation of alcohol or ester functional groups leads (amongst others) to a higher resistivity toward reduced interface (active layer–cathode) quality.

Finally, we also studied a small series of solution processable small molecule donor materials for OPV applications. The effect of the central donor unit in D-A-D-A-D type (D = donor, A = acceptor) small molecules related to the well-known high-performance DTS(FBTTh$_2$)$_2$ material was investigated. The central dithieno[3,2-*b*:2',3'-*d*]silole (DTS) moiety was replaced by CPDT, BDT (benzo[1,2-*b*:4,5-*b'*]dithiophene), DTP (dithieno[3,2-*b*:2',3'-*d*]pyrrole) and TT (thieno[3,2-*b*]thiophene). The best solar cell performance was obtained for CPDT and TT as central donor units (PCE ~3%). These results remain, however, far below the efficiency obtained for DTS(FBTTh$_2$)$_2$. For BDT(FBTTh$_2$)$_2$ and (especially) DTP(FBTTh$_2$)$_2$, the presence of small amounts of homo-coupled side products was observed by MALDI-TOF analysis, which might explain the unexpected low V_{OC} value obtained for the DTP-based devices. Despite extensive purification efforts, these side products could not be removed.

7.2 OUTLOOK

In this thesis it is demonstrated that copolymerization of a (relatively) strong electron donor (CPDT) and a (relatively) strong electron acceptor (Qx) building block results in copolymers with near-to-ideal bandgaps. Moreover, fluorination can be used to further decrease both the HOMO and LUMO energy levels, resulting in improved V_{OC} values for the polymer solar cells, with a minimal effect on the bandgap. It is also shown that optimization of the side chain density can be helpful to control the active layer morphology and, in addition, to improve the thermal stability of the solar cells. However, in this work, all copolymers are composed of CPDT, a building block with a demonstrated modest photochemical stability.[1] Therefore, it would be relevant to replace CPDT by other strong electron donors with increased photostability such as dithieno[3,2-*b*:2',3'-*d*]thiophene.[1] Control of the side chain density can also be applied to optimize the solar cell performance of other (known) copolymers. We have recently reported a series of low bandgap copolymers composed of *N*-acyl-substituted DTP's and fluorinated quinoxalines.[2] The non-fluorinated copolymer afforded a promising PCE of 4.8% in a standard bulk heterojunction OPV device, but Qx fluorination resulted in active layers with unfavorable morphologies (showing large domains), leading to decreased efficiencies. Variation of the side chain density could be a possible way to control the photoactive layer morphology and thereby optimize the polymer solar cell efficiency for this material class as well.

Two possible pathways to improve the thermal stability of polymer solar cells are explored in this PhD dissertation, i.e. control of the side chain density and addition of functional groups on the side chains. These concepts were demonstrated so far for copolymers affording moderate solar cell efficiencies. Translation of this

method to state of the art high-performance copolymers is an obvious next target. Both stabilizing principles described in this thesis could possibly be implemented on one single polymer (especially for low-T_g materials). Since photochemical stability is also of crucial importance for the creation of sustainable OPV products, care should also be taken to select materials composed of environmentally stable building blocks (e.g. PBDTTPD[3]).

In the last couple of years, it has been shown that small molecules can be possible alternatives for conjugated polymers as electron donor materials in organic solar cells. It is often postulated that the synthesis and especially the purification of these small molecules is more straightforward. However, even after extensive non-standard purification of some of our 'small' molecules (e.g. by preparative size exclusion chromatography), we have observed the presence of homo-coupled side products created during the final Stille cross-coupling reaction, which seems to have a detrimental effect on the solar cell performance.[4] Therefore, considerable care has to be taken during the synthesis of these materials to avoid the formation of these side products. In ongoing work on PTB7-based OPV devices, we have seen similar effects of homo-coupling defects (also in this case visualized by MALDI-TOF analysis). For both small molecules and polymers, these effects seem to be underappreciated, as their evaluation is almost absent in OPV literature. In this respect, small molecules can offer a useful scaffold to optimize the (Stille/Suzuki) polymerization conditions, since they allow for a more straightforward analysis of the byproducts. Furthermore, it could be interesting to study the effect of homo-coupling in more detail by deliberate addition of homo-coupled product to the pure small molecule. On the other hand, also for polymers MALDI-TOF analysis remains a useful technique to evaluate their structural quality, despite the possible issues for (very) high molar mass materials.

7.3 REFERENCES

[1]   M. Manceau, E. Bundgaard, J. E. Carlé, O. Hagemann, M. Helgesen, R. Søndergaard, M. Jørgensen and F. C. Krebs, *J. Mater. Chem.*, 2011, **21**, 4132.

[2]   J. Kesters, P. Verstappen, W. Vanormelingen, J. Drijkoningen, T. Vangerven, D. Devisscher, L. Marin, B. Champagne, J. Manca, L. Lutsen, D. Vanderzande and W. Maes, *Sol. Energy Mater. Sol. Cells*, 2015, DOI: 10.1016/j.solmat.2014.12.037.

[3]   A. Tournebize, J.-L. Gardette, C. Taviot-Guého, D. Bégué, M. A. Arnaud, C. Dagron-Lartigau, H. Medlej, R. C. Hiorns, S. Beaupré, M. Leclerc and A. Rivaton, *Polym. Degrad. Stab.*, 2015, DOI:10.1016/j.polymdegradstab.2014.12.018.

[4]   K. H. Hendriks, W. Li, G. H. L. Heintges, G. W. P. van Pruissen, M. M. Wienk and R. A. J. Janssen, *J. Am. Chem. Soc.*, 2014, **136**, 11128.

7.4 NEDERLANDSE SAMENVATTING

Tijdens het laatste decennium zijn de prestaties van organische zonnecellen spectaculair verbeterd en momenteel worden er efficiënties van meer dan 10% gerapporteerd voor *single junction* devices. Om commercialisatie toe te laten moet er echter aan drie belangrijke parameters voldaan worden, namelijk een hoge efficiëntie, een voldoende lange levensduur en de mogelijkheid om deze zonnecellen tegen een lage kostprijs te produceren. In deze thesis hebben we ons gericht op de optimalisatie van twee van deze parameters, nl. efficiëntie en stabiliteit, door de ontwikkeling van nieuwe *low bandgap* copolymeren en analoge kleine moleculen.

In eerste instantie hebben we ons gericht op de optimalisatie van het syntheseprotocol voor gealkyleerde 4*H*-cyclopenta[2,1-*b*:3,4-*b'*]dithiofenen (CPDT's), één van de courant gebruikte bouwstenen tijdens deze doctoraatsthesis. Om de complexe klassieke syntheseroute te vermijden werd er in 2010 binnen onze onderzoeksgroep een alternatieve drie-staps-synthese ontwikkeld, die daarenboven ook de introductie van (asymmetrisch) gefunctionaliseerde zijketens mogelijk maakt. Vermits tijdens deze procedure lage rendementen verkregen werden voor de finale ringsluiting, werd er getracht deze stap verder te optimaliseren. Door (voornamelijk) variatie van het extractiesolvent kon het rendement opgedreven worden van 55 tot 74%. Ondanks deze hoopgevende resultaten werden er echter nog steeds problemen ervaren tijdens de introductie van volumineuze zijketens. Dit heeft ons aangezet om een tweede, complementaire, syntheseroute te ontwikkelen die zich baseert op achtereenvolgens een Wittig carbonyl-olefinering en reductieve alkylering. Voor beide synthesestappen konden de producten in aanvaardbare opbrengsten (>

70%) geïsoleerd worden, waardoor deze Wittig route op dit moment het meest aangewezen lijkt (zeker voor de complexere zijketens).

Na optimalisatie van de monomeersynthese werd CPDT gecopolymeriseerd met een quinoxaline-derivaat (Qx), waardoor een PCPDTQx-type *low bandgap* copolymeer wordt verkregen. Door het elektronenrijk karakter van CPDT vertoonde dit polymeer niet enkel een kleine *bandgap*, maar ook een relatief hoog HOMO-energieniveau, waardoor de zonnecelprestatie gelimiteerd werd door een lage openklemspanning (V_{OC}). Om de V_{OC} te verhogen werden er vervolgens fluoratomen ingebouwd op de Qx-eenheid en de invloed hiervan op de fysicochemische materiaalkarakteristieken en zonneceleigenschappen werd onderzocht. Hoewel de optische eigenschappen van de polymeren amper beïnvloed werden, werden de posities van de HOMO en LUMO-energieniveaus in belangrijke mate bepaald door de introductie van de fluoratomen. Per geïntroduceerd fluoratoom werd er een daling van het HOMO-energieniveau met ∼0,1 eV waargenomen. Dit gaf aanleiding tot een stijging van de V_{OC} met ongeveer 0,1 V per fluoratoom tot een maximum van 0,83 V voor de PCPDTQx(2F):PC$_{71}$BM zonnecel. Fluorering had echter ook een belangrijke invloed op de morfologie van de actieve laag. Voor de PCPDTQx(2F):PC$_{71}$BM blend werden er grote domeinen (∼250 nm) waargenomen. De vorming van deze domeinen kon niet verhinderd worden door het gebruik van hoogkokende additieven, waardoor de zonnecelefficiëntie gelimiteerd bleef tot 5,26%.

In een vervolg-project werd de invloed van het aantal zijketens op het polymeer bestudeerd. Variatie van de zijketendichtheid leidde tot grote verschillen in de morfologie van de actieve laag van de zonnecellen. Daar waar domeingroottes van ongeveer 250 nm werden verkregen voor de PCPDTQx(2F):PC$_{71}$BM actieve laag, werd er al een geschikte nanomorfologie bekomen indien 50% van de

zijketens op de Qx-eenheid werden verwijderd. Dit gaf aanleiding tot zonnecellen met een maximumefficiëntie van 5,63%. Bovendien werd er, naast de invloed op de morfologie van de actieve laag, ook een groot effect waargenomen op de glastransitietemperatuur (T_g) van het polymeer. Aangezien de T_g van de polymeer:fullereen blend cruciaal is voor de thermische stabiliteit van polymere zonnecellen, werd ook een stabiliteitsstudie uitgevoerd. Verwijdering van de zijketens op alle Qx-eenheden gaf aanleiding tot zonnecellen met een verbeterde levensduur. Na een blootstelling aan 85 °C voor 120 u werden er voor dit polymeer nog steeds efficiënties van meer dan 80% van de initiële waarde bekomen, terwijl dit voor het volledig gealkyleerde polymeer gedaald was tot amper 50%.

Binnen onze onderzoeksgroep werd reeds eerder aangetoond dat de introductie van functionele groepen (ester, alcohol, cinnamoyl) op de zijketens van poly(3-alkylthiofenen) de thermische stabiliteit van de resulterende polymere zonnecellen gevoelig kan verbeteren. Dit effect kon gerelateerd worden aan de verminderde neiging tot fasescheiding van het polymeer en de fullereencomponent in de actieve laag. In deze thesis werden er inspanningen gedaan om dit mechanisme te vertalen naar *low bandgap* polymeren. Hiertoe werden PCPDTBT-type copolymeren (BT = 2,1,3-benzothiadiazool) gesynthetiseerd waarbij er alcohol- en estergroepen werden ingebouwd op de zijketens. Voor beide polymeren werd er een verhoging van de thermische stabiliteit van de resulterende polymeer:fullereen zonnecellen waargenomen tijdens een versnelde verouderingsstudie op 85 °C (in vergelijking met het niet-gefunctionaliseerde PCPDTBT). In tegenstelling tot de polythiofenen kon de verhoogde levensduur hier niet gelinkt worden aan vertraagde fasescheiding door de hoge T_g-waarden voor deze materialen (en resulterende blends). Voor de PCPDTBT-gebaseerde zonnecellen lijkt een hogere weerstand t.o.v. degradatie

van de interfase (actieve laag – kathode) aan de basis te liggen van de verbeterde thermische stabiliteit.

Tot slot werden er ook enkele uit oplossing verwerkbare 'kleine' moleculen bestudeerd als donormaterialen voor organische zonnecellen. Hierbij werd het effect van de centrale donoreenheid in D-A-D-A-D type materialen (D = donor, A = acceptor) bestudeerd. De onderzochte serie kleine moleculen werd verkregen door de centrale dithiëno[3,2-*b*:2',3'-*d*]silool-eenheid (DTS) van het welbekende DTS(FBTTh$_2$)$_2$ molecule te vervangen door CPDT, BDT (benzo[1,2-*b*:4,5-*b'*]dithiofeen), DTP (dithiëno[3,2-*b*:2',3'-*d*]pyrrool) en TT (thiëno[3,2-*b*]thiofeen). De beste zonnecelprestaties werden verkregen voor CPDT en TT als centrale donoreenheid (PCE ~ 3%). Deze resultaten blijven echter ver onder de gerapporteerde efficiëntie voor DTS(FBTTh$_2$)$_2$. Voor BDT(FBTTh$_2$)$_2$ en vooral DTP(FBTTh$_2$)$_2$ kon de aanwezigheid van homo-gekoppelde nevenproducten worden aangetoond met behulp van MALDI-TOF analyse. Dit kan mogelijk een verklaring zijn voor de onverwacht lage V_{OC}-waarden die verkregen werden voor de DTP-gebaseerde zonnecellen. Ondanks een uitgebreide zuivering werd er voorlopig niet in geslaagd om deze nevenproducten te verwijderen.

List of Publications

M. M. Kruk, T. H. Ngo, <u>P. Verstappen</u>, A. S. Starukhin, J. Hofkens, W. Dehaen, W. Maes, *Unraveling the fluorescence features of individual corrole NH tautomers*, J. Phys. Chem. A, **2012**, *116*, 10695.
Contribution: Corrole purification.

W. Vanormelingen, <u>P. Verstappen</u>, V. Maes, D. Bevk, L. Lutsen, D. Vanderzande and W. Maes, *Synthetic routes toward asymmetrically substituted (functionalized) 4H-cyclopenta[2,1-b:3,4-b']dithiophenes*, Synlett, **2013**, *24*, 2389.
Contribution: Development of the Wittig route.

W. Vanormelingen, J. Kesters, <u>P. Verstappen</u>, J. Drijkoningen, J. Kudrjasova, S. Koudjina, V. Liégeois, B. Champagne, J. Manca, L. Lutsen, D. Vanderzande, W. Maes, *Enhanced open-circuit voltage in polymer solar cells by dithieno[3,2-b:2',3'-d]pyrrole N-acylation*, J. Mater. Chem. A, **2014**, *2*, 7535.
Contribution: Synthesis of acceptor monomers.

<u>P. Verstappen</u>, J. Kesters, W. Vanormelingen, G. H. L. Heintges, J. Drijkoningen, T. Vangerven, L. Marin, S. Koudjina, B. Champagne, J. Manca, L. Lutsen, D. Vanderzande, W. Maes, *Fluorination as an effective tool to increase the open-circuit voltage and charge carrier mobility of organic solar cells based on poly(cyclopenta[2,1-b:3,4-b']dithiophene-alt-quinoxaline) copolymers*, J. Mater. Chem. A, **2015**, DOI: 10.1039/C4TA06054G.
Contribution: Synthesis and characterization of the monomers and polymers.

J. Kesters, <u>P. Verstappen</u>, W. Vanormelingen, J. Drijkoningen, T. Vangerven, D. Devisscher, L. Marin, B. Champagne, J. Manca, L. Lutsen, D. Vanderzande, W. Maes, *N-Acyl-dithieno[3,2-b:2′,3′-d]pyrrole-based low bandgap copolymers affording improved open-circuit voltages and efficiencies in polymer solar cells*, Sol. Energy Mater. Sol. Cells, DOI:10.1016/j.solmat.2014.12.037.
Contribution: Synthesis of the quinoxaline monomers.

K. Gilissen, J. Stryckers, <u>P. Verstappen</u>, J. Drijkoningen, G. H. L. Heintges, L. Lutsen, J. Manca, W. Maes, W. Deferme, *Ultrasonic spray coating as deposition technique for the light-emitting layer in polymer LEDs*, Org. Electron., DOI: 10.1016/j.orgel.2015.01.015.
Contribution: Characterization of the polymer before and after spraycoating.

L. Marin, J. Kudrjasova, <u>P. Verstappen</u>, H. Penxten, K. Robeyns, L. Lutsen, D. Vanderzande, W. Maes, *Quinoxaline-based cyclo(oligophenylenes)*, J. Org. Chem., manuscript accepted.
Contribution: Guidance of synthesis and purification.

J. Kesters, <u>P. Verstappen</u>, J. Raymakers, W. Vanormelingen, J. Drijkoningen, J. D'Haen, J. Manca, L. Lutsen, D. Vanderzande, W. Maes, *Enhanced organic solar cell stability by polymer (PCPDTBT) side chain functionalization*, Chem. Mater., manuscript under revision.
Contribution: Synthesis and characterization of the monomers and polymers.

D. Spoltore, T. Vangerven, <u>P. Verstappen</u>, F. Piersimoni, S. Bertho, K. Vandewal, N. Van den Brande, B. Van Mele, A. De Sio, J. Parisi, L. Lutsen, D. Vanderzande, W. Maes and J. V. Manca, *Effect of molecular weight on morphology and*

photovoltaic properties in P3HT:PCBM solar cells, Org. Electron., manuscript under revision.

Contribution: Fractionation and characterization of the P3HT samples.

F. Ouhib, M. Tomassetti, W. Dierckx, <u>P. Verstappen</u>, A. Wisley, A.-S. Duwez, V. Lemaur, R. Lazzaroni, J. Manca, W. Maes, C. Jérôme, C. Detrembleur, *Linear and star-shaped fluoro-isoindigo based donor-acceptor small molecules for organic solar cells*, Org. Electron., manuscript under revision.

Contribution: Guidance of synthesis and purification.

J. Kesters, <u>P. Verstappen</u>, M. Kelchtermans, L. Lutsen, D. Vanderzande, W. Maes, *Porphyrin-based bulk heterojunction organic photovoltaics: the rise of the colors of life*, Adv. Energy Mater., manuscript under revision.

Contribution: Article writing and revision.

<u>P. Verstappen</u>, J. Kesters, L. D'Olieslaeger J. Drijkoningen, I. Cardinaletti, T. Vangerven, J. D'Haen, J. Manca, L. Lutsen, D. Vanderzande, W. Maes, *Simultaneous enhancement of the solar cell efficiency and stability by reducing the side chain density on fluorinated PCPDTQx copolymers*, manuscript submitted.

Contribution: Synthesis and characterization of the monomers and polymers.

<u>P. Verstappen</u>, I. Cardinaletti, T. Vangerven, W. Vanormelingen, L. Lutsen, D. Vanderzande, J. Manca, W. Maes, *Variation of the central donor unit in D-A-D-A-D small molecules for organic solar cells*, to be submitted.

Contribution: Synthesis and characterization of the small molecules.

Dankwoord

Oef, na veel zweten en zwoegen ben ik eindelijk aangekomen op het einde van mijn PhD thesis. Daarmee is ook de tijd aangebroken om enkele mensen te bedanken die hebben bijgedragen aan de verwezenlijking van dit werk.

Op de eerste plaats wil ik graag even de tijd nemen om mijn promotor, Prof. dr. Wouter Maes, te bedanken. Ik vond het fantastisch dat je me de vrijheid hebt gelaten om mijn eigen weg te zoeken, al heb je waarschijnlijk wel een paar keer gevloekt toen ik mij weer eens op één of ander zot idee stortte ☺, maar toch heb je mij altijd het gevoel gegeven dat ik nuttig werk aan het verrichten was. Je wist als geen ander je studenten te motiveren en jouw punctualiteit en kritisch denken hebben mijn werk en mijzelf zeker positief beïnvloed (al heb ik het soms ook verwenst tijdens het schrijven ☺). Bedankt voor alles. Het was een voorrecht om met jou te mogen samenwerken.

Verder verdient natuurlijk ook mijn copromotor, Prof. dr. Dirk Vanderzande, een woordje van dank. Hiervoor zou ik zelfs graag teruggaan naar mijn bachelorjaren. Het aanstekelijk enthousiasme dat u tijdens de lessen tentoonspreidde heeft er mee voor gezorgd dat ik deze richting ben ingeslagen. Tijdens de doctoraatsjaren hebben we elkaar wat minder gezien, maar telkens ik u tegen het lijf liep had u toch enkele nuttige tips in petto, waarvoor dank.

Of course, I would also like to thank my second copromoter, dr. Laurence Lutsen. Thank you for guiding the daily operation of our lab and dealing with some urgent orders.

Furthermore, I would like to thank all the members of the jury for taking the time to evaluate my work and the IWT for financial support.

Natuurlijk heb ik ook altijd kunnen rekenen op de nodige hulp van mijn naaste collega's tijdens het uitvoeren van mijn doctoraatsonderzoek. Daarvoor verdienen zij nu een welgemeend woordje van dank. Ik zou graag willen beginnen bij de oude garde. Sarah en Hanne, bedank voor de begeleiding tijdens de eerste maanden van mijn doctoraatsonderzoek. Jullie enthousiasme heeft ervoor gezorgd dat ik er met heel veel plezier direct "vollenbak" tegenaan gegaan ben. Lidia, thanks for helping me with my CPDT synthesis problems during the early days of my PhD. I hope you will find a nice job soon. En toen kwam de Vanormelingen, de man die mij van mijn polymerisatiefobie afgeholpen heeft. Wouter, het was echt een plezier om met u te kunnen samenwerken en bedankt om ook af en toe eens de tijd te nemen om mijn geklaag te aanhoren wanneer het weer eens tegen zat. Jurgen, kom binnen een week of twee nog eens terug dan zal ik het wel klaar hebben ☺. Nee, jou moet ik ook voor heel wat zaken bedanken. Niet alleen heb je een heleboel dagen zonnecelmetingen uitgevoerd voor mij, maar heb je mij ook op tijd en stond eens achter mijn veren gezeten. Zonder jou was mijn boekje waarschijnlijk de helft dunner. Rafael, mijn brother-in-arms tijdens de avondlijke labo uurtjes, bedankt voor al het constructieve (en minder constructieve) gekribbel op mijn trekkast en voor al je advies in verband met mijn synthese- en PC-problemen.

Het zou me te ver leiden om alle collega's gedurende de vier jaar apart te bedanken, daarom wil ik jullie graag gezamenlijk bedanken. Jullie hebben allemaal bijgedragen aan de toffe ongedwongen sfeer die aanwezig was, waardoor ik vier jaar lang met heel veel plezier ben komen werken. Bedankt Tom, Inge, Toon, Ans, Joke, Neomy, Evelien, Stephan, Kayte, Veronique, Julija, David B., Geert, Joris, Mathias, Sanne, Yasmine, David C., Brecht, Rebecca, Tien, Benjamin, Joachim, Matthias, Ya-Mi.

Natuurlijk mag ik ook het vast personeel niet vergeten. Zij zorgen er immers voor dat wij uberhaupt kunnen werken. Bedankt Iris, Huguette, Gunter, Koen en Jan-de-massa-man.

Verder heb ik ook het geluk gehad om enkele thesisstudenten te mogen begeleiden tijdens hun bachelorstage. Ik hoop vooral dat jullie iets opgestoken hebben van deze periode. Er zijn in elke geval enkele mooie resultaten uit voortgevloeid, waarvoor mijn dank. Bedankt Jeroen, Gaël, Wout en Jorne.

Verder dien ik ook nog enkele collega's van het IMO te bedanken. Ilaria, thanks for all the work on the small molecules. I realize these were not the most motivating materials, but you kept on optimizing and in the end we finally got some decent results. Tim, Jeroen, Lien en Prof. dr. Jan D'Haen, bedankt voor alle fysische analyses en om deze begrijpelijk uit te leggen aan een leek als mij ☺.

Vervolgens wil ik ook alle externe collega's bedanken waarmee ik heb samengewerkt. Prof. dr. Bruno Van Mele, Niko en Maxime van de Vrije Universiteit Brussel voor alle thermische analyses. Prof. dr. Benoît Champagne of the University of Namur for the theoretical calculations.

Tot slot wil ik ook nog mijn familie en vrienden bedanken voor hun steun tijdens deze periode.

<div align="right">BEDANKT ALLEMAAL!</div>